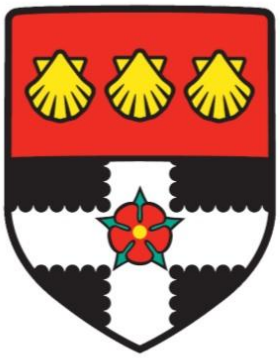

University of Reading

Smoking induced muscle dysfunction: Unravelling the mechanisms leading to diminished regeneration

Husain M Bin Haidar

Thesis submitted for the degree of Doctor of Philosophy

School of Biological Sciences

July 2025

Declaration

I confirm that the work in this thesis is my own work, and the use of all material from other sources has been fully acknowledged.

Husain M A J A Bin Haidar

Acknowledgments

I am grateful to Professor Ketan Patel for giving me this opportunity to learn and grow, I thank you for your guidance and advice. To me you are more than a tutor and a friend, you are family.

Ali Al Qallaf you are a brother to me, your contribution and aid have been invaluable for the past years and for that I thank you, I will always be indebted to you.

My wife Danah, the rock on which I lean, my support structure and my number one fan. Thank you for your patience, perseverance and love. Without you I would not be where I am today.

I dedicate this work to my parents, my wife, and my boys.

Abstract

With an estimated 1 billion smokers worldwide, cigarette smoke is the leading cause of cancer and cardiovascular disease. Cigarette smoke has been found to cause weakness and wasting of skeletal muscle, the mechanism of which is still not completely understood. Recently, electronic cigarette use has become prominent worldwide. Consumption has been linked with multiple respiratory diseases but the effect on muscle is still not fully known. We hypothesize that cigarette smoke and vaping causes incomplete regeneration of muscle after acute damage. The aim of the project is to understand how cigarette smoke media (CSM) and vape media (VM) affects the growth, survival and regeneration of muscle by investigating the direct effect on immortalized myoblasts and mouse models. Then using gene expression along with a bio-informatic approach called "connectivity-mapping", identify compounds that could be repurposed as therapies to promote muscle growth and function in smokers. Here we found that CSM reduced viability in several cell lines, reduced the migratory abilities of myoblasts and caused atrophy in myotubes. Both CSM and VM increased senescence, reduced fusion, induced organellar stress and dysregulated cytokine levels in vitro. In vivo CSM and VM did not affect animal weights, muscle weights, fibre cross sectional area or cause fibrosis after acute damage. However, they prolonged regeneration, and dysregulated cytokine levels. The gene expression data of CSM revealed several differentially expressed genes. The expression data was introduced into the C-map which identified harmine and asiaticoside as compounds that could potentially reverse the effects of CSM on muscle. We found that these compounds failed to rescue cells in a viability assay, therefore suggest a combination of transcriptomics and proteomics as a more robust solution to find alternatives.

Table of Contents:

Abbreviations

Ab	Antibody
Ach	Acetylcholine
ADP	Adenine diphosphate
AKT	Protein kinase B
AP-1	Activator protein-1
ATP	Adenosine triphosphate
BAP	Benzo[*a*]pyrene
CHD	Coronary heart disease
COPD	Chronic obstructive pulmonary disease
CM	Conditioned media
CS	Cigarette smoke
CSM	Cigarette smoke conditioned media
CVD	Cardiovascular disease
DEG	Differentially expressed gene
DM	Differentiation media
E-cig	Electronic cigarette
ECM	Extracellular matrix
EGFR	Epidermal growth factor receptor
ERK	Extracellular signal-regulated kinases
FBS	Foetal bovine serum
FCS	Foetal calf serum
GM	Growth media
IHC	Immunohistochemistry
MAFbx	Muscle atrophy F-box
MAPK	Mitogen-activated protein kinases
Myf5	Myogenic factor 5
MyoD	Myoblast determination protein-1
MRFs	Myogenic regulatory factors
nAChRs	Neuronal nicotinic acetylcholine receptors

NF-κB	Nuclear factor-kappa-B
NHS	National Health Service
NMJ	Neuromuscular junction
NNK	4-(methylnitrosamino)-1-(3-pyridyl)-1-butanone
NNN	*N'*nitrosonornicotine
PAD	Peripheral artery disease
PAH	Polycyclic aromatic hydrocarbon
PAX3	Paired box 3
PAX7	Paired box 7
PBS	Phosphate buffered saline
PCA	Principal component analysis
P_i	Inorganic phosphate
PKA	Protein kinase A
PKC	Protein kinase C
qPCR	Quantitative real-time polymerase chain reaction
RNA	Ribonucleic acid
ROS	Reactive oxygen species
SASP	Senescence associated secretory phenotype
SC	Satellite cells
sActRIIB	Soluble activin receptor 2 B
SMA	Spinal muscular atrophy
T-tubules	Transverse tubules
UPS	Ubiquitin proteasome system
USP-19	Ubiquitin specific protease-19
VM	Vape extract conditioned media
WHO	World health organization

Chapter 1: Introduction

1.1. Tobacco and health

Tobacco consumption became mainstream in the early 20th century (Hoffmann & Hoffmann, 1997) and today is marketed to the public to consume in various ways, which include chewable tobacco and conventional cigarettes. The World Health Organization (WHO) estimates that there are more than 1 billion smokers worldwide and approximately 7 million smoking related deaths annually (WHO, 2020). The National Health Service (NHS) has reported that almost 500,000 hospital admissions and approximately 80,000 deaths are attributed to smoking in 2020 (NHS, 2020).

It is now widely accepted that smoking increases the risk of a multitude of diseases (figure 1.1) including lung cancer, chronic obstructive pulmonary disease (COPD) and cardiovascular disease (CVD).

1.1

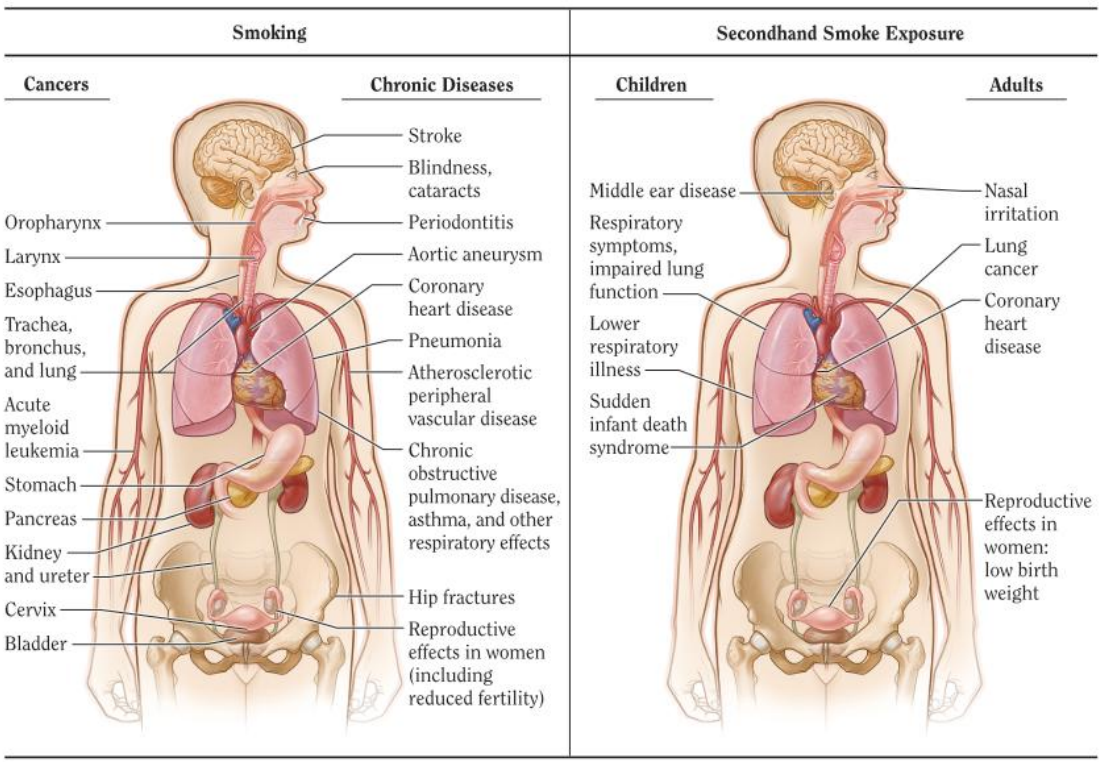

Figure 1.1. Diseases linked to smoking. Image sourced from (Centers for Disease et al., 2010).

The many diseases attributed to smoking are a consequence of the many constituents in cigarettes; it is reported that more than 5000 chemicals can be found in cigarette smoke, with many designated as toxic or carcinogenic (Borgerding & Klus, 2005). These chemicals include the likes of hydrogen cyanide, formaldehyde, acrolein, lead, arsenic, benzene, benzo[*a*]pyrene (BAP); a polycyclic aromatic hydrocarbon (PAH), a class of chemical known to cause DNA damage, *N*-nitrosamines such as 4-(methylnitrosamino)-1-(3-pyridyl)-1-butanone (NNK) and *N'*nitrosonornicotine (NNN) both established as tumourogenic in multiple *in-vivo* experiments, tar, carbon monoxide and the addictive component nicotine. Several publications (Borgerding & Klus, 2005; Hoffmann & Hoffmann, 1997; Hoffmann et al., 2001; Jaccard et al., 2019; Li & Hecht, 2022; Smith et al., 2003; Talhout et al., 2011) have comprehensive data with regards to the cigarette smoke constituents.

Similarly, the electronic cigarette, marketed as the safe alternative, has the same chemical constituents (Beauval et al., 2017; Eshraghian & Al-Delaimy, 2021; Famele et al., 2017; Goniewicz et al., 2014; Han et al., 2016; Kamilari et al., 2018; Sleiman et al., 2016). The effects of these chemicals are felt within seconds after the consumer takes the first puff. Briefly, the mouth, tongue and nose are the first to be affected by causing inflammation and damage to the tissue and nerve endings resulting in the loss of taste and smell. The smoke travels down to the lungs reaching the bronchi, bronchioles and the alveoli. Here, pulmonary absorption occurs, and the systemic effect is initiated. Nicotine rapidly diffuses into the pulmonary circulation and reaches the brain within seconds activating the nicotinic acetylcholine receptors (nAChRs) and dopamine release, the major addictive consequence. Carbon monoxide competes with oxygen and binds to hemoglobin forming carboxyhemoglobin and reducing the oxygen carrying capacity of blood. Acrolein and formaldehyde cause inflammation and alveolar damage, tar deposits in the bronchial epithelium cause damage and impaired cilia function leading to increased mucus and decreasing pathogen clearance. Generally, the systemic effect results in chronic

inflammation, vasoconstriction leading to increased heart rate and hypertension. Eventually, long term exposure leads to atherosclerosis, chronic obstructive pulmonary disorder, cancer and cardiovascular disease.(Centers for Disease et al., 2010; Hahad et al., 2023; Munzel et al., 2020).

1.2. Lung cancer

In the UK approximately 50,000 people are diagnosed annually with lung cancer (Navani et al., 2022; NHS, 2025), on the global scale it is the leading smoking related cause of mortality (WHO, 2025). A possible route of carcinogenesis is through DNA mutations (Centers for Disease et al., 2010) (figure 1.2), the toxic and carcinogenic nature of the cigarette constituents causes DNA adducts, either directly; via enzymatic hypermethylation of promoter regions of genes that may result in silencing; or through metabolic activation catalyzed by cytochrome P-450 enzymes, glutathione *S*-transferases and UDP-glucuronosyl transferases that transform the carcinogens to water soluble forms which are detoxified and excreted. However, this process produces electrophilic compounds such as carbocations or epoxides which can mediate a reaction with the nucleophilic locations in DNA causing adducts. Either way these adducts may elude repair mechanisms; due to overwhelming damage or dysfunction, resulting in mutations in the DNA sequence, should the mutations occur in growth regulatory genes then this would lead to unchecked proliferation, more mutations and eventually cancer. Some of the most significant mutations develop in tumour suppressor genes and oncogenes such as RB, PTEN, CDKN2A, STK11, KRAS and TP53 (Centers for Disease et al., 2010). The second route of carcinogenesis is through receptor binding, nicotine and NNK may bind to neuronal nicotinic acetylcholine receptors (nAChRs), β-adrenergic receptors and the epidermal growth factor receptor (EGFR) family ERBB. The binding of cigarette smoke (CS) constituents to these receptors activates downstream kinases such as protein kinase C (PKC), protein kinase A (PKA), extracellular

signal-regulated kinases (ERK), and the most significant of all, protein kinase B (AKT). Originally nAChRs were thought to exist only in neuronal cells, but since then they have been discovered in lung tissues (Schuller & Orloff, 1998; Tarroni et al., 1992). The activation of nAChRs by nicotine and NNK in lung epithelial cells promoted properties such as proliferation, angiogenesis, cell survival and decreased contact inhibition, all properties of carcinogenesis (Hanahan & Weinberg, 2011; Schuller & Orloff, 1998; Tsurutani et al., 2005). B-adrenergic receptors are stimulated by NNK due to its similar structure to adrenaline (the natural ligand for the receptor), after binding it mediates the release of arachidonic acid which is then converted by COX-2 to prostaglandin E_2 thus promoting inflammation, proliferation and cell survival in cancer. The most significant influencer of signaling induced by CS is AKT, it controls multiple cellular mechanisms that promote proliferation and cell survival as well as tumour resistance to chemotherapy as shown by (Tsurutani et al., 2005) when they found that in human lung cancer cells the AKT-dependant proliferation was activated by nicotine and NNK binding to nAChRs.

1.2

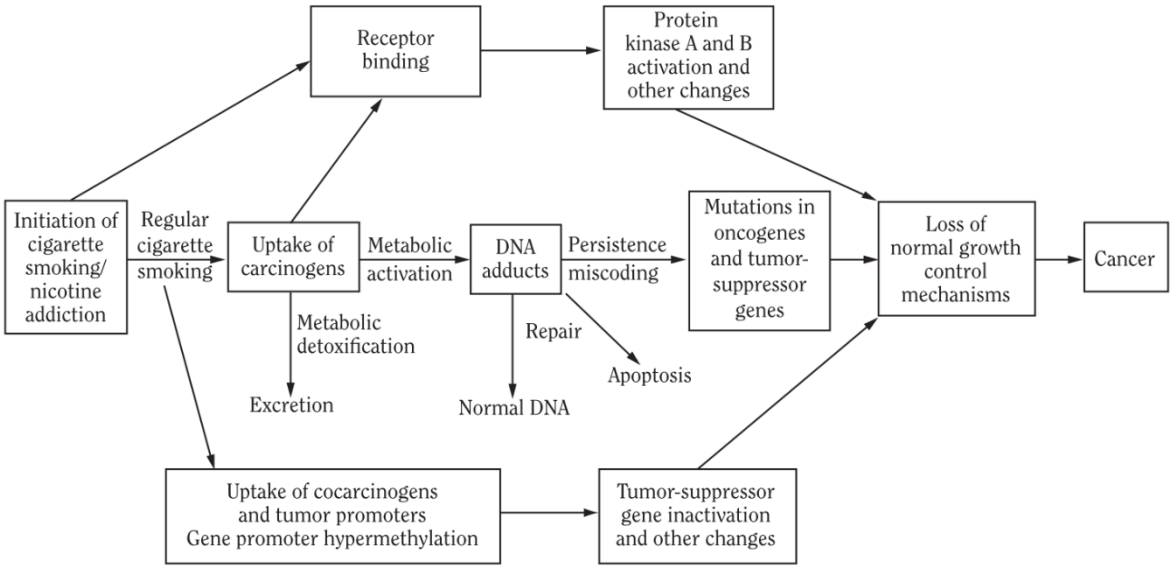

Figure 1.2. Routes of carcinogenesis via cigarette smoke consumption. Sourced from (Centers for Disease et al., 2010).

1.3. Respiratory disorders

Cigarette smoke (CS) causes multiple non-malignant respiratory diseases that may lead to malignancy, these diseases are not exclusive and may arise simultaneously. Emphysema, chronic bronchitis, and asthma are some of the major CS-induced respiratory diseases which the WHO estimates to cause 3 million deaths annually. Even though the lungs have ample defense mechanisms that combat injury caused by inhaling CS, these defenses are eventually overwhelmed by constant exposure. The primary mechanisms leading to respiratory disease formation are endothelial and epithelial injury, increased alveolar epithelial permeability through CS and oxidative stress. CS has a high oxidant potential with elevated concentrations of free radicals (Repine et al., 1997), protease-antiprotease imbalance and chronic inflammation; oxidative stress promotes gene expression of pro-inflammatory mediators via transcription factors, such as activator protein-1(AP-1) and nuclear factor-kappa-B (NF-κB) (Centers for Disease et al., 2010). The only way to avoid these respiratory diseases remains the cessation of smoking.

1.4. Cardiovascular disease

Cardiovascular disease (CVD) refers to conditions that affect the heart and blood vessels, these include coronary heart disease (CHD), hypertension, stroke, heart attack, aneurysms, and peripheral artery disease (PAD). The NHS estimates that 25,000 deaths per year can be attributed to smoking related CVD. The constituents of CS play many roles in promoting and increasing the risk of CVD (figure 1.3), nicotine for example is considered a sympathomimetic drug that releases catecholamines from neurons and the adrenal gland leading to elevated heart rate through continued stimulation of the sympathetic nervous system (Benowitz & Jacob, 1984), this elevated heart rate means increased myocardial contractility and blood pressure which eventually may cause stress to the heart and can be contributory to CVD. In a study performed on fifty-two smoking subjects they found that cigarette smoking acutely increases heart rate, brachial blood pressure and heart-femoral pulse wave velocity (Rhee et al., 2007). Chronically the association between cigarette smoking and hypertension has been thoroughly investigated but remains divisive. A study conducted on adolescents concluded that cigarette smoking reduces blood pressure (Alomari & Al-Sheyab, 2016). On the other hand, a more recent study performed longitudinally on more than five thousand participants concluded that cigarette smoking significantly increased the risk of hypertension (Gao et al., 2023). These inconsistencies in the findings were explained by (Leone, 2011) where initially nicotine mediated vasoconstriction induces an acute but transient elevation in blood pressure. Afterwards, a decrease in blood pressure is the result of the chronic depressant effects of nicotine. Concurrently, the arterial wall is being exposed to carbon monoxide which in the long run causes irreversible structural changes. This cycle eventually results in increased blood pressure. Carbon monoxide binds to hemoglobin, this decreases the amount of hemoglobin available for oxygen transport. In a long-term smoker this results in hypoxemia, in response red blood cells increase in mass as a mechanism to compensate for the oxygen needed by the body. Consequently, this leads

to increased blood viscosity which in turn increases the workload of the heart i.e. increased blood pressure and coagulation (Benowitz, 2003). Every inhalation distributes a high number of oxidizing chemicals, and metals such as lead, mercury, and cadmium; found elevated in serum of smokers and concentrated in the aortic wall (Abu-Hayyeh et al., 2001), into the blood stream. The oxidizing chemicals delivered cause endothelial dysfunction, inflammation, and platelet activation (Burke & Fitzgerald, 2003). The metals can catalyze the oxidation of cellular proteins causing structural damage and endothelial detachment from blood vessel walls (Bernhard et al., 2005) leading to inflammation, and possible clot formation.

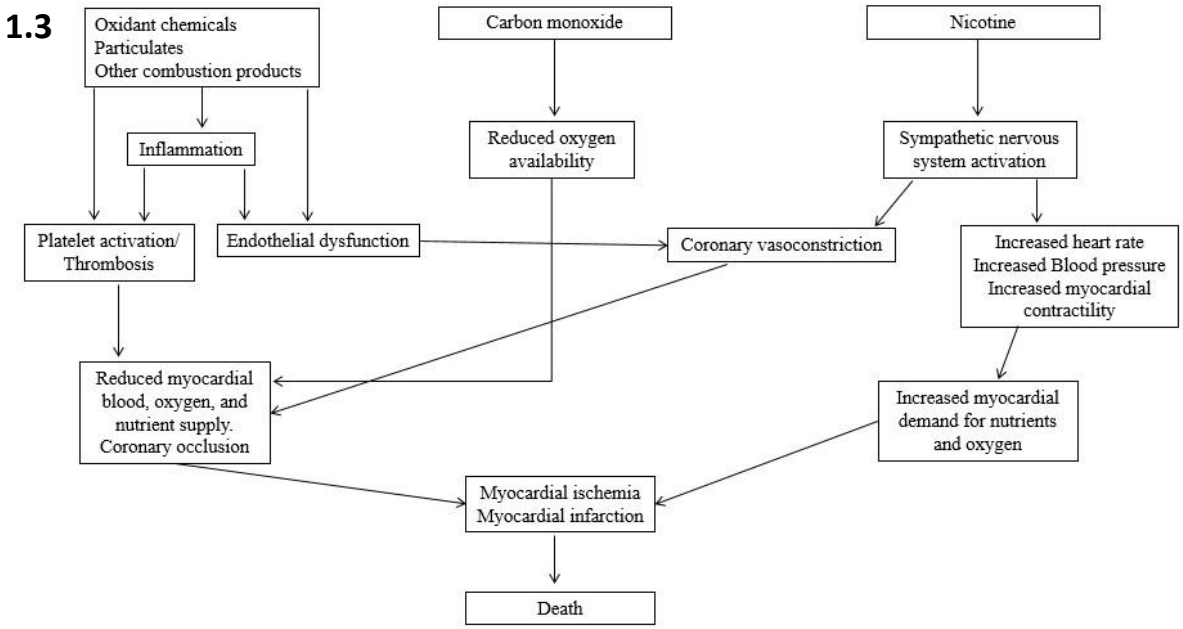

Figure 1.3. Overview of mechanisms by which CS causes a CDV event. Image modified from (Benowitz, 2003).

Muscles are not immune to the effects of smoking (Kok et al., 2012; Kumar & Kumar, 1998; Lee et al., 2007; Saito et al., 2012) reported that smokers showed decreased muscle strength to their non-smoking counterparts, this will be further explored later.

1.5. Muscle overview

Muscle, which accounts for approximately 50% of our body weight, can be defined as tissue with contractile capabilities, achieved with the aid of specialized components. This allows groups of muscle cells to perform multiple tasks, ranging from deliberate movements such as picking up a bottle of water, to more involuntary actions such as peristalsis. There are three forms of muscle tissue, smooth, skeletal, and cardiac, each of which has different structural properties that promote specific metabolic and mechanical functions. Cardiac muscle, as the name implies, is located exclusively in the heart, skeletal muscle is attached to the bones of the skeleton and smooth muscle can be found lining the interior of hollow organs (figure 1.4).

1.4

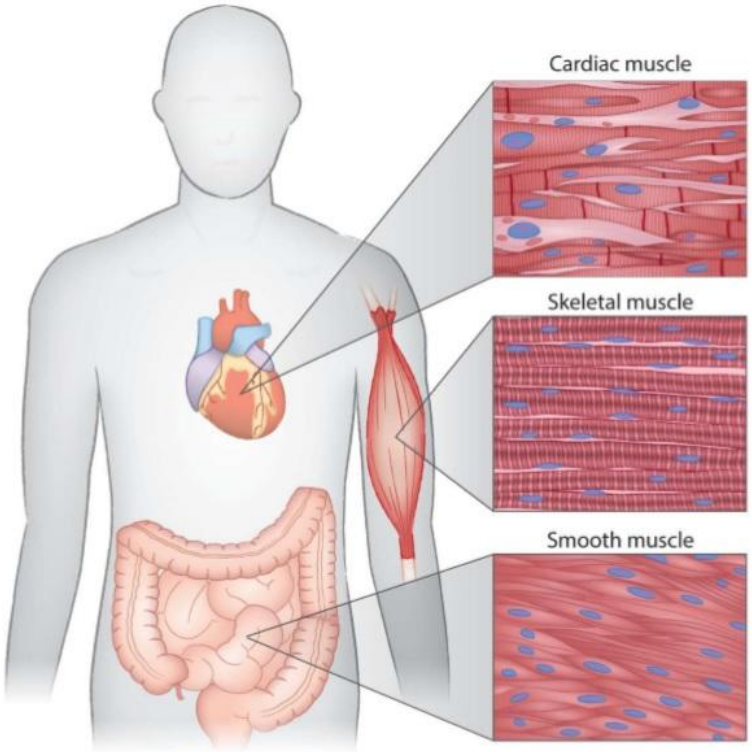

Figure 1.4. Location and structure of the three muscle types; cardiac, skeletal and smooth. Sourced from (McNamara & Sadayappan, 2018).

There are two ways to classify muscle tissue. They are either “striated or unstriated” and “voluntary or involuntary” (figure 1.5). The term “striation” reflects the light and dark

bands that are visible under light microscopy. Cardiac and skeletal muscle fall under this term, smooth muscle is thus termed “unstriated”. Furthermore, the terms “voluntary and involuntary” reflect conscious (somatic nervous system) and subconscious (autonomous nervous system) control of the muscle tissue.

1.5

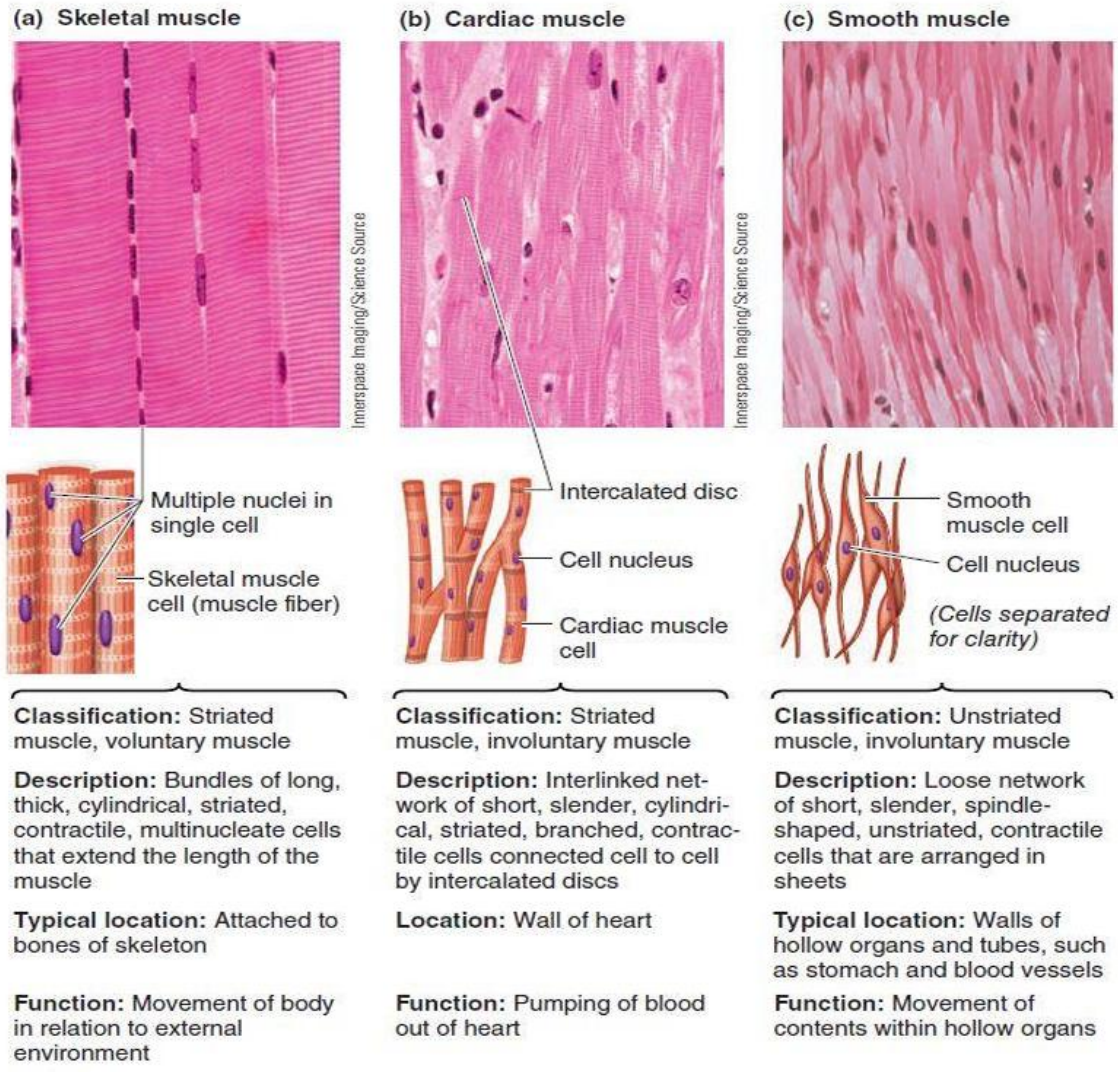

Figure 1.5. Characterization of different muscle types. Representative images of longitudinal sections taken from (A) skeletal muscle, (B) cardiac muscle and (C) smooth muscle. Sourced from (Sherwood, 2015).

1.5.1. Smooth muscle

Smooth muscle cells are spindle shaped, mononucleated with poorly developed sarcoplasmic reticulum and are usually arranged in sheets within the walls of hollow organs,

tubes, and blood vessels. The autonomous nervous system drives contractions through calcium ion influx, and even though smooth muscle tissue is unstriated (i.e. lacking in sarcomeric organization) they do however have "dense bodies" comprised of actin and myosin chains that facilitate contraction (Sherwood, 2015). A major difference between smooth and skeletal muscle is the initiation of contraction, smooth muscle instigates a chemical change to the thick filament (myosin) to initiate cross-bridge cycling whereas skeletal muscle induces a physical change to the thin filament. Smooth muscle contraction occurs when cytosolic Ca^{2+} binds to intracellular calmodulin, the resulting complex activates myosin light chain kinase, an enzyme, which in turn phosphorylates the myosin light chain allowing for cross bridge formation with actin and the cycling to begin (Sherwood, 2015). Some of the functions performed by smooth muscle include iris constriction, peristalsis in the bowels and vascular constriction.

1.5.2. Cardiac muscle

The heart, the life pump which beats over 3 billion times in a lifetime is made up of multiple cell types including endothelial cells, fibroblasts, vascular smooth muscle cells and myocytes. Each of these cells contribute to the function of the heart, however it is the myocyte which is the contractile unit of the heart. Cardiac muscle cells (cardiomyocytes) and skeletal muscle cells are similar with regards to striation (or sarcomeric organization) and fibre banding. However, cardiomyocytes are shorter in length, are usually mononucleated and are dense with both mitochondria and myoglobin. The branched fibres are linked at their ends by intercalated discs (figure 1.6) which allow the muscle cells to contract in a wave-like form (Sherwood, 2015). These synchronized contractions allow the heart to act as a pump, driving blood through systemic circulation. Intercalated discs have two structures that are vital for contraction, desmosomes, and gap junctions. Desmosomes act as safety-buckles, keeping muscle cells coupled at the ends and stopping them from

pulling apart during contraction. Gap junctions have multiple channels between neighboring cells that form intercellular pathways for swift conduction of action potential through the cells, resulting in the synchronized contraction of the heart (functional syncytia) (figure 1.6). This synchronized contraction begins with specialized cardiac muscle cells known as "pacemaker cells", which in turn react to signals from the autonomic nervous system and hormones to regulate blood pressure and heart rate (Betts, 2013).

1.6

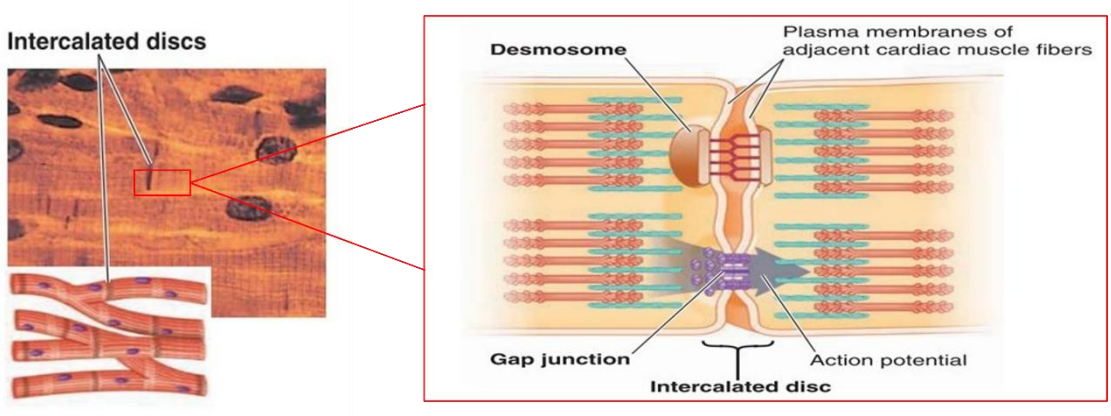

Figure 1.6. Branching cardiac muscle cells are linked by intercalated discs which have two types of membrane junctions. Desmosomes which hold adjacent cardiac muscles together, and gap junctions that allow swift transfer of action potential. Sourced from (Sherwood, 2015).

1.5.3. Skeletal muscle

Skeletal muscle contraction induces movement and generates force. It aids in the maintenance of posture and protection of the joints, bones, and internal organs. Skeletal muscle is controlled voluntarily via the somatic nervous system. Mechanically, it converts chemical energy to motion. Metabolically, it acts as storage for carbohydrates and amino acids which may later be utilized for activity (Frontera & Ochala, 2015) or donated to other organs for protein synthesis (Wolfe, 2006). Each muscle consists of connective tissue, blood vessels, nerves, and muscle fibres. The connective tissue encapsulates the muscle

maintaining integrity and structure when the muscle contracts. The outermost layer of connective tissue is called the epimysium, which acts as a barrier, keeping the muscle away from other organs allowing it freedom of movement. Within the muscle an arrangement of fibres, bundled together by the middle layer of connective tissue known as perimysium, is a fascicle. Within the fascicle every muscle fibre is enveloped by a thin layer of collagen and reticular fibre called the endomysium, this houses extracellular nutrients that support the muscle fibres (figure 1.7) (Betts, 2013).

1.7

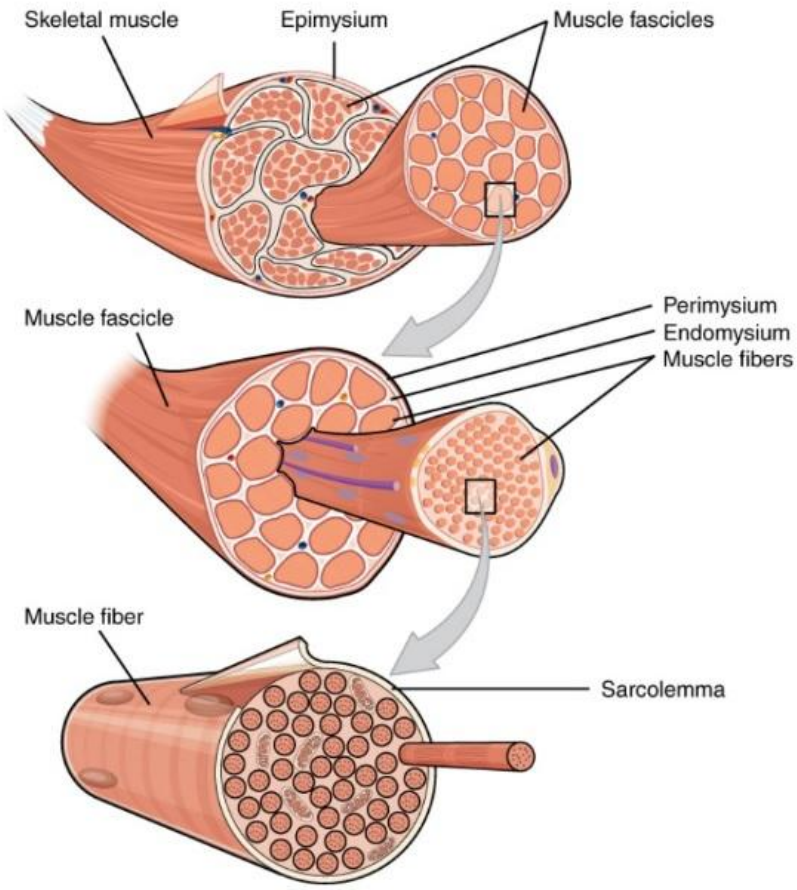

Figure 1.7. Muscle layout within the extracellular matrices. Sourced from (Betts, 2013).

Muscle fibres are long, cylindrical, dense with mitochondria and multinucleated, a result of myoblast fusion in early embryonic development. A high number of nuclei means multiple

copies of genes, which in succession means creation of large amounts of proteins and enzymes needed for contraction. These nuclei reside under the plasma membrane or "sarcolemma", the mitochondria and myofibrils within the cytoplasm or "sarcoplasm". The endoplasmic reticulum or "sarcoplasmic reticulum" is responsible for storage, release, and retrieval of calcium ions vital to contraction. The contractile unit of a muscle fibre resides within the myofibril and is called the Sarcomere; it houses an arrangement of thin and thick myofilaments that give skeletal muscle striated appearance (figure 1.8).

1.8

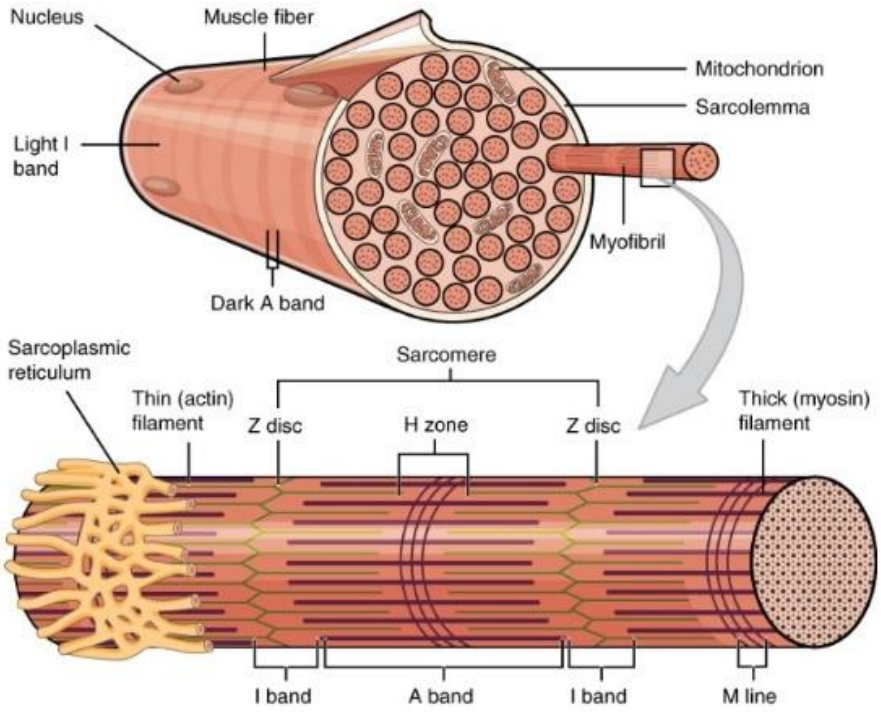

Figure 1.8. Arrangement of the thin and thick filaments of the sarcomere within a muscle fibre. Sourced from (Betts, 2013).

Sarcomere are packed within the myofibril, spanning the whole length of the muscle fibre. Each sarcomere is approximately 2 µm in length, the borders which anchor the thin filaments are called the Z-lines. The thin filament is comprised of actin, troponin, and tropomyosin. The thick filament, anchored in the middle of the sarcomere (M-line) by myomesin, is

comprised of myosin, it extends from the center of the sarcomere towards (but not all the way) to the Z-line (figure 1.9). Contraction of the muscle occurs when the filaments slide across one another (Betts, 2013; Lange et al., 2020).

1.9

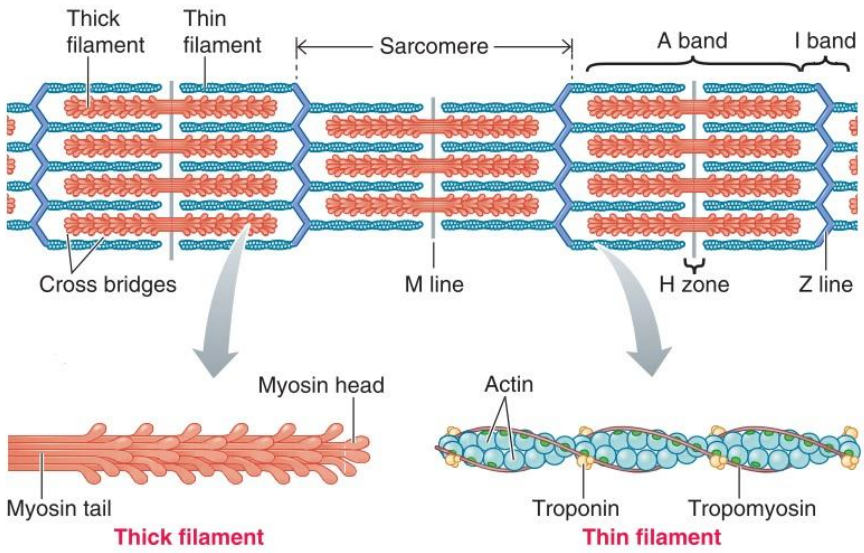

Figure 1.9. The sarcomere is comprised of thin and thick filaments organized to form cross bridges producing the sliding filament model observed in contraction. Sourced from (Sherwood, 2015).

Contraction of skeletal muscle starts at the neuromuscular junction (NMJ). This is where the motor neuron meets the muscle fibre. The axon terminal releases acetylcholine (ACh) which diffuses across the synaptic cleft and binds to ACh receptors on the motor endplate of the sarcolemma. This opens an ion channel on the receptor allowing positively charged ions to pass into the muscle fibre causing it to depolarize. The depolarization triggers voltage-gated sodium channels to open, firing the action potential along the sarcolemma, into the transverse tubules (T-tubules). These tubules run perpendicularly from the surface of the sarcolemma into the muscle fibre. As the action potential travels the T-tubules, it activates the dihydropyridine receptors, which in turn trigger ryanodine receptors on the lateral sacs of the sarcoplasmic reticulum releasing calcium ions (Ca^{2+}) into the cytosol (figure 1.10).

1.10

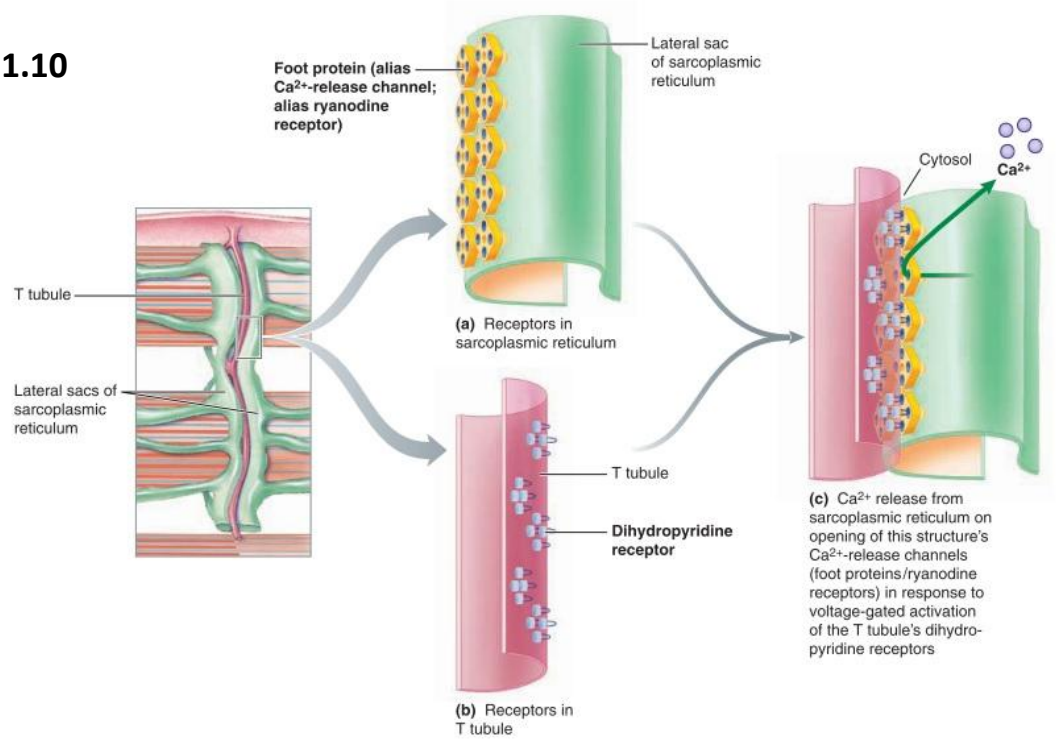

Figure 1.10. The action potential travels through the sarcolemma, down the T-tubules activating the dihydropyridine receptors, this triggers the release of Ca^{2+} through the ryanodine receptor into the cytosol. Sourced from (Sherwood, 2015).

Once released, Ca^{2+} binds to troponin (on the thin filament of the sarcomere), shifting tropomyosin uncovering the myosin binding sites on actin and initiating cross-bridging. The binding of myosin and actin triggers a power stroke pulling the thin filament inwards towards the center of the thick filament. The cross-bridges and power stroke, driven by adenosine-triphosphate (ATP), continues successively and in cycles (figure 1.11).

1.11

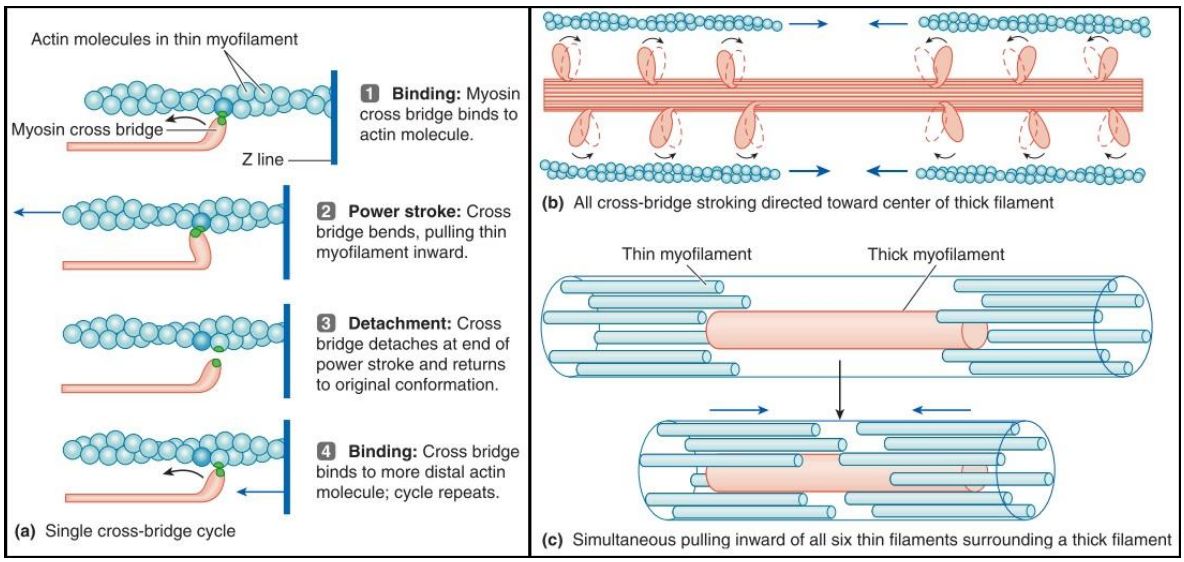

Figure 1.11. The cross-bridge activity and power stroke. Sourced from (Sherwood, 2015).

Each cycle of the cross-bridge to power stroke consumes ATP as the energy source. Myosin has an actin binding site and an ATPase binding site. This is responsible for the energized myosin state through splitting ATP to adenosine diphosphate (ADP) and inorganic phosphate (P_i). The crossbridge cycle starts when Ca^{2+} is released, allowing myosin to bind with actin forming a cross bridge. The contact produces a power stroke pulling the thin filament towards the centre. During the power stroke P_i is released and once its complete ADP is released. This permits the now empty myosin ATPase site to bind another ATP molecule. Once the ATP binds the cross bridge detaches, returning myosin to the unbent form and ready for the next cycle. The new ATP molecule is now split by myosin ATPase to give an "energized" crossbridge (figure 1.12). The cycles continue as long as Ca^{2+} is present in the cytosol.

1.12

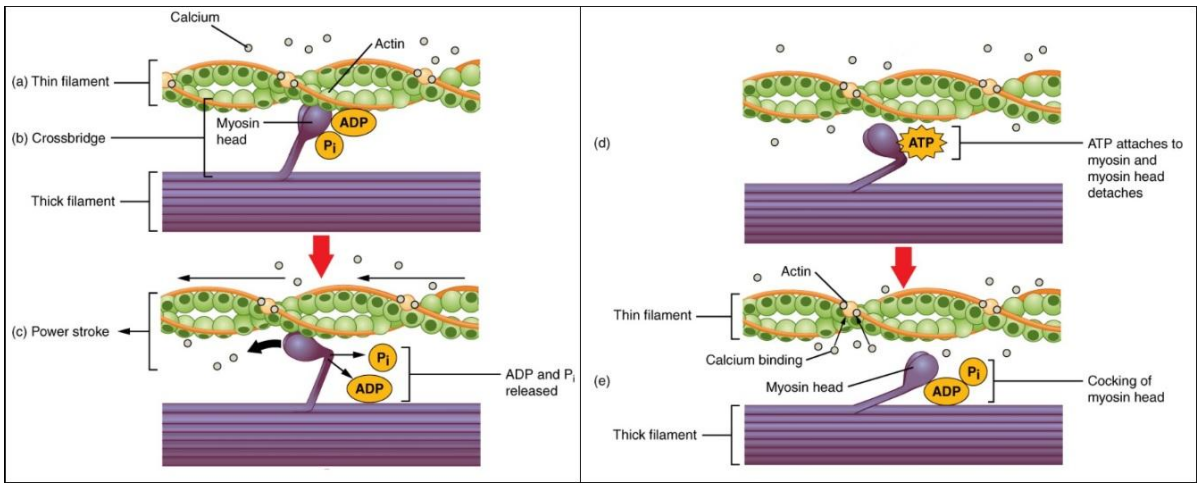

Figure 1.12. ATP drives crossbridge and power stroke. (A) presence of calcium allows myosin to bind actin forming a crossbridge (B), (C) a power stroke upon contact pulls the thin filament towards the center of the sarcomere releasing P_i in the process and ADP at the end, (D) the empty ATPase binding site recruits ATP detaching the crossbridge and "cocking" the myosin. (E) ATPase splits ATP into ADP and P_i, the cycle is now ready to be repeated. Sourced and modified from (Betts, 2013).

Skeletal muscle relaxation occurs when the electrical impulse stops, this allows Ca^{2+}-ATPase pumps in the sarcoplasmic reticulum to transfer Ca^{2+} from the cytosol back into the lateral sacs. The removal of Ca^{2+} from the cytosol allows troponin-tropomyosin to return to its blocking position on actin. Consequently, the cross-bridges can no longer form thus allowing the thin filament to slide back into its resting position relaxing the myofibre.

Due to high demand for ATP to continue activity, skeletal muscle has adopted three pathways to maintain supply: Creatine phosphate, oxidative phosphorylation, and glycolysis (Sherwood, 2015). Creatine phosphate is the first energy source used upon contraction from rest. It is rapidly hydrolyzed by donating a phosphate directly to ADP forming ATP and creatine, a process catalyzed by creatine kinase. At rest excess ATP is stored by transferring the energy phosphate back to creatine forming creatine phosphate and ADP (figure 1.13).

1.13

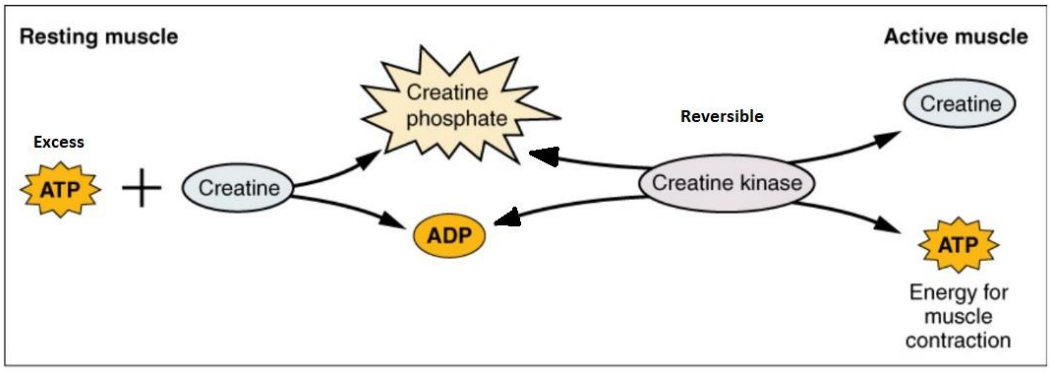

Figure 1.13. The creatine phosphate metabolic pathway first utilized at contraction from rest. Sourced and modified from (Betts, 2013).

For prolonged contractile activity, the muscle diverts energy production to either oxidative phosphorylation or glycolysis (figure 1.14).

1.14

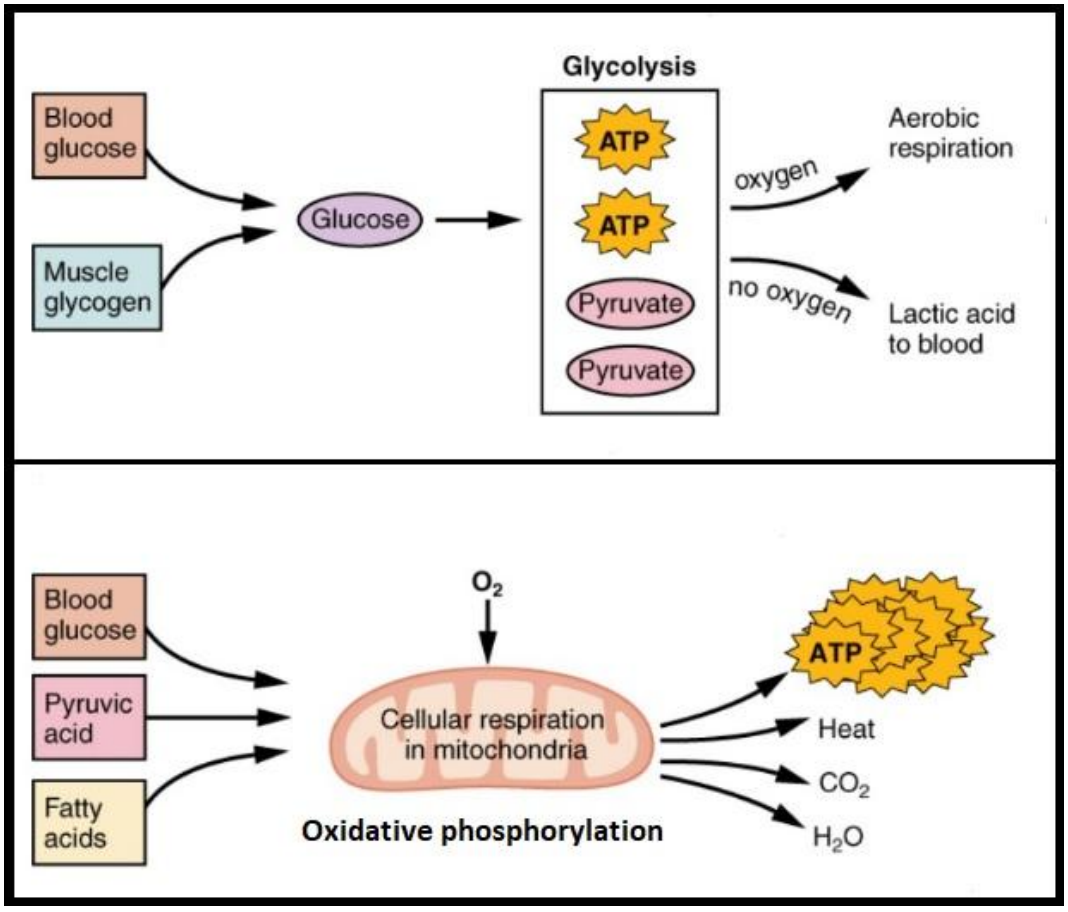

Figure 1.14. Glycolysis and oxidative phosphorylation are metabolic pathways used to generate energy during prolonged muscle activity. Sourced and modified from (Betts, 2013).

Oxidative phosphorylation occurs within the mitochondria of muscle cells if a sufficient quantity of oxygen is present. This pathway is powered by glucose and fatty acids from the blood stream to generate a high yield of ATP molecules per molecule processed, in a relatively slow process. Hence, due to physiological limitations, if there is a lack of oxygen or energy supply to the muscle, the glycolysis pathway is activated. Glucose from the blood stream or glycogen stored in the muscle are converted into pyruvate and ATP. The pyruvate may further be utilized in oxidative phosphorylation when oxygen is present, however, in an anaerobic environment it is converted to lactate (Sherwood, 2015).

1.5.4. Types of skeletal muscle fibre.

Skeletal muscle fibres can be classified into many specialized types that have variations in contractility, metabolism and morphology. For example, skeletal muscles involved in maintaining posture need to sustain tension for prolonged durations while resisting fatigue. Whereas muscles responsible for eyelid and eye movement require fast contraction. These variations are the outcome of the diverse expression of contractile protein isoforms in muscle cells as well as metabolic influences that control the supply and utilization of oxygen. Skeletal muscle fibres can be classified depending on their main pathway for ATP synthesis; oxidative phosphorylation or glycolysis, and on the maximum rate of contraction; fast or slow twitch fibres (Mescher, 2023). Fast-twitch fibres have a high myosin ATPase activity, while the slow-twitch skeletal muscle fibres have lower myosin ATPase activity (Sherwood, 2015). Multiple combinations of these isoforms can be found within a single fibre, but ultimately the most common isoform determines the functional characteristics such as resilience to fatigue and contraction speed (Graziotti et al., 2001).

There are three major types of skeletal muscle fibres (Mescher, 2023):

I. Slow oxidative (type I) fibres are adapted for slower contractions for prolonged periods without fatigue. They have a high number of mitochondria, an increased amount of myoglobin and surrounding capillaries.

II. Fast glycolytic (type IIb) fibres are adapted for short, rapid contractions. They have a lower number of mitochondria and capillaries than type I fibres. Relying mostly on anaerobic metabolism of glucose in stored glycogen results in rapid fatigue due to accumulation of lactic acid from glycolysis.

III. Fast oxidative-glycolytic (type IIa) fibres have histological and physiological features that are intermediary to the other two.

The characteristics of skeletal muscle fibre types are summarized in table 1.1.

	Slow, Oxidative Fibers (Type I)	Fast, Oxidative-Glycolytic Fibers (Type IIa)	Fast, Glycolytic Fibers (Type IIb)
Mitochondria	Numerous	Numerous	Sparse
Capillaries	Numerous	Numerous	Sparse
Fiber diameter	Small	Intermediate	Large
Size of motor unit	Small	Intermediate	Large
Myoglobin content	High (red fibers)	High (red fibers)	Low (white fibers)
Glycogen content	Low	Intermediate	High
Major source of ATP	Oxidative phosphorylation	Oxidative phosphorylation	Anaerobic glycolysis
Glycolytic enzyme activity	Low	Intermediate	High
Rate of fatigue	Slow	Intermediate	Fast
Myosin-ATPase activity	Low	High	High
Speed of contraction	Slow	Fast	Fast
Typical major locations	Postural muscles of back	Major muscles of legs	Extraocular muscles

Table 1.1. The characteristics of different skeletal muscle fibres according to twitch speed and ATP synthesis. Sourced from (Mescher, 2023)

1.5.5. Skeletal muscle regeneration.

Muscle damage is inevitable in a person's lifetime, it may occur due to disease, such as Duchenne muscular dystrophy, stress from excessive exercise or trauma such as stab or laceration and chemical interactions from sources that may be medicinal or recreational. Some features of muscle damage include centrally located nuclei, distortion of contractile components, presence of necrotic fibres, inflammatory cells and phagocytosis are visible. To combat damage, muscle cells have varying capabilities for regeneration, cardiac muscle has very poor ability to regenerate, skeletal and smooth muscle show sturdy regeneration (Mescher, 2023; Sherwood, 2015). Keeping this in mind, if the damage is however extensive and beyond repair capabilities, then fibrosis and scar tissue is formed hindering muscle function and contractile efficacy. Skeletal muscle regeneration occurs in five inter-dependent stages (figure 1.15), beginning with degeneration then inflammation/regeneration followed by remodeling of the extracellular matrix and finally maturation/innervation.

1.15

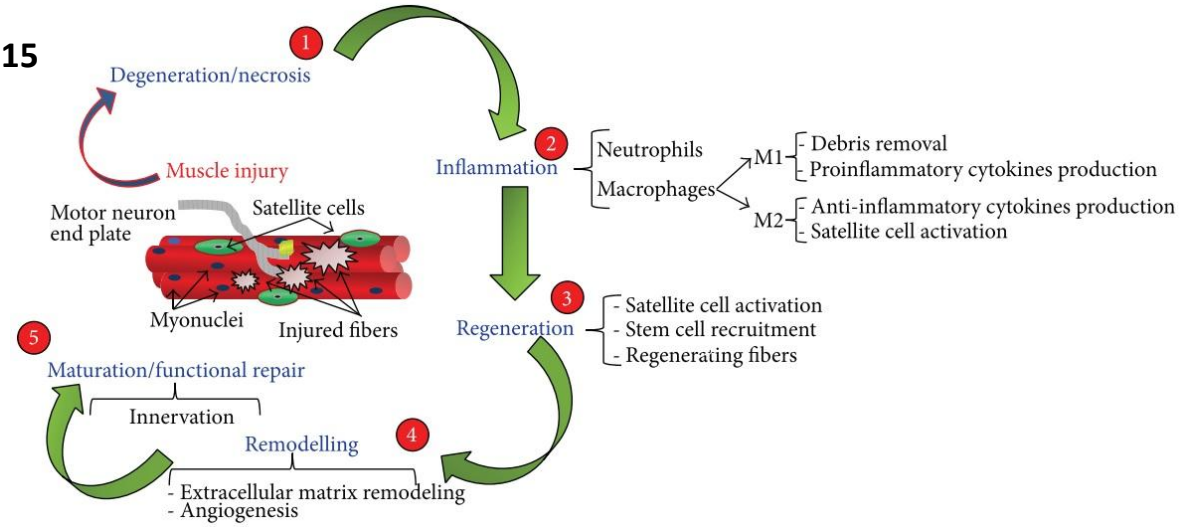

Figure 1.15. Skeletal muscle regeneration cycle. (1) Degeneration and necrosis of damaged fibres. (2) Inflammation, neutrophil and M1/M2 macrophage recruitment. (3) Regeneration of damage by satellite cell activation, proliferation, differentiation. (4) Remodelling of extracellular matrix and angiogenesis. (5) functional repair and innervation of myofibres. Sourced from (Musarò, 2014).

During degeneration, a necrosis cascade is seen. The sarcolemma is disrupted, increasing permeability of the myofibre leading to the breakdown and discharge of intracellular materials. When the intracellular components are released into the extracellular space they act as signals, known as damage-associated molecular patterns (DAMPs), that trigger an inflammatory response (Forcina et al., 2020). Neutrophils and macrophages infiltrate the affected tissue. Their activity results in the secretion of a variety of cytokines and growth factors that regulate tissue regeneration response and promote stem cell activation. Neutrophils recruited to the damage site release numerous proinflammatory molecules that include cytokines (TNF-α, IL-1, IL-6, IL-8 and ADAM8) and growth factors (IGF-I, VEGF, TGF-β1) this creates an environment that attracts other inflammatory cells that include monocytes and macrophages. Macrophage activity is split into two stages; **M1** which is pro-inflammatory and responsible for debris removal via phagocytosis and secretion of molecules to stimulate myoblast proliferation from satellite cells. **M2** is non-phagocytic, anti-inflammatory macrophage invasion which stops myoblast proliferation, promotes differentiation, fusion, and growth of myofibres (Sass et al., 2018). Regeneration is dictated by satellite cells (SC), which reside between the sarcolemma and basal lamina, they proliferate and generate myoblasts that will either fuse with damaged fibres repairing them, or fuse to each other forming new fibres (Gayraud-Morel et al., 2009). This process of regeneration and renewal results in expression, up-regulation, and down-regulation of multiple molecular markers (figure 1.16), most notable are Pax7, CD34, Myf5, MyoD and Myogenin. The expression of Pax7 and CD34 in quiescent SC is up-regulated as they activate and proliferate but once differentiation begins Pax7 is down-regulated and CD34 is no longer expressed. MyoD and Myf5 are expressed once SC proliferate, upon differentiation and fusion into myotubes Myf5 is downregulated and Myogenin is expressed (Beauchamp et al., 2000; Forcina et al., 2020; Musarò, 2014; Scharner & Zammit, 2011).

1.16

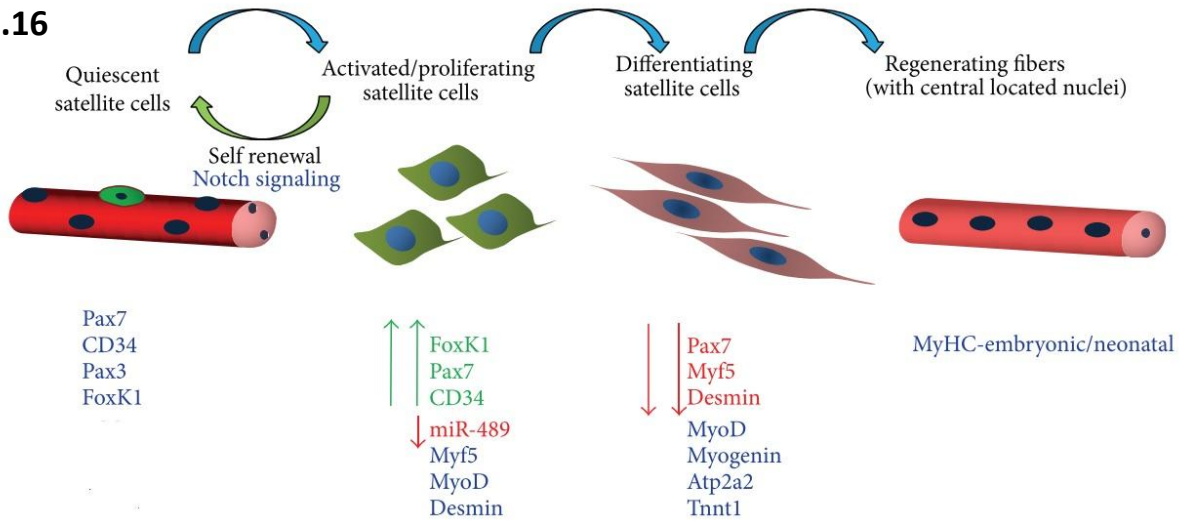

Figure 1.16. During regeneration, satellite cells activate, proliferate, differentiate and fuse. Associated with each stage are several markers that are either expressed, up regulated or down regulated. (Blue represents expression, green is up regulation, red is down regulation). Sourced and modified from (Musarò, 2014).

The remodeling process involves angiogenesis and the activation of the extracellular matrix (ECM) resulting in production of fibrotic framework for support of the newly differentiated muscle fibres and innervating them through establishing the neuromuscular junctions (NMJs). The final step of repair is the innervation of muscle fibres before returning to functionality (Lluri et al., 2006).

1.5.6. Effect of smoking on muscle.

Cigarette smoke (CS) has a long history of causing multiple diseases, all of them life threatening (Centers for Disease et al., 2010). The chemicals enter our blood stream causing a chain reaction in the entire body. Extensive studies have been performed to link CS to cancer, COPD, CVD as well as how muscle is affected, however, not much is understood about the mechanism of how it affects skeletal muscle. A study was performed on 4249 Japanese men (Saito et al., 2012). Aged between 20 to 79 years they underwent an annual checkup over a period of ten years. During these annual investigations the muscle strength, exercise habits and smoking habits were evaluated. Of the subjects that took part 1618 were

current smokers and 2631 were nonsmokers. The study concluded that smokers had diminished grip strength when compared to the non-smokers in the study cohort. However, there were some limitations to this study. Only men were examined thus the results cannot be generalized to women. Additionally, former smokers were not included removing the possibility to complete the classification profile of (i) smokers, (ii) past smokers and (iii) nonsmokers. Furthermore, no biological mechanisms that are detrimental to muscle strength such as hormonal changes or nutritional deficits were accounted for.

In a more comprehensive study performed longitudinally over a period of 15 years on both men and women aimed to assess whether smoking is related to muscle strength and if lifestyle choices influence this relation (Kok et al., 2012). Kok et al, tested knee muscle strength using an isokinetic strength test. Measurements of the subjects were taken at the ages of 21, 27, 32, and 36. During the investigation, smoking habits and lifestyle covariates such as daily physical activity and diet were evaluated using interviews and questionnaires. Subsequently they found that smoking 100g of tobacco a week resulted in diminished strength in both men and women, furthermore this effect was mostly independent of variations in lifestyle choices. This study agrees with the findings of Saito et al (Saito et al., 2012) and builds upon it with the inclusion of diet and lifestyle choices, however it has its limitations as well. In the last timepoint of the study the device used to measure the knee muscle strength was different to the previous examinations. Even though the device was standardized this still could introduce a form of measurement bias. Questionnaires are a valid form of data collection but still do not exclude the possibility of recall bias. Additionally, hormonal factors were not accounted for and not tested limiting the biological insight. Finally, the age range of the subjects was limited to young adults thus missing out on the effects that may occur in an older population.

The decrease in strength in the previous studies could possibly be attributed to CS induced muscle atrophy. A previous study (Montes de Oca et al., 2008) performed on 34 subjects

investigated the effect of smoking on skeletal muscle. By comparing fourteen healthy smokers with twenty nonsmokers, they found that smokers exhibited atrophy in the oxidative fibres of the *Vastus Lateralis*. Similarly, Petersen et al, (Petersen et al., 2007) linked CS to increased gene expression of muscle atrophy F-box (MAFbx/atrogin-1) and myostatin. Both play a prominent role in muscle catabolism. MAFbx/atrogin-1 is an E3 ubiquitin ligase involved in protein degradation via the ubiquitin proteasome system (UPS) (Foletta et al., 2011) and myostatin is a known inhibitor of muscle growth and differentiation (Carnac et al., 2006). Another study (Liu et al., 2011) performed *in-vitro* and *in-vivo* experiments to determine if CS induced skeletal muscle atrophy. They exposed rats to cigarette smoke and L6 myotubes were incubated with cigarette smoke extract. Then using western blotting and quantitative real-time polymerase chain reaction (qPCR) they found that ubiquitin-specific-protease-19 (USP-19) was indeed upregulated and myosin heavy chain (MYH) downregulated, this was coupled with inhibition of myogenic differentiation via p38, ERK, and mitogen-activated protein kinases (MAPK).

1.5.7. Effect of vaping on muscle.

In the past decade there has been an increase in use of electronic cigarettes otherwise known as vape (Pepper & Brewer, 2014). The popularity of vaping has led to more than twenty million users worldwide due to the belief that it is safe (Theron et al., 2019). It has been reported that the presence of chemicals like formaldehyde and acrolein is lower than traditional cigarettes (Goniewicz et al., 2014; Margham et al., 2016; Sleiman et al., 2016), however, these chemicals are still present in vaping. Acute exogenous lipoid pneumonia, diffuse alveolar hemorrhage and many other lung related injuries have been reported after the use of vape (Theron et al., 2019). Systemically it is believed to cause an inflammatory response. A study performed on human alveolar macrophages (Scott et al., 2018) found that vaping caused inflammation and inhibited phagocytosis. Vaping may be considered a new trend, where scientific findings are still emerging and the mechanism of its systemic effect is yet to be fully understood, especially on muscle.

1.6. Hypothesis

Hypothesis 1.

Cigarette smoke induced muscular dysfunction is still not fully understood, we postulate that using *in-vitro* and *in-vivo* experiments we will see delayed muscle regeneration, then using gene expression analysis and the bio-informatic approach known as "Connectivity-mapping" (Lamb et al., 2006) we will identify already clinically approved medications for repurposing as possible therapies to promote muscle function in smokers.

Hypothesis 2.

Vaping is a recent trend marketed as the safe alternative to cigarette smoking. However, many of the constituents remain the same as those found in cigarettes. We hypothesize that the effect of vape smoke will be similar to that of cigarette smoke in both in vitro and in vivo experiments.

1.7. Objectives

- To determine whether CSM and VM have a direct effect on myoblast viability, proliferation, migration, fusion and atrophy.
- Use genetic expression analysis and bioinformatic approaches to determine clinically approved compounds that can be repurposed as therapeutics to counter the effects of CSM on myoblasts.
- To determine whether CSM and VM diminish regenerative capabilities of skeletal muscle following acute injury in mouse models.

Chapter 2: Methods

2.1. Cell culture

The C_2C_{12} mouse muscle derived myoblasts were cultured in growth media (GM) comprised of high glucose Dulbecco's modified eagles' medium (DMEM) (Gibco) supplemented with 10% (v/v) heat-inactivated foetal bovine serum (FBS) (Gibco) and 1% (v/v) penicillin/streptomycin (Gibco), at 37^o C in a humidified incubator with 5% CO_2.

The AB1190, AB1167 and AB678 human muscle derived myoblasts were cultured in growth media comprised of skeletal muscle cell growth medium (SMGM) (PromoCell) with supplement mix (PromoCell) and 1% (v/v) Gentamicin (Gibco), at 37^o C in a humidified incubator with 5% CO_2.

To differentiate the myoblasts (all cell lines), cells were allowed to reach 85-95% confluence then, the relative growth media was replaced with differentiation media (DM) (high glucose DMEM (Gibco) supplemented with 5% (v/v) heat-inactivated horse serum and 1% (v/v) penicillin/streptomycin).

The IMR90 cell line was cultured in minimum essential medium (MEM) (Gibco) with 10% (v/v) FBS (Gibco), 1% (v/v) penicillin/streptomycin (Gibco) and 1% (v/v) 100mM sodium pyruvate. Dr. Anand Rai from Micregen Ltd. conducted the maintenance and culture of the IMR90 cells.

2.2. Mice maintenance and model

All experiments conducted on the mice were performed in accordance with the Animals (Scientific Procedures) Act 1986 (UK). Male C57BL/6J mice (10 weeks old) were from Charles Rivers, Harlow (UK) and housed in the Biological Resource Unit at the University of Reading. Four to five mice were kept per cage under standard environmental conditions (12h light/dark cycles and a temperature of 20/22°C) with food and water provided ad libitum.

2.3. Conditioned media preparation

2.3.1. Cigarette smoke Conditioned media

Filtered 1R6F research cigarettes, purchased from the Centre for Tobacco Reference Products at the University of Kentucky (Kentucky, USA) were connected to a 60ml syringe with rubber tubing. After a cigarette was lit, air was withdrawn by fully retracting the plunger in a process that lasted on average eight seconds. The withdrawn smoke was then bubbled through 10 ml of phosphate buffered saline (PBS); every "exhalation" would last an average of 20 seconds. The process was repeated until the cigarette was fully consumed a process that would require on average nine draws (figure 2.1). The absorbance (optical density (OD)) of the smoke bubbled PBS was measured at 220 nm and recorded. Thereafter dilutions were made in PBS to investigate various concentrations of cigarette smoke conditioned media (CSM), however, the final working dilution was a 1:10 into either growth (GM) or differentiation media (DM) depending on the requirements of the experiment.

To prepare the cigarette smoke conditioned media (CSM) that was used for the in-vivo experiments, a single cigarette was bubbled through 10 mL of PBS producing an optical density of 1.8 at 220 nm. The CSM was filtered using 0.22 μm filter (Merck) then injected in the mice intraperitoneally.

2.1

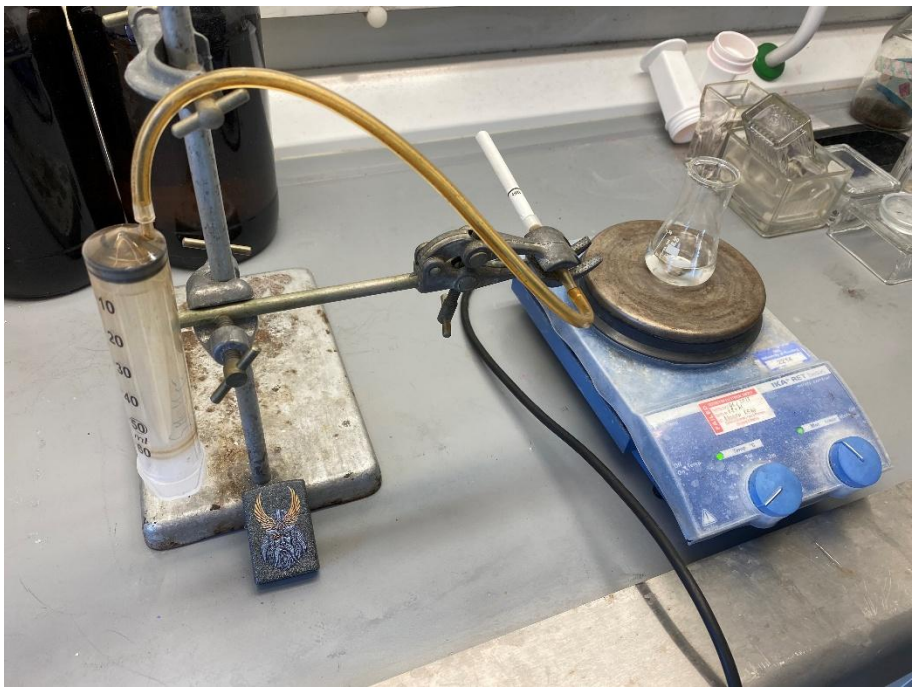

Figure 2.1. Setup used to extract cigarette smoke media.

2.3.2. Electronic cigarette conditioned media

The electronic cigarette "PockeX" used to produce the vape conditioned media (VM), was purchased from Aspire Electronic Cigarettes (UK) LTD and has a 0.6 Ω atomizer (replaced after five preparations) with the power pre-set to run between 18-23 watts. An E-liquid; Menthol 3 mg nicotine made by "VS Fifty Fifty", purchased commercially from an online retailer was used for all VM preparations. The device was connected to a 60 ml syringe using rubber tubing. The aerosol was withdrawn the full length of the syringe at an average of eight seconds. The smoke was then bubbled through 10 ml PBS at an average of 20 seconds. The "bubbling" would end when the absorbance reached at least 1.0 OD at 220 nm, this was recorded, and the subsequent dilutions were made in PBS, however, the final working dilution was a 1:10 into GM or DM depending on the requirements of the experiment.

To prepare the vape conditioned media that was used for the in-vivo experiments the extract was bubbled through 10 mL of PBS until an optical density of 1.0 at 220 nm was reached. The VM was filtered using 0.22 µm filter (Merck) then injected in the mice intraperitoneally.

2.4. Viability assay (MTS)

The CellTiter96® AQ_{ueous} one solution cell proliferation assay kit (Promega) was used to assess the effect of CSM and VM on myoblast viability. The MTS assay is a colorimetric method of determining the number of viable cells, the solution contains a tetrazolium compound which is reduced to a coloured formazan compound by dehydrogenase enzymes in metabolically active cells. In concordance with the supplier protocol, 10'000 cells per well were seeded into a 96-well plate and allowed to adhere overnight, a well omitting cells was kept for each condition of treatment as a blank to insure there is no interference with the MTS reagent (Promega). The cells were exposed to different concentrations of the conditioned media for 24 h (10 µl of CM with 90 µl of GM per well), then 20 µl of the MTS reagent (Promega) was added and incubated for 4 hours at 37° C. Afterwards, the absorbance was recorded at 490 nm using a plate reader.

2.5. Coverslip etching

The etching process provides a rough surface on which the cells can adhere. The coverslips were first soaked in absolute ethanol (Sigma) for 15 minutes, then placed in 2.5 M HCl (Fisher Scientific) for 30 minutes. Coverslips were then washed in sterile water for three consecutive times 5 minutes each, followed by 5 minutes in absolute ethanol. The coverslips were then air dried and placed inside a biological hood to be sterilised by exposure to UV light for 2 hours at least.

2.6. Fusion assay

Myoblast fusion analysis was performed to assess the effect of our conditioned media on myogenic differentiation. Initially, etched coverslips were placed in the wells of a 12-well plate before seeding $4.5x10^5$ cells per well. The myoblasts were allowed to reach 85-95% confluence before the media was changed to differentiation medium with the addition of various concentrations of the conditioned media (CSM/VM). The cells were allowed to

differentiate at 37° C and 5% CO_2 until the characteristic elongated morphology of the myotubes in the control was identified with a light microscope, this was approximately 96-120 hours for C_2C_{12} and 72-96 hours for the human cell lines. The myotubes were then fixed using 2% (w/v) paraformaldehyde (PFA) (Fisher Scientific) in PBS followed by immunostaining and imaging with an epifluorescence microscope (Zeiss AxioImager) with Axiovision SE64 Rel. 4.9.1 software installed. Fusion was judged to have occurred when a minimum of three nuclei were seen in a myosin-positive myotube. The fusion index (FI) was used as a parameter of analysis and was calculated as the percentage of nuclei within myotubes compared to the total number of nuclei in a field of view.

2.7. Atrophy assay

To investigate the effect of the conditioned media (CSM/VM) on muscle atrophy, $4.5x10^5$ cells were seeded on etched coverslips within a 12 well plate. The myoblasts were allowed to reach at least 85% confluence before the growth media (GM) [DMEM, 10% (v/v) FBS and 1% (v/v) penicillin-streptomycin for C_2C_{12} or SMGM with supplement mix and 1% (v/v) gentamycin for AB1190] was changed to differentiation media (DM) [DMEM, 5% (v/v) FBS and 1% (v/v) penicillin-streptomycin] inducing differentiation. The cells were cultured at 37° C and 5% CO_2 until the characteristic elongated morphology of the myotubes was seen, this was approximately 96-120 hours for C_2C_{12} and 72-96 hours for the human cell lines. Subsequently the DM was replaced with DM containing the various concentrations of conditioned media (CSM/VM) along with fresh DM for the control. The cells were then cultured for a further 24 h before being fixed in 2% (w/v) PFA followed by immunostaining and imaging with an epifluorescence microscope (Zeiss AxioImager) with Axiovision SE64 Rel. 4.9.1 software installed. ImageJ was used to measure the mean area of the myotubes as the parameter to assess atrophy.

2.8. Cell migration

2.8.1. Individual cell tracking

The myoblasts were seeded at low confluence (3000 per well in a 12-well plate) and allowed to adhere overnight. The next day, prior to the start of timelapse, the environmental chamber was turned on and allowed to equilibrate to 37º C and 5% CO_2. Next, the myoblasts were exposed to different concentrations of the conditioned media (CSM/VM), tracked for 24 h and cell position captured using a timelapse (Nikon TIE) microscope at a rate of one frame taken every 10 minutes with a 10X objective (NIS-elements AR software). Single cell tracking was performed on ImageJ using the MTrackJ plugin. Selection of cells was based on them being isolated at the beginning of the assessment and must remain in the field of view throughout the recoding period. A minimum of five fields of view were taken per well, with each condition having 3 wells at least.

2.8.2. Scratch assay

To assess migration using the scratch assay 40,000 myoblasts were seeded per well in a 24-well plate. They were allowed to adhere overnight at 37º C and 5% CO_2 before a scratch was made using a sterile 10µL pipette tip across the middle of the well. The media was removed, and the cells were gently washed with PBS to remove any debris, then fresh growth media (GM) including the various concentrations of conditioned media (CSM/VM) were added. The plate was transferred to an environmental chamber at 37º C with 5% CO_2 and imaged using a timelapse (Nikon TIE) microscope for 24 h at a rate of one frame every 10 minutes with a 10X objective (NIS-elements AR software). Myoblasts were tracked Using ImageJ, and when the first cells met from opposite sides the timepoint was taken as the migration parameter.

2.9. Focal adhesion assessment

To investigate the effect of conditioned media (CSM/VM) on focal adhesions, 5,000 cells were seeded on etched coverslips within the wells of a 12-well plate. The cells were allowed to adhere overnight at 37° C and 5% CO_2 then exposed to the different concentrations of CSM or VM for at least 4 h. The myoblasts were then fixed with 2% (w/v) PFA for 20 min followed by two washes in PBS for 1 minute each. The cell membranes were then disrupted using permeabilization buffer at room temperature for 15 min, followed by three washes in PBS for 5 min. Blocking of non-specific binding sites was performed using 10% (v/v) goat serum in PBS for 30 min. To stain for focal adhesions the cells were incubated with anti-paxillin antibody (Y113) (1:200 dilution; Abcam) overnight at 4° C then washed five times with PBS for 3 minutes. The secondary antibody (Alexaflour 488 goat anti-rabbit, 1:200; Invitrogen) was added and kept for 1 h in the dark at room temperature. This was then followed by two washes in PBS for 5 minutes, subsequently incubating the slides using rhodamine conjugated phalloidin (ThermoFisher) for 20 minutes at room temperature to stain for actin, and finally two more 5-minute washes in PBS before DAPI was added. The slides were then imaged (Nikon A1R confocal microscope) at a 100X magnification and analysed using ImageJ. Expression of paxillin that colocalised to phalloidin was judged as the presence of focal adhesions and the presence of stress fibres was judged when they met the size parameters reported previously (Horzum et al., 2014).

Dr. Bokai Guo from the University of Reading conducted the staining and imaging of the focal adhesion slides.

2.10. Cellular senescence

Prior to staining, in a 12-well plate, 5000 cells were seeded per well and allowed to adhere overnight, the next day they were exposed to different concentrations of CSM or VM for at least 48 hours at 37° C and 5% CO_2. Thereafter the media was aspirated and replaced with

fresh growth media (GM) for 24 hours. To assess the possibility of the conditioned media inducing senescence, the Abcam senescence detection kit (ab65351) was utilised. The staining process and all solutions were prepared according to the manufacturers protocol prior to application on samples. In brief, the media was aspirated from the wells, the cells were washed once with PBS then fixed for 15 minutes at room temperature with the fixative solution provided in the kit. Two 5-minute washes with PBS ensued, followed by the addition of the senescence staining solution into each well and incubation at 37° C overnight. Afterwards, the wells were washed twice with PBS and images were taken on a Zeiss A1 Inverted epifluorescent microscope and analysis was carried out using ImageJ by counting the percentage of senescent cells (stained blue).

Dr. Anand Rai from Micregen Ltd. conducted the maintenance, exposure, fixation and staining of the IMR90 cells.

2.11. Cellular and mitochondrial analysis

Seven thousand cells were seeded per well in a black 96-well plate (Gernier, G655090) and allowed to adhere overnight at 37° C and 5% CO_2. The following day the cells were exposed to various concentrations of the conditioned media (CSM/VM) and allowed to incubate for 3 hours. Meanwhile, the staining dye mix was prepared in the growth media without any supplement (serum free) (only antibiotics), Calcein green AM (Invitrogen) which labels the cytoplasm of viable cells was used at a final concentration of 1 µM and to label the mitochondria a final concentration of 0.2 µM Mitotracker Orange (Invitrogen). After the 3-hour exposure to CSM or VM was complete, the media was aspirated, and the cells were twice washed in PBS for 5 minutes, then for 30 minutes the cells were incubated with the staining solution in 37° C with 5% CO_2. Subsequently, the cells were fixed with 2% PFA (Fisher scientific) for 15 minutes followed by two washes of PBS for 3 minutes. The nuclei were stained with DAPI (Fisher scientific), a 1:10000 dilution in PBS and left for 15 minutes

at room temperature, two more washes of PBS followed before finally 100 µl of 0.1% (w/v) sodium azide (Fluka) in PBS was added to each well. For image acquisition the plate was transferred to the Operetta® high content imaging system (PerkinElmer) under cell culture environmental conditions. At a 40X magnification, 10 to 20 images were taken per well and analysed using the Oparetta® software (PerkinElmer). The parameters interrogated were number of cells, nuclear area, nuclear roundness, nuclear staining intensity, cell area, cell roundness, cytoplasmic staining intensity, Mitotracker intensity and Mitotracker area, results were taken as mean per well.

Mustafa Al Asady from the University of Reading conducted the staining, imaging and analysis of the assay.

2.12. Haematoxylin and eosin

The muscle tissue slides were removed from -80º C and allowed to dry for at least 15 minutes at room temperature. Then they were washed for two minutes in PBS to remove the freezing media and transferred to Harris haematoxylin (Sigma-aldrich) for 2 minutes to stain the nuclei. The slides were then placed in distilled water for one minute before being transferred under the tap where the water was allowed to wash the slides for up to five minutes to remove any excess background staining. As a counter stain, the slides were placed in 1% eosin for 1 minute followed by immersing the slides in in 70% ethanol for 1 minute, 90% ethanol for 2 minutes, then 100% ethanol for 2 minutes repeated thrice. Finally, the slides were cleared in two washes of xylene, 3 minutes each then mounted with DPX mounting media (Fisher) and cover slipped. The slides were allowed to dry for 15 minutes in a fume cupboard before being imaged using the NanoZoomer-SQ (Hamamatsu) digital slide scanner.

2.13. Picrosirius Red staining

The muscle tissue slides were removed from -80º C and allowed to dry for at least 15 minutes at room temperature. The Picrosirius red stain kit (Abcam – ab150681) was used, the

manufacturers protocol was followed and performed in a fume hood. Briefly, to stain the cytoplasm the slides were placed in Bouin solution (prewarmed to 56^{o} C in a water bath) for 15 minutes, then rinsed and washed in tap water for 15 minutes at room temperature. This was followed by a 1-hour incubation in Picrosirius red at room temperature and in the dark to stain for collagen. The slides were then rinsed quickly (two dips only) in two consecutive washes of acidified water (0.5% v/v glacial acetic acid in distilled water) and dehydrated in 3 washes of ethanol 100% for 5 minutes each. Finally, the slides were cleared in xylene for 5 minutes then mounted with DPX mounting media (Fisher) and cover slipped. The slides were allowed to dry overnight in a fume cupboard before being imaged using the NanoZoomer-SQ (Hamamatsu) digital slide scanner.

2.14. Immunostaining

The slides were removed from -80^{o} C and allowed to dry for at least 15 minutes at room temperature. Using a hydrophobic pen (Merck) a barrier was drawn around the desired section (to maintain the antisera used in the protocol) and allowed to dry for 15 minutes. The slides were washed three times with PBS for 5 minutes, then to expose the antigens they were left in permeabilization buffer (Sucrose 20.54 g, HEPES 0.952 g, NaCl 0.584 g, $MgCl_2$ 0.260 g, sodium azide 0.1 g, Triton X-100 1 mL) for 15 minutes. The slides were washed once again three times with PBS for 5 minutes followed by 30 minutes in blocking buffer (FBS 25 mL, sodium azide 200 mg, Triton X-100 250 µL dissolved in 1X PBS to make a final volume of 500 mL) at room temperature, and then overnight incubation at 4^{o} C with the desired primary antibody. Next, the slides underwent three 10-minute washes in blocking wash buffer to remove the unbound primary antibodies, concurrently the corresponding secondary antibody was prepared in blocking wash buffer. Once the washes were completed the secondary antibody (200 – 300 µL depending on section size) was applied and left for 1 hour in the dark at room temperature followed by three more 10-minute washes in PBS to remove any excess antibody. If multiple antibodies were required for profiling, then another

primary antibody would be introduced at this stage and the previous steps of incubation, washing, adding secondary antibodies and further washes would be repeated. Ultimately, the slides were mounted with 4′,6-diamidino-2-phenylindole (DAPI) and imaged using an epifluorescence microscope (Zeiss AxioImager) with Axiovision SE64 Rel. 4.9.1 software installed. Analysis of images was performed with ImageJ software and where required; Adobe Photoshop was used to merge the exported images creating the whole muscle sections.

2.15. In-vivo muscle damage

The first phase of the study involved an 8-week pre-conditioning period where the mice were split into three cohorts receiving intraperitoneal injections (IP) twice a week, a control batch (n = 12) of PBS, a cigarette smoke conditioned media batch (n = 15) and a vape conditioned media batch (n = 15). Following every injection the mice were weighed and monitored for at least 30 minutes before being housed. After 8 weeks, 30 µL of 50 µM Cardiotoxin (CTX) from *Naja Pallida* (Latoxan) was injected into the right tibialis anterior (TA) of all the mice, they were monitored for 30 minutes before being returned to housing. The second phase of the study was the regeneration period, the mice still received IP injections twice a week until they were euthanised on day 5, 10 and 20 after injection of CTX. Then the TA, extensor digitorum longus (EDL), gastrocnemius and soleus muscles of both legs were collected (figure 2.2). Finally, the muscles were blocked, cryo-sectioned and immunostained.

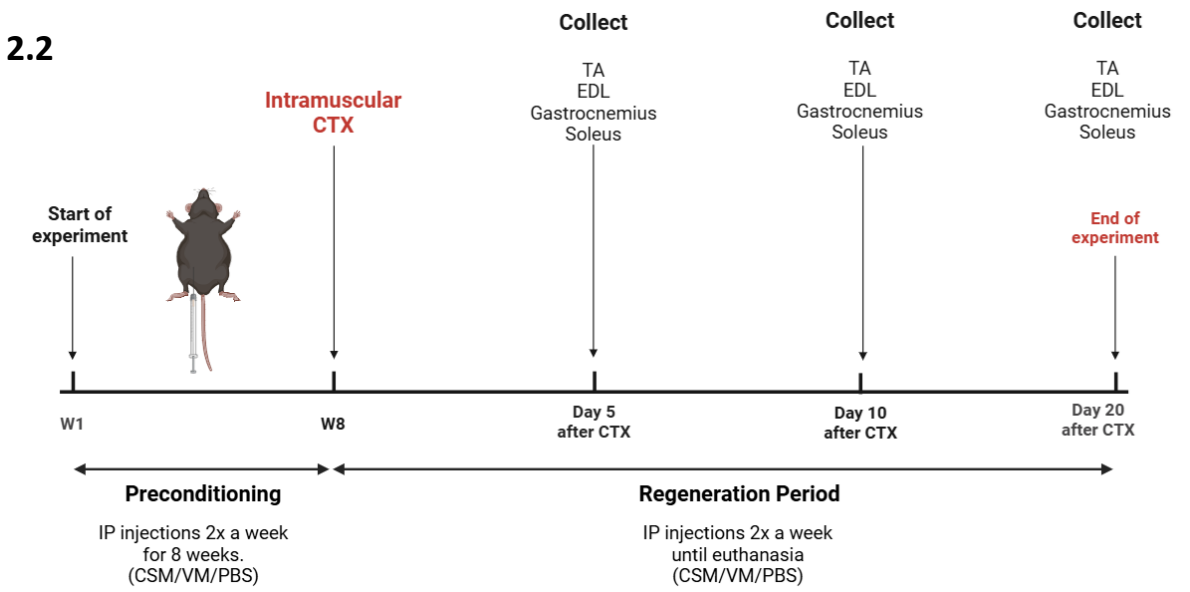

Figure 2.2. The in-vivo study plan.

2.16. Intraperitoneal injections

The conditioned media was prepared in 25G, 500µL syringes (Insumed). To start the mice were weighed, then scruffed with the head oriented upwards, the needle was inserted into the peritoneum on the right side of the mouse at a point proximal and lateral to the last nipple, 100 µL of the CSM, VM or PBS was injected. The mice were then returned to the cage and monitored for 30 minutes before being returned to housing.

2.17. Anaesthesia

Anaesthesia was performed with 3.5% isoflurane in oxygen, then maintained at 2% during the procedure. Afterwards, the mice were returned to the cages and monitored for 30 minutes to ensure recovery.

2.18. Intramuscular injections

First the cardiotoxin was prepared in 30G, 8 mm long needles with 300 µL syringes (Insumed). The mice were anesthetised and the area around the TA was shaved to allow accurate delivery. The first injection was inserted parallel to the muscle at the distal end of the anterior of the TA, the needle was inserted approximately 7 mm into the muscle and 10

µL of cardiotoxin was administered. The next two injections were delivered perpendicular to the muscle, lateral to the right and left of the proximal end of the TA, similarly 10 µL of solution was administered in each site. In total the animals received 30 µL of 50 µM cardiotoxin from *Naja Pallida* (Latoxan) in the right TA, thereafter they were returned to their cages where they were monitored for at least 30 minutes ensuring full recovery.

Dr. Robert Mitchell from Micregen Ltd. conducted the intramuscular injections.

2.19. Euthanasia

Euthanasia was performed by CO_2 asphyxiation, followed by cervical dislocation as confirmation. The procedure conformed with Guidance on the operations of the ASPA issued by the Home Office.

2.20. Cardiac puncture

This procedure was only carried out on mice from day 20 after cardiotoxin injection to ensure that mice received the maximum number of conditioned media (CSM/VM) injections before the blood was utilised. Euthanasia was performed via CO_2 for 70 seconds; the mice were thoroughly checked by pinching of the foot or ear to confirm loss of consciousness. Then, the rodent was laid on its back and using a 19G needle inserted below the thorax towards the heart the blood was slowly drawn. Immediately after, cervical dislocation was conducted to confirm death. The blood was centrifuged at 10,000 G for 20 minutes and the serum was collected in a tube and stored at -80^{o} C.

Andrew Parnell from the University of Reading aided with the cardiac puncture.

2.21. Muscle dissection

Muscle dissection was performed within 10 minutes after euthanasia. The mice were sprayed with 70% ethanol before being secured on a corkboard, the fur around the circumference of the belly was cut and drawn down to the feet exposing the muscles and tendons. The skin

covering the ankle and foot was gently sliced downwards towards the toes then pulled free by hand. Using surgical forceps, the fascia layer covering the TA and EDL along with muscle covering the proximal EDL tendon were removed exposing the muscles and tendons. Using surgical micro-scissors, the distal tendon of the TA was severed where it crossed the medial side of the limb. Thereafter, using surgical forceps the TA was pried proximally to the knee by the tendon and liberated by cutting at the origin then temporarily placed in PBS. Next, the distal tendons of the EDL were severed using micro-scissors, then using surgical forceps carefully pried through the ankle. The muscle was drawn proximally to the knee by the tendons, and while the muscle was kept taut the proximal tendons were severed freeing the EDL, it was then temporarily placed in PBS. Afterwards, the mice were turned to the prone position and secured on the corkboard using pins. The gastrocnemius tendon at the distal end was cut before it was lifted proximally exposing the plantaris and soleus. The proximal tendon of the soleus was carefully cut, then drawn distally by the tendon while the muscle was taut, the distal end was cut without damaging the gastrocnemius. The soleus was then temporarily stored in PBS. Subsequently, the plantaris was removed by separating the distal tendon from the gastrocnemius tendon and liberating it by severing the proximal tendon. Finally, to liberate the gastrocnemius, the tissue surrounding the muscle was removed exposing it entirely, then using surgical forceps it was drawn proximally and cut at the origin before it was temporarily placed in PBS. When all the required muscles of a mouse were collected in PBS they were individually weighed, imaged and snap-frozen by placing them on foil before transferring the foil to a bed of pre-prepared frozen isopentane in liquid nitrogen. The frozen muscles were then moved into pre-labelled and pre-cooled (on dry ice) Eppendorf tubes before being stored in -80^{o} C.

Mustafa Al Asady from the University of Reading aided with the weighing, imaging and freezing of the muscles.

2.22. Muscle blocking and cryosectioning

A dry-ice alcohol bath was set up with a metal block placed in the middle, along with the forceps being used they were allowed to cool to the temperature of the dry-ice for at least 20 minutes. The muscles were transferred from -80° C in a dry-ice container to prevent freeze-thaw. Individually the muscles were set on the chilled metal block and overlayed with Optimal Cutting Temperature compound (OCT) (CellPath) in a dropwise manner until completely enveloped. The muscle was rapidly placed into an appropriately sized aluminium foil container of OCT and floated in the dry-ice alcohol bath causing the OCT to freeze into a block. Temporarily, the blocks were stored in dry-ice until all muscles were completed then stored in -80° C.

The blocked muscles were transversely sectioned at 12 μm thickness using a Hacker Bright OTF5000 cryostat and collected serially onto pre-labelled glass slides then stored in -80° C until utilised for immunostaining.

2.23. Inflammatory cytokine analysis

Inflammatory cytokine assessment was performed on samples taken from a human cell line (AB1190) and mice serum.

In a 6-well plate, 60’000 cells per well were seeded and allowed to adhere overnight at 37° C and 5% CO_2. The following day the cells were incubated with the conditioned media for 72 hours. Afterwards, the media was collected and spun for 10 minutes at 500 G at 4° C to remove cell debris, and subsequently another centrifugation at 2000 G for 20 minutes at 4° C. The supernatant was collected and stored at -80° C until it was sent to Eve Technologies Corporation (Canada). The multiplexing analysis was performed using the Luminex™ 200 system (Luminex, USA) by Eve Technologies Corp. (Calgary, Alberta). Fifteen markers were simultaneously measured in the samples using Eve Technologies' Human Focused 15-Plex Discovery Assay® (MilliporeSigma, USA) according to the manufacturer's protocol.

The 15-plex consisted of GM-CSF, IFNγ, IL-1β, IL-1Ra, IL-2, IL-4, IL-5, IL-6, IL-8, IL-10, IL-12p40, IL-12p70, IL-13, MCP-1 and TNF-α. Assay sensitivities of these markers range from 0.14 – 5.39 pg/mL for the 13-plex. Individual analyte sensitivity values are available in the MilliporeSigma MILLIPLEX® MAP protocol.

To assess inflammatory cytokines in mice, after the cardiac puncture of the day 20 dissections the blood was centrifuged at 10'000 G for 20 minutes and the serum was collected in a tube and stored at -80° C until it was sent to Eve Technologies Corporation (Canada). The multiplexing analysis was performed using the Luminex™ 200 system (Luminex, USA) by Eve Technologies Corp. (Calgary, Alberta). Thirty-two markers were simultaneously measured in the samples using Eve Technologies' Mouse Cytokine 32-Plex Discovery Assay® (MilliporeSigma, USA) according to the manufacturer's protocol. The 32-plex consisted of Eotaxin, G-CSF, GM-CSF, IFNγ, IL-1α, IL-1β, IL-2, IL-3, IL-4, IL-5, IL-6, IL-7, IL-9, IL-10, IL-12(p40), IL-12(p70), IL-13, IL-15, IL-17, IP-10, KC, LIF, LIX, MCP-1, M-CSF, MIG, MIP-1α, MIP-1β, MIP-2, RANTES, TNFα, and VEGF. Assay sensitivities of these markers range from 0.3 – 30.6 pg/mL for the 32-plex. Individual analyte sensitivity values are available in the MilliporeSigma MILLIPLEX® MAP protocol.

2.24. Microarray

The C_2C_{12} cell lines were investigated as both myoblasts and myotubes. The myoblasts were allowed to grow to 60% confluence before they were exposed to CSM for 24 hours then lysed and collected for microarray. For myotubes, the cells were allowed to reach confluence before differentiation, then they were exposed to CSM for 24 hours before lysis and collection. The transcriptomic expression profiles for each biological replicate were generated on the Affymetrix Mouse Genome 430_2 Array platform from ThermoFisher Scientific. For each treatment, total RNA was extracted by direct cell lysis and recovery

using the Absolutely RNA Microprep Kit (Agilent, as per the manufacturer's guidelines). Each treatment series also incorporated a vehicle-only control set of triplicate cultures. Integrity of total RNAs was determined using an Agilent Bioanalyser as per the manufacturer's instructions and only samples with RNA integrity number >7 were progressed to transcriptome analysis. Transcriptome changes driven by exposure to the treatments were determined using the Nugen Ovation V2 labelling system (https://www.nugen.com/ products) followed by Mouse Genome 430_2 GeneChips as per the manufacturer's instructions (https://www.thermofisher.com/order/catalog/product/902490). Gene expression data was analysed in the Transcript Analysis Console (TAC): https://www.thermofisher.com/uk/en/home/life-science/microarray-analysis/microarray-analysis-instruments-software-services/microarray-analysis-software/affymetrix-transcriptome-analysis-console-software.html). Raw data was extracted and normalised (MAS_5) and differentially expressed genes (DEGs) were generated for each treatment profile ($P<0.05$). CMAP treatment profiles were based on statistically significant DEGs derived from treatment and control groups.

Professor David Chambers from the University College London performed the Microarray experimentation. Transcriptomic analysis was performed by Professor Darius Widera at the University of Reading, Daniela Gerovska and Marcos Arauzo-Bravo from the group of computational biology and systems biomedicine at the Basque foundation for science, Spain.

2.25. Connectivity Mapping

CMAP data were generated by comparison of the treatment-specific DEGs (see above) to the Broad connectivity map database (www.broadinstitute.org/connectivitymap-cmap) as previously described:

(https://pmc.ncbi.nlm.nih.gov/articles/PMC6731247/pdf/41398_2019_Article_555.pdf) and using the SPIED web portal (http://92.205.225.222/HGNC-SPIED3-QF.py) [https://bmcgenomics.biomedcentral.com/articles/10.1186/1471-2164-14-765]. CMAP 'hits' were ranked according to their correlation with the treatment-specific cohort of DEGs.

Professor David Chambers from the University College London performed the C-Mapping.

2.26. Statistical analysis

Data was presented as the mean ± standard error of the mean (SEM). Statistical analysis was carried out with GraphPad Prism using unpaired Student's t-test or a one-way analysis of variance or a two-way analysis of variance followed by post hoc Tukey's test or Bonferroni's multiple comparison or Dunnet's multiple comparison tests. A minimum of 95% confidence interval was used for significance; p values on figures were indicated by $p < 0.05$ (one asterisk), $p < 0.01$ (two asterisks), $p < 0.001$ (three asterisks) and $p < 0.0001$ (four asterisks).

Chapter 3: Investigating the effects of cigarette smoke media and vape media on early stages of skeletal muscle cell development.

3.1. Introduction

Muscle damage may occur due to disease, trauma and stress from excessive exercise or lifestyle choices. Smoking and recently vaping is popular, according to the Office for National Statistics in 2023 an estimated 6 million people aged over 18 smoked, additionally 5.1 million over the age of 16 vape in the UK (Statistics, 2024). Disease outcomes from the use of cigarettes and vaping are well documented, they include a variety of cardiovascular and respiratory diseases. Furthermore, studies have shown that cigarette smoke causes cell death (Feng et al., 2021; Kunzi & Holt, 2019), delays wound closure (Luppi et al., 2005) and bone healing (Patel et al., 2013).

Skeletal muscle regeneration is driven by the resident satellite cell population located between the basal lamina and sarcolemma (Mauro, 1961). They remain quiescent until required for growth or repair, once activated they undergo symmetric and asymmetric division. The former leads to repopulating the resident stem cell pool, the later results in a daughter cell that can migrate (Schultz et al., 1985), differentiate and fuse generating new myofibres (Yin et al., 2013).

Cigarette smoke induced muscle dysfunction has been well documented with a focus on functionality, fatigue, atrophy and weakness (Chan et al., 2020; Degens et al., 2015; Luppi et al., 2005; Nogueira et al., 2018; Saito et al., 2012). Much less is known about the impact on muscle regeneration. This chapter investigates the impact of both cigarette smoke and vape on the initial stages of muscle biology. We believe that smoking or vaping (Churg et al., 2002; Lee et al., 2012) leads to diminished satellite cell biology. Thus, we investigated the direct impact of CSM, VM on mice and human myoblasts to assess viability, proliferation, migration, differentiation, and fusion. We suggest that dysfunction in any or all these stages would potentially result in delayed regeneration.

3.2. Results:

3.2.1. Cigarette smoke and vape extract conditioned media.

The first hurdle was to devise a method of exposing cells to cigarette and vape smoke. This method had to be feasible and reproducible. Therefore, the work of (Nogueira et al., 2018) was used as launching point and a similar method was devised. The conditioned media was prepared by bubbling the combusted smoke of a cigarette or vape through PBS until the cigarette was consumed, or an equal number of "inhalations" to that for the vape. Afterwards an optical spectrum analysis was performed to determine and visualize the chemical constitution. This was found to be between the UV range (190 nm to 400 nm) (figure 3.1). Phosphate buffered saline (PBS) (figure 3.1A) which was used as the vehicle for the conditioned media had no effect on absorbance. Cigarette smoke media (CSM) (figure 3.1B) showed a peak starting at 210 nm then dropping and extending to 350 nm. Vape extract media (VM) (figure 3.1C) showed a similar trend to CSM where a peak is visible starting at 210 nm then dropping immediately after.

3.1

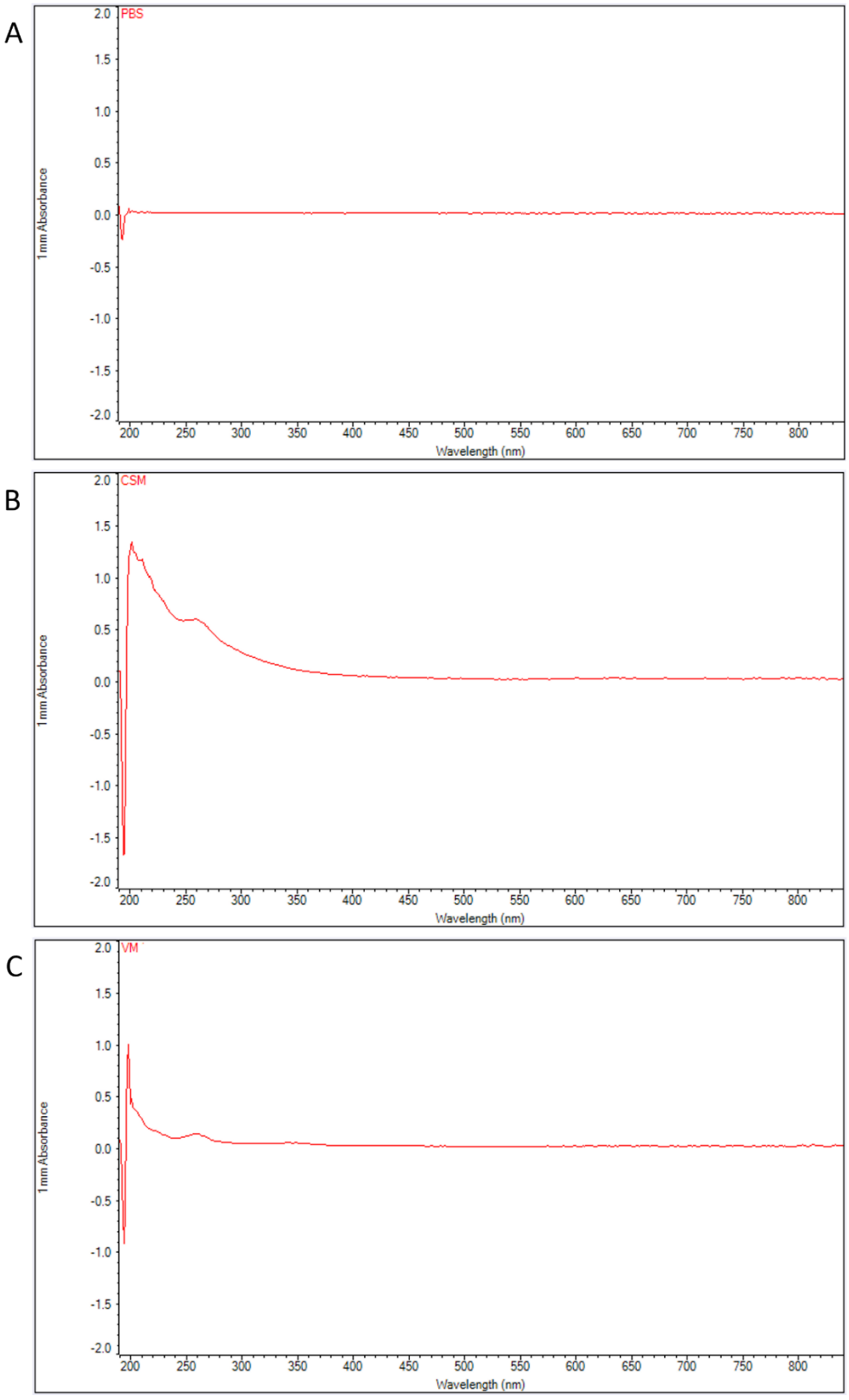

Figure 3.1. Spectrum analysis of conditioned media. (A) PBS, (B) cigarette smoke conditioned media (CSM) and (C) vape conditioned media (VM) used in experimental procedures. (n=3).

To determine functional concentrations that were used to calculate multiple dilutions implemented in the experiments, absorbance of the conditioned media was measured individually at different wavelengths falling within the UV range. Both CSM (figure 3.2 A) and VM (figure 3.2 B) presented a peak absorbance at 220 nm. Going forward all absorbance measurements were performed at 220 nm as the reference point for calculations of dilutions. The maximum absorbance that was measured using a single cigarette in 10ml PBS was 1.8 OD at 220 nm. Similarly, the maximum optical density measured for VM was 1.3 OD in 10 ml of PBS.

3.2

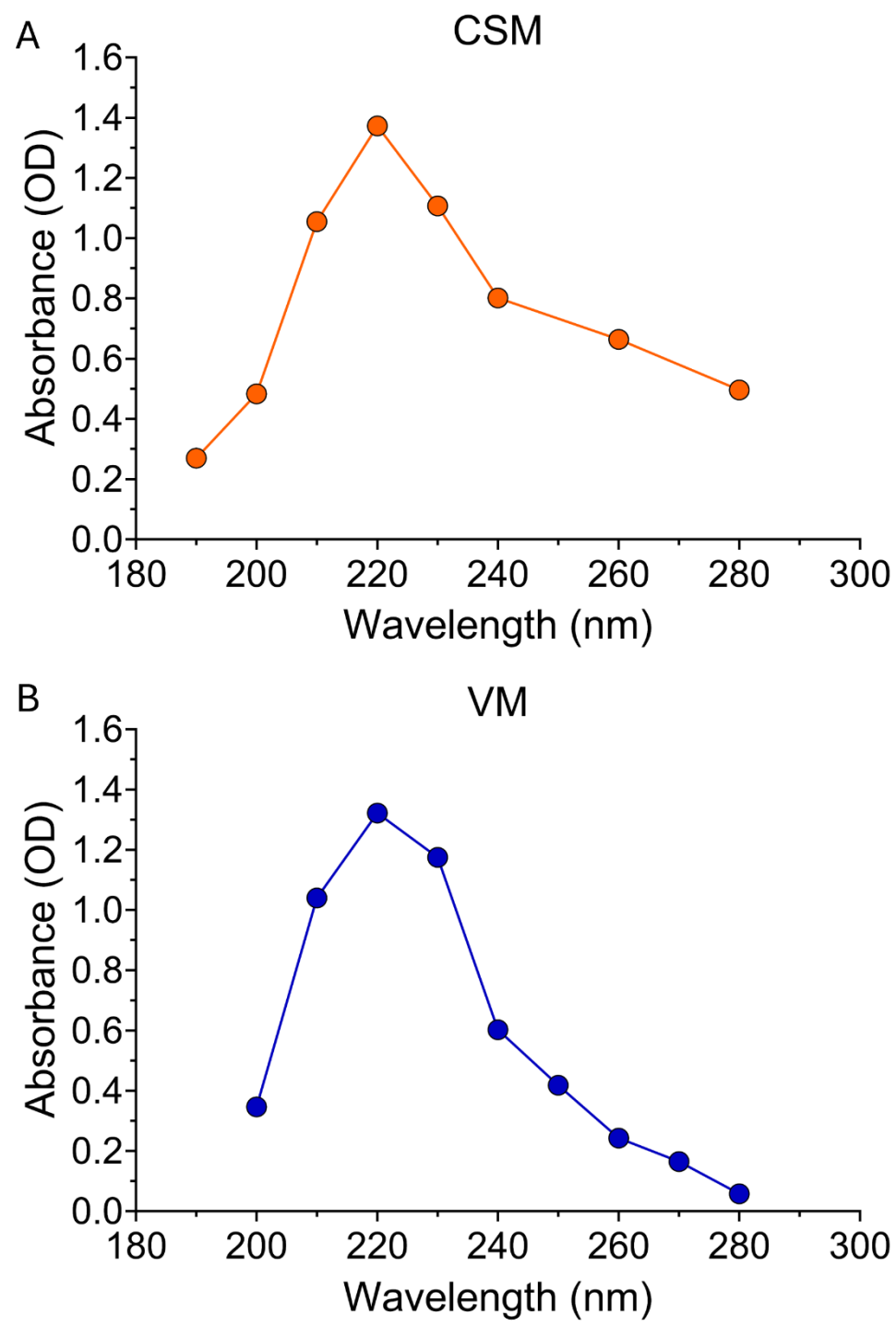

Figure 3.2. Absorbance measurements of the conditioned media within a portion of the UV range. The peak absorbance wavelength was determined for both CSM (A), and VM (B) allowing us to standardize the use of this wavelength to determine concentrations of conditioned media used in future experiments.

3.2.2. Cigarette smoke media diminished cell viability

The first test was to assess cell viability using an MTS assay (Promega) after exposure to conditioned media for 24 hours. The C_2C_{12} cell line was exposed to increasing concentrations of conditioned media starting from 0.001 OD to 0.24 OD with CSM (figure 3.3 A) and from 0.001 OD to 0.1 OD with VM (figure 3.3 B). After 24 h exposure, a concentration dependent decrease in viability was seen starting from 0.05 CSM (figure 3.3 C), however with the VM there was no effect (figure 3.3 D).

3.3

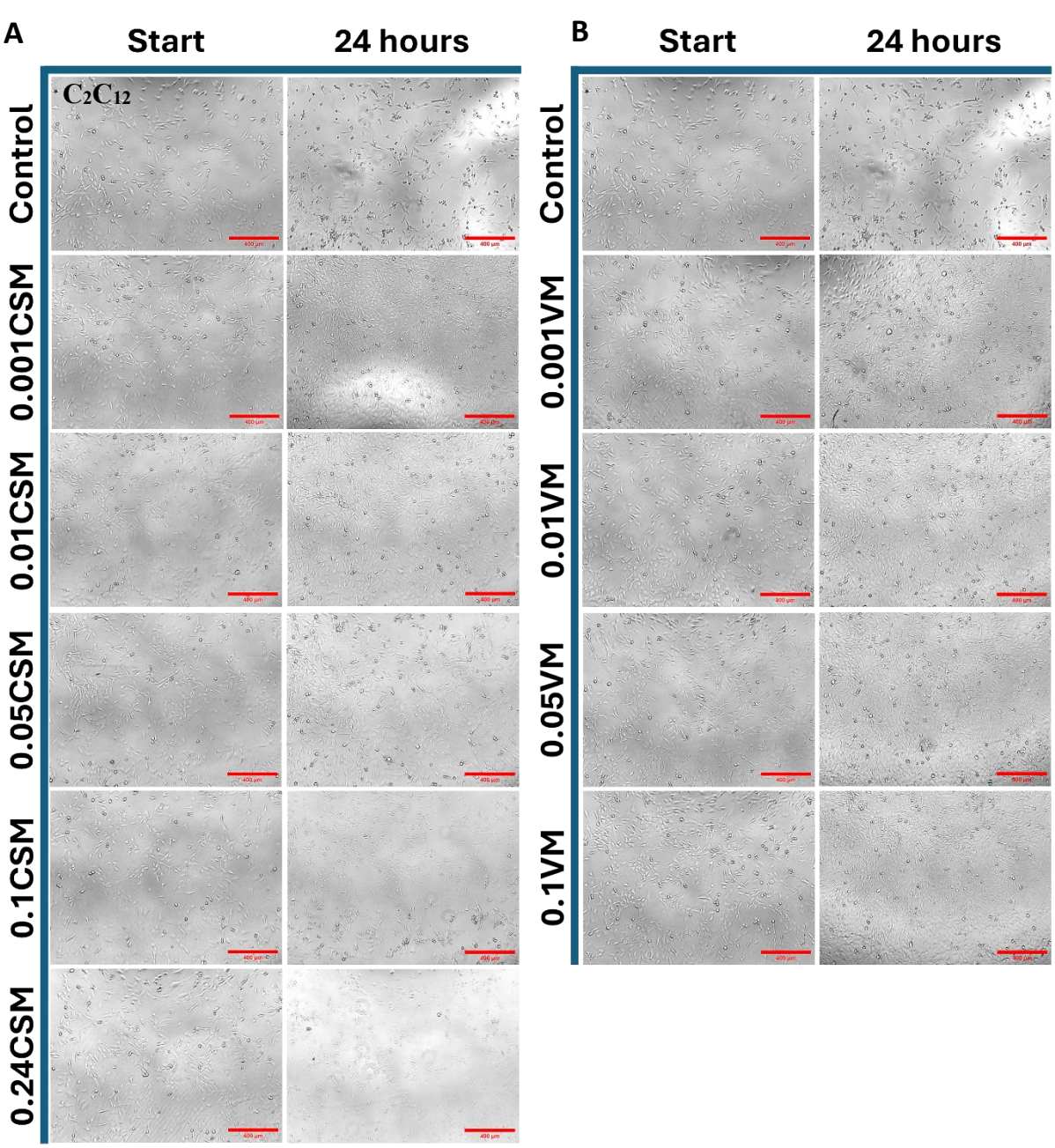
A
Start
24 hours
C2C12
Control
0.001CSM
0.01CSM
0.05CSM
0.1CSM
0.24CSM
B
Start
24 hours
Control
0.001VM
0.01VM
0.05VM
0.1VM

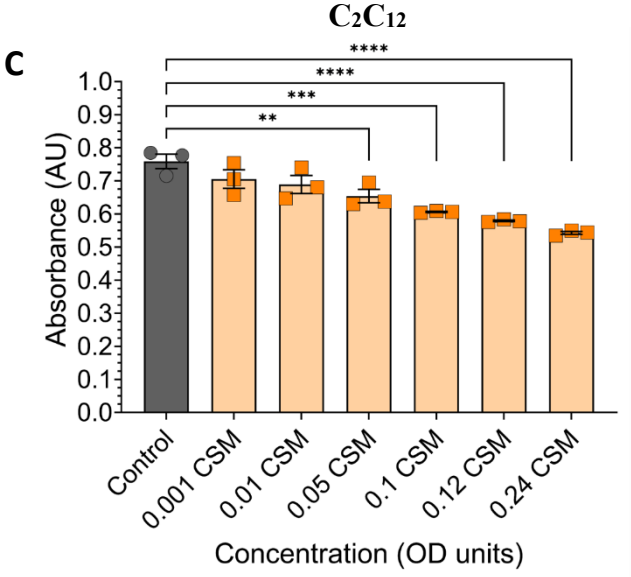
C2C12
C
Absorbance (AU)
1.0
0.9
0.8
0.7
0.6
0.5
0.4
0.3
0.2
0.1
0.0
****
****
***
**
Control
0.001 CSM
0.01 CSM
0.05 CSM
0.1 CSM
0.12 CSM
0.24 CSM
Concentration (OD units)

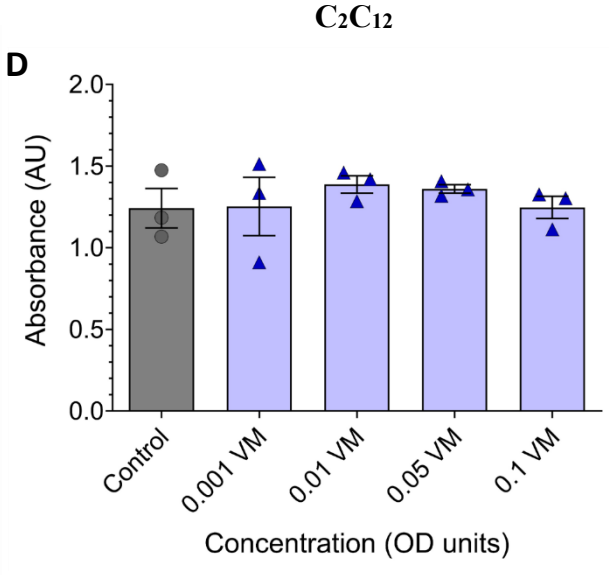
C2C12
D
Absorbance (AU)
2.0
1.5
1.0
0.5
0.0
Control
0.001 VM
0.01 VM
0.05 VM
0.1 VM
Concentration (OD units)

Figure 3.3. Viability assay of C_2C_{12}. Cells were exposed to increasing concentrations of CSM (A) and VM (B) for 24 hours. Afterwards viability was assessed and quantified (using an MTS reagent) for (C) CSM and (D) VM exposed cells. Data presented as the mean +/- SEM using one-way ANOVA with Dunnett's multiple comparison test. **p<0.01, ***p<0.001, ****p<0.0001, (n=3). Scale bar is 400µm.

Next three human cell lines were examined. These were, AB1190 sourced from the paravertebral muscles of a 16-year-old boy. The AB678 sourced from the quadriceps of a 53-year-old man, and AB1167 sourced from the fascia lata of a 20-year-old-man. This allowed us to investigate the effect of genetic variability as well as cell origin. The AB1190 was exposed to various concentrations of CSM (figure3.4 A) for 24 hours, which resulted in a significant increase in absorbance at the lower concentrations of 0.001 OD to 0.05 OD, no change at 0.1 OD and then a significant decrease at 0.12 OD and 0.24 OD (figure 3.4 C). However, when exposed to VM (figure 3.4 B) all concentrations showed a significant increase (figure 3.4 C). With AB678 a significant decrease in absorbance was seen at 0.1 OD and 0.2 OD after 24 hours exposure to CSM, and at 0.05 and 0.1 OD with VM (figure 3.4 D). AB1167 showed a significant drop in absorbance from 0.05 OD through to 0.2 OD after exposure with CSM, similarly after 24 hours exposure to VM, a significant decrease in absorbance was observed from 0.025 OD to 0.1 OD (figure 3.4 E). These results are very interesting as they display a variable reaction to CSM and VM from muscle cells sourced from different donors and locations.

3.4

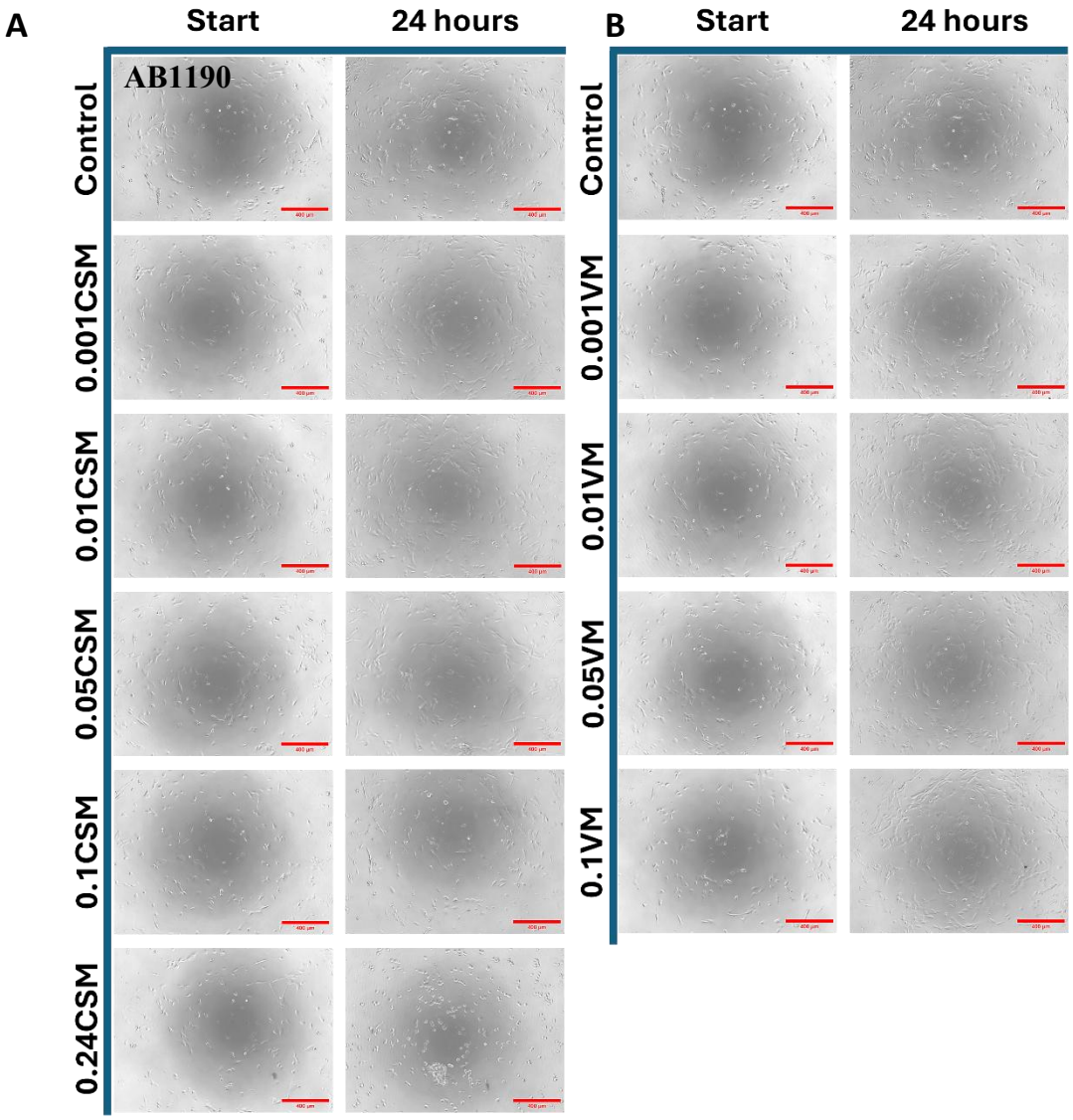
A
Start
24 hours
AB1190
Control
0.001CSM
0.01CSM
0.05CSM
0.1CSM
0.24CSM
B
Start
24 hours
Control
0.001VM
0.01VM
0.05VM
0.1VM

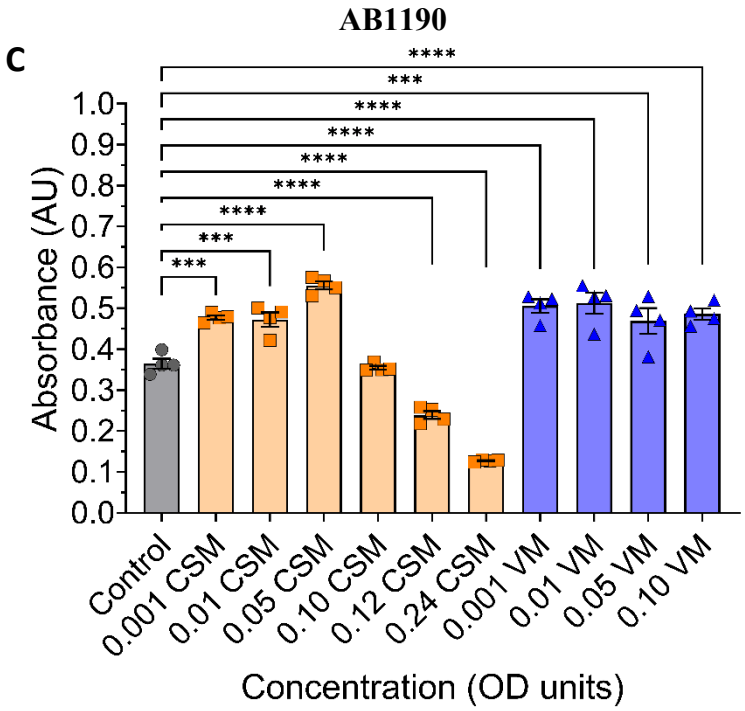
AB1190
C
Absorbance (AU)
1.0
0.9
0.8
0.7
0.6
0.5
0.4
0.3
0.2
0.1
0.0
****
***
****
****
****
****
***
***
Control
0.001 CSM
0.01 CSM
0.05 CSM
0.10 CSM
0.12 CSM
0.24 CSM
0.001 VM
0.01 VM
0.05 VM
0.10 VM
Concentration (OD units)

3.4

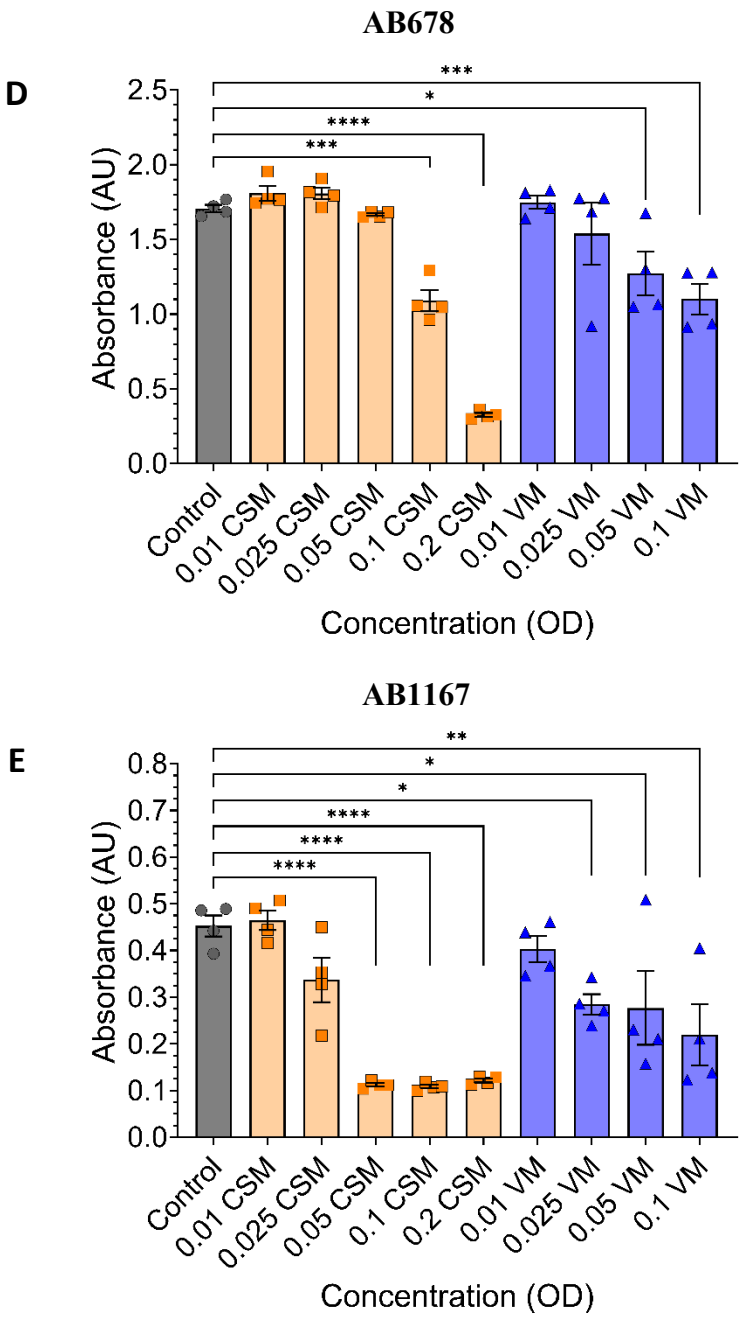

Figure 3.4. Viability assay of human cell lines. Cells were exposed to increasing concentrations of CSM and VM for 24 hours before viability was assessed and quantified (using an MTS reagent). (A) representative images of AB1190 exposed to CSM. (B) representative images of AB1190 exposed to VM. (C) quantified data of AB1190 exposed to CSM and VM. (D) MTS results of AB678 cells and (E) AB1167 after 24 hours exposure to CSM and VM. Data presented as the mean +/- SEM using one-way ANOVA with Dunnett's multiple comparison test. *p<0.05, **p<0.01, ***p<0.001, ****p<0.0001, (AB1190 n=4, AB678 n=4, AB1167 n=4). Scale bar is 400µm.

3.2.3. CSM drives cellular senescence in AB1190 myoblasts

The ability to proliferate is essential to muscle regeneration. Senescence is where cells stop proliferating permanently due to stress and avoid apoptosis. They remain metabolically active and dysfunctional. This leads to the release of pro-inflammatory cytokines and proteases into the surrounding environment causing damage and promoting chronic inflammation. This cascade of events is also known as the senescence associated secretory phenotype (SASP) which leads to tissue degeneration and is a hallmark of aging (Borghesan et al., 2020; Gorgoulis et al., 2019). Etoposide (EP) is a toxin found in American Mayapple; it was first synthesized in 1966 and was approved as a cancer therapeutic by the U.S food and drug administration in 1983. Etoposide targets DNA topoisomerase II inhibiting its activity and preventing DNA re-ligation. This leads to increasing numbers of DNA double strand breaks, halting of the cell cycle and eventually senescence or cell death (Montecucco et al., 2015; Muqaddas & Siddiqui, 2015).

In this experiment, we determine whether CSM and VM would induce senescence. First, the C_2C_{12} cell line was exposed to increasing concentrations of conditioned media for 72 hours, we used etoposide (EP) 50 μM as a positive control, a known chemical that induces senescence (Kellers et al., 2022), was incubated with the cells (figure 3.5 A). The results showed that there was limited to no β-Gal staining in the positive control and across all concentrations of conditioned media used. Furthermore, the number of countable cells was low with the EP and decreased in a concentration dependent manner when exposed to CSM (figure 3.5 B).

3.5

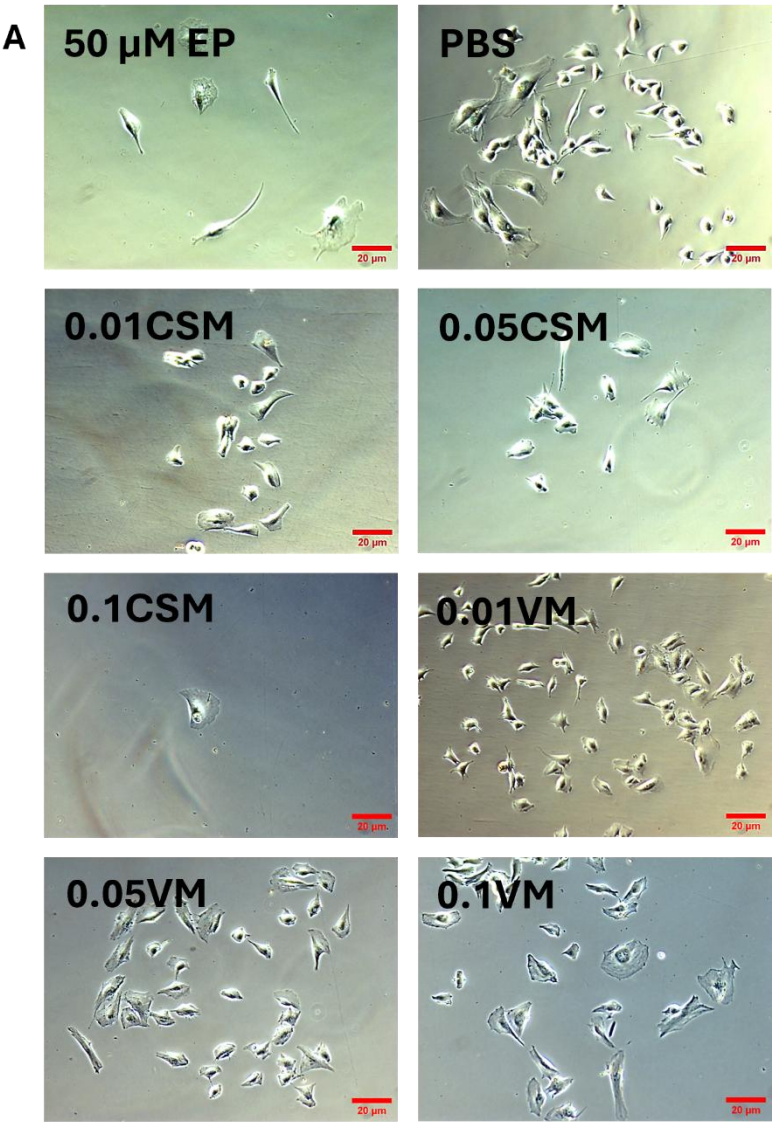
A
50 µM EP
PBS
0.01CSM
0.05CSM
0.1CSM
0.01VM
0.05VM
0.1VM
20 µm

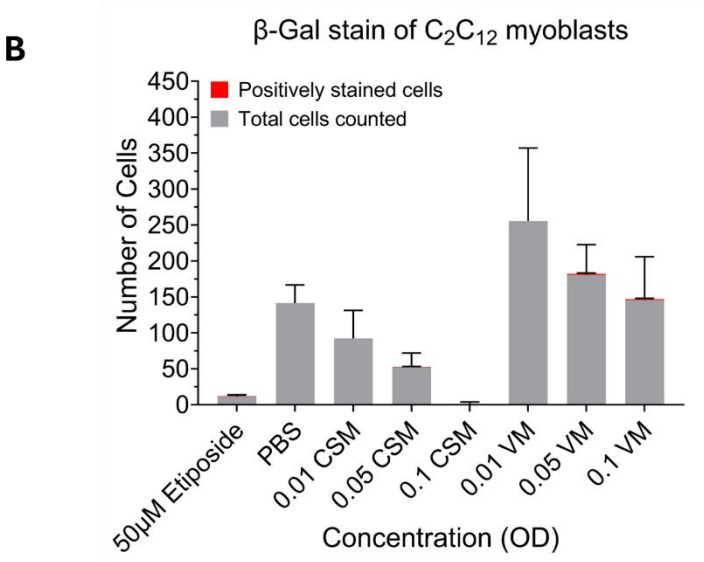
B
β-Gal stain of C2C12 myoblasts
Positively stained cells
Total cells counted
Number of Cells
450
400
350
300
250
200
150
100
50
0
50µM Etiposide
PBS
0.01 CSM
0.05 CSM
0.1 CSM
0.01 VM
0.05 VM
0.1 VM
Concentration (OD)

Figure 3.5. β-Gal staining of C_2C_{12} myoblasts exposed to conditioned media for 72 hours. (A) Representative images of staining. (B) Total number of cells counted, and number of positive cells observed. Data presented as the mean +/- SEM using one-way ANOVA with Dunnett's multiple comparison test (n=3). Scale bar is 20µm.

To investigate if the conditioned media drives the AB1190 cell line into senescence, they were exposed for 72 hours before fixing and staining with β-gal (figure 3.6 A). Five images were taken from each well and the number of stained cells was counted as a percentage of all cells in the field of view. The VM had no significant effect on the myoblasts, however the two concentrations of CSM (0.05 & 0.1 OD) revealed a significant increase in positively stained cells (figure 3.6 B), furthermore there was visible number of dead cells with the higher concentration of CSM.

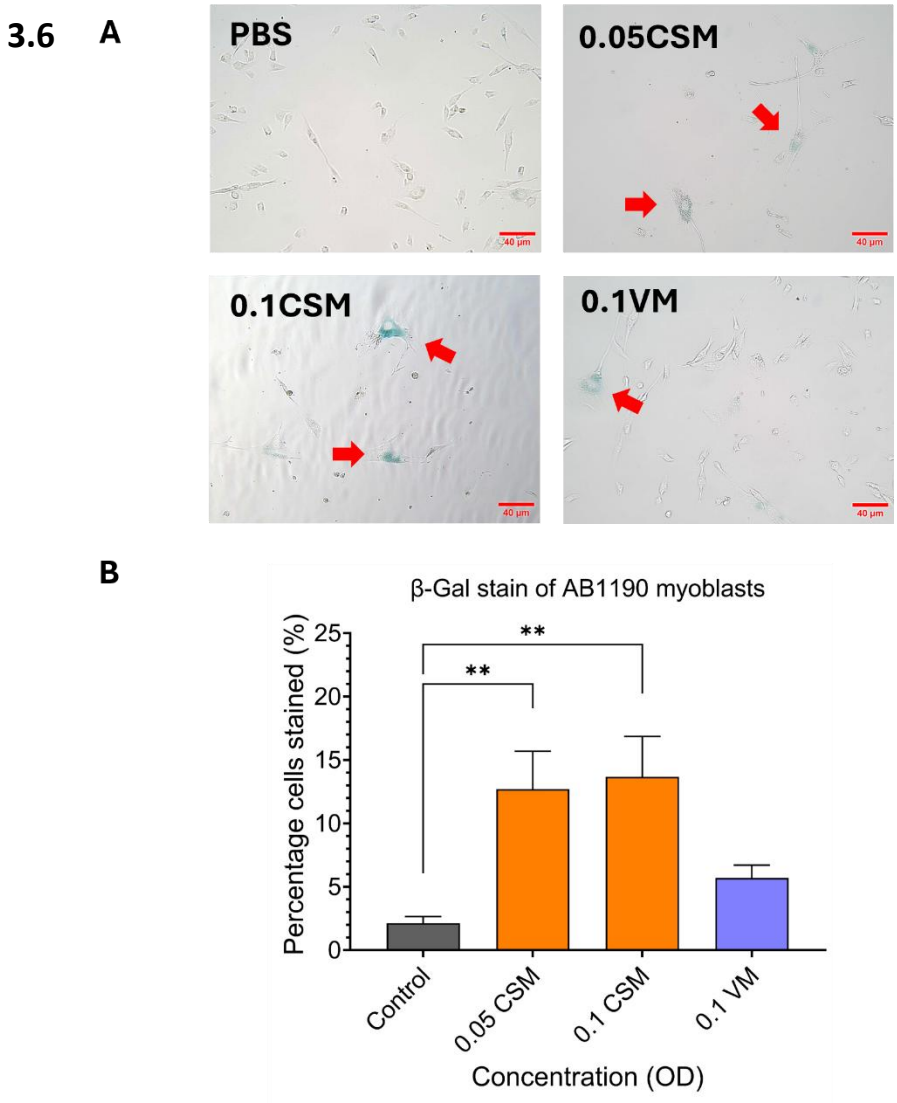

Figure 3.6. β-Gal staining on AB1190 myoblasts. Cells were exposed to CSM and VM for 72 hours before staining for β-Gal activity. (A) representative images of positively stained cells (shown by the red arrows). (B) shows the percentage of positive stained cells. Data presented as the mean +/- SEM using one-way ANOVA with Dunnett's multiple comparison test. **p<0.01, (n=3). Scale bar is 40µm.

To confirm that the conditioned media was indeed driving the cell lines to senescence, since there were varying results between the C_2C_{12} and AB1190, the IMR-90 human fibroblast cell line was similarly exposed to the conditioned media, fixed, stained and imaged (figure 3.7 A). Both CSM and VM (figure 3.7 B) showed no significant increase in positively stained cells in all concentrations. Furthermore, due to the negative control showing a high percentage of staining, the cells on the plate were lysed, collected and the absorbance was measured at 630 nm to ensure results were accurate. The absorbance measures of CSM and VM exposed IMR-90 lysates revealed a significant increase of staining with 0.05 OD, 0.1 OD CSM, and the highest concentration of 0.1 OD VM (figure 3.7 C).

3.7

A

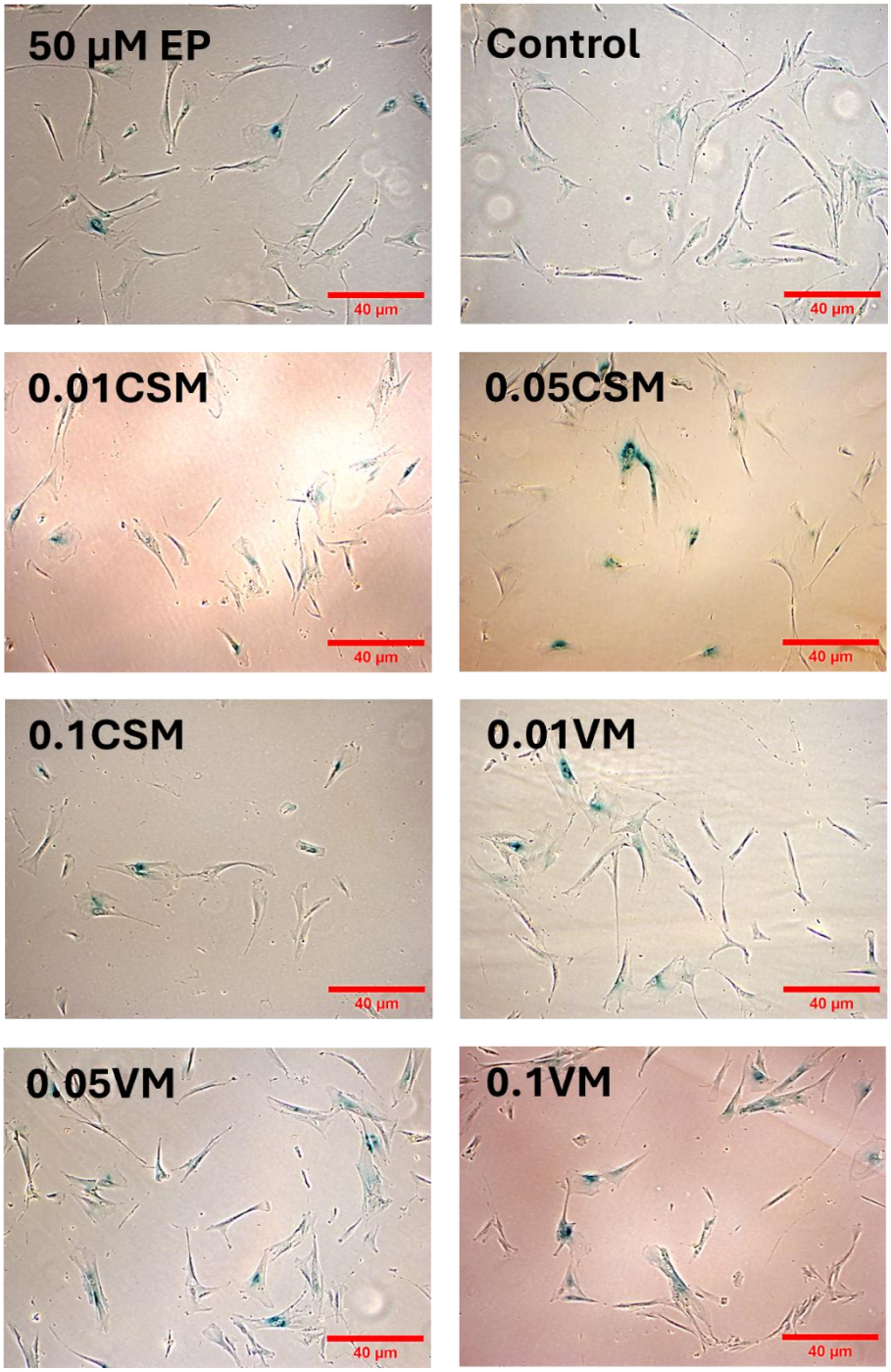

3.7

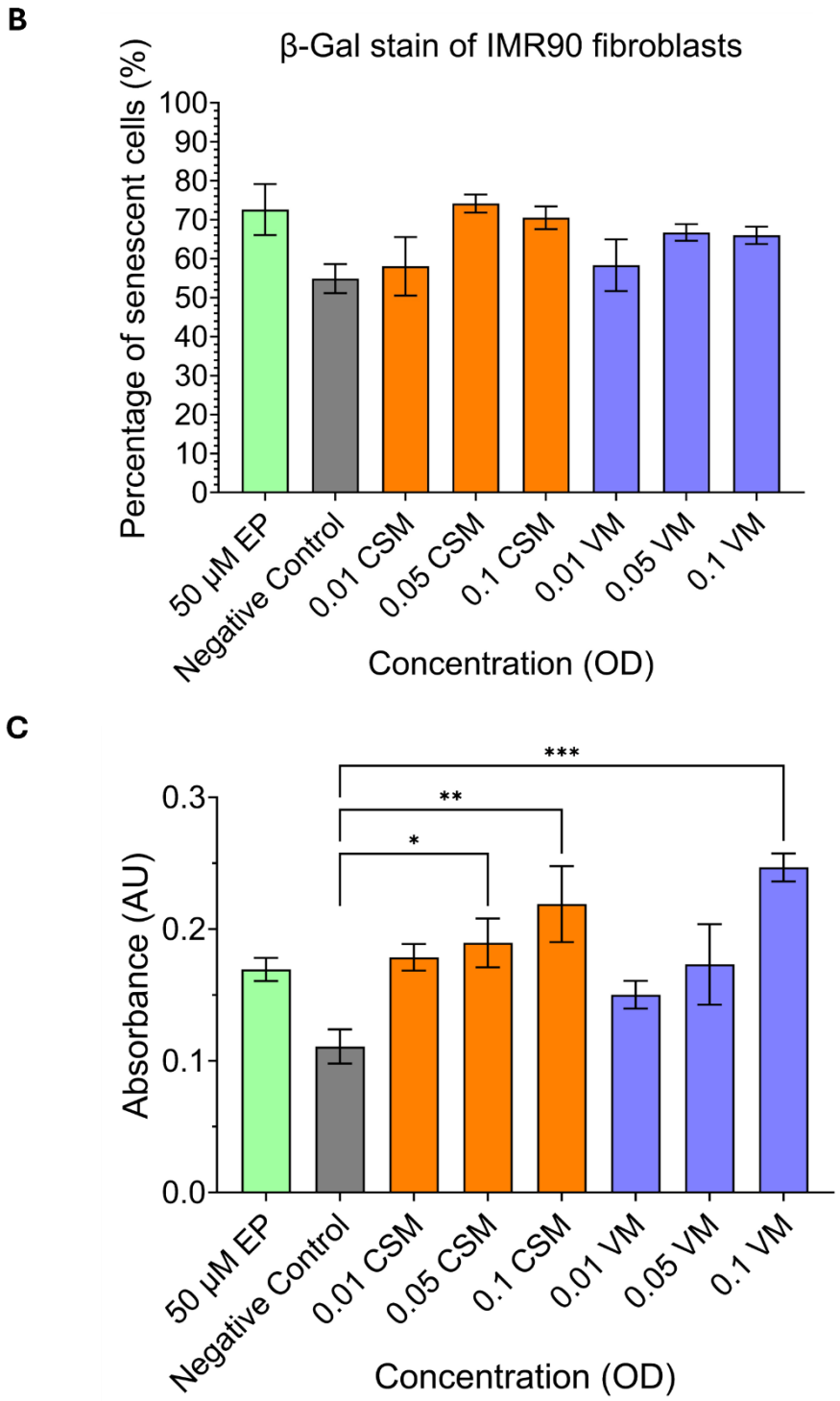

Figure 3.7. β-Gal staining on IMR-90. Cells were exposed to CSM and VM for 72 hours before staining for β-Gal activity. (A) representative images of positively stained cells (presented with blue dye). (B) shows the percentage of positively stained cells. Subsequently, the cells were lysed, and the absorbance was measured at 630 nm (C). Data presented as the mean +/- SEM using one-way ANOVA with Dunnett's multiple comparison test. *p<0.05, **p<0.01, ***p<0.001, (n=3). Scale bar is 40µm.

3.2.4. Cellular migration was impaired by cigarette smoke media

Cell migration is essential to regenerating muscle fibres, satellite cells residing between the sarcolemma and the endomysium (Mauro, 1961) generate myoblasts that migrate towards the damaged area and repair the fibres (Morgan et al., 1987; Siegel et al., 2009; Watt et al., 1987). To determine the effect of the conditioned media on C_2C_{12} myoblast migration two methods were employed: single cell tracking and the scratch assay. First the cells were exposed to three concentrations, 0.01 OD, 0.05 OD and 0.1OD of CSM then directly tracked for 24 hours under timelapse (figure 3.8 A). Similarly, the cells were exposed to three concentrations of VM and 0.05 OD CSM as a positive control (we observed a delay in migration and then a significant decrease after 24 hours, thus we used this concentration of CSM as a positive control) then tracked for 24 hours (figure 3.9 A). Subsequently the same parameters were employed in the scratch assay (figure 3.10 A). Single cell tracking revealed a reduction in the distance travelled with 0.05 OD, 0.1 OD CSM (figure 3.8 B) and only 0.1 OD VM (figure 3.9 B). When the speed was calculated over 2-hour intervals; the myoblasts exposed to 0.05 OD CSM displayed a period of 10 hours where the myoblasts had reduced speed but then recovered by 12 hours after exposure. The highest concentration of 0.1 OD CSM showed most cells dying except for a few that had limited motility (figure 3.8 C). The speed of myoblasts exposed to VM showed similar speeds to the control until the 24^{th} hour when 0.1 OD VM had a significant reduction (figure 3.9 C).

The scratch assay (figure 3.10) exhibited similar findings where cells exposed to 0.05 OD CSM resulted in a delay of cells crossing the scratch (figure 3.10 B) whereas exposure to VM had no effect on cell traversal (figure 3.10 C). Cells exposed to 0.1 OD CSM failed to cross the scratch even after the 24-hour threshold had passed and therefore removed from the analysis.

3.8

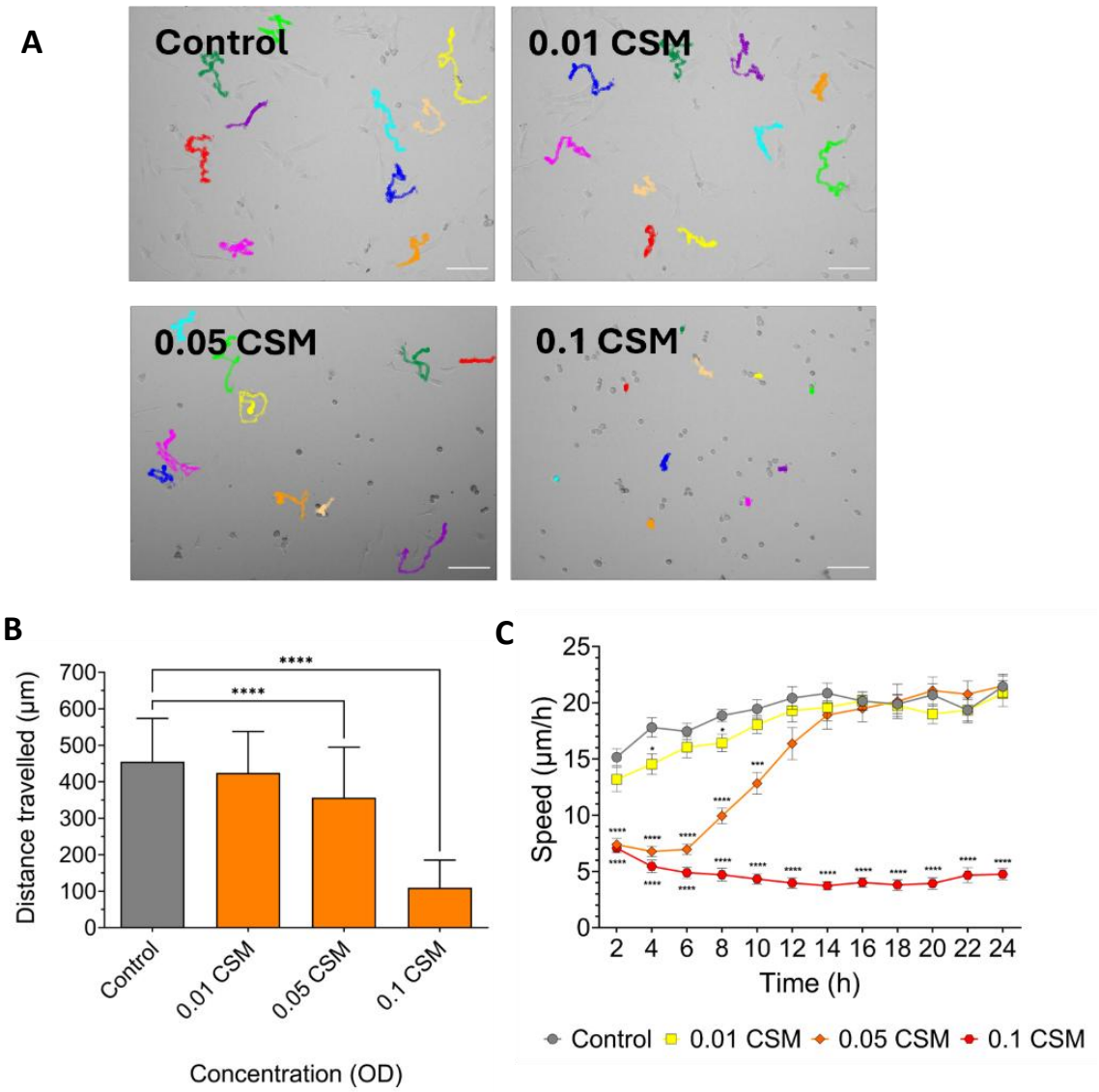

Figure 3.8. Effect of CSM on C_2C_{12} myoblast migration. Cells were exposed to CSM then monitored for 24 hours using timelapse microscopy. (A) representative images of cell migration tracks (coloured lines) and (B) the distance travelled after 24 hours. (C) the average speed of myoblasts during the 24-hour timelapse. Data presented as the mean +/- SEM using one-way ANOVA with Dunnett's multiple comparison test for the distance travelled. A two-way ANOVA with Dunnett's multiple comparison test was used for the analysis of the speed. *p<0.05, **p<0.01, ***p<0.001, ****p<0.0001, (n=3) scale bar is 100µm.

3.9

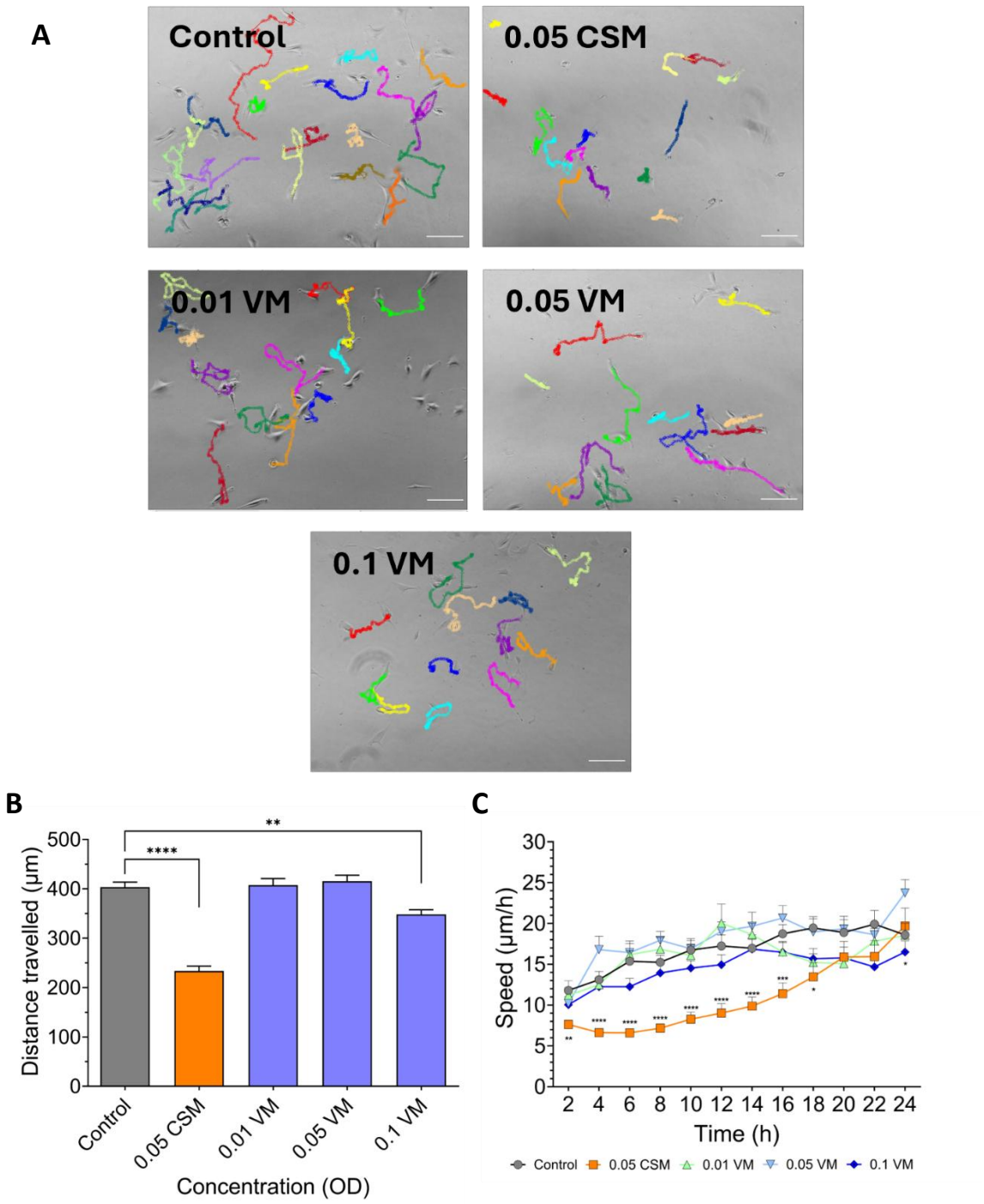

Figure 3.9. Effect of VM on C_2C_{12} myoblast migration. Cells were exposed to VM then monitored for 24 hours using timelapse microscopy. (A) representative images of cell migration tracks (coloured lines) and (B) the distance travelled after 24 hours. (C) the average speed of myoblasts during the 24-hour timelapse. Data presented as the mean +/- SEM using one-way ANOVA with Dunnett's multiple comparison test for the distance travelled. A two-way ANOVA with Dunnett's multiple comparison test was used for the analysis of the speed. *p<0.05, **p<0.01, ***p<0.001, ****p<0.0001, (n=3) scale bar is 100µm.

3.10

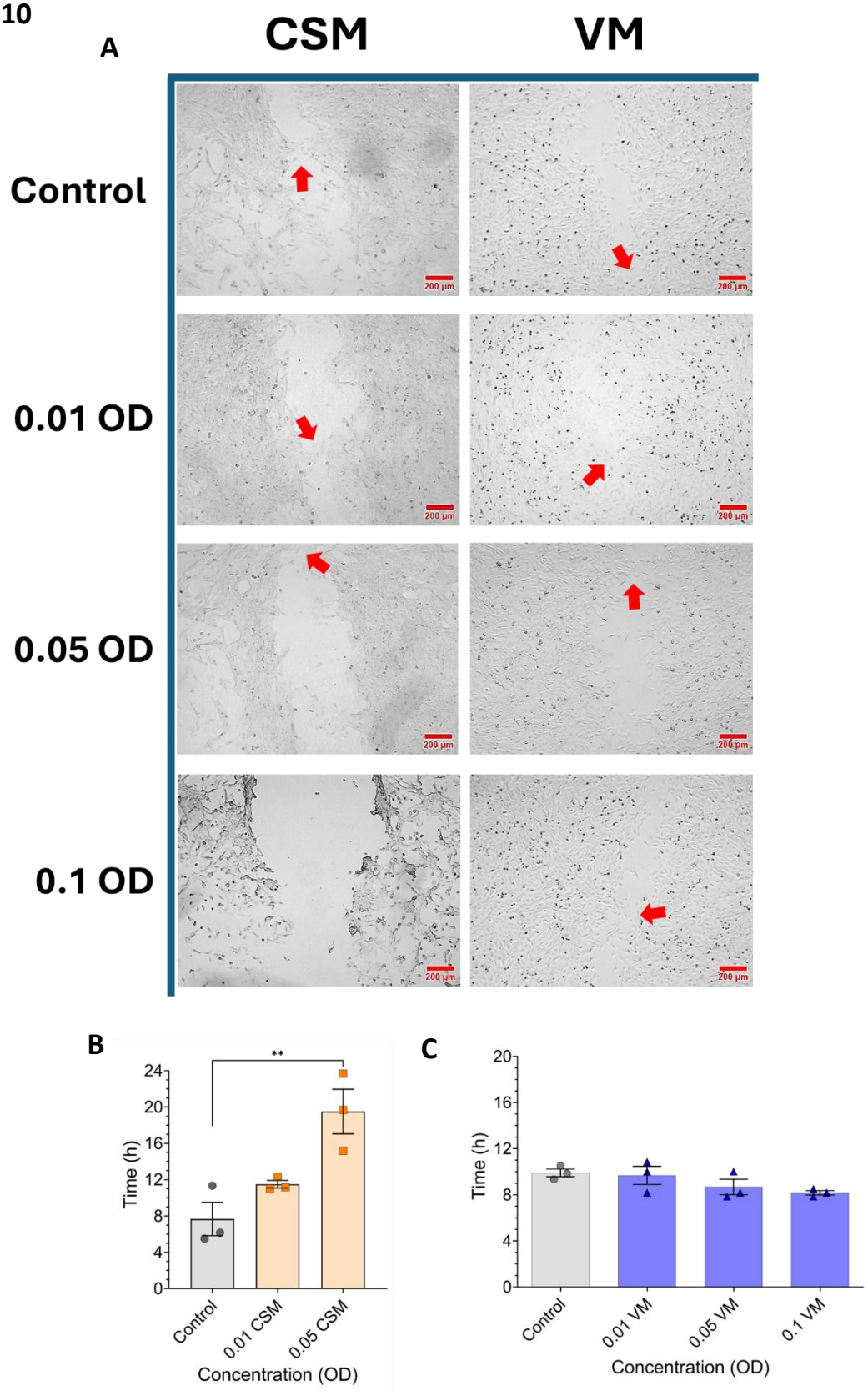
A
CSM
VM
Control
0.01 OD
0.05 OD
0.1 OD
200 µm
B
**
Time (h)
24
20
16
12
8
4
0
Control
0.01 CSM
0.05 CSM
Concentration (OD)
C
Time (h)
20
16
12
8
4
0
Control
0.01 VM
0.05 VM
0.1 VM
Concentration (OD)

Figure 3.10. Scratch assay of C_2C_{12} myoblasts. Cells were plated overnight then a scratch was formed across the face of the well. This was followed by exposing to CSM or VM and monitoring using a timelapse microscope for 24 hours. (A) representative images of the end of the experiment (arrows indicate cells meeting). The time taken for the first cell to meet another from the other side with CSM (B) and VM (C) was used as the scratch closure time. Data presented as the mean +/- SEM using one-way ANOVA with Dunnett's multiple comparison test. **p<0.01, (n=3) scale bar is 200µm.

The effect of the conditioned media on migration was replicated using the AB1190 myoblasts (figure 3.11 A). The findings revealed a decrease in distance travelled (figure 3.11 B) and diminished speed when tracked over 24 hours (figure 3.11 C) with 0.05 OD and 0.1 OD CSM. However, there was no effect on distance travelled and speed with VM. These findings were supported by the scratch assay; myoblasts were incubated with the two conditioned media for 24 hours (figure 3.12 A) and the time taken for cells to cross the scratch and meet was recorded. Myoblasts exposed to 0.05 OD CSM took significantly longer to cross (figure 3.12 B), meanwhile cells exposed to 0.1 OD CSM barely moved even after 24 hours and were subsequently removed from the analysis. On the other hand, myoblasts exposed to VM displayed no difference to control (figure 3.12 C).

3.11

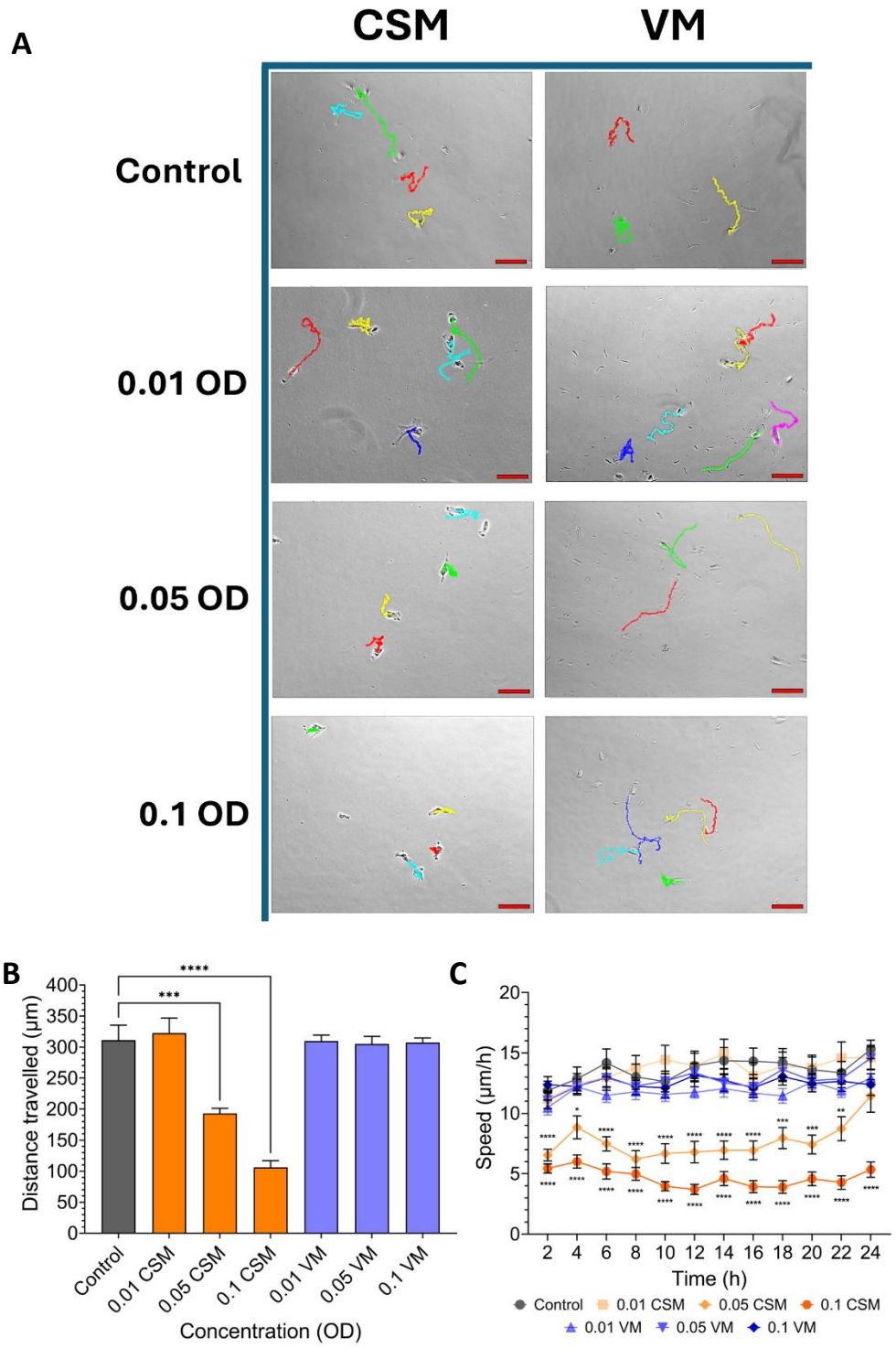

Figure 3.11. Effect of CSM and VM on AB1190 myoblast migration. Cells were exposed to CSM and VM then monitored for 24 hours using timelapse microscopy. (A) representative images of cell migration tracks (coloured lines) and (B) the distance travelled after 24 hours. (C) the average speed of myoblasts during the 24-hour timelapse. Data presented as the mean +/- SEM using one-way ANOVA with Dunnett's multiple comparison test for the distance travelled. A two-way ANOVA with Dunnett's multiple comparison test was used for the analysis of the speed. *p<0.05, **p<0.01, ***p<0.001, ****p<0.0001, (n=3) scale bar is 100µm.

3.12

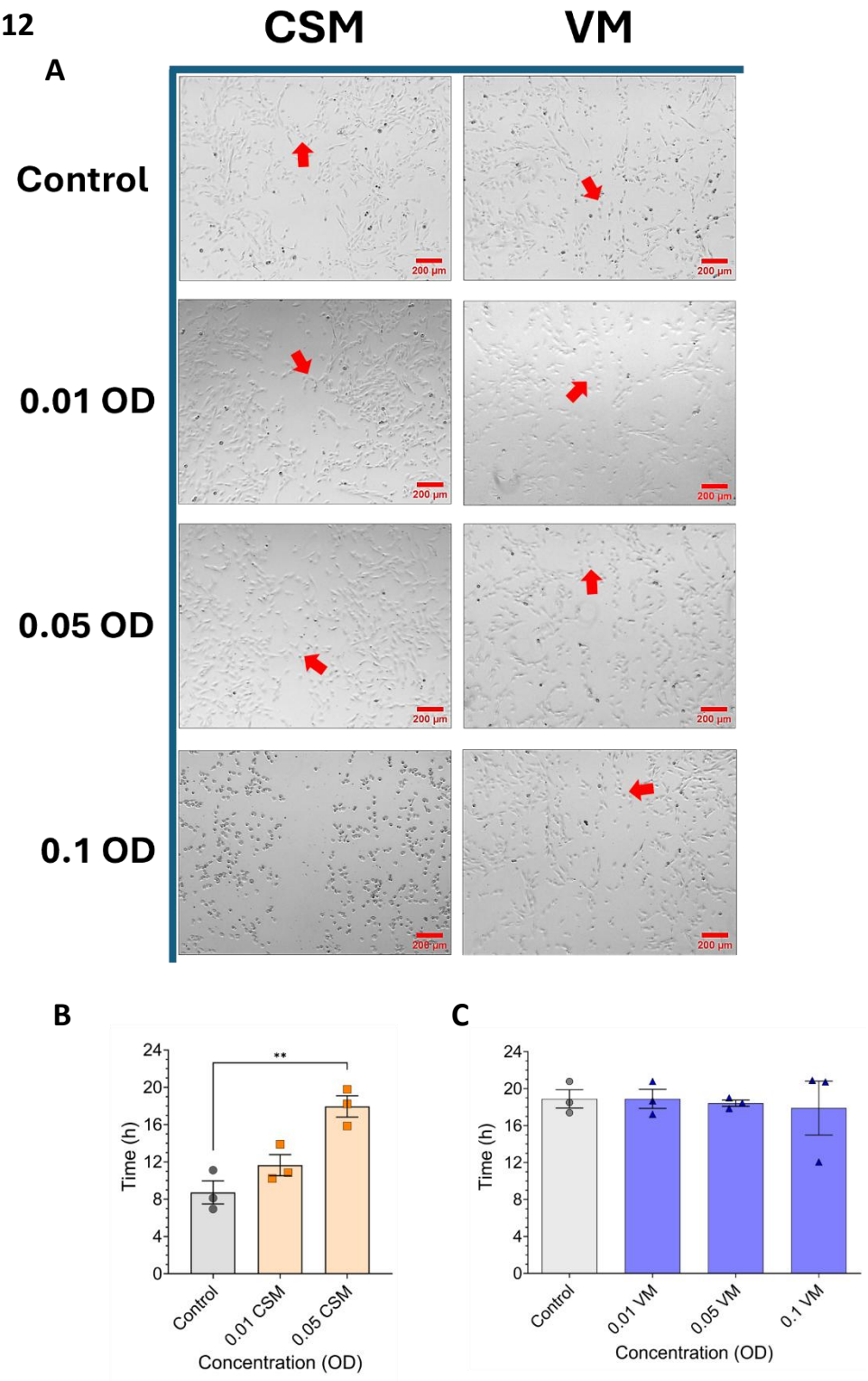

Figure 3.12. Scratch assay of AB1190 myoblasts. Cells were plated overnight then a scratch was formed across the face of the well. This was followed by exposing to CSM or VM and monitoring using a timelapse microscope for 24 hours. (A) representative images of the end of the experiment (arrows indicate cells meeting). The time taken for the first cell to meet another from the other side with CSM (B) and VM (C) was used as the scratch closure time. Data presented as the mean +/- SEM using one-way ANOVA with Dunnett's multiple comparison test. **p<0.01, (n=3) scale bar is 200µm.

3.2.5. Examining impact of CSM and VM on focal adhesions.

The ability of a cell to adhere to the extracellular matrix and respond to external stimulatory factors can determine the cell's fate, proliferation, migration and differentiation (Turner, 2000). Focal adhesions play a critical role in cell motility. They form connection points to the extracellular matrix and undergo cycles of turnover allowing the cell to crawl along surfaces (Choi et al., 2020). Investigating the effect of CSM and VM on focal adhesions (FA) and filamentous actin / stress fibres (SF) was developed to explain why decreased motility was observed previously. The C_2C_{12} (figure 3.13 A) underwent conditioned media exposure for at least 4 hours before fixing and staining for paxillin, and filamentous actin (using phalloidin). Paxillin is a protein located at focal adhesions and phalloidin is an extract that binds tightly to filamentous actin revealing cellular cytoskeleton (Melak et al., 2017; Turner, 2000). C_2C_{12} cells exposed to 0.05 OD CSM had no change in the number of focal adhesions or the number of stress fibres compared to the control, however there was a significant decrease in the total area of focal adhesions and stress fibres (figure 3.13 B). Furthermore, with VM the number and total area of focal adhesions along with total area of stress fibres were significantly higher than the control (figure 3.13 C).

3.13

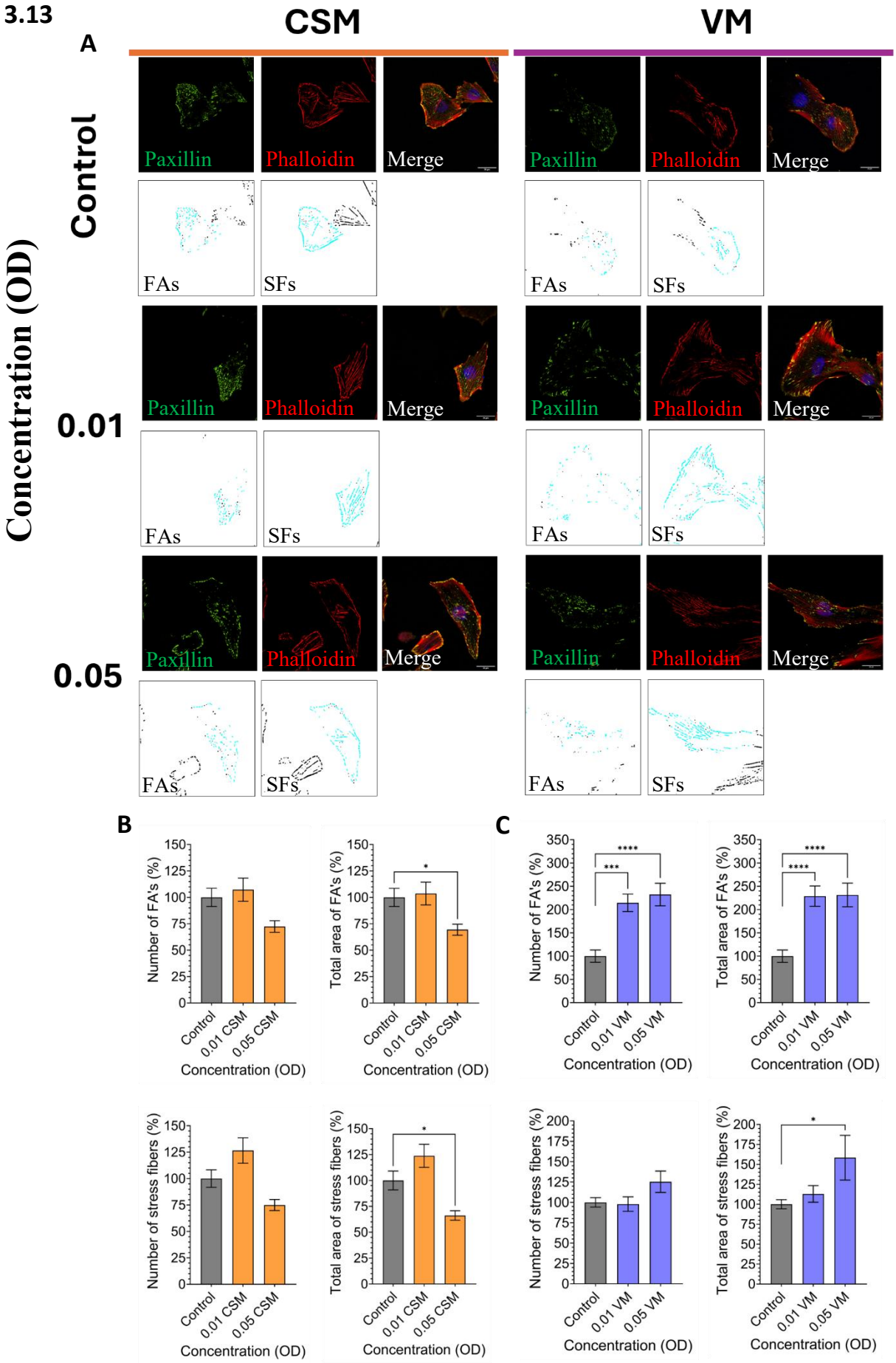
A
CSM
VM
Concentration (OD)
Control
0.01
0.05
Paxillin
Phalloidin
Merge
FAs
SFs
B
C
Number of FA's (%)
Total area of FA's (%)
Number of stress fibers (%)
Total area of stress fibers (%)
Control
0.01 CSM
0.05 CSM
0.01 VM
0.05 VM
Concentration (OD)

Figure 3.13. Effect of CSM and VM on C_2C_{12} focal adhesions. The cells were exposed to different concentrations of CSM and VM for at least 4 hours before they were fixed and stained. (A) representative images of CSM and VM exposed myoblasts stained with paxillin, phalloidin and DAPI. The number and area of focal adhesions with stress fibres of (B) CSM and (C) VM exposed myoblasts. Data presented as the mean +/- SEM using one-way ANOVA with Dunnett's multiple comparison test. *p<0.05, ***p<0.001, ****p<0.0001, (n=4) scale bar is 20µm.

When the AB1190 myoblasts (figure 3.14 A) were examined an increase in the number and total area of focal adhesions was seen in the cells exposed to 0.05 OD CSM, furthermore a decrease in the number of stress fibres was observed in the 0.01 OD CSM cohort (figure 3.14 B). Moreover, the VM had no significant effect on the number and area of either the focal adhesions or stress fibres (figure 3.14 C).

3.14

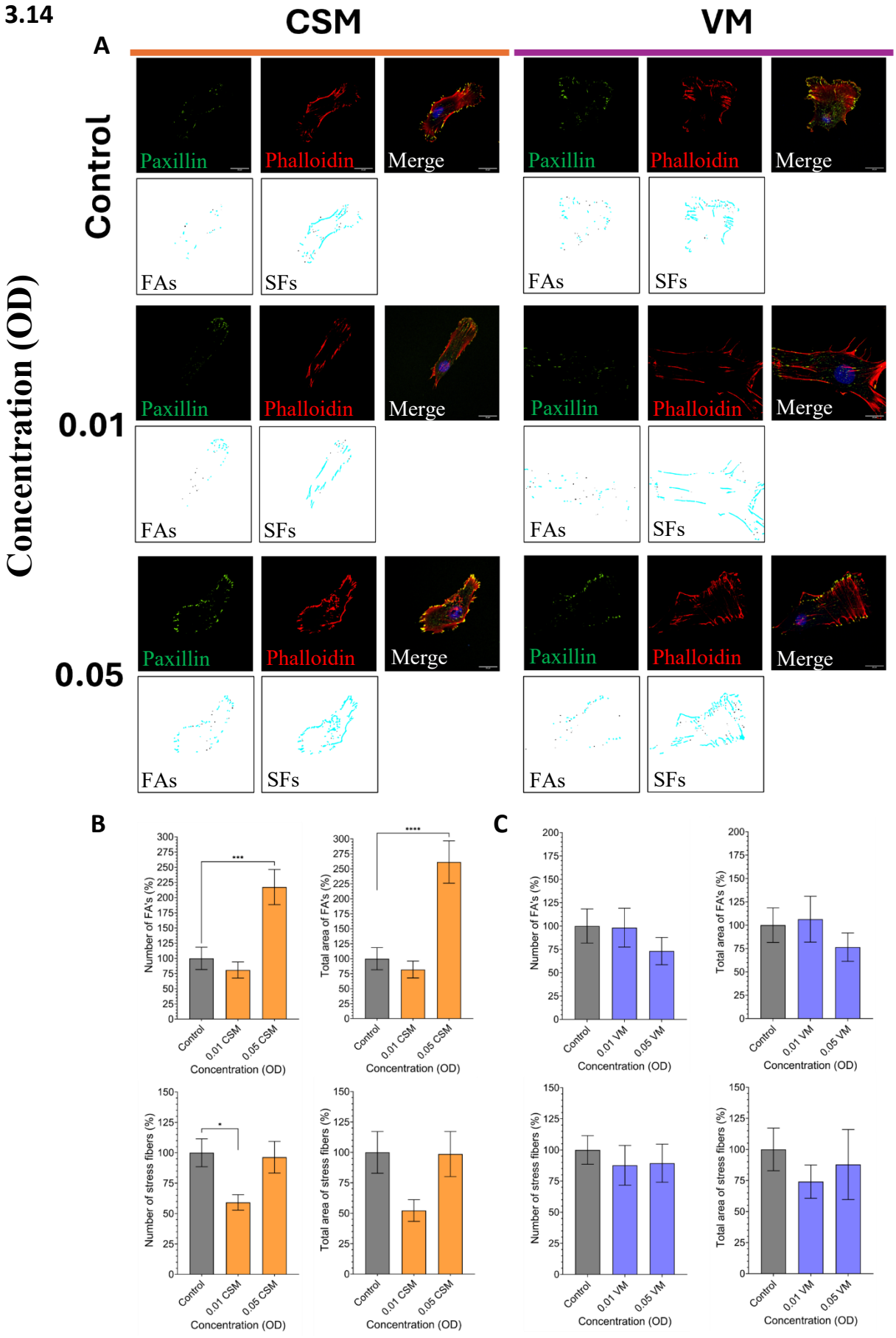
CSM
VM
A
Control
0.01
0.05
Concentration (OD)
Paxillin
Phalloidin
Merge
FAs
SFs
B
C
Number of FA's (%)
Total area of FA's (%)
Number of stress fibers (%)
Total area of stress fibers (%)
Control
0.01 CSM
0.05 CSM
0.01 VM
0.05 VM
Concentration (OD)

Figure 3.14. Effect of CSM and VM on AB1190 focal adhesions. The cells were exposed to different concentrations of CSM and VM for at least 4 hours before they were fixed and stained. (A) representative images of conditioned media exposed myoblasts stained with paxillin, phalloidin and DAPI. The number and area of focal adhesions with stress fibres of (B) CSM and (C) VM exposed myoblasts. Data presented as the mean +/- SEM using one-way ANOVA with Dunnett's multiple comparison test. *p<0.05, ***p<0.001, ****p<0.0001, (n=4) scale bar is 20µm.

3.2.6. CSM and VM affect myogenic differentiation and fusion.

To determine the impact of the conditioned media on myogenic differentiation and fusion, C_2C_{12} cells were cultured to 85% confluence followed by induction of differentiation by changing the growth media (GM) to differentiation media (DM) containing the various concentrations of CSM or VM and then incubating them a further 5 days (figure 3.15).

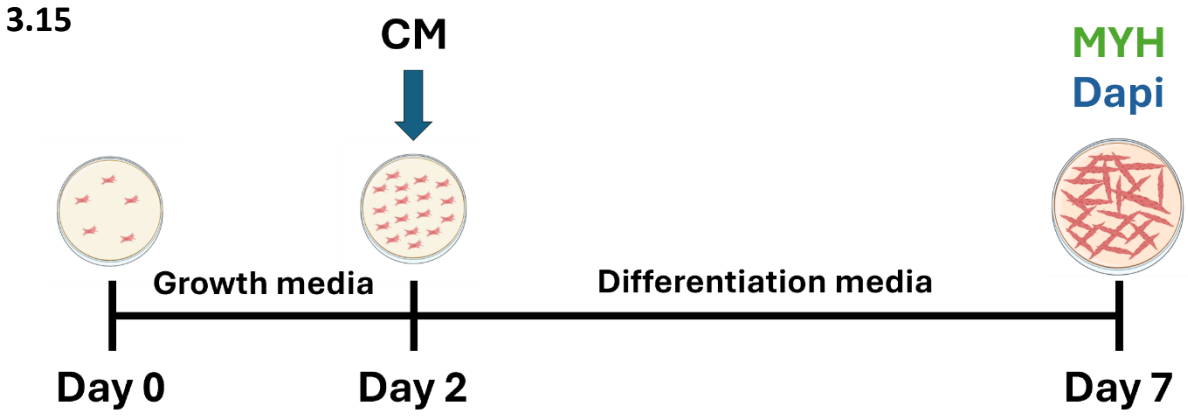

Figure 3.15. Schematic representation of the procedure used to investigate the effect of both the conditioned media (CM) on C_2C_{12} myoblast fusion.

After differentiation, staining for myosin heavy chain 1 (MYH1) to identify the myotubes was performed. The addition of CSM resulted in myotubes smaller than control (figure 3.16 A). Furthermore, when the fusion index (FI) was calculated, (by counting the number of nuclei within myotubes and calculating it as a percentage from the total number of nuclei), a significant decrease in all concentrations of CSM was seen (figure 3.16 B).

3.16

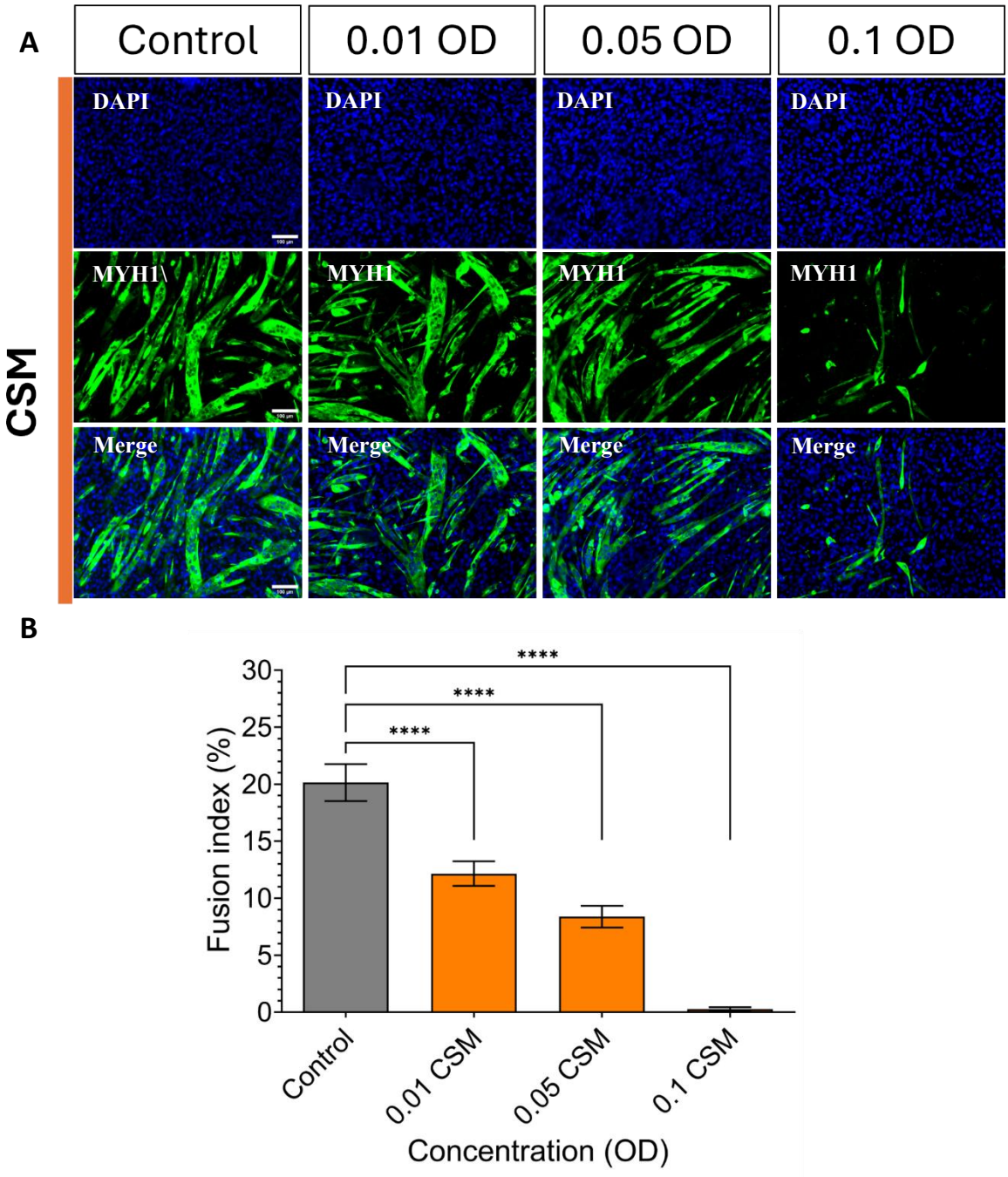

Figure 3.16. Impact of CSM on C_2C_{12} fusion. (A) Representative images of MYH1 stained myotubes incubated with various concentrations of CSM. (B) The percentage of fusion index was quantified and compared to the control. Data presented as the mean +/- SEM using one-way ANOVA with Dunnett's multiple comparison test. ****p<0.0001, (n=3) scale bar is 100µm.

The impact of VM on C_2C_{12} fusion capabilities was tested by incubating the cells with VM and initiating differentiation. After staining MYH1 (figure 3.17 A) the myotubes that were exposed to the 0.05 OD CSM (used as a positive control) and the higher concentrations of VM appeared smaller than the control, furthermore, the fusion index was found to be significantly lower in 0.05 OD & 0.1 OD of VM (figure 3.17 B).

3.17

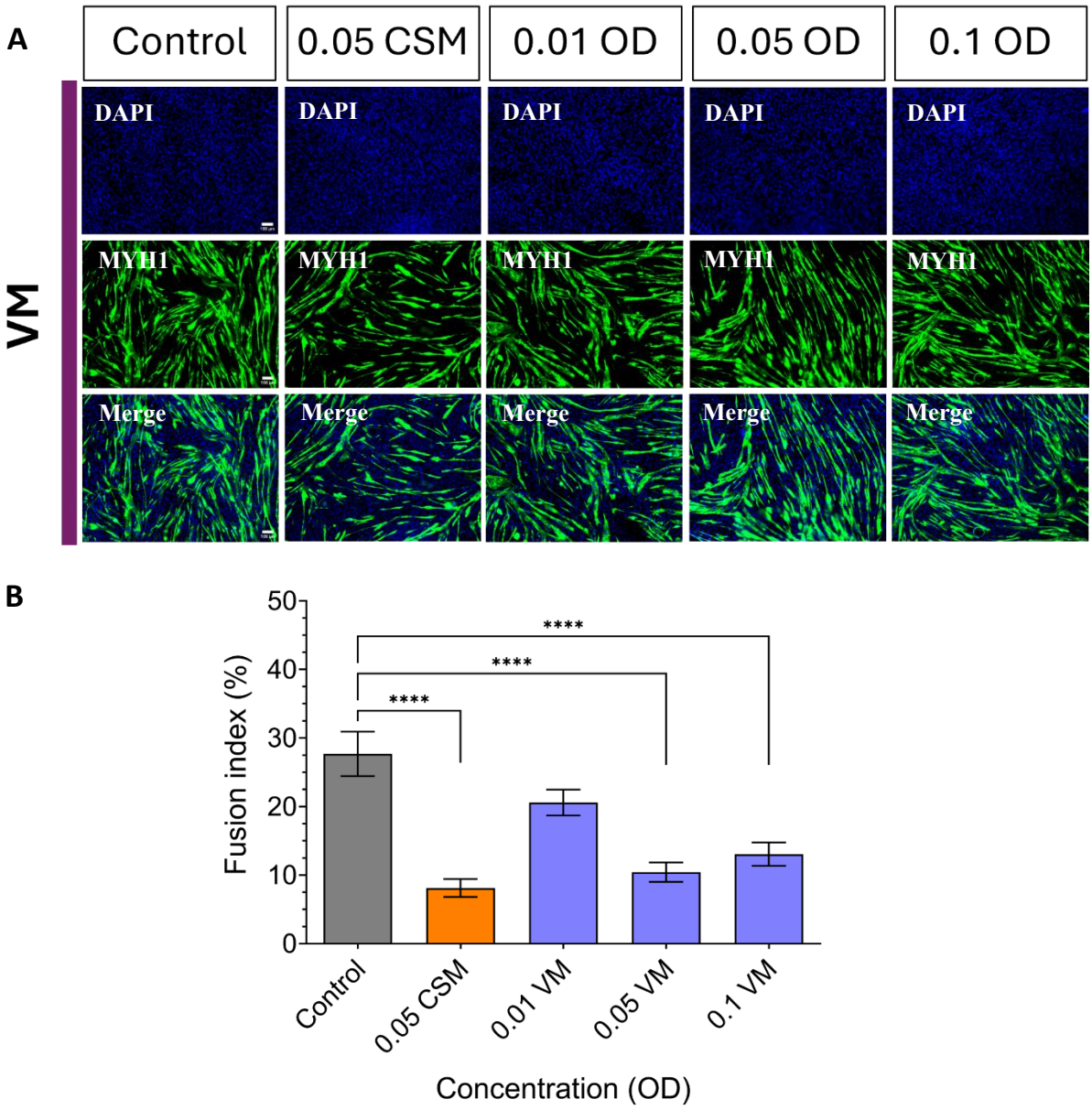

Figure 3.17. Impact of VM on C_2C_{12} fusion. (A) Representative images of MYH1 stained myotubes incubated with various concentrations of VM. (B) The percentage of fusion index was quantified and compared to the control. Data presented as the mean +/- SEM using one-way ANOVA with Dunnett's multiple comparison test. ****p<0.0001, (n=3) scale bar is 100µm.

Based on these findings, the experiment was repeated with the human AB1190 cell line to investigate if they responded in a similar manner. The cells were grown to confluence then induced to differentiate for at least 72 hours (AB1190 differentiate quicker than C_2C_{12}) with various concentrations of CSM and VM (figure 3.18) before immunostaining.

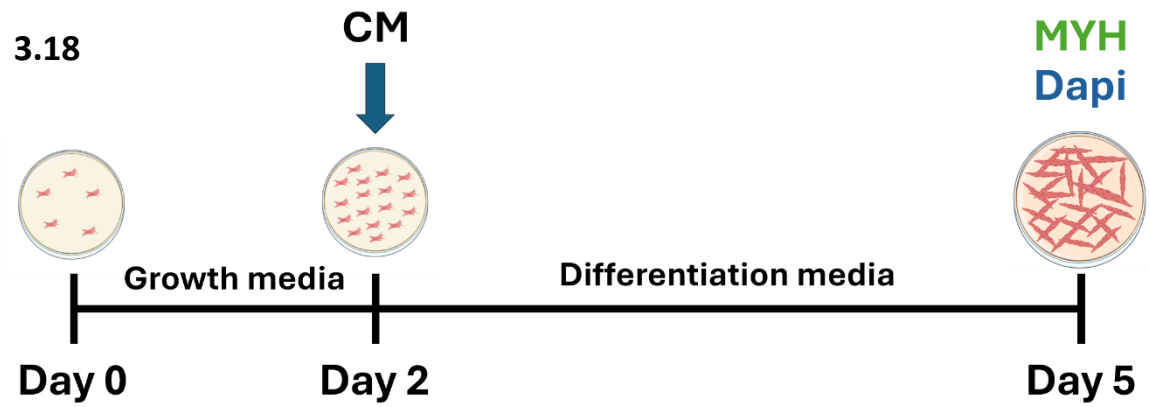

Figure 3.18. Schematic representation of the procedure used to investigate the effect of conditioned media (CM) on AB1190 myoblast fusion. The AB1190 cell line differentiates quicker than the C_2C_{12}.

From the myosin staining it was visible that the myotubes formed were smaller in size and had fewer nuclei within as the concentration of CSM and VM increased (figure 3.19 A). Furthermore, when the fusion index was calculated a significant decline was observed in all concentrations of CSM (figure 3.19 B) and in the two higher concentrations of VM (figure 3.19 C).

3.19

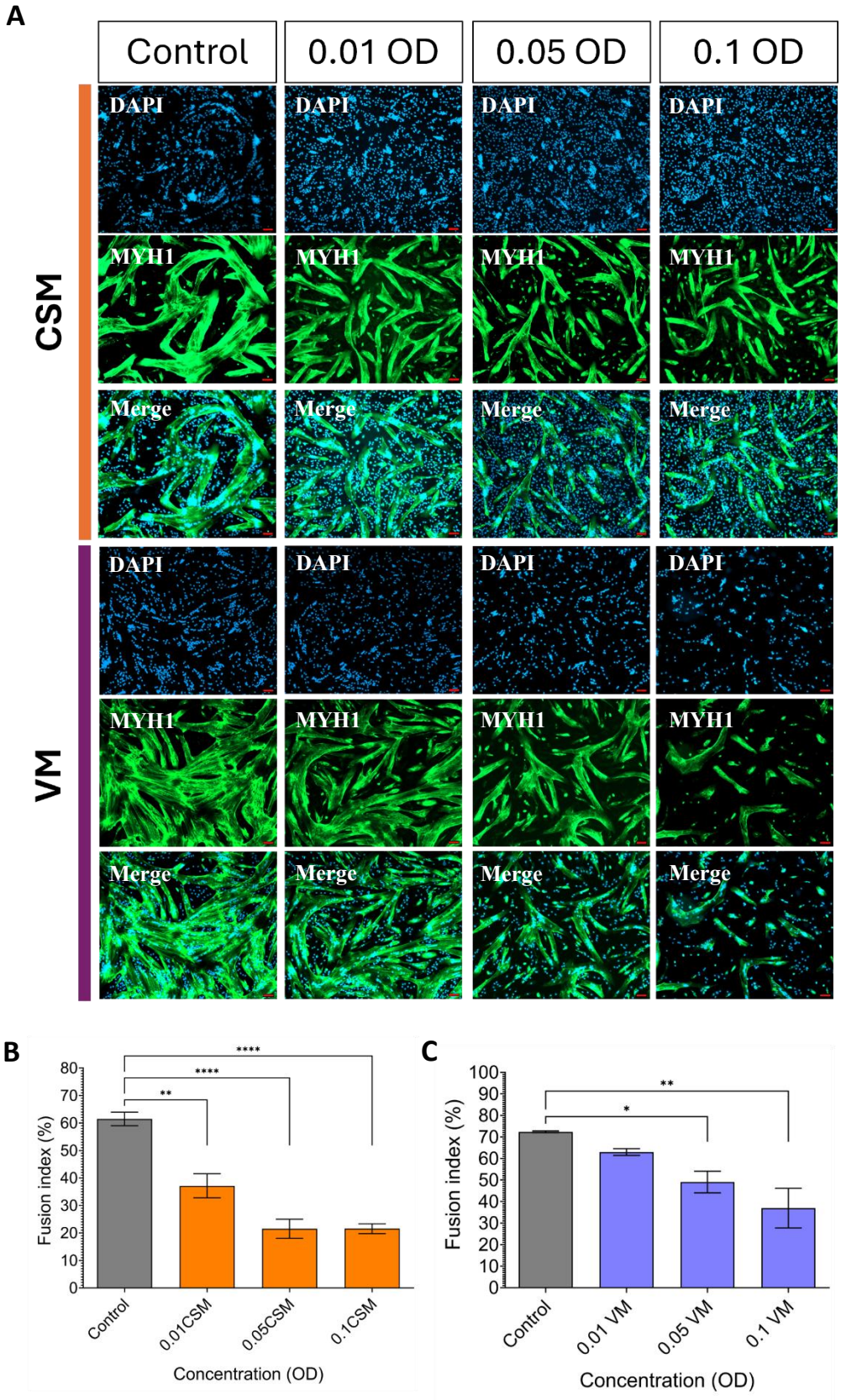

Figure 3.19. Impact of CSM and VM on AB1190 fusion. (A) Representative images of MYH1 stained myotubes incubated with various concentrations of CSM and VM. (B) quantification of the fusion index of CSM, and (C) VM. Data presented as the mean +/- SEM using one-way ANOVA with Dunnett's multiple comparison test. *p<0.05, **p<0.01, ***p<0.001, ****p<0.0001, (n=3) scale bar is 100 µm.

3.2.7. Only Cigarette smoke media caused myotube atrophy.

Muscle atrophy can occur due to inactivation, damage and denervation but also in response to systemic influences such as aging, malnutrition and disease. The C_2C_{12} and AB1190 cell lines were used to assess whether the conditioned media causes atrophy in-vitro. The myoblasts were cultured until confluence then differentiated, once myotubes had formed (72 hours for AB1190, 120 hours for C_2C_{12}) the media was changed to include different concentrations of CSM or VM and then cultured for a further 24 hours (figure 3.20, figure 3.23).

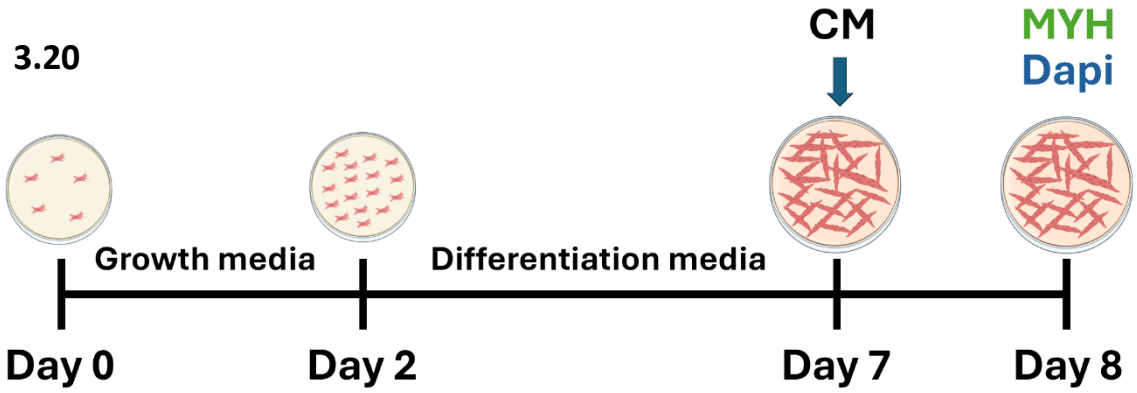

Figure 3.20. Experimental procedure used to investigate the effect of the conditioned media (CM) on C_2C_{12} myotube atrophy.

Once incubation with the conditioned media was completed, the cells were stained for MYH1 and imaged. After 24 hours with CSM the area of MYH1 was significantly lower in both 0.05 OD and 0.1 OD (figure 3.21 A, B). However, myotubes exposed to VM exhibited no change (figure 3.22 A, B).

3.21

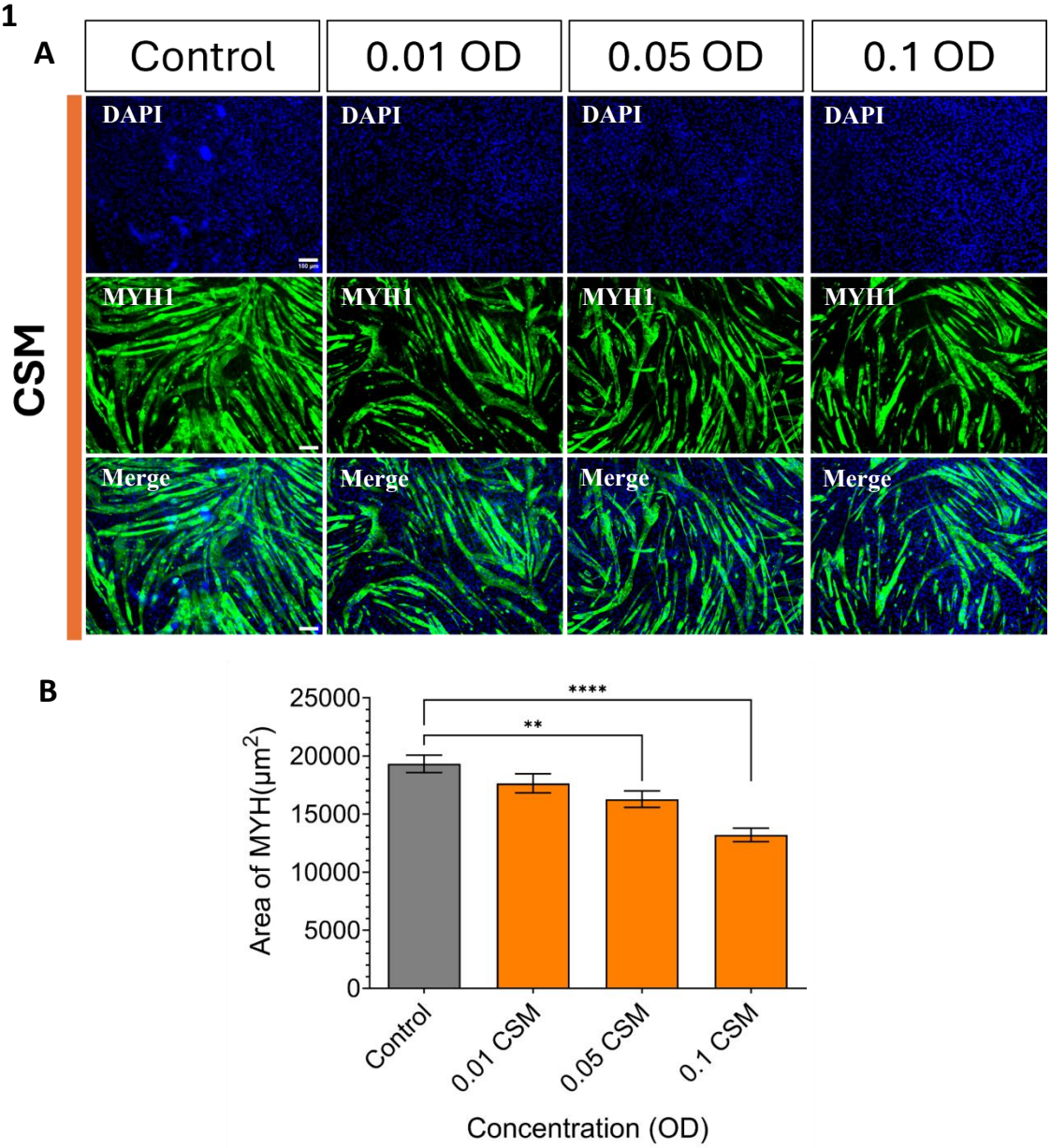

Figure 3.21. Impact of CSM on C_2C_{12} myotubes. (A) Representative images of MYH1 stained myotubes incubated with various concentrations of CSM. (B) quantification of the area of the myotubes. Data presented as the mean +/- SEM using one-way ANOVA with Dunnett's multiple comparison test. **p<0.01, ****p<0.0001, (n=3) scale bar is 100μm.

3.22

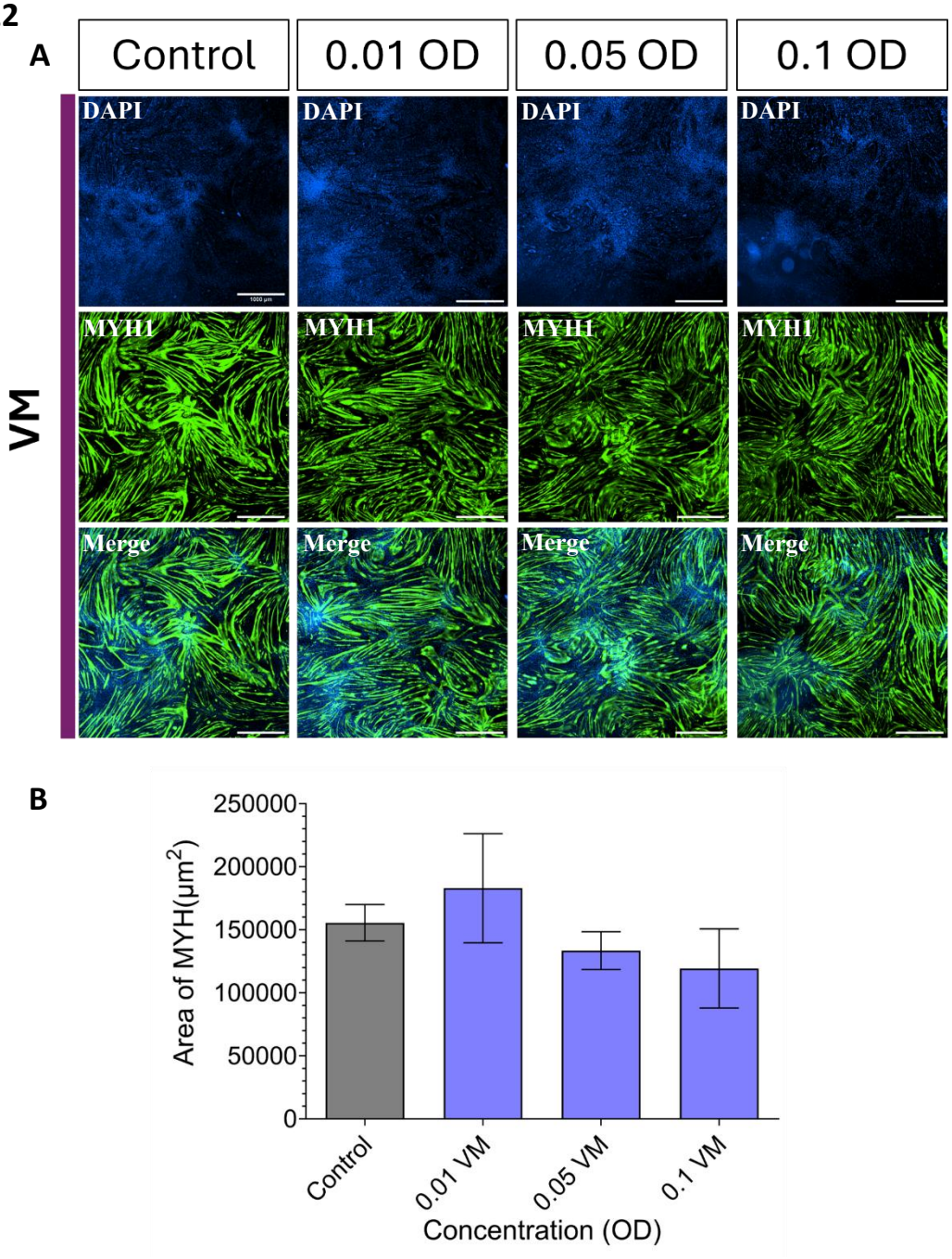

Figure 3.22. Impact of VM on C_2C_{12} myotubes. (A) Representative images of MYH1 stained myotubes incubated with various concentrations of VM. (B) quantification of the area of the myotubes. Data presented as the mean +/- SEM using one-way ANOVA with Dunnett's multiple comparison test. (n=3) scale bar is 1000µm.

AB1190 myotubes cultured with CSM and VM proved more robust than the C_2C_{12} cells. After 24 hours with CSM the area of myotubes exhibited a concentration dependent decrease from 0.1 OD, albeit only 0.24 OD was significant (figure 3.24 A, C). The myotubes exposed to VM demonstrated no change (figure 3.24 B, C).

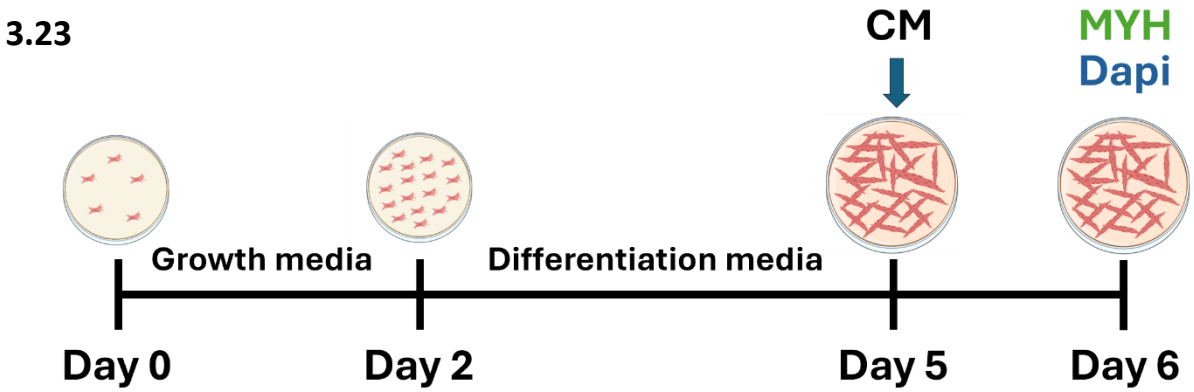

Figure 3.23. Experimental procedure used to investigate the effect of the conditioned media (CM) on AB1190 myotube atrophy.

3.24

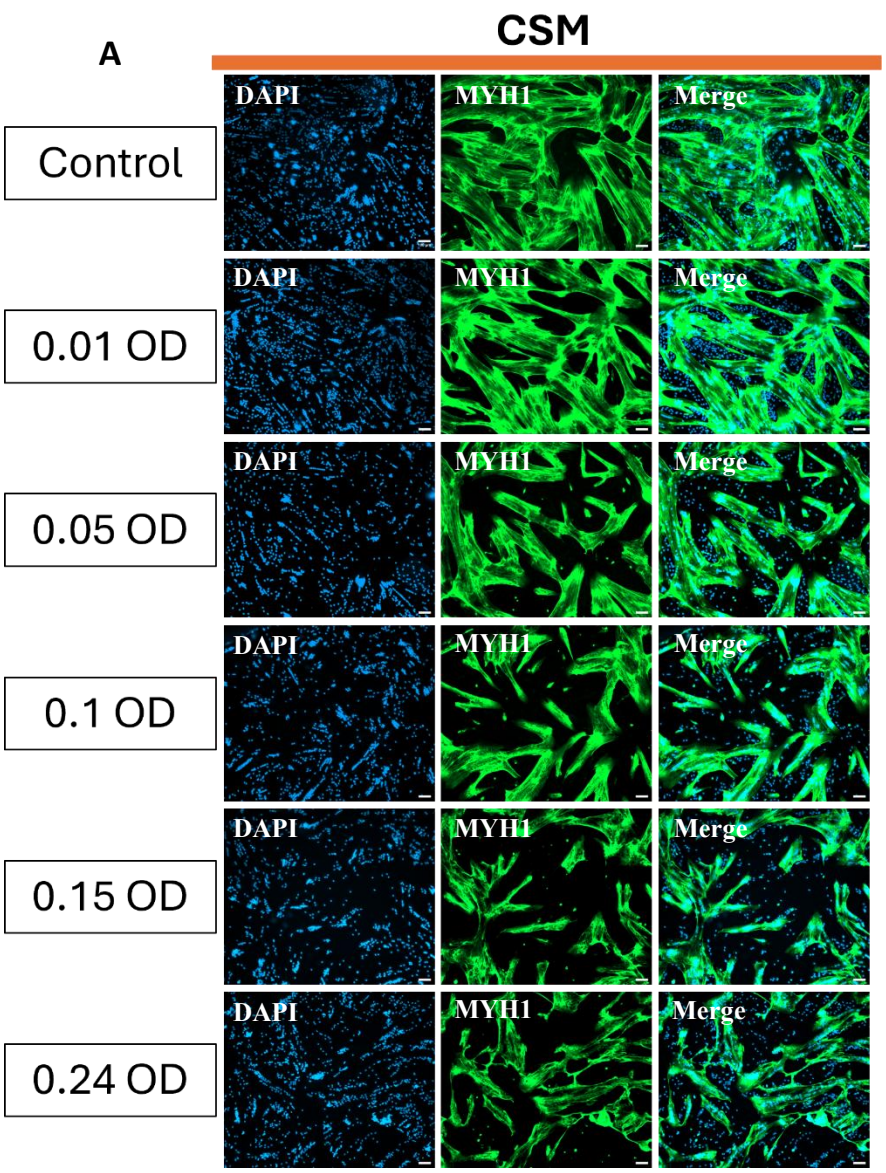

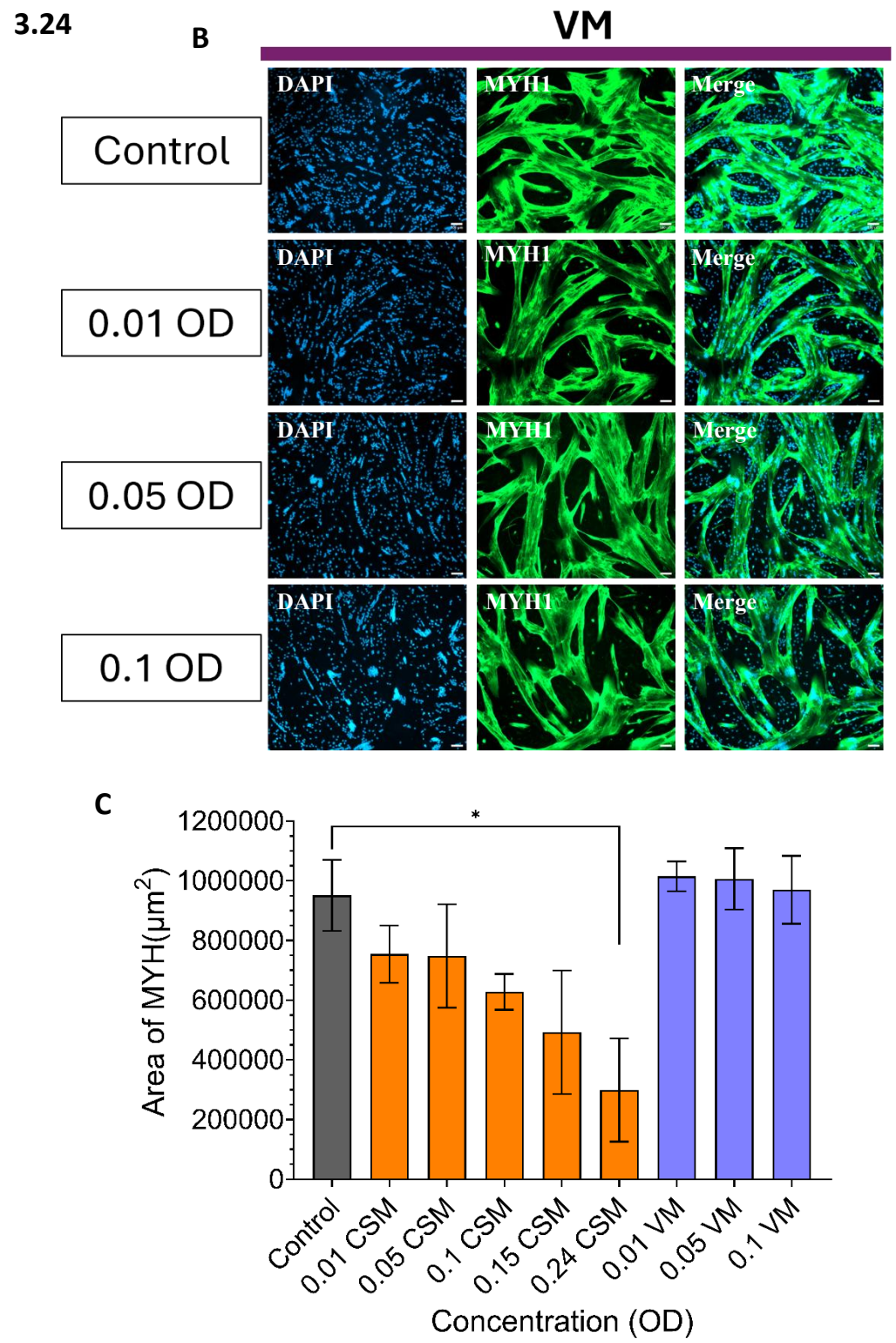

Figure 3.24. Impact of CSM and VM on AB1190 myotubes. Representative images of MYH1 stained myotubes incubated with various concentrations of (A) CSM and (B) VM. (C) quantification of the area of the myotubes. Data presented as the mean +/- SEM using one-way ANOVA with Dunnett's multiple comparison test. *p<0.05, (n=3), scale bar is 100µm.

Following these findings another experiment was performed where the myotubes were cultured for 48 hours with 0.1 OD CSM and 0.1 OD VM (figure 3.25 A). We wanted to find out if longer exposure even to a lower concentration of CSM would have an effect. This resulted in a significant decrease in the area of myotubes with CSM (figure 3.25 B, C). With VM we observed a decrease in the area, however it was not significant (figure 3.25 D, E).

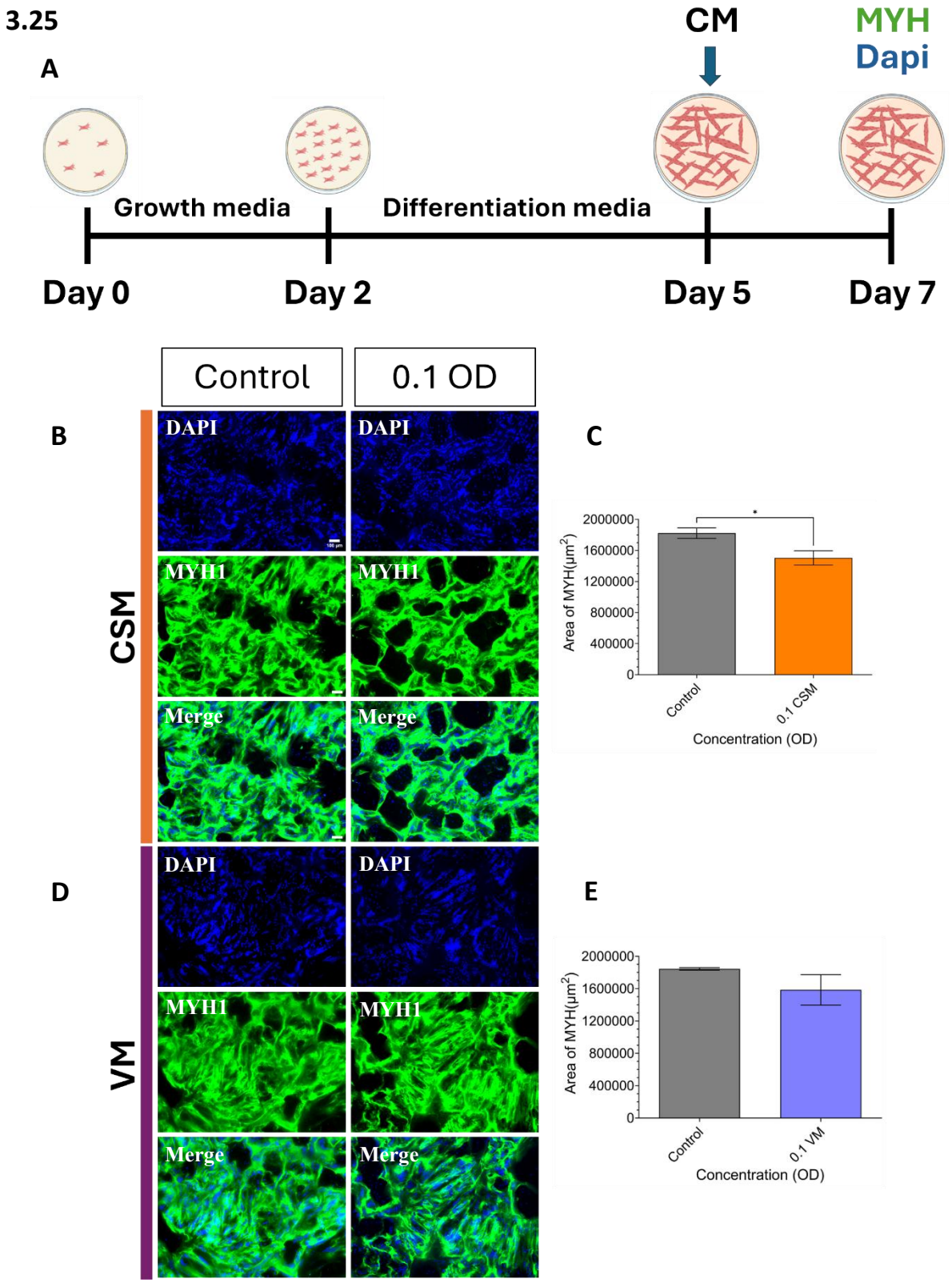

Figure 3.25. Impact of extended incubation (48 hours) of conditioned media (CM) on AB1190 myotubes. (A) Schematic representation of the experimental timeline. Representative images of MYH1 stained myotubes incubated with (B) 0.1 OD CSM and (D) 0.1 OD VM. (C, E) quantification of the area of the myotubes. Data presented as the mean +/- SEM using a Student's t-test. *p<0.05, (n=3), scale bar is 100µm.

3.2.8. A myostatin ligand trap (sActRIIB) rescues CSM induced atrophy.

Myostatin is part of the transforming growth factor-β (TGF-β) family and predominantly expressed in skeletal muscle tissue. It acts as a negative regulator of skeletal muscle growth (Grobet et al., 1997; McPherron et al., 1997). Therefore, compounds that target myostatin and activin, such as soluble activin receptor IIB (sActRIIB), and block the signaling pathway have been found to cause hypertrophy in mice (Lee et al., 2005). An experiment using sActRIIB was set up to investigate if CSM induced atrophy could be prevented (figure 3.26). The myoblasts were cultured until confluence and differentiated. Then we exposed the C_2C_{12} to 0.05 OD CSM with 1µg/mL sActRIIB for 24 hours (figure 3.27), while AB1190 cells were incubated with 0.24 OD CSM and 1µg/mL sActRIIB for the same duration (figure 3.28). The difference in CSM concentrations used was due to the 0.05 OD CSM producing an effect on the C_2C_{12} myotubes whereas AB1190 myotubes showed no impact. The AB1190 myotubes were more robust and therefore the higher concentration of 0.24 OD CSM was used to elicit a significant effect. The addition of 1µg/mL of sActRIIB resulted in the "rescue" of both myotube cell lines after exposure to an atrophy inducing concentration of CSM (figure 3.27 and 3.28).

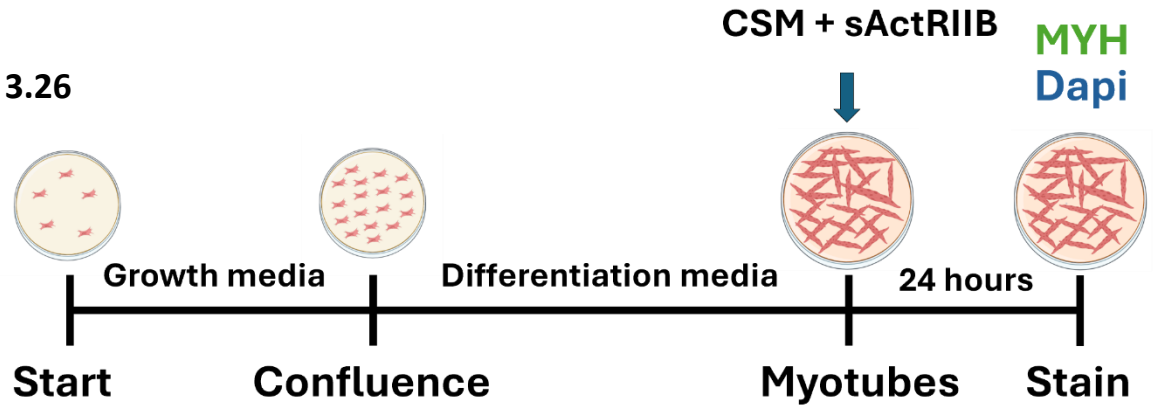

Figure 3.26. Experimental design used to investigate CSM atrophy induced prevention by sActRIIB.

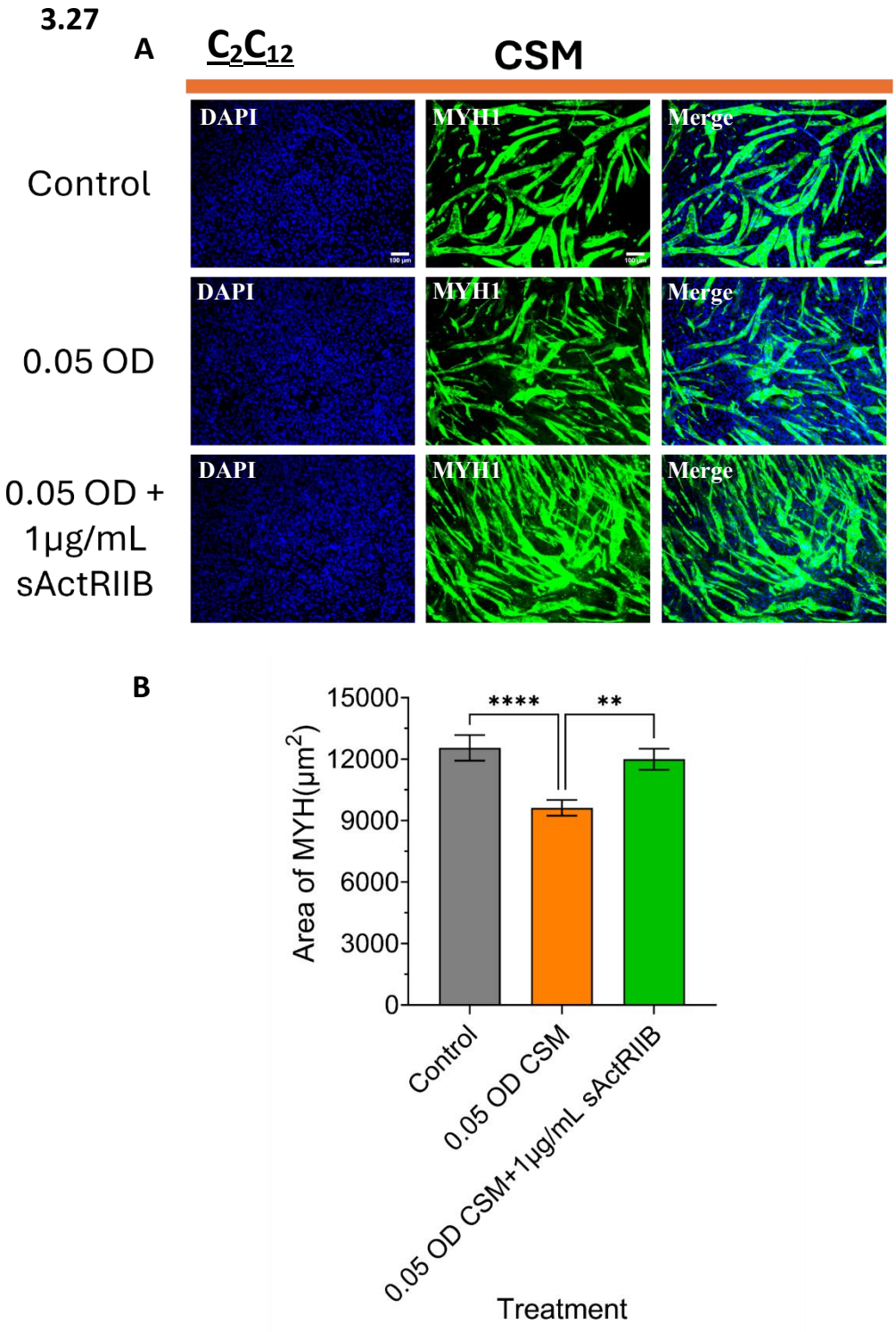

Figure 3.27. Impact of sActRIIB on C_2C_{12} CSM induced atrophy. (A) Representative images of MYH1 stained myotubes incubated with 0.05 OD CSM and sActRIIB. (B) quantification of the area of the myotubes. Data presented as the mean +/- SEM using one-way ANOVA with Bonferroni's multiple comparison test. **p<0.01, ****p<0.0001 (n=3), scale bar is 100µm.

3.28

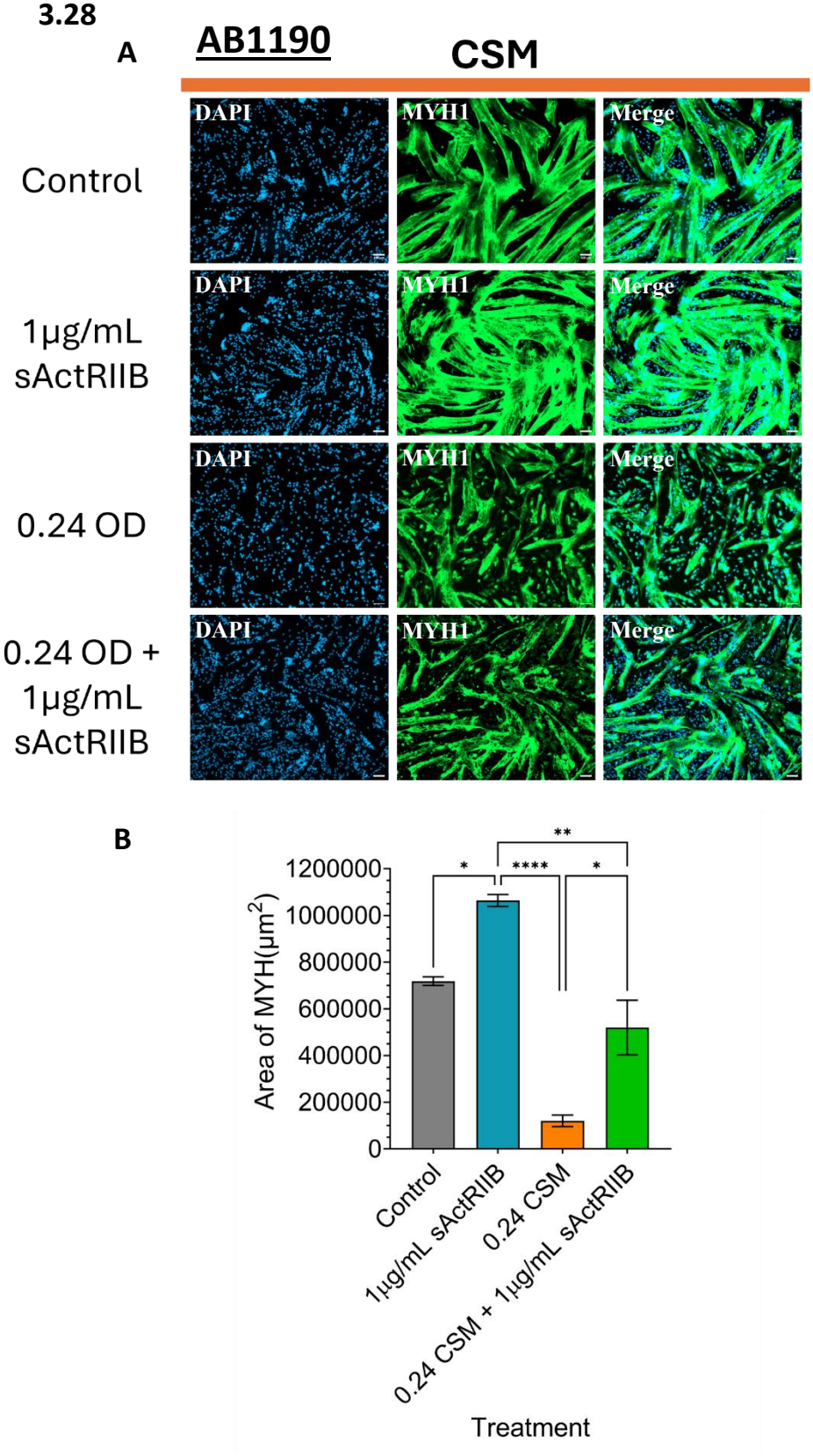

Figure 3.28. Impact of sActRIIB on AB1190 CSM induced atrophy. (A) Representative images of MYH1 stained myotubes incubated with 0.24 OD CSM and sActRIIB. (B) quantification of the area of the myotubes. Data presented as the mean +/- SEM using one-way ANOVA with Bonferroni's multiple comparison test. *p<0.05, **p<0.01, ****p<0.0001 (n=3), scale bar is 100µm.

3.2.9. Conditioned media increased the area of nucleoli.

Cell organelles control cell behavior, each structure has a specific role that contributes to overall health of the cell. We observed dysfunctional muscle cells in our previous experiments. We therefore investigated the effect of CSM and VM on nuclei, nucleoli, mitochondria and cytoskeleton (Schieweck & Gotz, 2024). The nucleolus, a nuclear organelle involved in the regulation of the cell cycle under stress or in response to damage, produces and assembles ribosomes which are essential for protein synthesis (Cmarko et al., 2008). Fibrillarin is a nucleolar protein involved in ribosome assembly and plays an essential role in cell growth (Amin et al., 2007). To investigate how the nucleoli respond the AB1190 myoblasts and myotubes were exposed to both conditioned media for 24 hours. Subsequently, fixed and immuno-stained for fibrillarin; a nucleolar stain, and with phalloidin; stains the actin filaments to visualize the cytoskeleton (figure 3.29 A). Consequently, myoblasts exhibited no significant change in the area or number of nucleoli (figure 3.29 B and C). When the same investigation was carried out on myotubes (figure 3.30 A) a significant increase in the area of nucleoli was observed in both CSM and VM (figure 3.30 B), additionally there was a significant decrease in the number of nucleoli with CSM alone (figure 3.30 C). The increased size of nucleoli after exposure to CSM and VM suggests stress induced dysfunction. An increased nucleolar size has been associated with neoplasms such as prostate cancer (Koh et al., 2011).

3.29

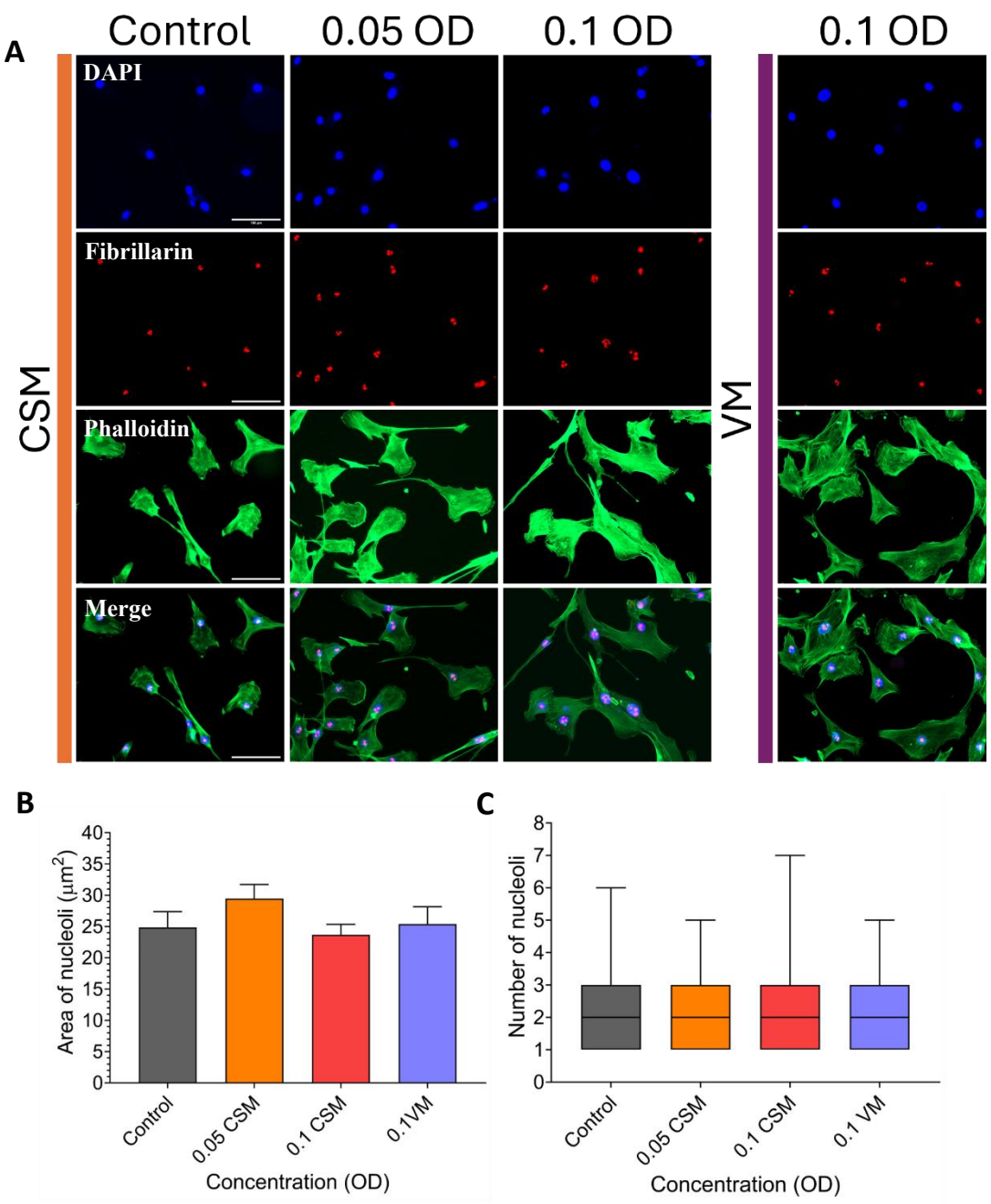

Figure 3.29. Impact of CSM and VM on the nucleoli of AB1190 myoblasts. Myoblasts were exposed to CSM or VM for 24 hours then stained with fibrillarin and phalloidin to show the nucleoli and cell cytoskeleton. (A) Representative images of myoblasts after 24 hours exposure to CSM or VM. (B) quantification of the area of nucleoli, and (C) number of nucleoli counted. Data presented as the mean +/- SEM using one-way ANOVA with Dunnett's multiple comparison test. (n=3), Scale bar is 100µm.

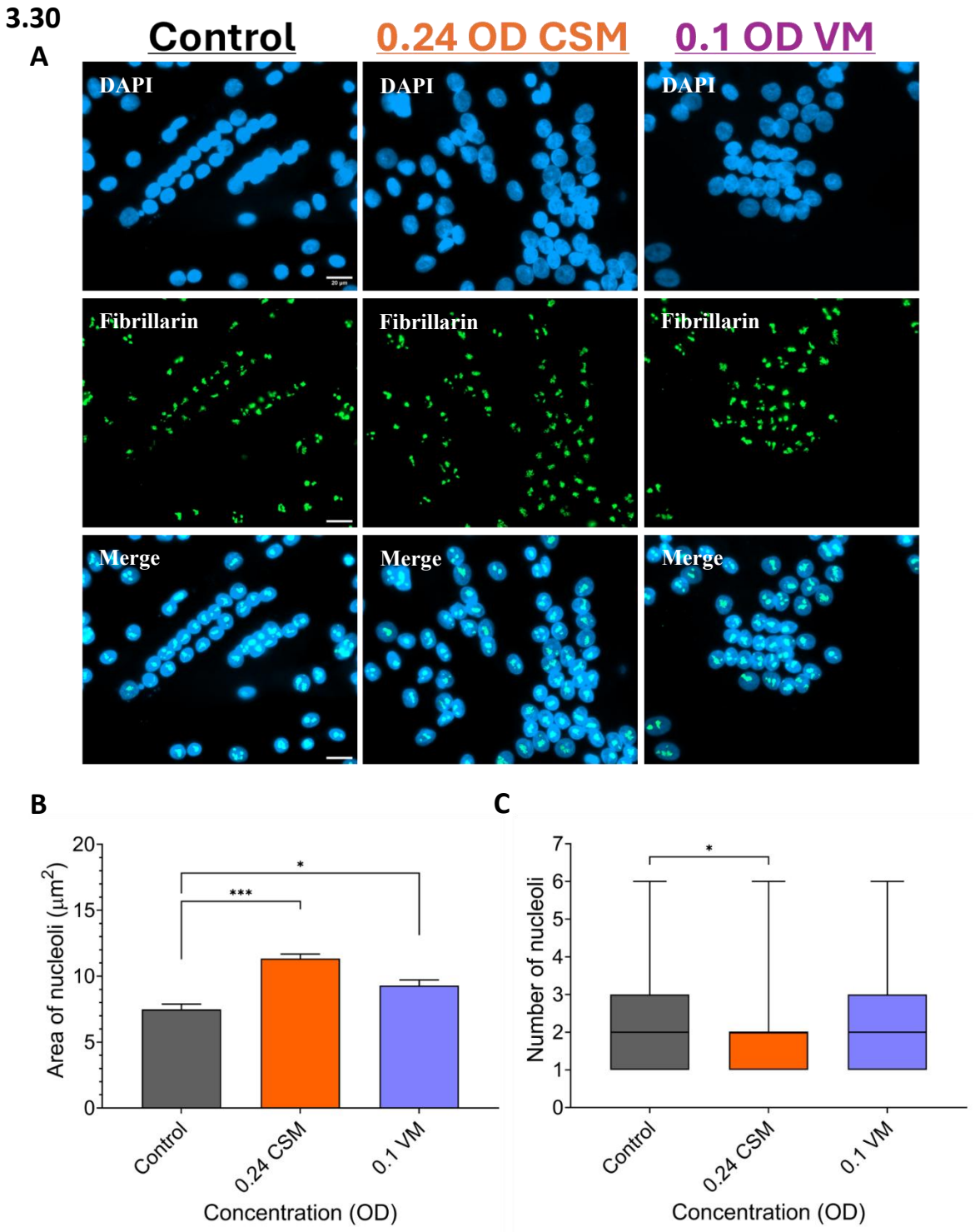

Figure 3.30. Impact of CSM and VM on the nucleoli of AB1190 myotubes. Myotubes were exposed to CSM or VM for 24 hours then stained with fibrillarin to show the nucleoli. (A) Representative images of myotubes after 24 hours exposure to CSM or VM. (B) quantification of the area of nucleoli, and (C) number of nucleoli counted. Data presented as the mean +/- SEM using a one-way ANOVA with Dunnett's multiple comparison test. *p<0.05, ***p<0.001 (n=3), scale bar is 20µm.

3.2.10. CSM and VM affect AB1190 mitochondria and nucleus.

Mitochondria are membranous organelles responsible for the cell's energy production. They are responsible for the regulation of cellular metabolism and play a critical role in apoptosis. Mitochondrial dysfunction caused by cigarette smoke (CS) increases reactive oxygen species (ROS) production, alters mitochondrial membrane potential, reduces respiration and leads to apoptosis in lung tissue and cells (Kanithi et al., 2022) (Maremanda et al., 2021). We investigated the effect of 0.05 OD, 0.1 OD CSM and 0.1 OD VM on AB1190 cell line by incubating for 3 hours. The switch to a shorter incubation period from 24 hours was because we believed that mitochondrial dysfunction due to CSM exposure occurs rapidly. Afterwards, staining with Mitotracker™ for mitochondrial labelling, Calcein green for cytoplasmic staining of live cells and DAPI for the nucleus (figure 3.31 A) was performed. This was then followed by interrogating multiple parameters using the Oparetta® high content imaging system. We observed a significant decrease in the number of nuclei (figure 3.31 B) and intensity of DAPI staining (figure 3.31 E) with 0.1 OD in both CSM and VM. A significant decrease in the area of nucleus in all concentrations of both conditioned media (figure 3.31 C). A significant increase in the nuclear roundness with all conditioned media concentrations (figure 3.31 D). There was a significant drop in cell area (figure 3.31 F) with 0.1 OD CSM only and all concentrations of conditioned media in the intensity of cytoplasmic staining (figure 3.31 H). Finally, the area of mitochondrial staining was significantly higher with 0.05 OD CSM (figure 3.31 I) and the staining intensity was significantly higher with 0.1 OD VM.

3.31

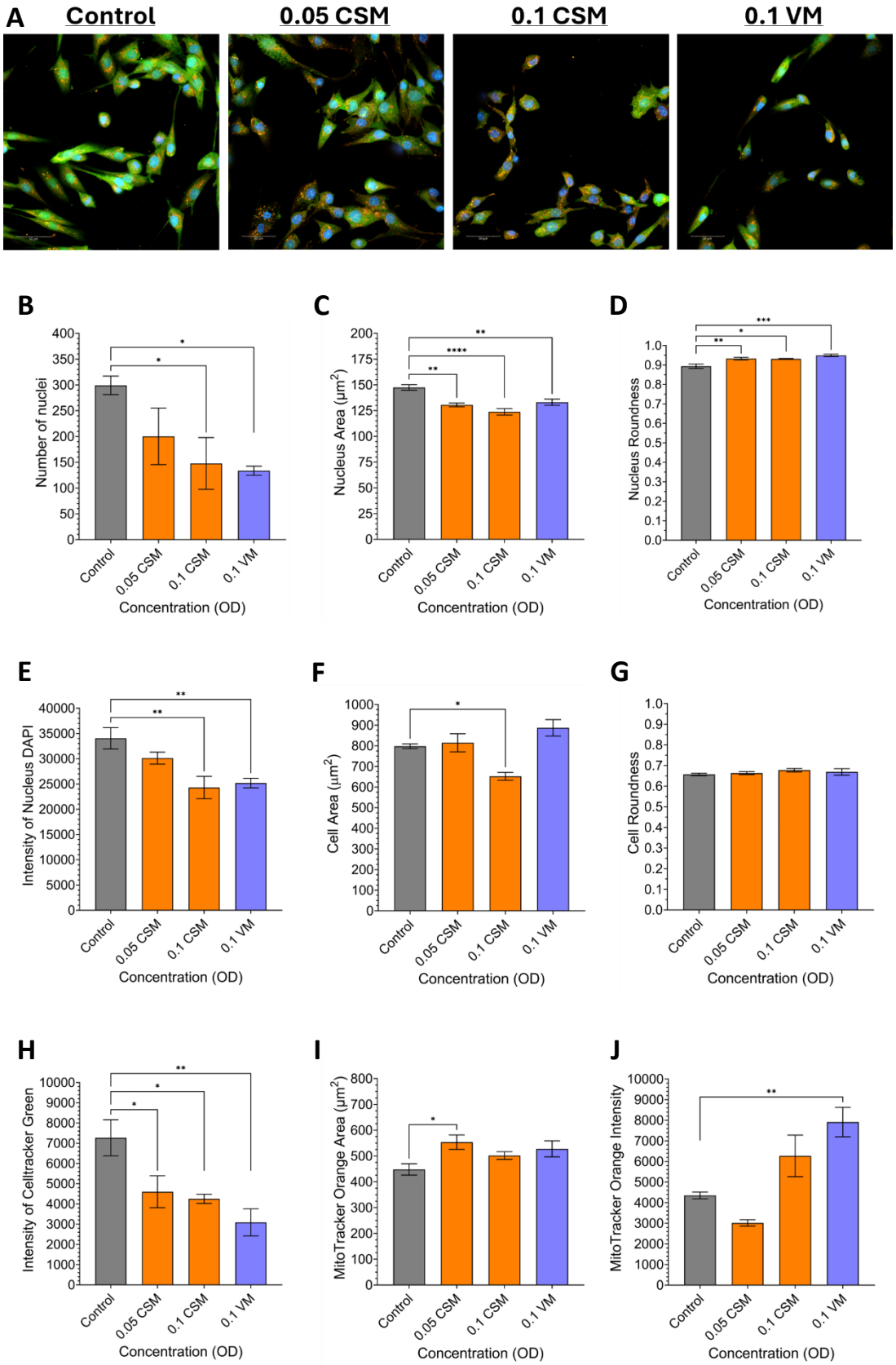
A
Control
0.05 CSM
0.1 CSM
0.1 VM
B
Number of nuclei
C
Nucleus Area (µm²)
D
Nucleus Roundness
E
Intensity of Nucleus DAPI
F
Cell Area (µm²)
G
Cell Roundness
H
Intensity of Celltracker Green
I
MitoTracker Orange Area (µm²)
J
MitoTracker Orange Intensity
Control
0.05 CSM
0.1 CSM
0.1 VM
Concentration (OD)

Figure 3.31. Organellar analysis of AB1190 myoblasts exposed to CSM or VM. The myoblasts were exposed to CSM or VM for 3 hours before staining with Mitotracker™, calcein green and DAPI. (A) Representative images of myoblasts after staining. (B) Quantification of the number of nuclei. (C) Quantification of nucleus area (μm^2). (D) Quantification of the roundness of the nucleus. (E) Quantification of the intensity of nuclear staining. (F) Quantification of the area of the cells (μm^2). (G) Quantification of the roundness of the cells. (H) Quantification of the intensity of cytoplasmic staining. (I) Quantification of the area of mitochondrial staining (μm^2). (J) Quantification of the intensity of mitochondrial staining. Data presented as the mean +/- SEM using one way ANOVA with Dunnett's multiple comparison test. *p<0.05, **p<0.01, ***p<0.001, ****p<0.0001 (n=5), scale bar is 50µm.

3.2.11. Cigarette smoke elevated the IL-8 inflammatory cytokine in AB1190.

Smoking is a factor in many pathological conditions. It has been found to have immune compromising properties (Sopori & Kozak, 1998) and to modulate inflammatory and anti-inflammatory cytokines in human airways (Hagiwara et al., 2001), in alveolar macrophages (Lugg et al., 2022), and alveolar epithelial cells (Szoka et al., 2019). We believe that CSM and VM will cause a pro-inflammatory response in muscle myoblasts and therefore investigated the effects directly on muscle cells. The AB1190 cells were exposed to CSM and VM then the inflammatory response was measured. The myoblasts were seeded into 6 well plates and allowed to adhere overnight. They were then exposed to different concentrations of CSM and VM for 72 hours. Afterwards, the media was collected from the wells and frozen at -80^{o} C before sending to Eve technologies (Calgary, Alberta) for investigation. The multiplex analysis of 15 human focused markers investigated the levels of GM-CSF, IFNγ, IL-1β, IL-1RA, IL-2, IL-4, IL-5, IL-6, IL-8, IL-10, IL-12p40, IL-12p70, IL-13, MCP-1, and TNFα (figure 3.32). The analysis revealed a significant increase in the levels of IL-8 only with 0.025 OD CSM. Fluctuations were observed but none were significant, furthermore the cytokines that displayed no change have not been presented in (figure 3.32 B).

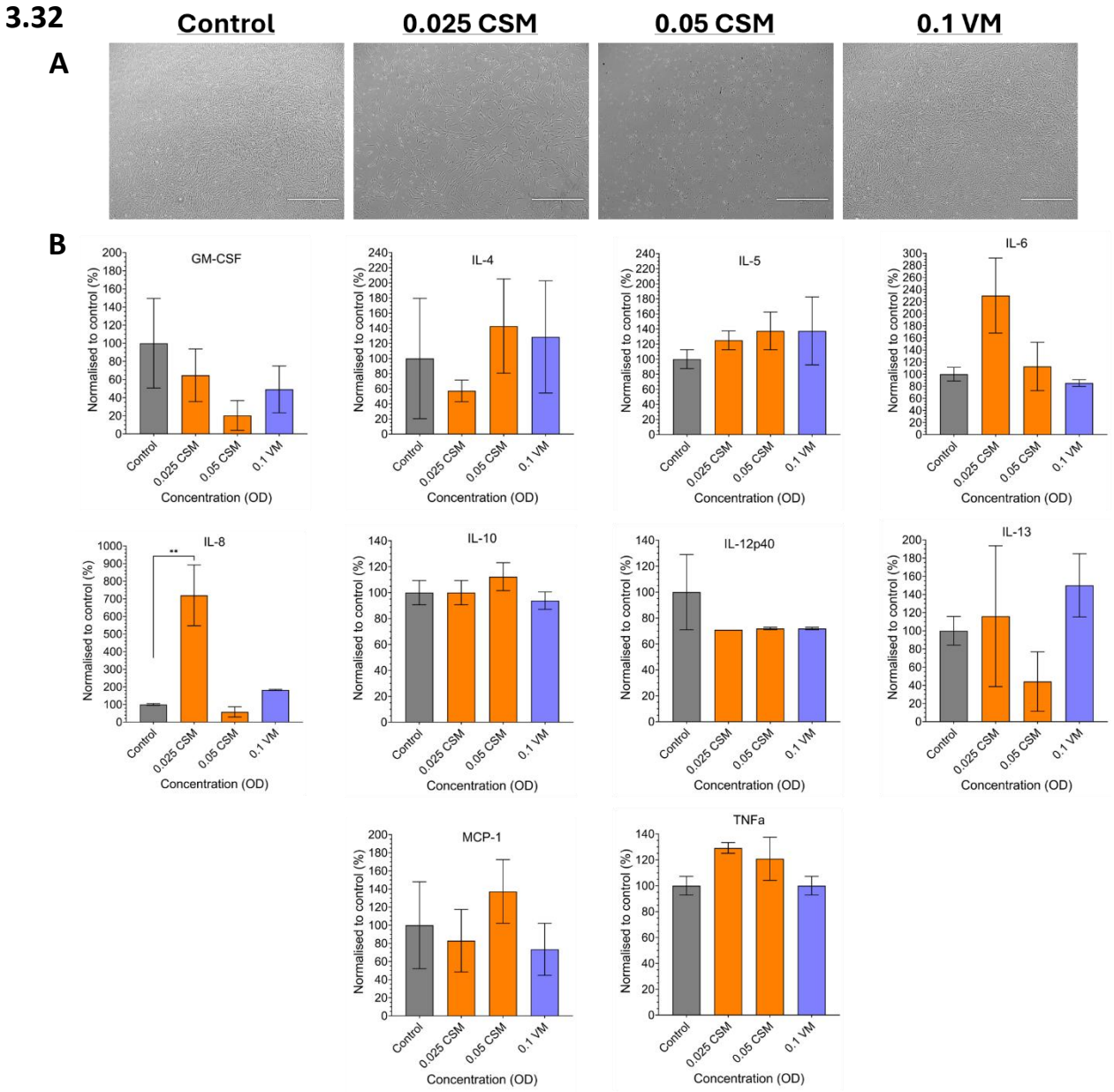

Figure 3.32. Effect of CSM and VM on AB1190 inflammatory cytokine profile. The myoblasts were exposed to CSM or VM for 72 hours, the media was then collected, and a multiplex analysis of 15 human focused markers was performed. (A) representative images of cells after 72 hours exposure to CSM or VM. (B) quantification of the multiplex analysis of inflammatory cytokines. Data presented as the mean +/- SEM using one way ANOVA with Dunnett's multiple comparison test. **p<0.01, (n=3), scale bar is 1000µm.

3.3. Discussion

We have shown that CSM alone diminished viability, slowed migration through decreased areas of focal adhesions (FAs) and stress fibres (SFs), induced senescence as well as atrophy and elevated IL-8 release. Furthermore, both CSM and VM reduced fusion capabilities, increased the area of nucleoli, and decreased the area of the nucleus.

The immortalized myoblast cell lines were chosen for the in-vitro experiments due to their sustainability and malleable nature. They proliferate rapidly and differentiate to functional myotubes capable of contracting and generating force in low serum conditions making them the ideal precursor to in-vivo experiments (McMahon et al., 1994). The C_2C_{12} cell line was chosen to represent the mouse subject throughout the project and the human counterpart AB1190; sourced from paravertebral muscle of a 16-year-old boy, was chosen as the transition from a lower to a higher mammal under in-vitro conditions, subsequently allowing for comparisons of any outcomes.

Cigarette smoking remains popular, more recently electric cigarettes or vaping have become more prevalent (Statistics, 2024). Many studies have investigated the outcomes of cigarette smoke, even on muscle, however the knowledge we have about how smoking and vaping affects early-stage regeneration remains scarce.

This project investigates how the early steps of muscle regeneration were affected by both cigarette smoke conditioned media (CSM) and vape conditioned media (VM). The initial hurdle was to produce a method of reproducible and accurate delivery of cigarette smoke and vape constituents. Based off the work from (Nogueira et al., 2018) the cigarette smoke and vape were bubbled through PBS. The CSM was pH 6.1 and VM was pH 7.0, then using spectrum analysis the solubilized aerosols were detected within the ultraviolet range (UV), similar to the findings of (Luppi et al., 2005) however, the difference was that we found the highest optical density (OD) measurements between 210 nm and 220 nm unlike their

findings of 270 nm to 280 nm. Going forward absorbance was measured at 220 nm and all dilutions were derived from this optical density.

The first experiment performed was to investigate the effect of the conditioned media on cell viability and proliferation. With C_2C_{12} there was a dose dependent decrease in absorbance with CSM only, interestingly with AB1190 an increase in absorbance was seen with all concentrations of VM and lower concentrations of CSM, however no significance visible at 0.1 OD CSM and a significant decrease with the higher concentrations. The MTS assay had been used previously as a metabolic measure (Heher et al., 2022; Wong et al., 2022) and the findings here potentially indicate metabolic dysfunction. The two other human myoblast cell lines were used here to investigate variability in response to the conditioned media. AB678 sourced from the quadriceps of a 53-year-old man presented with a decrease in viability beyond 0.1 OD CSM and 0.05 OD VM, furthermore AB1167 from the fascia lata of a 20-year-old man was highly susceptible exhibiting decreased viability from 0.05 OD CSM and at 0.025 OD VM. The varying responses of the human cell lines can be due to differing metabolic profiles and genetic variations between sources.

During regeneration activated satellite cells proliferate in an essential step to replenish the satellite cell pool and as myoblasts before differentiating (Wang & Rudnicki, 2011). Should this proliferative ability be hindered surely as a consequence the regenerative robustness of skeletal muscle would be diminished through exhaustion of the satellite cell pool. Cigarette smoke had previously been shown to stop the proliferation of lung fibroblasts through increased p53, p21 and p16 activity (Nyunoya et al., 2006). Our investigation showed that C_2C_{12} did not undergo senescence but rather; based on the images, we suspect it was cell death in a dose dependent manner with CSM. Furthermore, both AB1190 and IMR-90 displayed signs of cell death however they also showed significant senescence after exposure to the conditioned media for at least 24 hours. These variations in response could be due to the method of immortalization or even inherent genetic mutations within the cell line; it is

quite possible that the C_2C_{12} has a mutation in the p53 gene thus preventing the cells from senescing. Initially, this experiment was performed on AB1190 then C_2C_{12} both displaying contradicting findings. The IMR-90 cell line can be induced into senescence with the addition of etoposide (Anerillas et al., 2022), this was used to resolve this problem by confirming that indeed both CSM and VM have senescence inducing constituents.

Migration of myoblasts is vital for muscle development and successful regeneration (Choi et al., 2020). The migration assay revealed that exposure to CSM decreased travelled distance and speed in both cell lines. Exposure to VM resulted in a reduction of distance travelled by C_2C_{12} in the highest concentration only. Furthermore, when a wound closure assay was implemented, the findings corroborated single cell tracking. The migratory ability of myoblasts is vital for muscle regeneration; they need to travel along the fibre before differentiation occurs. CSM significantly increased the time taken for cells to travel across the scratch in both cell lines, no significant effect was observed with any concentration of VM. The findings here indicate that CSM hinders migration, this correlates to the findings of other studies (Ng et al., 2015; Wahl et al., 2016), to explore this further, phalloidin and paxillin staining was used to quantify the area of F-actin and focal adhesion scaffolds respectively, both are needed to create the tension required for traction. The size of focal adhesions is linked to a cells migratory ability (Kim & Wirtz, 2013) our findings displayed varying results; in C_2C_{12} a decrease in the area of FA's with 0.05 CSM and an increase with VM, this explains why migration is inhibited in CSM and possibly why the VM exposed cells displayed slightly elevated speeds. Interestingly, in AB1190 the number and area of focal adhesions almost tripled compared to the control with CSM which could explain the inhibited migration, VM had no effect. Indeed Kim et al (Kim & Wirtz, 2013) commented that size of focal adhesions is linked to migratory ability. Furthermore, from their results this indicates that any increase or decrease could influence migration. Subsequently, the focal adhesion data corroborates the findings of the migration, however further investigations in

this are warranted possibly in the assembly of less complex structures (Wozniak et al., 2004) or FA turnover.

Differentiation and fusion of myoblasts is crucial during regeneration, considering this significance, the effect of CSM and VM on the fusibility of the myotubes was examined. Following the addition of differentiation media, the control groups in both cell lines generated multinucleated myotubes with the characteristic pattern of striated muscle. Conversely, the addition of both conditioned media resulted in a reduction in the myotube areas and the number of fused nuclei. Previous studies performed on other stem cells (Ng et al., 2015; Wahl et al., 2016) also reported that cigarette smoke caused aberrant cellular differentiation. Fusion is a stepwise sensitive process that involves the adhesion of myoblasts, membrane remodeling and specific changes in protein expression (Millay, 2022). Therefore, it's plausible that the constituents of the conditioned media could impact these proteins and membrane integrity, potentially obstructing fusion.

Muscle injuries require significant time for healing, this often leads to atrophy due to disuse and damage, however the bodies regenerative capabilities restore muscle mass and function over time. In studies conducted on smokers (Kok et al., 2012; Saito et al., 2012) researchers observed that smokers exhibited reduced muscle strength and mass compared to non-smokers. Additionally, Peterson et al (Petersen et al., 2007) reported that smoking impaired protein synthesis and increased the expression of myostatin, a muscle growth inhibitor (McPherron et al., 1997). Exposing the myotubes to VM after differentiation in the atrophy assay displayed no significant changes in both cell lines, however C_2C_{12} and AB1190 myotubes displayed a reduction in area after exposure to CSM, albeit the AB1190 myotubes were more robust and significance was only found at the highest concentration. Due to the trend seen in the findings of the human myoblasts a second prolonged exposure at a lower concentration of 0.1 OD was performed, this time significance was seen with CSM but not VM. Our results corroborate the findings of (Liu et al., 2011) in vitro, and (Petersen et al.,

2007) reported similar findings in human subjects. Furthermore, they reported increased myostatin expression in cigarette smoke cohort; based on this and the findings of (Lee et al., 2020; Suh et al., 2020) on the inhibition of myostatin and preservation of muscle mass we examined whether atrophy could be prevented or rescued by inhibiting the activin/myostatin signaling pathway. Myostatin binds to activin receptor II and activin receptor IIB with high affinity (Lee et al., 2005), therefore using a soluble transmembrane receptor (sActRIIB) would trap myostatin and prevent it from binding to its target nullifying its effect (Lee et al., 2005). Stemming from this and previous work done within our group, soluble activin receptor IIB (sActRIIB) was used in an atrophy assay with CSM, and found to rescue both cell lines from atrophy similar to the findings of (Bin Haidar et al., 2024; Lee et al., 2005).

A functional nucleolus is essential for ribosome production as well as regulating cell survival and proliferation (Dubois & Boisvert, 2016). An enlarged nucleoli has been reported as a phenotype in senescent cells (Kasselimi et al., 2022), as well as an increased demand for protein synthesis in cancerous cells (Derenzini et al., 2009), therefore fibrillarin a nucleolar protein, was stained to determine the size of the nucleolus in our experiment. Our findings in myoblasts revealed no change in the area of nucleoli with both conditioned media. Furthermore, the number of nucleoli was not affected by the CSM or VM. In myotubes however, the highest concentration of 0.24 OD CSM was used because it significantly induced atrophy. After exposure the number of nucleoli with CSM was significantly lower than control, however the area of nucleoli was larger in both conditioned media. These findings may be indicative of increased ribosomal RNA production for protein synthesis, and aberrant nucleolar behavior similar to what is seen in tumor cells (Correll et al., 2019), the speculation here is that this increased ribosomal biogenesis could be in response to the atrophy inducing conditioned media.

Mitochondrial response to cigarette smoke has been well documented in lung tissue and epithelial cells within. Hara et al (Hara et al., 2013) observed disrupted mitochondrial

dynamics through increased ROS production which led to senescence in primary human bronchial epithelial cells. Similarly, Hoffmann (Hoffmann et al., 2013) demonstrated changes in mitochondrial structure and function in human bronchial epithelial cells (BEAS-2B), where prolonged exposure to cigarette smoke extract (CSE) resulted in increased fragmentation, branching and density of the matrix. Additionally, Sundar et al (Sundar et al., 2019) observed altered OXPHOS protein complexes. There are a few studies performed on muscle mitochondria but none of them investigate the effect at the satellite cell (SC) level. For instance, Örlander et al (Orlander et al., 1979) and Barreiro et al (Barreiro et al., 2010) investigated the effect on biopsies from the quadriceps and both concluded with dysregulated mitochondrial enzyme activity. Alternatively Alonso et al (Alonso et al., 2003) isolated the mitochondria from the quadriceps and investigated the effect of carbon monoxide (CO); a known chemical found in cigarettes (Talhout et al., 2011). They observed dose dependent inhibition of cytochrome *c* oxidase with CO. Our study investigates the direct effect of satellite cell exposure and the mitochondrial response to CSM and VM. Our findings show that both conditioned media are disrupting mitochondrial homeostasis and altering nuclear morphology. Organelles such as the nucleus and mitochondria display distinct morphological features during apoptosis. Mitochondria become more condensed and form perinuclear masses (Bottone et al., 2013). The nuclei shrink and become more rounded as the chromatin condenses (Kerr et al., 1972; Prokhorova et al., 2015). These could be corroborated by performing Western Blots to investigate cleaved caspases (Nicholson et al., 1995) or through flowcytometry, analyzing the cells with annexin V (Vermes et al., 1995), both techniques known for evaluating apoptosis.

Cytokines are involved in the immune response and mediate communication within the immune network. They are proteins that can be secreted by several cells such as macrophages, lymphocytes and even muscle cells. Imbalanced or abnormal cytokine levels can cause a multitude of diseases and in severe cases lead to death (Liu et al., 2021).

Inflammatory cytokines also play a key role in inducing cellular senescence, some of the inflammatory cytokines involved in inducing the senescence associated secretory phenotype (SASP) are IL-6, IL-8 and TNF-α (Davalos et al., 2010). Our data showed dysregulated cytokine levels when CSM and VM were added to the cells. This dysregulation ultimately could be the driving force behind the senescence seen previously. A notable finding is the increased IL-8 expression with the lower dose of CSM. This could be because the cells were incubated with the conditioned media for 72 hours. This prolonged exposure with 0.5 OD CSM has led to increased cell death as seen from the representative images in figure 3.33 A resulting in the decreased IL-8 levels. Another notable finding is the decrease in GM-CSF levels. This colony stimulating factor is involved in immune response and host defense systems (Becher et al., 2016). It is usually found to be elevated in senescent fibroblasts (Coppe et al., 2008). Our findings may be different, but this is expected due to the nature of the conditioned media and the different cell lines. In fact, two studies by one group that investigated the effects of smoking on inflammation (Barreiro et al., 2010) (Barreiro et al., 2012) observed differing results with regards to cytokine levels based on the type, species and location of the sample collected. The takeaway message here is that both CSM and VM have a direct effect on muscle cells.

3.4. Limitations and future work

The cigarette and vape smoke were both solubilized in PBS, this provided significant results, however, had drawbacks. The smoke released from a combusted cigarette and e-liquid contains many organic chemicals (Eshraghian & Al-Delaimy, 2021; Jaccard et al., 2019) which only dissolve in organic solutions such as ethanol, or chloroform. In fact, when this was attempted with ethanol (EtOH), the spectrum analysis performed resulted in different shaped graphs, furthermore when this conditioned EtOH was used on the cells in the same manner as the infused PBS complete cell death was observed in all concentrations of conditioned media. This experiment does not remove the potential effects of ethanol. An

alternative would have to be considered, perhaps with more time available this would have been achieved. Furthermore, the CSM was recorded at pH 6.1. It may be argued that this decrease in the pH could have significant repercussions on our experiments. However, the CSM was diluted in growth or differentiation media to a dilution factor of 1:10 before use. We believe that this was enough to make the pH neutral, and a possible way to test this would have been to simply measure it before use.

The β-Gal assay was used to assess senescence; this was to be coupled with Click-iT EdU flow cytometry cell proliferation assay (Thermofisher) to assess the cell cycle. Had this been completed we would have a better understanding of the effect of the conditioned media on proliferative dynamics. Furthermore, etoposide didn't show a significant increase in staining with the IMR-90, this could be attributed to the low "n" numbers used in this experiment as well as the high positivity of the negative control. Additionally, etoposide was not used on AB1190 due to it being the first experiment done to investigate senescence. The atrophy assay was conducted to determine the effect of our CSM and VM on myotubes. An argument can be made that our findings do not show atrophy but rather impaired growth. This could be settled by repeating the experiment with two control cohorts. One would be fixed at the beginning of the conditioned media exposure and the other at the end. Then we would compare the myotube area. If both are indeed equal, then what we observed would be CSM induced atrophy, alternatively if there is a difference then this would be proof that it is indeed impaired growth. Another aspect that wasn't addressed was when sActRIIB was used to rescue atrophy in C_2C_{12}, there wasn't a cohort exposed to sActRIIB alone, this was however remedied in the subsequent experiment involving AB1190. Additionally, the organellar investigations were only performed on AB1190 cells. Had this experiment been completed with the C_2C_{12} cell line we could have compared the findings. Based on the varying mechanistic response of the cell lines we suspect that this would carry into the organelles.

In the laboratory there were several human cell lines including the AB678 and AB1167, it would have been interesting to investigate how they all respond to the CSM and VM under the panel of assays performed here. This would allow us to thoroughly investigate any similarities or differences between muscle cells sourced from different locations.

3.5. Conclusion

We set out to explore the effect of CSM and VM on the early phases of regeneration with an aim to understand how muscle regeneration is impacted at the satellite cell level. Both cigarette smoke and vaping cause systemic inflammation (Barreiro et al., 2012; Farrell et al., 2021) which we speculate impacts the satellite cell functionality. Here we employed two stem cell-like cell lines to investigate the multistep process of regeneration from a physical and mechanical aspect. Our findings demonstrate that our conditioned media affected viability and metabolism, induced senescence, limited migration, disrupted focal adhesions, obstructed fusion, induced atrophy and dysregulated nucleoli.

From a physical and mechanical standpoint, our findings could provide evidence of delayed muscle regeneration and offer insights into the underlying mechanisms.

Chapter 4: Investigating the effects of cigarette smoke media and vape media on skeletal muscle regeneration

4.1. Introduction

Mouse models have become integral to the study of muscular damage and regeneration. The genetic lineage is easily traceable, immune responses are well characterized, and muscle injuries can be easily induced through mechanical trauma, exercise or even chemically using cardiotoxin (CTX) or barium chloride. Derived from *Naja pallida,* cardiotoxin induces a reproducible and momentary muscular injury, without affecting the nerves or vasculature, followed by complete regeneration and without causing severe consequences to the animal (Wang et al., 2022). Muscle regeneration is a tightly regulated process that restores function and architecture following injury through distinct but overlapping phases. Initially following injury there is degeneration/necrosis of fibres, followed by an inflammatory response which in turn initiates regeneration through activation, proliferation and differentiation of satellite cells (SC). Maturation of new fibres occurs concurrently with extra-cellular matrix (ECM) remodeling, angiogenesis, and innervation through establishment of neuromuscular junctions (NMJ), eventually leading to functional recovery (Forcina et al., 2020). In chronic degenerative muscular diseases, or due to extensive muscle damage, the inflammatory cells and fibroblasts persist during regeneration leading to fibrosis within regenerating fibres (Mann et al., 2011).

Tobacco smoking and vaping are now widely accepted to cause significant health risks. They contain thousands of chemicals that include heavy metals and carcinogens (Goniewicz et al., 2014; Jaccard et al., 2019). Consumers of cigarettes have been shown to have weakened muscles (Kok et al., 2012), exhibit muscular atrophy (Liu et al., 2011; Montes de Oca et al., 2008) and impaired function through altered calcium kinetics (Nogueira et al., 2018). Furthermore, they display diminished orthopedic regeneration and wound healing (Kanneganti et al., 2012; Sloan et al., 2010). In studies investigating the effects of vaping there is increasing evidence linking it to elevated systemic inflammation and an increased risk of cardiovascular diseases (CVD's) (Hua et al., 2013; Wang et al., 2018; Zong et al.,

2024), notwithstanding the psychological disorders that may arise (Farrell et al., 2021). However, not much is known about the effects within the musculoskeletal system. In our in-vitro experiments we observed a direct effect of cigarette smoke conditioned media (CSM) and vape conditioned media (VM) on myoblasts. Viability, proliferation, migration and fusion were all dysregulated. These processes are all vital steps in early regeneration. Therefore, based on the in vitro findings we suspect that muscle regeneration would be diminished in an in vivo setting.

In this chapter we investigated the effects of cigarette and vape extracts in-vivo. The aim was to determine how systemic exposure to the conditioned media affects mice, and specifically the impact it may have on skeletal muscle regeneration. Additionally, we investigated whether there is a difference in effect between CSM and VM in the context of skeletal muscle maintenance and regeneration.

We hypothesized based on the literature available and the previous in-vitro experiments that both CSM and VM would cause muscle atrophy and disturb regeneration following acute injury.

4.2. Results

4.2.1. Animal weights were not affected by IP injections of CSM and VM.

The experiments were conducted on forty-two C57BL/6 adult male mice. Animals were split into three cohorts, the control cohort which consisted of 12 animals received phosphate buffered saline (PBS) intraperitoneal (IP) injections. The second cohort and third consisted of 15 animals each and received either CSM or VM IP injections. They were preconditioned for 8 weeks with IP injections of 1.8 OD CSM and 1.0 OD VM twice a week. This period of preconditioning allows the mice to become habitual smokers as shown previously by the findings of (Nogueira et al., 2018) when the cotinine levels were measured by ELISA and proved to be high as those of smokers. Afterwards, an intramuscular (IM) injection into the right hind limb (into the tibialis anterior (TA) muscle) of the mice was performed using cardiotoxin (CTX) to induce damage. Collection of the muscles was performed on day 5, 10 and 20 post CTX injections. At every time point four control animals, five CSM injected and five VM injected were sacrificed (figure 4.1).

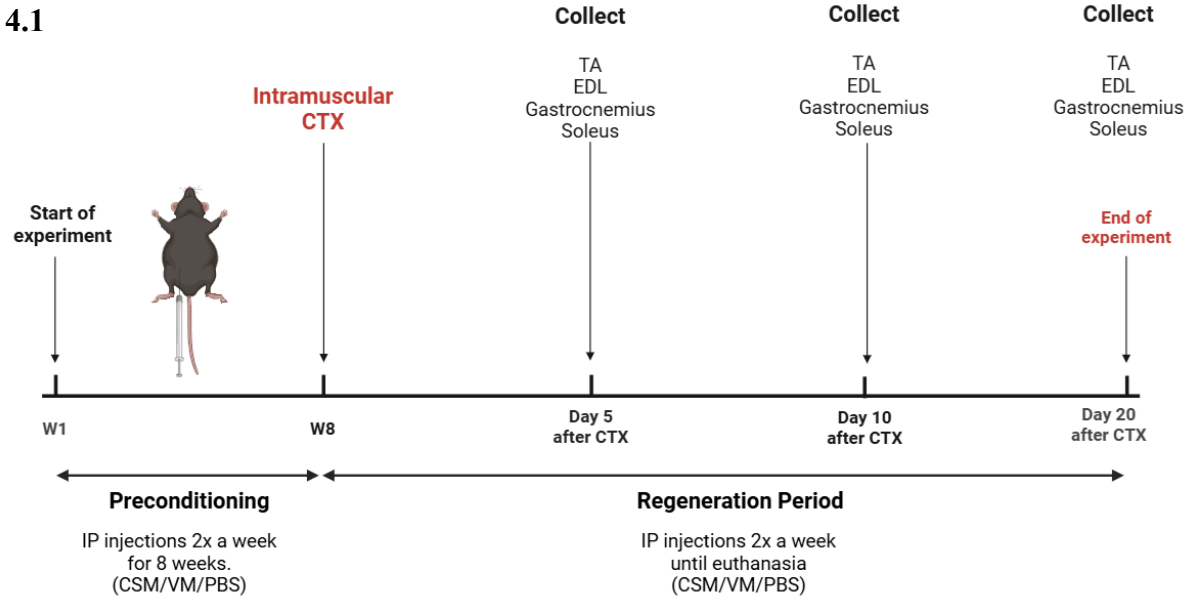

Figure 4.1. In-vivo project outline.

The animals were weighed before every injection until the day of sacrifice. Both CSM and VM had no effect on animal weights throughout the experiment (figure 4.2).

4.2

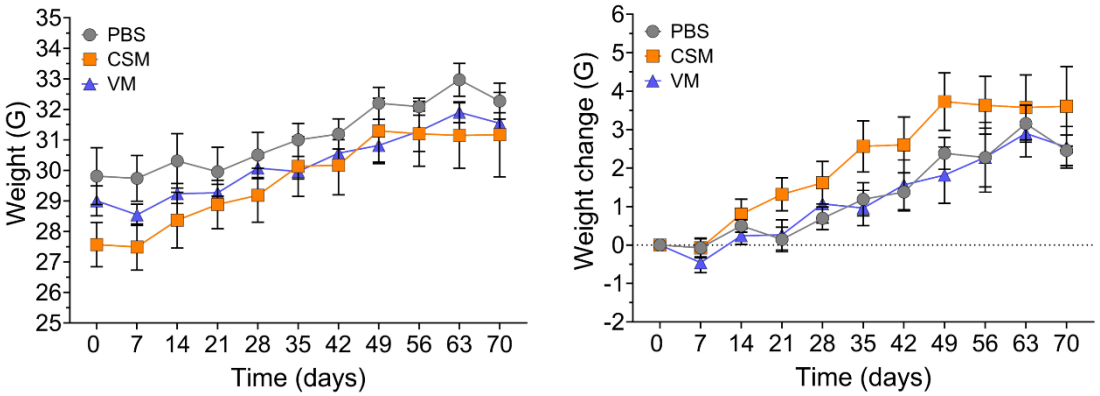

Figure 4.2. The effect of conditioned media IP injections on animal weights. The mice were weighed twice a week before every IP injection until they were sacrificed. Data presented as mean +/- SEM using two-way ANOVA with Dunnett's multiple comparison tests, (n=4 for control, n=5 for CSM and n=5 for VM injections).

4.2.2. Muscle weights weren't affected by exposure after day 20.

The right and left tibialis anterior (TA), extensor digitorum longus (EDL), soleus and gastrocnemius were collected from animals on days 5, 10 and 20 post CTX injections. They were photographed and weighed before flash freezing and storage.

The muscle weights collected were normalized to body weight to account for variability in animal sizes. We observed a significant increase in day 5 collections of the left EDL and right gastrocnemius of mice injected with CSM. Furthermore, there was a significant increase in the right TA of VM injected mice (figure 4.3). No changes were detected in the remaining collections.

4.3

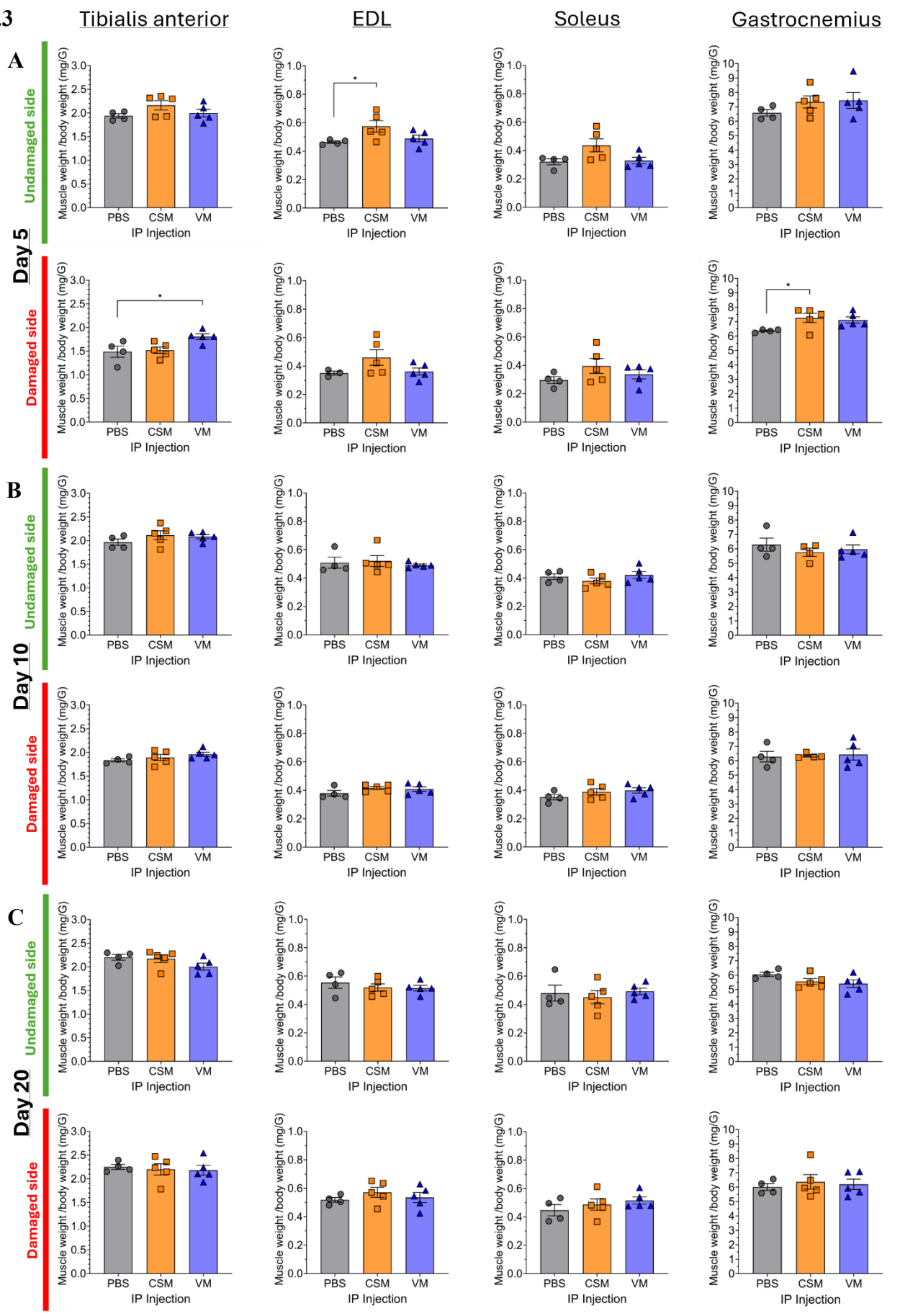
Tibialis anterior
EDL
Soleus
Gastrocnemius
A
B
C
Undamaged side
Damaged side
Day 5
Day 10
Day 20
Muscle weight /body weight (mg/G)
PBS
CSM
VM
IP Injection
*

Figure 4.3. Effect of conditioned media IP injections on muscle weights. The tibialis anterior (TA), extensor digitorum longus (EDL), soleus and gastrocnemius were collected and the normalized muscle weights to body weights was analyzed. (A) Day 5 collections, (B) Day 10 collections, (C) day 20 collections. Data presented as mean +/- SEM using one-way ANOVA with Dunnett's multiple comparison tests, *$p<0.05$. (n=4 for control and n=5 for CSM and n=5 for VM injections)

4.2.3. Fibre area wasn't affected by CSM or VM after 20 days post cardiotoxin injections (CTX).

Following the muscle weight measurements haematoxylin and eosin (H&E) staining was performed on the TA sections. This revealed considerable damage caused by the cardiotoxin (CTX) 5 days post IM injections, widespread myofibre necrosis with plenty of infiltration of inflammatory cells were visible in all cohorts. By day 10 the infiltration was mostly cleared, the myofibres appeared compact with centrally located nuclei. At day 20 the inflammatory infiltration seemed to completely clear with the myofibres appearing normal in size and shape but remain with centrally located nuclei (figure 4.4).

4.4

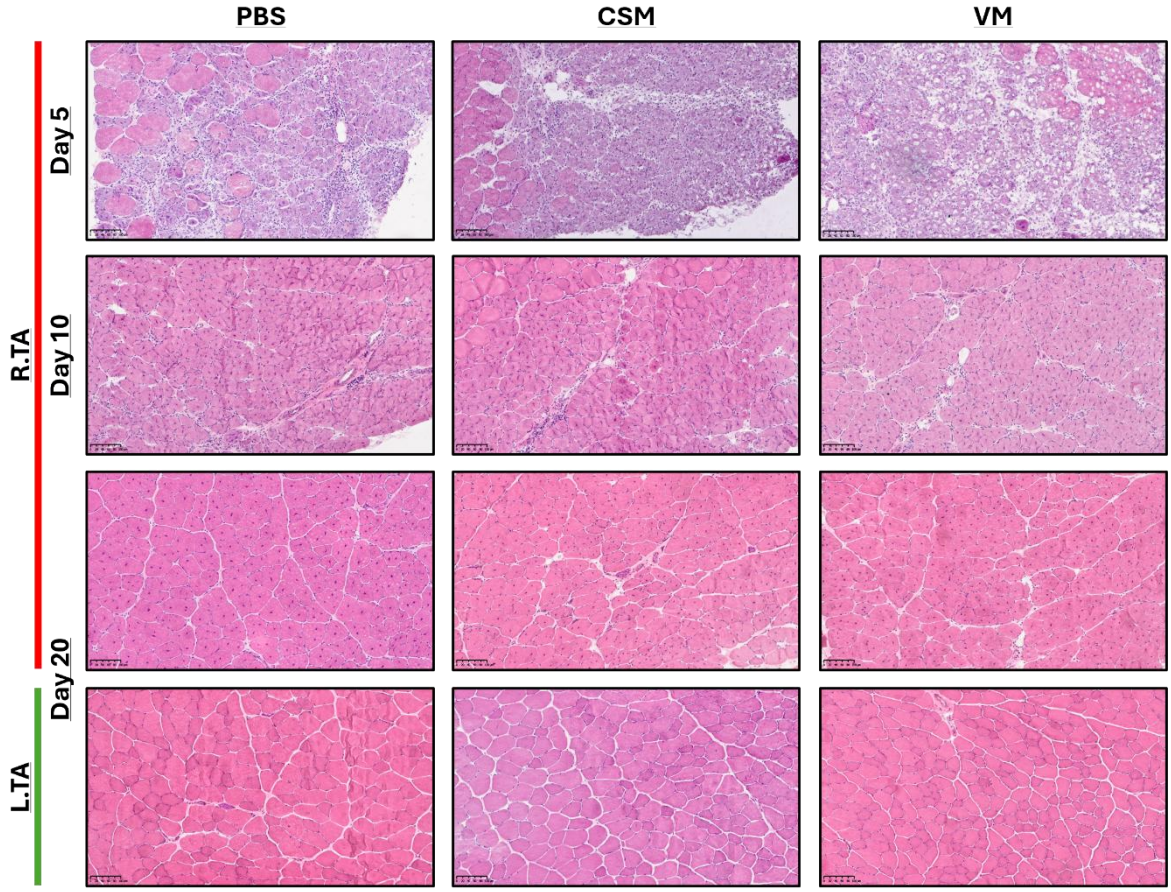

Figure 4.4. H&E stain of TA's 5-, 10- and 20-days post CTX injections. Scale bar is 100µm.

The damaged area (centrally located nuclei only) of fibres from day 20 collections were measured then compared with an undamaged area within the same section (figure 4.5). This revealed that by day 20 damaged fibres had no significant difference in fibre area to the undamaged. Moreover, there was no difference between the CSM, VM and PBS injected mice either (figure 4.5 B).

4.5

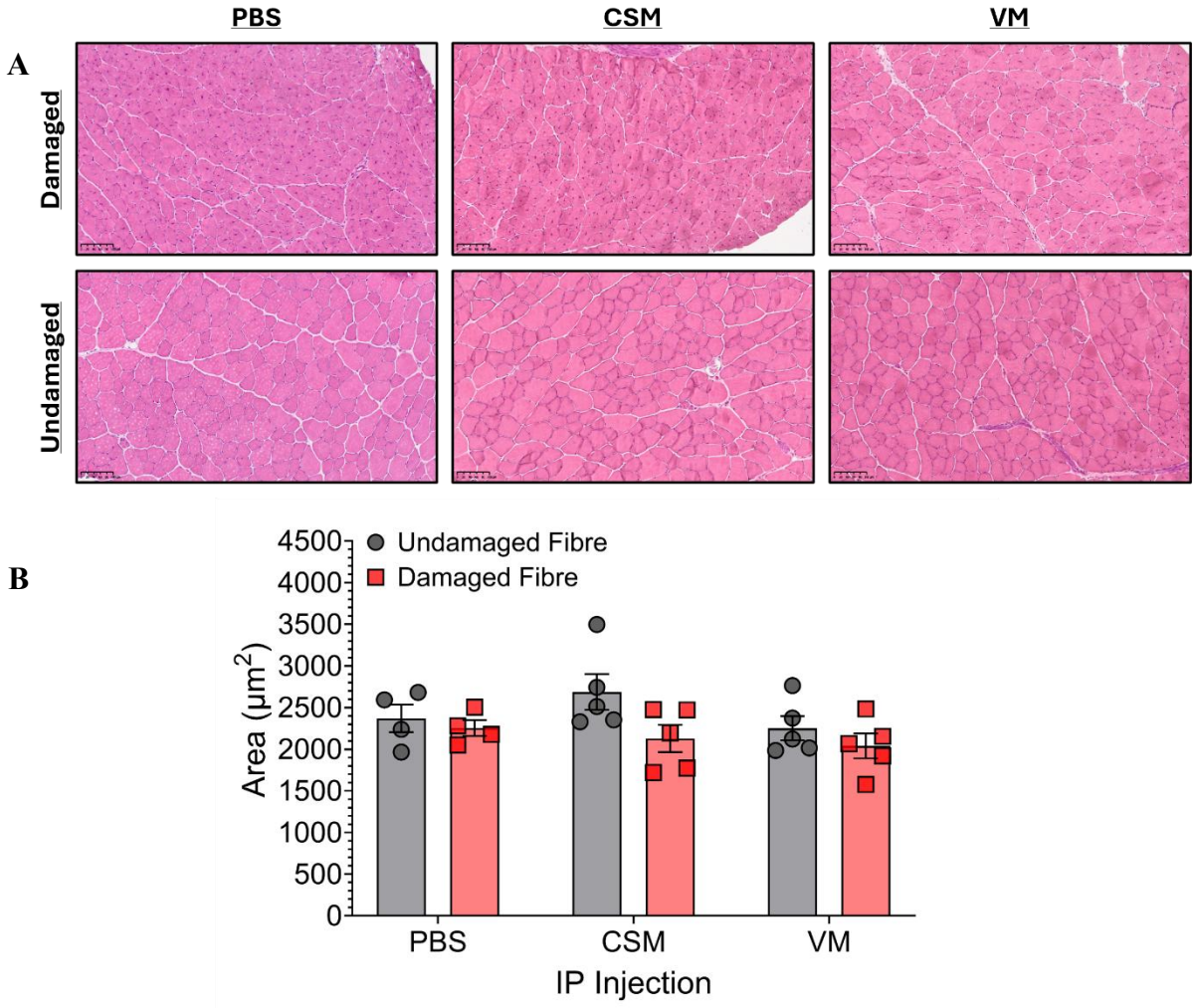

Figure 4.5. The effect of CSM and VM on fibre area 20 days post CTX injections. The area of damaged fibres was compared to the undamaged fibres within the same section. (A) Representative images of H&E sections. (B) Quantification of the fibre areas. Data presented as mean +/- SEM using a Two-way ANOVA with Tukey's multiple comparisons test. (n=4 for control, n=5 for CSM and n=5 for VM injections). Scale bar is 100 µm.

4.2.4. CSM and VM have no effect on IgG^+ infiltration after damage.

Following the H&E staining we investigated the effect of CSM and VM on immune cell infiltration after damage. The muscle sections from day 5, 10 and 20 post CTX injections were stained for IgG (figure 4.6 A). This allowed us to detect muscle fibre damage due to a leaky membrane. IgG is normally extracellular and once the sarcolemma is damaged it infiltrates the cell (Oxenhandler et al., 1977). Once measured the IgG^+ area (figure 4.6 B) of damaged muscle revealed that there was no difference in percentage area of infiltration with the conditioned media injected mice when compared to PBS in any of the time points. This means that the conditioned media had no effect on immune cell infiltration.

4.6

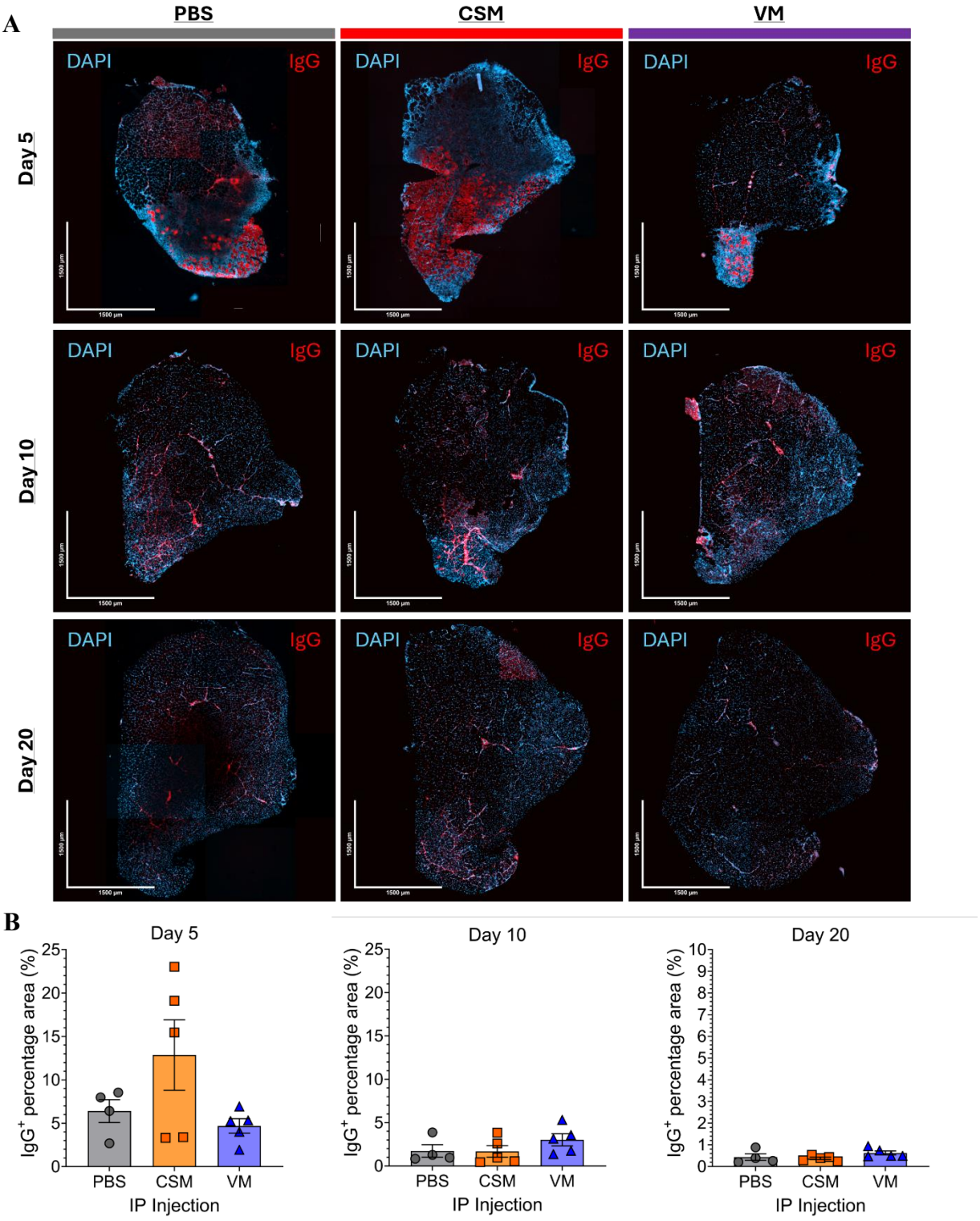

Figure 4.6. The effect of CSM and VM on IgG infiltration of damaged muscle. (A) representative images showing IgG$^+$ infiltration (seen in red) of days 5, 10 and 20 post CTX injected mice. (B) Quantification of the percentage area of IgG$^+$ fibres. Data presented as mean +/- SEM using a One-way ANOVA with Dunnett's multiple comparison tests. (n=4 for control and n=5 for CSM & VM injections). Scale bar is 1500 µm.

4.2.5. Embryonic myosin persists with CSM and VM injected mice.

Embryonic myosin was used as a marker for regenerating fibres (Guiraud et al., 2019). Muscle sections from day 5, 10 and 20 collections were stained and imaged (figure 4.7). Upon analysis, the size of embryonic myosin (eMYHC/MYH3) positive fibres was similar in all injected mice on day 5. Day 10 quantification revealed a significant increase in both CSM and VM injected mice. Finally, there was no eMYH detected in all samples by day 20 (figure 4.7 D). The results here suggest that regeneration does ultimately occur but may be hindered by the CSM and VM.

4.7

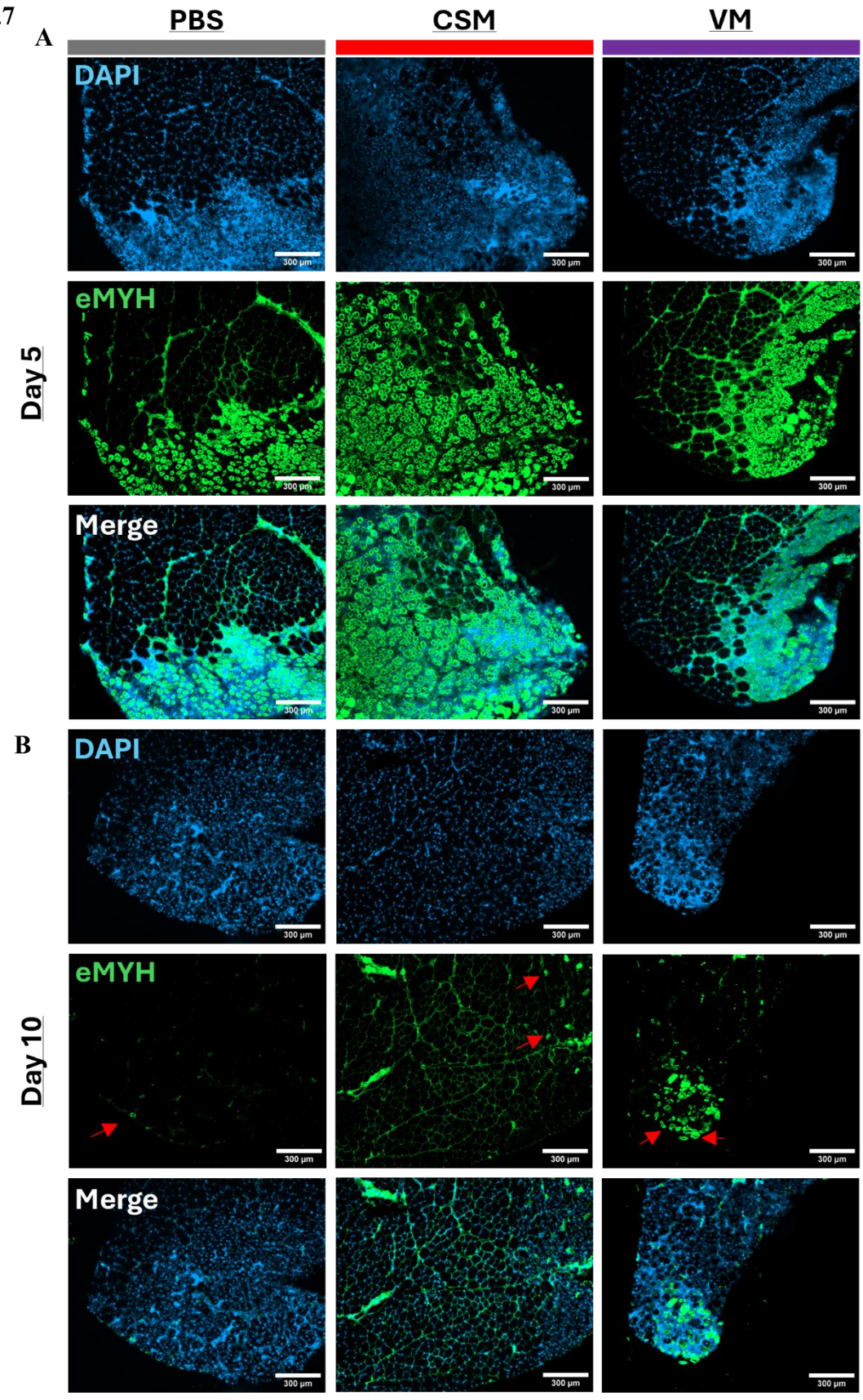
A
PBS
CSM
VM
DAPI
eMYH
Merge
Day 5
B
DAPI
eMYH
Merge
Day 10
300 µm

4.7

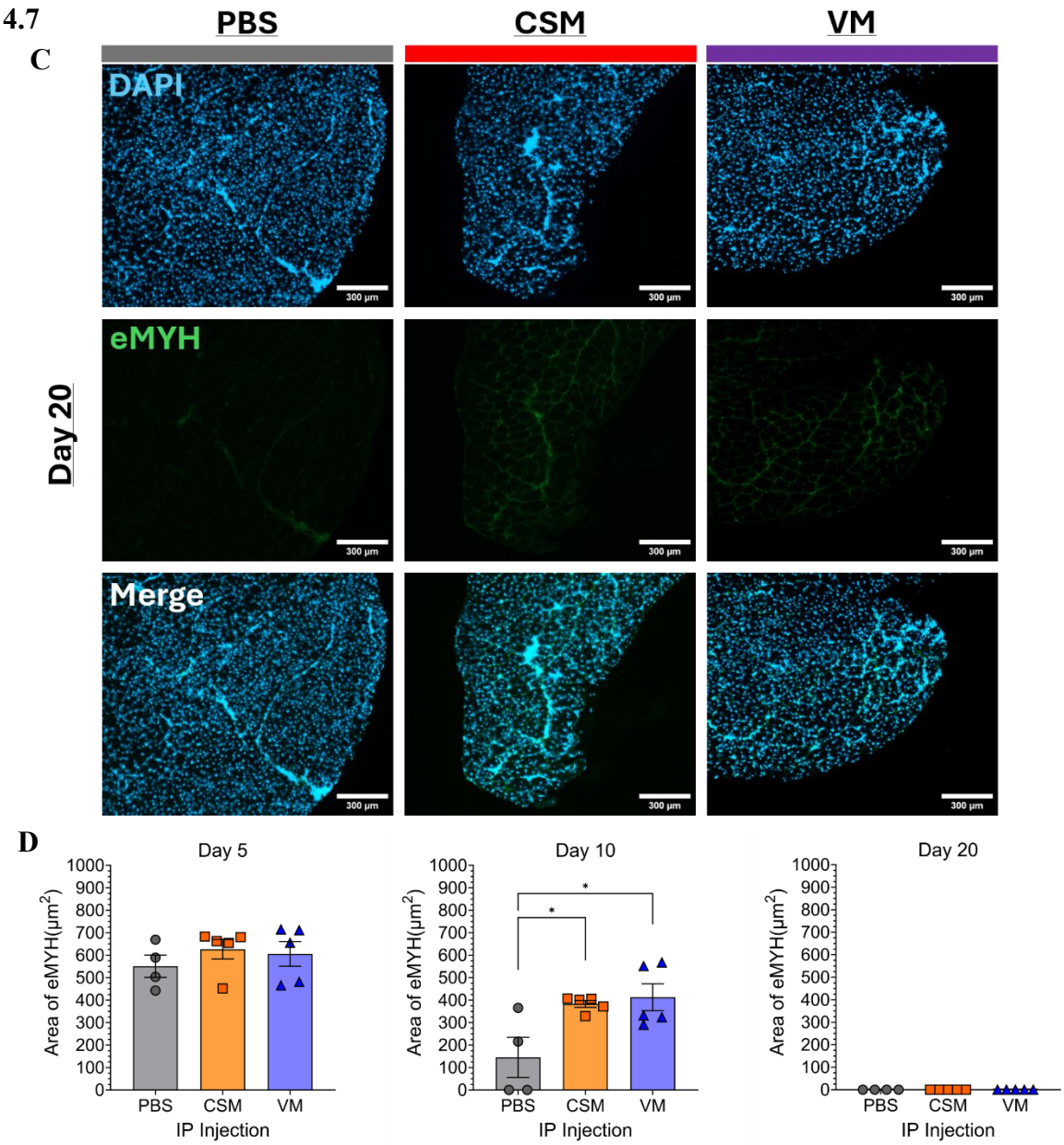

Figure 4.7. Effect of CSM and VM on area of eMYH after injury with CTX. (A) Representative images showing eMYH staining (seen in green) on day 5-, (B) day 10-, (C) day 20- post CTX injury. (D) Quantification of the area of eMYH. Data presented as mean +/- SEM using a One-way ANOVA with Dunnett's multiple comparison tests. *p<0.05, (n=4 for control and n=5 for CSM and n= 5 for VM injections). Scale bar is 300 µm.

4.2.6. Fibre maturity is affected twenty days post CTX injury by conditioned media exposure.

Dystrophin is essential for muscle membrane stability and is used as an indicator of fibre maturity, it is naturally distributed evenly around the myofibre. Following damage, the expression of dystrophin under the sarcolemma is lost. It returns over time, with the development of multiple foci that gradually extend to ultimately form a continuous band under the sarcolemma. (Gao & McNally, 2015). Therefore day 20 sections post CTX damage were stained (figure 4.8 A) and the expression of dystrophin was quantified as a percentage of each fibre's perimeter (figure 4.8 B). The analysis revealed that there was a significant decrease in dystrophin perimeter of damaged fibres of mice injected with CSM and VM when compared to those injected with PBS. Once again, the findings here suggest that regeneration ultimately occurred but was delayed.

4.8

A

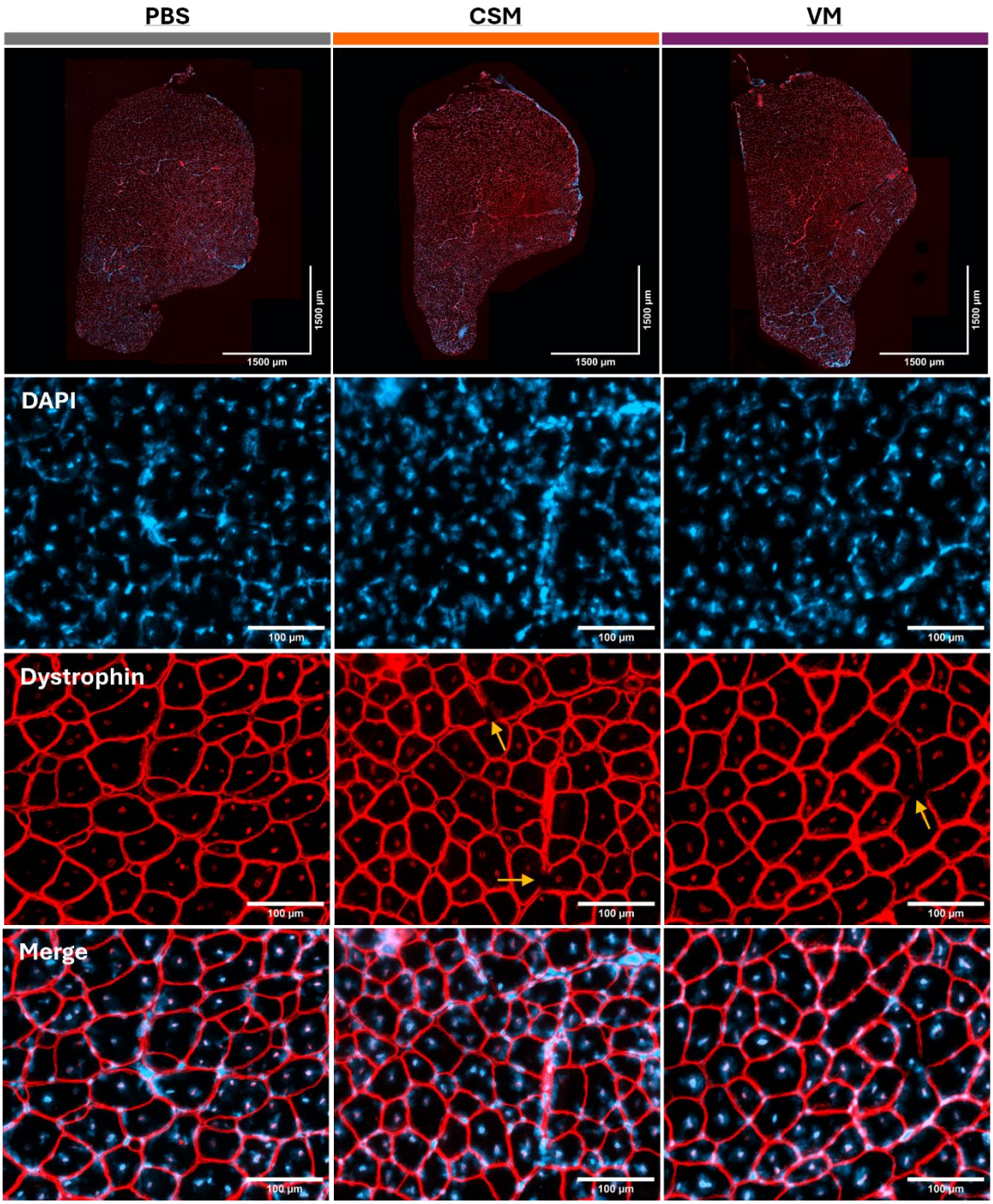
PBS
CSM
VM
1500 µm
DAPI
Dystrophin
Merge
100 µm

B

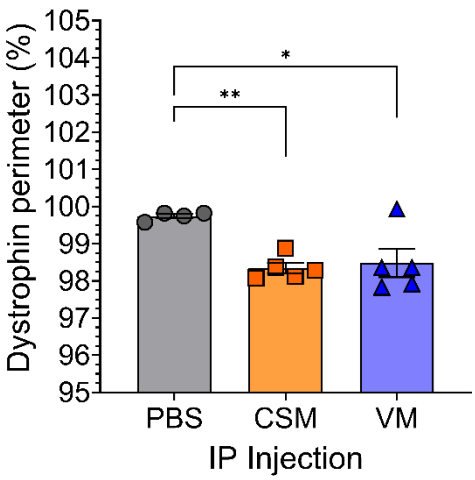
Dystrophin perimeter (%)
105
104
103
102
101
100
99
98
97
96
95
*
**
PBS
CSM
VM
IP Injection

Figure 4.8. The effect of CSM and VM on fibre maturity. The expression of dystrophin (seen in red) and perimeter values were measured 20 days post CTX injections. (A) Representative images of dystrophin staining with arrows pointing to low expression areas. (B) quantification of perimeter percentage of dystrophin. Data presented as mean +/- SEM using a One-way ANOVA with Dunnett's multiple comparison tests. *$p<0.05$, **$p<0.01$. (n=4 for control and n=5 for CSM and n = 5 for VM injections). Scale bar is 1500 µm for full muscle sections and 100 µm for magnified cross sectional images.

4.2.7. Levels of fibrosis were not affected in damaged sections.

Fibrosis occurs when there is excessive deposition of collagen in the ECM by fibroblasts and fibro adipogenic progenitors (FAPs) resulting in fibrotic scar tissue. This leads to impaired muscle function and affects regeneration (Mahdy, 2019). Here the levels of fibrosis were assessed in damaged sections of day 20 collections using picrosirius red staining (figure 4.9 A). The results showed that the levels of fibrosis in CSM and VM injected mice are the same as those injected with PBS (figure 4.9 B).

4.9

A

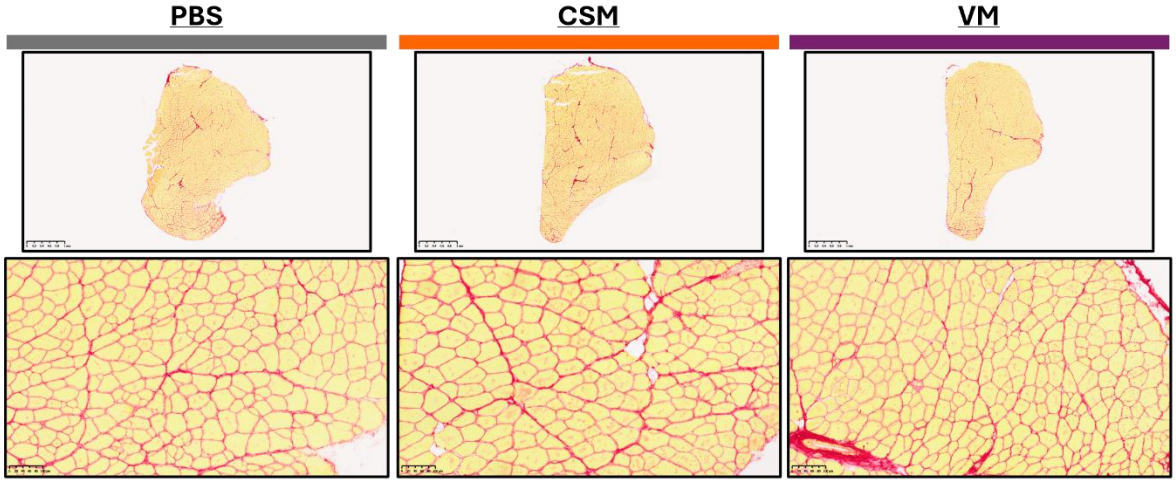

B

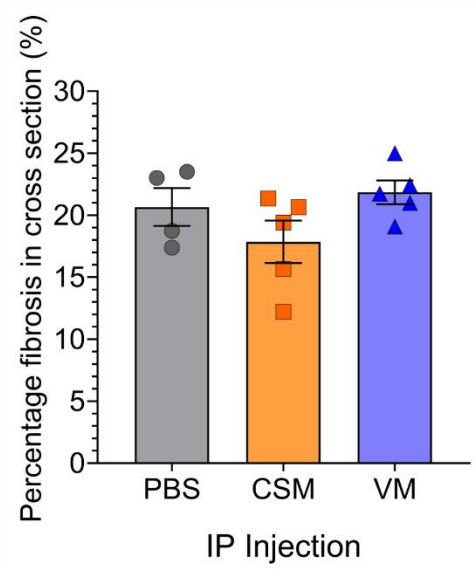

Figure 4.9. Effect of CSM and VM on fibrosis. Picrosirius staining was performed, and the area of fibrosis was measured on day 20 post CTX sections. (A) Representative images of PBS, CSM and VM injected mice. (B) quantification of percentage of picrosirius staining in cross sections. Data presented as mean +/- SEM using a One-way ANOVA with Dunnett's multiple comparison tests. (n=4 for control and n=5 for CSM and n = 5 for VM injections). Scale bar is 1 mm for full muscle sections and 100 µm for magnified cross sectional images.

The in-vivo experiments were conducted with two aims in mind. To determine how systemic exposure to CSM and VM impacts skeletal muscle maintenance and regeneration. To summarize, CSM and VM had no major impact on muscle weights following damage with CTX. However, from the staining performed everything suggests delayed but ultimately successful regeneration.

4.2.8. Atrophy wasn't observed in contralateral undamaged muscle sections of CSM and VM injected mice.

The second part of the in vivo experiments aimed to determine the effect of CSM and VM on muscle fibre homeostasis. Hence, muscle sections were taken from the contralateral undamaged TA 20 days post CTX to assess fibre area. The sections were examined with antibodies to identify the different fibre types, IIA (MHC-IIA), IIB (MHC-IIB), IIX (MHC-IIX) and laminin for the extra cellular matrix (figure 4.10 A). Type IIA fibres are oxidative, fatigue resistant, are considered fast twitch and produce high force similar to glycolytic fibres. Type IIB fibres are glycolytic, with low fatigue resistance, can generate high force and are considered fast twitch. Type IIX fibres are fast twitch glycolytic fibres that generate explosive power and have extremely low fatigue resistance. The antibodies used bind to the different myosin heavy chain (MHC) isoforms that are expressed in the sarcomeric thick filament (Mescher, 2023; Schiaffino et al., 2015). A 1500 µm cross section was taken from the deep and superficial regions then the areas of each fibre were measured, pooled and averaged (figure 4.10 B). There was no significant change detected in the area of any of the fibre types when compared to the PBS.

4.10

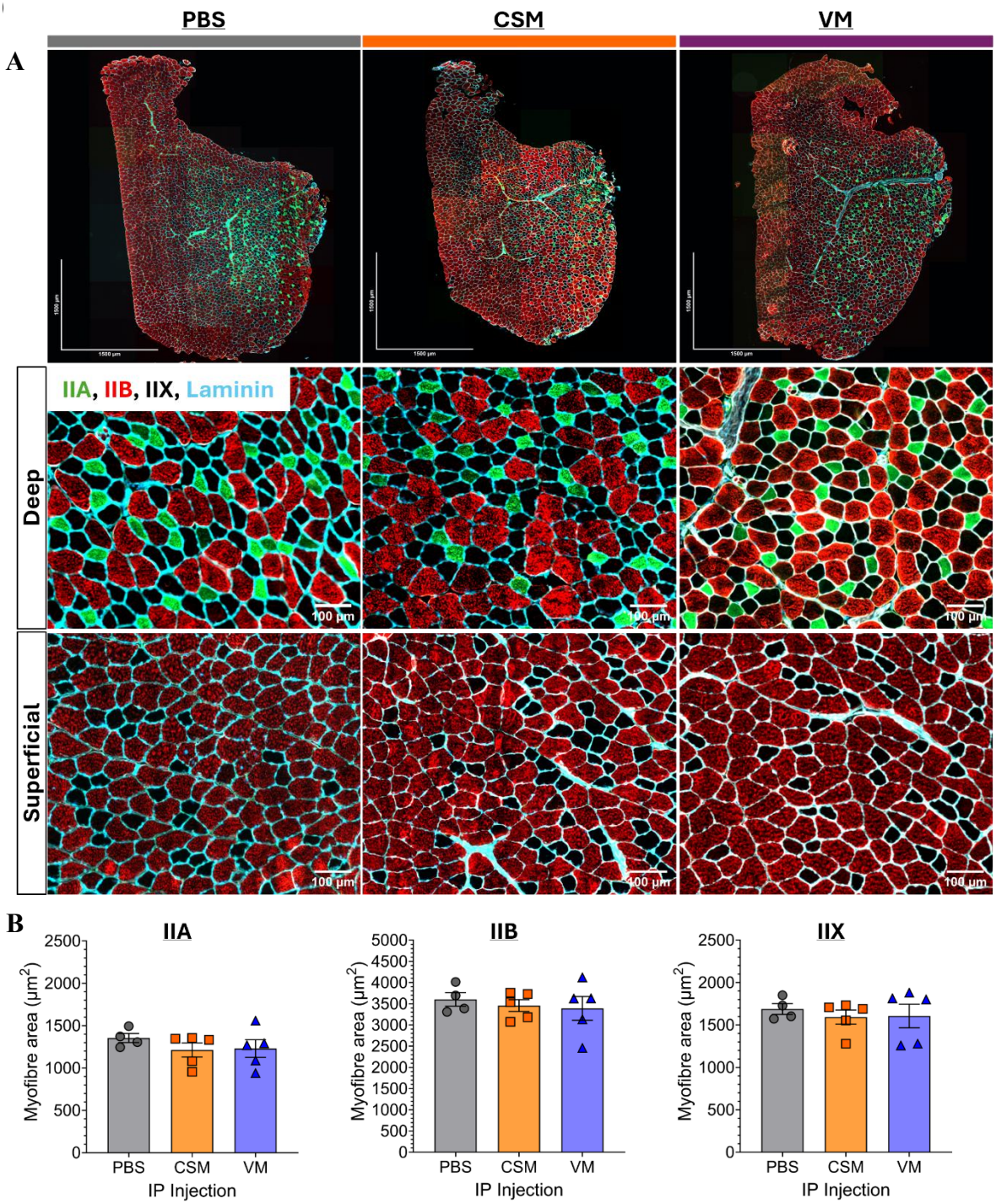

Figure 4.10. The effect of CSM and VM on fibre areas of contralateral undamaged TA. The areas of IIA (green), IIB (red), and IIX (black) were analyzed from day 20 collections post CTX injury. (A) Representative images of PBS, CSM and VM exposed mice. (B) quantification of muscle fibre areas. Data presented as mean +/- SEM using a One-way ANOVA with Dunnett's multiple comparison tests. (n=4 for control and n=5 for CSM and n = 5 for VM injections). Scale bar is 1500 µm for full muscle sections and 100 µm for magnified cross sectional images.

4.2.9. CSM and VM cause Inflammatory cytokine dysregulation.

Inflammatory cytokines are essential for immunity and regeneration. When dysregulated it can lead to chronic inflammation, fibrosis, and an autoimmune response. To investigate the effect of CSM and VM on the inflammatory response of mice we collected blood through cardiac puncture of the day 20 cohorts. The blood was centrifuged, and the serum was collected. Afterwards, the analysis was performed by Eve technologies (Calgary, Alberta, Canada) which targeted 32 known inflammatory markers. Our findings showed that both CSM and VM injections caused inflammatory cytokine dysregulation (figure 4.11). Most notably there was a decrease in G-CSF, IP-10, and LIX levels. However, this was only significant with VM. Additionally, there was a significant decrease in IL-5 with CSM only (figures 4.11 A & B). Our results show a trend in many of the cytokines tested however it is likely that due to the small "n" numbers we don't have significance.

4.11

A

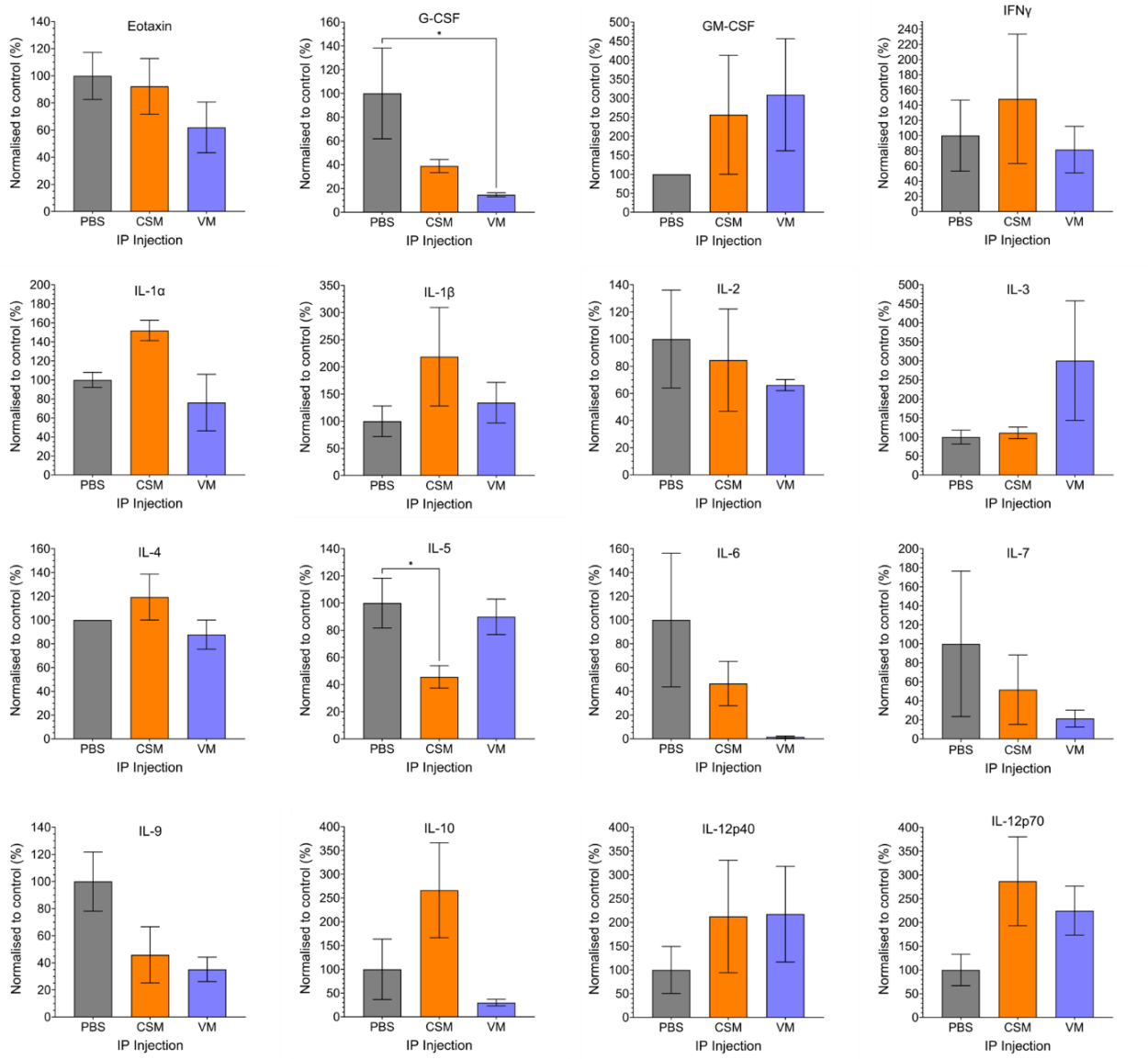
Eotaxin
G-CSF
GM-CSF
IFNγ
IL-1α
IL-1β
IL-2
IL-3
IL-4
IL-5
IL-6
IL-7
IL-9
IL-10
IL-12p40
IL-12p70
Normalised to control (%)
PBS
CSM
VM
IP Injection

4.11

B

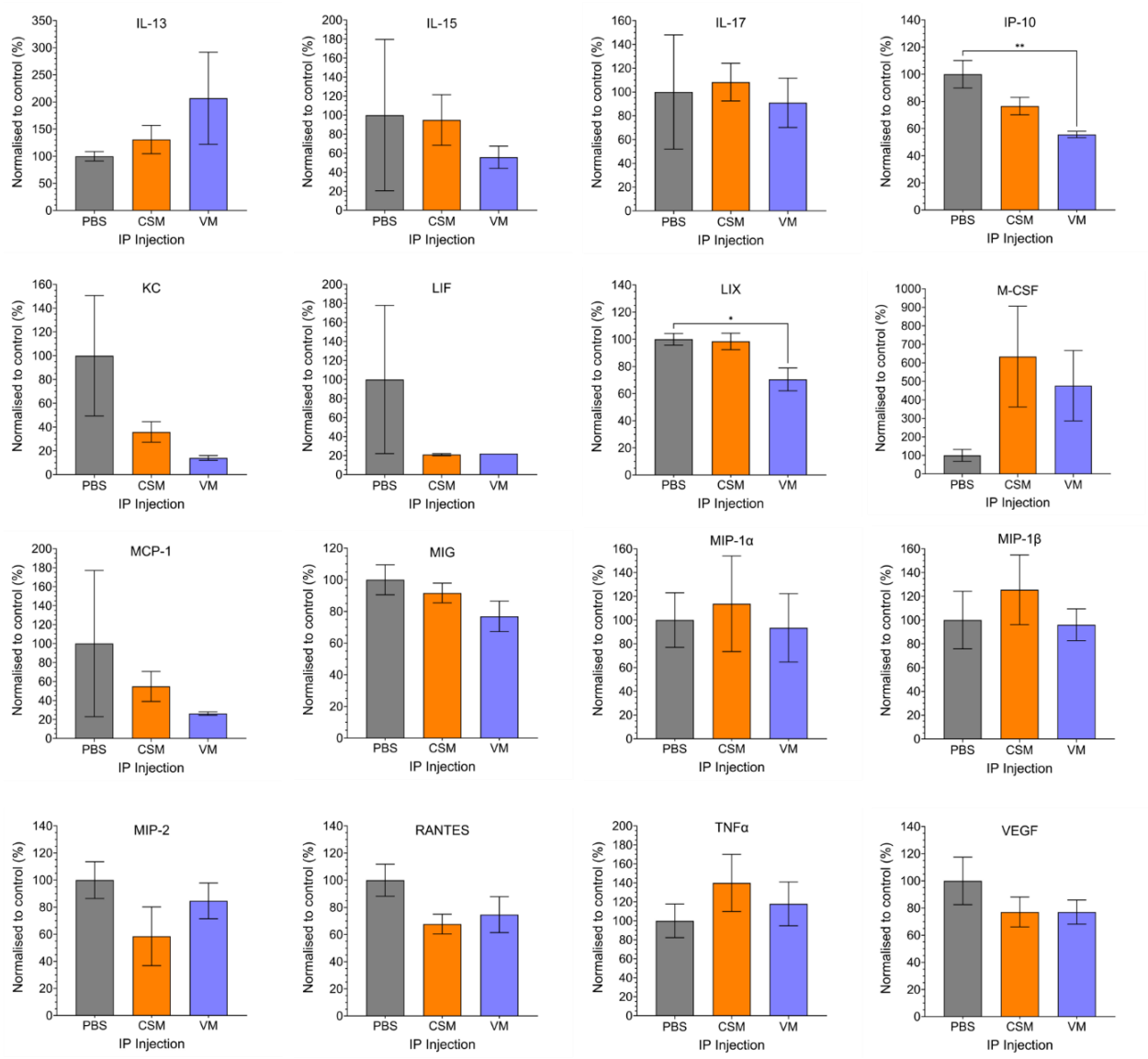

Figure 4.11. Inflammatory cytokine response to CSM and VM exposure. Blood was collected from the day 20 cohorts of mice, the serum was collected and analyzed for 32 known inflammatory markers (A) & (B). Data presented as the mean +/- SEM using one way ANOVA with Dunnett's multiple comparison test. *p<0.05, **p<0.01 (n=4 for the control and 5 for CSM and VM injected).

Our findings indicate that there was no atrophy seen in the undamaged contralateral muscle. However, muscle homeostasis was affected by CSM and VM through dysregulated inflammatory cytokines.

4.3. Discussion

This experiment was based on the previous findings that conditioned media affected satellite cell viability, migration, proliferation and differentiation in-vitro. The hypothesis was that systemic exposure of CSM and VM would affect the regenerative capacity, not only through a heightened state of inflammation, but also through affecting the resident stem cell. The conditioned media exposure had no effect on animal weights and muscle weights. Additionally, there was no notable fibrosis after 20 days regeneration. The regenerating fibres were the same size as the control. IgG infiltration was similar in all cohorts; however, more regenerating fibres were visible in conditioned media injected cohorts by day 10, and incomplete dystrophin perimeters were seen 20 days post-CTX injections. Furthermore, the undamaged contralateral TA muscle fibres displayed no atrophy in IIA, IIB or IIX fibres after 20 days post CTX.

Smoking and now more recently vaping have become prevalent amongst the population in the UK (Tattan-Birch et al., 2023). These are easily consumed through inhalation when the tobacco or e-liquid are combusted through heat. Translating this experience to the mice meant that, due to Home-Office regulations, it required a different route than the most obvious being a smoke chamber. This resulted in mice having two weekly intraperitoneal injections of the conditioned media which would introduce the smoking/vaping constituents to their systems. The preconditioning phase of 8 weeks was to induce a habit within the cohorts and ensure that cotinine levels are similar to those in regular smokers (Nogueira et al., 2018). In this investigation CTX was used to induce skeletal muscle injury, the assumption is that damage would be uniform throughout the muscle due to the concentration of CTX and the same target locations used. This doesn't absolve variability in location of damage but standardizes the strength of injury. The animal weights were not affected by systemic exposure through IP injections. This is similar to previous findings from (Nogueira et al., 2018), they investigated both full body exposure to cigarette smoke (CS) and cigarette

smoke extract (CSE) IP injections. Interestingly, they found that only mice exposed through inhalation don't gain weight.

Damage was induced to the right TA of the mice, with the left used as contralateral control. Collections of the muscles included the EDL, soleus and gastrocnemius. Each of these has a different fibre composition and would be useful for future experiments. When the right hind limb muscle weights were recorded and normalized to body weights, a significant difference in the right gastrocnemius was observed between conditioned media injected and PBS on day 5 dissections. Moreover, a significant increase in weight was observed in the right TA of VM injected mice only. This is interesting, vape smoke has been shown to increase the inflammatory response in the lungs (Masso-Silva et al., 2021), and also gut epithelium (Sharma et al., 2021). Recent studies investigating the effect of "E-cigarette aerosols" (Bahmed et al., 2019; Ma et al., 2021; Wang et al., 2020) show that immune cells including macrophages, neutrophils, eosinophils and t-cells were recruited to the lungs and airways upon exposure to vape smoke. It is possible that due to edema from the inflammatory status of vape exposed mice resulted in increased recruitment of the inflammatory cells leading to heavier TA weights.

Muscle regeneration is a coordinated process that involves inflammation, regeneration leading to fibre maturation, which is tied into extracellular matrix remodeling before functional recovery through innervation. Our experiment targeted some aspects of every step of this process. Initially IgG^+ area used to detect fibre necrosis (Forcina et al., 2020; Morgan et al., 2018) and the early stages of inflammation, which from our results shows to be unaffected in the conditioned media exposed cohorts. This continues with the detection of eMYH a marker for regenerating fibres that was still significantly higher in the CSM and VM injected cohorts by day 10 collections. Additionally, the incomplete ECM remodeling seen by dystrophin staining 20 days post CTX in the conditioned media exposed cohorts leads us to believe that regeneration is delayed but not impeded. We can assume this due to

the similar fibre area size of damaged and undamaged, aided by no significant fibrosis observed in the damaged sections from the picrosirius staining. The secondary aim of this experiment was to investigate if conditioned media induced atrophy in muscle fibres. We stained the contralateral undamaged TA and stained for IIA, IIB and IIX muscle fibres. Previous studies on smokers and cigarette smoke extracts demonstrated atrophy (Chan et al., 2020; Montes de Oca et al., 2008; Stevens et al., 2024) a finding that was unfortunately not shared by our results, we believe that this could be due to the mode of exposure and the concentration of CSM/VM administered.

4.4. Limitations and future work

The first limitation faced in our experiments was the smoke and vape delivery method. Due to rules and regulations, a respiratory method of delivery was not an option under our licence. Therefore, the IP systemic delivery route was adopted. Even though (Nogueira et al., 2018) provides evidence that IP delivery of CSM is just as effective, the main route of consumption within the population remains through inhalation. Ideally, we would have opted for a side-by-side comparison.

The number of mice used in these experiments is minimal compared to similar projects investigating the outcomes of smoking and vaping. The study would benefit from more animals, namely the muscle weights in section 4.2.2 and the comparisons of fibre size of damaged vs undamaged in section 4.2.3. Here we saw a trend of decreased weights and sizes and potentially with higher numbers this trend would become significant. But our findings remain substantial even with the cohort sizes used.

Following IgG^+ staining, an F4/80 fluorescence or immunohistochemical stain would have provided insight into the recruitment of macrophages to the damage site. A recent study by (Tan et al., 2025) concluded that TNF-α released by cigarette smoke induced macrophages promoted skeletal muscle pyroptosis and likely contributing to muscle atrophy.

Staining for fibre type would provide insights into which could be affected by systemic exposure to the conditioned media. Even though fibre area was measured using H&E in the damaged area, cross sectional measurements by fibre type was intended, and would have added value to the current study. We observed a decrease in fibre size with CSM and VM; (though insignificant and perhaps with larger cohorts this would be different), this may be due to reduced protein synthesis. The best way to investigate this would be to prepare western blots using antibodies against 26S proteasome and LC3 for autophagy.

The experiment has three time points of muscle collection post CTX, this allowed for visualization of the regenerative process. However, extension of the timeline by adding one more cohort, would have provided more insight into the remodeling of the ECM, ideally we would have preferred to have a timepoint where we could visualize the complete expression of dystrophin.

Future studies would involve profiling the neuromuscular junction (NMJ). Cross sections would be stained with α-Bungarotoxin; an antibody used to visualize the (NMJ) (Hsieh & Chen, 2024) to determine the outcome on innervation and potential functionality of the muscle fibres. Then, RNA sequencing of the gastrocnemius to determine any differences in expression. The EDL's would undergo single fibre isolation and then (I) on-fibre analysis of the stem cell, where we interrogate activation, proliferation and migration (II) expansion of the primary satellite cells on a petri dish then investigate how they respond to CSM/VM and compare to immortalized cell lines.

4.5. Conclusion

In this study we set out to investigate if cigarette smoke and vape smoke media affected muscle regeneration in-vivo. We hypothesized that due to the inflammatory nature of both conditioned media and the previous findings from in-vitro experiments that regeneration would be hindered or impeded, leading to increased fibrosis in damaged areas.

We found that animals exposed to the conditioned media had hindered regeneration and incomplete fibre maturation by day 20 after CTX induced muscle injury. Most literature alludes to the cardiovascular and respiratory outcomes of e-cigarettes and as far as we know, this is the first instance proving that vaping has the same implications as cigarette smoke on muscle regeneration.

Chapter 5: Using transcriptomic analysis coupled to bioinformatic based drug repurposing platforms to identify novel therapies to reverse the effects of cigarette smoke

5.1. Introduction

Protein turnover is critical to muscle homeostasis. The balance between protein synthesis and degradation is integral to maintaining muscle integrity, mass and function in both the resting and active state. Muscle protein turnover can be influenced by nutrient supply, hormonal stimuli, exercise and stress. Disruption in the balance can lead to sarcopenia and atrophy. Smoking has been found to cause muscle weakness and atrophy. One mechanism was described in a longitudinal study performed on 16 individuals concluded that smoking impaired muscle protein synthesis and increased the expression of myostatin, a myokine that inhibits muscle growth, and muscle atrophy F-box (MAFbx), an E3 ubiquitin ligase that mediates skeletal muscle atrophy (Petersen et al., 2007). Alternatively, Liu et al (Liu et al., 2011) described a different pathway involving the over-expression of USP-19 through MAPK phosphorylation. Several studies reported hindered cellular differentiation (Ng et al., 2015; Wahl et al., 2016), furthermore (Liu et al., 2011) specifically reported inhibited myogenic differentiation and myotube formation after cigarette smoke extract exposure. From our in vitro studies we showed that cigarette smoke conditioned media (CSM) affects viability, proliferation, migration, differentiation of muscle cells, and metabolism potentially causing atrophy. These effects are a result of direct exposure to CSM as evidenced by our work and supported by the works of (Feng et al., 2021), where cigarette smoke (CS) induced apoptosis of Raw264.7 macrophages, (Martinez et al., 2022) impeded osteoblast differentiation and (Liu et al., 2011) inhibition of myogenic differentiation in L6 rat cells, (Horinouchi & Miwa, 2021) and attenuated mitochondrial metabolic activity in human vascular endothelial cells. The changes in cell function could be due to alterations in transcription. Liu et al (Liu et al., 2011) reported that CS exposure upregulated USP-19 gene expression in L6 myotubes. Similarly, Wang et al (Wang et al., 2021) reported changes in transcription of IL-1α, IL-1β, TNF-α and TGF-β after exposing BEAS-2B (a human bronchial epithelial cell line) to cigarette smoke condensate. Currently, there are multiple

methods to process gene expression, these include northern blotting, quantitative polymerase chain reaction (qPCR), DNA microarray and RNA-seq.

Northern blotting is used to measure the size and quantity of a particular RNA in a sample through separation by electrophoresis, transfer to a nylon or nitrocellulose (NC) membrane, and hybridisation with labelled complementary probes. Despite the simplicity and low cost, the technique is limited by time consumption, low sample throughput and high demand of starting materials (Singh et al., 2018).

qPCR quantifies gene expression in real time by amplifying cDNA and labelling with florescence dyes. The cycle threshold (Ct) is used as an indicator of the initial transcript abundance. Absolute quantification is accomplished using a standard curve derived from known DNA concentrations. It is possible to detect multiple transcripts in a single reaction by using different probes labelled with different florescent dyes, also known as multiplex qPCR. While qPCR is efficient and offers multiplex detection, it relies on pre-existing knowledge of target sequences and is limited to the number of transcripts that can be analysed (VanGuilder et al., 2008).

DNA microarrays measure gene expression by hybridizing labelled cDNA to probes on a chip. This allows for the simultaneous quantification of thousands of transcripts at once. There are two main types of microarray technology, cDNA microarrays and in-situ synthesized oligonucleotide microarrays. They differ in probe design but follow a similar approach, RNA extraction, cDNA synthesis, labelling then hybridisation and finally fluorescence scanning. The fluorescent signal intensity is proportional to transcript quantity. Microarrays are cost effective; they do not require prior sequence knowledge (unlike qPCR) and can run thousands of transcripts. However, they cannot test multiple samples; a control and test must be run separately. Moreover, they require dedicated software and statistical tools for analysis (Singh et al., 2018; Sinicropi et al., 2006).

RNA-seq quantifies RNA through direct sequencing and measurement of RNA fragments. There are several methods of RNA sequencing and choice depends on the objective of the study. However, they all share similar principles. RNA is extracted and purified, then enriched and fragmented followed by ligation with adapter molecules. Then, the RNA is amplified creating a sequencing library and finally high throughput sequencing. This technology is valuable because it can detect thousands of differentially expressed gene variants, and transcript isoforms up to a resolution of a single nucleotide. Consequently, this comes with a high cost and computational burden for data analysis (Kukurba & Montgomery, 2015; Singh et al., 2018).

Bioinformatics can be used to identify molecular pathways by analysing large scale data such as transcriptomics, proteomics and metabolomics. Using pathway databases, differentially expressed genes or proteins can be mapped to biological pathways revealing functional associations and regulative pathways. This allows for the identification of key signalling cascades that can be linked to therapeutic targets for various conditions. The basis of Connectivity mapping (CMAP) is that different compounds which are readily translatable, and accepted by the food and drug administration (FDA) are introduced to various cell lines. Thereafter the transcriptome of the cell line is determined either using RNAseq or by microarrays. This signature is the response of cells to a particular drug. What an investigator can subsequently do is to take their intervention on any cellular basis or tissue and develop a transcriptome. Thereafter, match the experimental transcriptome versus the transcriptome induced by an FDA approved drug on the cell lines examined by the Broad institute. This gives two possibilities; one is you match the transcriptome of your intervention to the Broad transcriptome and thereby you identify a drug which mimics your experimental set up. The converse could also be done; you look for a transcriptome which is opposite to the one you induced and therefore you find the antagonist (Lamb et al., 2006).

In the previous two chapters we investigated the effects of cigarette smoke conditioned media (CSM) and vape conditioned media (VM) on the organellar, cellular, and tissue level. In this chapter we delve into the gene expression of C_2C_{12} before and after exposure to CSM, in both myoblasts and myotubes. We aimed to identify differentially expressed genes. Then, using C-mapping we aimed to identify compounds that could potentially alleviate or counter the effects of the cigarette smoke in vitro. The two chosen compounds, asiaticoside and harmine were initially tested for cytotoxicity then potential therapeutic effects in a viability assay with CSM exposure.

5.2. Results

5.2.1. Exposure to CSM causes differential gene expression in C_2C_{12} myoblasts and myotubes.

To investigate the potential changes in gene expression at mRNA level we cultured the C_2C_{12} cell lines and analysed both myoblasts and myotubes. Briefly, the myoblasts were allowed to grow until 60% confluence before they were exposed to CSM for 24 hours then lysed and collected for microarray. For myotubes, the cells were allowed to reach confluence before differentiation, then they were exposed to CSM for 24 hours before lysis and collection. This was then followed by RNA recovery and integrity analysis. Samples with RNA integrity number greater than 7 progressed to microarrays. Principal component analysis (PCA) is a technique used to simplify complicated sets of data. It Enables us to visualize correlations or variances between thousands of genes using 3-D scatter plots. The principal component analysis of the microarray revealed distinct differences between the controls and CSM exposed myoblasts (figure 5.1) and myotubes (figure 5.2). However, there was no visible clustering of the samples with both controls and the cigarette smoke exposed cohort. The variations in locations of the samples; blue dots for cigarette exposed samples and red dots for control samples, does suggest that CSM exposure causes significant changes on the overall gene expression pattern compared to the control.

5.1

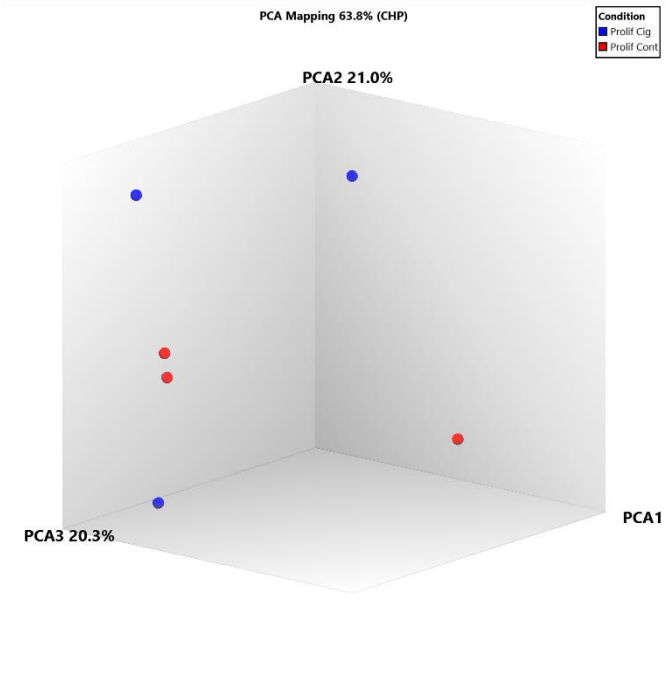

Figure 5.1. Principal component analysis (PCA) of the gene expression data of myoblasts control vs myoblasts cigarette exposed. Each dot represents a sample.

5.2

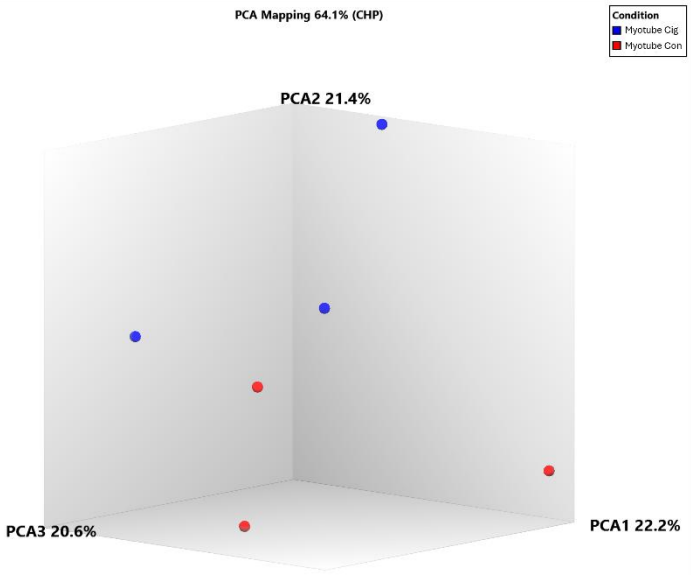

Figure 5.2. Principal component analysis (PCA) of the gene expression data of myotubes control vs myotubes cigarette exposed. Each dot represents a sample.

In the volcano plot of the myoblast exposed cohort (figure 5.3) a fold change of 0.5 in log 2 scale corresponds to a fold change of 1.4142 in linear scale. The x-axis represents the log2 value of fold change and the y-axis represents the t-statistic as log10 p value. Each gene is represented by a dot in the graph. We identified the highest differentially expressed genes as Cyp1a1, Ahrr, and Ell. There were 45012 similar, and a total of 89 were found to be differentially expressed. The upregulated were 43 and downregulated were 46. This was further correlated when a more detailed view of the upregulated and downregulated genes was viewed in a heat map of cigarette exposed in relation to control myoblasts (figure 5.4 & 5.6).

5.3

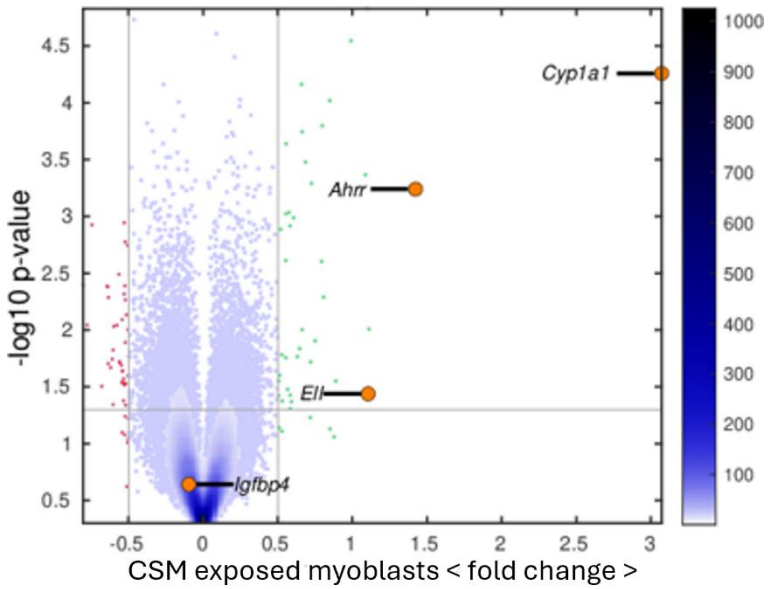

Figure 5.3. Pairwise volcano plot of differentially expressed transcripts (DEGS) between control myoblasts and cigarette exposed myoblasts. Each gene is represented by a dot in the graph. There were 45012 similar, and 89 were found to be differentially expressed. The upregulated were 43 and downregulated were 46.

In the heatmap of upregulated genes after myoblast exposure to CSM (figure 5.4) we find all the highest differentially expressed genes. Cyp1a1 is involved in the metabolism of xenobiotics. It is involved in the oxidative metabolism of benzo[α]pyrene; a component in cigarette smoke, and polycyclic aromatic hydrocarbons converting them into potent carcinogens (Mescher & Haarmann-Stemmann, 2018). Similarly, Ahrr is activated by pollutants and is involved in the xenobiotic signalling pathway (Baba et al., 2001). Elongation factor for RNA polymerase II (Ell) increases the rate of transcription and acts as a negative regulator of p53 (Shinobu et al., 1999). The functional enrichment analysis of upregulated genes in smoke exposed myoblasts in relation to control (figure 5.5) revealed several highly significant terms with the majority falling within the metabolic processes. But the term with highest significance was “response to xenobiotic stimulus”.

5.4

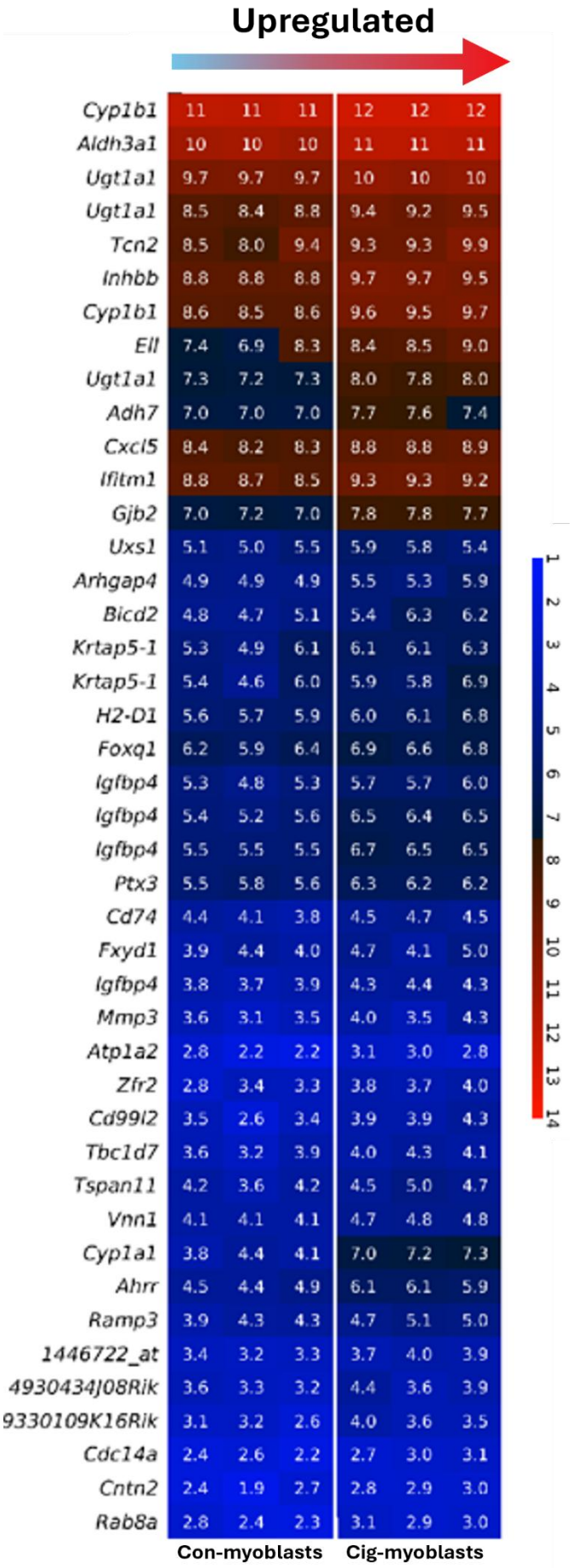
Upregulated
Cyp1b1 11 11 11 12 12 12
Aldh3a1 10 10 10 11 11 11
Ugt1a1 9.7 9.7 9.7 10 10 10
Ugt1a1 8.5 8.4 8.8 9.4 9.2 9.5
Tcn2 8.5 8.0 9.4 9.3 9.3 9.9
Inhbb 8.8 8.8 8.8 9.7 9.7 9.5
Cyp1b1 8.6 8.5 8.6 9.6 9.5 9.7
Ell 7.4 6.9 8.3 8.4 8.5 9.0
Ugt1a1 7.3 7.2 7.3 8.0 7.8 8.0
Adh7 7.0 7.0 7.0 7.7 7.6 7.4
Cxcl5 8.4 8.2 8.3 8.8 8.8 8.9
Ifitm1 8.8 8.7 8.5 9.3 9.3 9.2
Gjb2 7.0 7.2 7.0 7.8 7.8 7.7
Uxs1 5.1 5.0 5.5 5.9 5.8 5.4
Arhgap4 4.9 4.9 4.9 5.5 5.3 5.9
Bicd2 4.8 4.7 5.1 5.4 6.3 6.2
Krtap5-1 5.3 4.9 6.1 6.1 6.1 6.3
Krtap5-1 5.4 4.6 6.0 5.9 5.8 6.9
H2-D1 5.6 5.7 5.9 6.0 6.1 6.8
Foxq1 6.2 5.9 6.4 6.9 6.6 6.8
Igfbp4 5.3 4.8 5.3 5.7 5.7 6.0
Igfbp4 5.4 5.2 5.6 6.5 6.4 6.5
Igfbp4 5.5 5.5 5.5 6.7 6.5 6.5
Ptx3 5.5 5.8 5.6 6.3 6.2 6.2
Cd74 4.4 4.1 3.8 4.5 4.7 4.5
Fxyd1 3.9 4.4 4.0 4.7 4.1 5.0
Igfbp4 3.8 3.7 3.9 4.3 4.4 4.3
Mmp3 3.6 3.1 3.5 4.0 3.5 4.3
Atp1a2 2.8 2.2 2.2 3.1 3.0 2.8
Zfr2 2.8 3.4 3.3 3.8 3.7 4.0
Cd99l2 3.5 2.6 3.4 3.9 3.9 4.3
Tbc1d7 3.6 3.2 3.9 4.0 4.3 4.1
Tspan11 4.2 3.6 4.2 4.5 5.0 4.7
Vnn1 4.1 4.1 4.1 4.7 4.8 4.8
Cyp1a1 3.8 4.4 4.1 7.0 7.2 7.3
Ahrr 4.5 4.4 4.9 6.1 6.1 5.9
Ramp3 3.9 4.3 4.3 4.7 5.1 5.0
1446722_at 3.4 3.2 3.3 3.7 4.0 3.9
4930434J08Rik 3.6 3.3 3.2 4.4 3.6 3.9
9330109K16Rik 3.1 3.2 2.6 4.0 3.6 3.5
Cdc14a 2.4 2.6 2.2 2.7 3.0 3.1
Cntn2 2.4 1.9 2.7 2.8 2.9 3.0
Rab8a 2.8 2.4 2.3 3.1 2.9 3.0
Con-myoblasts
Cig-myoblasts
1 2 3 4 5 6 7 8 9 10 11 12 13 14

Figure 5.4. Heat map of up regulated genes in cigarette exposed myoblasts in relation to control myoblasts. Each column represents one sample. The colour bar on the side codifies gene expression in $\log_2$ scale, the higher the gene expression the more red the colour.

5.5

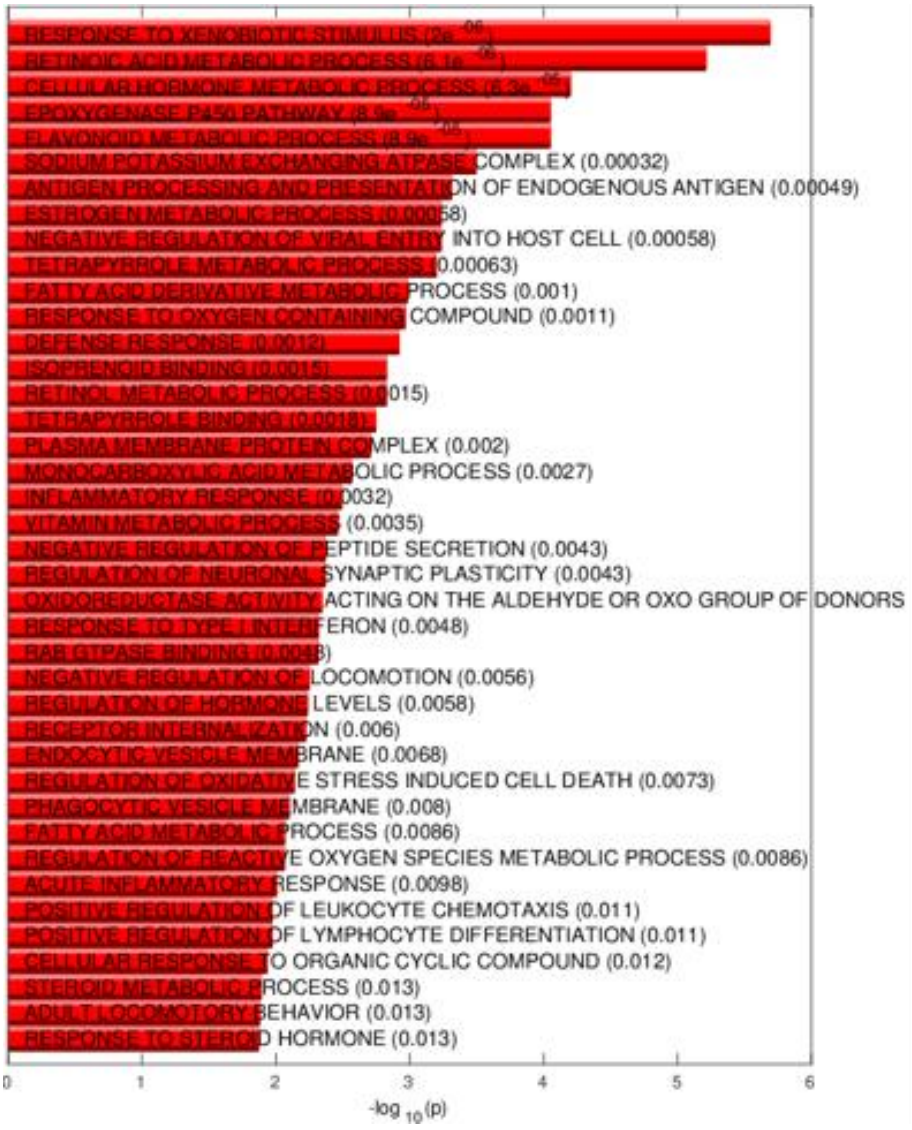

Figure 5.5. Bar plot of the significantly enriched terms of cigarette exposed myoblasts up regulated in relation to control. Longer bars correspond to higher statistical significance of the enrichment (the p-values are given in parentheses).

The heatmap of cigarette smoke exposed myoblasts down regulated genes (figure 5.6) in relation to control yielded some interesting findings. Gm7325 otherwise known as myomixer (myomerger) (Quinn et al., 2017) was a standout of the downregulated genes. Furthermore, Nov also known as Ccn3 is a part of the CCN family that are associated with the extracellular matrix and play a role in cardiovascular and skeletal muscle development (Heath et al., 2008). Igf2 (Insulin like growth factor 2) a member of the insulin family and is involved in development and growth. Finally, Actc1 (Actin alpha cardiac muscle 1), α-actins are a major component of the contractile apparatus and together with tropomyosin form the thin contractile filament that connects the Z-disc to myosin (thick filament) (Frank et al., 2019). Upon investigating the functional enrichment analysis (Figure 5.7) some of the standout terms of downregulated genes include the negative regulation of calcium mediated signalling, tissue migration, positive regulation of protein complex assembly, wound healing, extracellular matrix binding and growth factor activity.

5.6

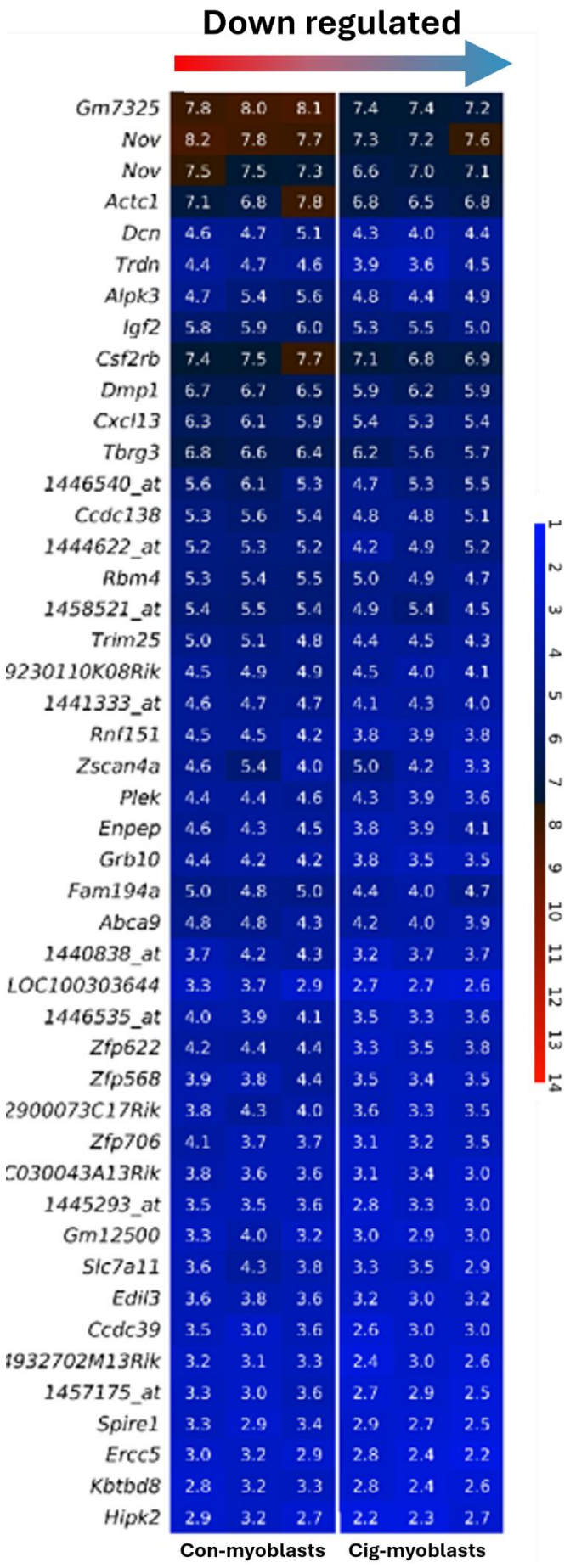
Down regulated
Gm7325 7.8 8.0 8.1 7.4 7.4 7.2
Nov 8.2 7.8 7.7 7.3 7.2 7.6
Nov 7.5 7.5 7.3 6.6 7.0 7.1
Actc1 7.1 6.8 7.8 6.8 6.5 6.8
Dcn 4.6 4.7 5.1 4.3 4.0 4.4
Trdn 4.4 4.7 4.6 3.9 3.6 4.5
Alpk3 4.7 5.4 5.6 4.8 4.4 4.9
Igf2 5.8 5.9 6.0 5.3 5.5 5.0
Csf2rb 7.4 7.5 7.7 7.1 6.8 6.9
Dmp1 6.7 6.7 6.5 5.9 6.2 5.9
Cxcl13 6.3 6.1 5.9 5.4 5.3 5.4
Tbrg3 6.8 6.6 6.4 6.2 5.6 5.7
1446540_at 5.6 6.1 5.3 4.7 5.3 5.5
Ccdc138 5.3 5.6 5.4 4.8 4.8 5.1
1444622_at 5.2 5.3 5.2 4.2 4.9 5.2
Rbm4 5.3 5.4 5.5 5.0 4.9 4.7
1458521_at 5.4 5.5 5.4 4.9 5.4 4.5
Trim25 5.0 5.1 4.8 4.4 4.5 4.3
9230110K08Rik 4.5 4.9 4.9 4.5 4.0 4.1
1441333_at 4.6 4.7 4.7 4.1 4.3 4.0
Rnf151 4.5 4.5 4.2 3.8 3.9 3.8
Zscan4a 4.6 5.4 4.0 5.0 4.2 3.3
Plek 4.4 4.4 4.6 4.3 3.9 3.6
Enpep 4.6 4.3 4.5 3.8 3.9 4.1
Grb10 4.4 4.2 4.2 3.8 3.5 3.5
Fam194a 5.0 4.8 5.0 4.4 4.0 4.7
Abca9 4.8 4.8 4.3 4.2 4.0 3.9
1440838_at 3.7 4.2 4.3 3.2 3.7 3.7
LOC100303644 3.3 3.7 2.9 2.7 2.7 2.6
1446535_at 4.0 3.9 4.1 3.5 3.3 3.6
Zfp622 4.2 4.4 4.4 3.3 3.5 3.8
Zfp568 3.9 3.8 4.4 3.5 3.4 3.5
2900073C17Rik 3.8 4.3 4.0 3.6 3.3 3.5
Zfp706 4.1 3.7 3.7 3.1 3.2 3.5
C030043A13Rik 3.8 3.6 3.6 3.1 3.4 3.0
1445293_at 3.5 3.5 3.6 2.8 3.3 3.0
Gm12500 3.3 4.0 3.2 3.0 2.9 3.0
Slc7a11 3.6 4.3 3.8 3.3 3.5 2.9
Edil3 3.6 3.8 3.6 3.2 3.0 3.2
Ccdc39 3.5 3.0 3.6 2.6 3.0 3.0
1932702M13Rik 3.2 3.1 3.3 2.4 3.0 2.6
1457175_at 3.3 3.0 3.6 2.7 2.9 2.5
Spire1 3.3 2.9 3.4 2.9 2.7 2.5
Ercc5 3.0 3.2 2.9 2.8 2.4 2.2
Kbtbd8 2.8 3.2 3.3 2.8 2.4 2.6
Hipk2 2.9 3.2 2.7 2.2 2.3 2.7
Con-myoblasts
Cig-myoblasts
1 2 3 4 5 6 7 8 9 10 11 12 13 14

Figure 5.6. Heat map of down regulated genes in cigarette exposed myoblasts in relation to control. Each column represents one sample. The colour bar on the side codifies gene expression in log_2 scale, the higher the gene expression the more red the colour.

5.7

Figure 5.7. Bar plot of the significantly enriched terms of cigarette exposed myoblasts downregulated in relation to control. Loner bars correspond to higher statistical significance of the enrichment (the p-values are given in parentheses).

Next volcano plots of the myotubes exposed cohort (figure 5.8) identified the highest differentially expressed genes as Calr3, Adamts15, Myl10 and Adh7. A fold change of 0.5 in log 2 scale corresponds to a fold change of 1.4142 in linear scale. The x-axis represents the log2 value of fold change and the y-axis represents the t-statistic as log10 p value. Moreover, 231 differentially expressed transcripts were detected between CSM exposed and control myotubes (98 upregulated and 133 downregulated genes). These were further correlated when a more detailed view of the upregulated and down regulated genes was viewed in a heat map of cigarette exposed in relation to control myotubes (figure 5.9 & 5.11). Calr3 is a member of the calreticulin family which are calcium binding chaperones and mainly found in the endoplasmic reticulum. Adh7 is part of the alcohol dehydrogenases (ADHs) which are mostly involved in the metabolism of drugs and metabolites that contain alcohol functional groups (Di et al., 2021). Adamts15 is involved in the extracellular matrix remodelling and myoblast fusion (Stupka et al., 2013)

5.8

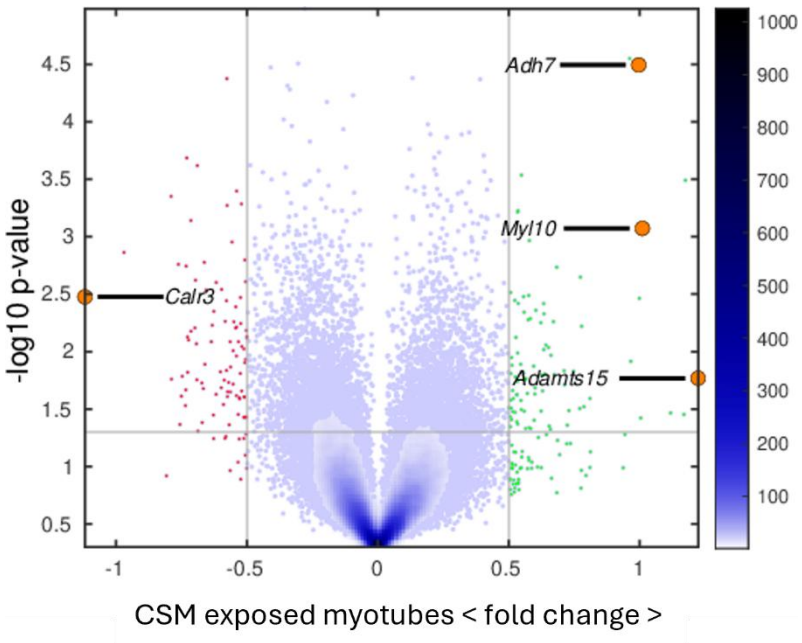

Figure 5.8. Pairwise Volcano plot of differentially expressed transcripts (DEGS) between control and cigarette exposed myotubes. Each gene is represented by a dot in the graph. There were 44870 similar, and a total of 231 were found to be differentially expressed. The up regulated were 98 and downregulated were 133.

Some noteworthy mentions of upregulated genes (figure 5.9) in response to CSM induced stress include Klf15 which regulates lipid flux and metabolic homeostasis in muscle (Fan et al., 2021) and Nfix which is involved in muscle regeneration (Rossi et al., 2017). Noteworthy mentions of down regulated genes (figure 5.11) due to CSM induced stress include Gpr35 which is implicated in multiple tumours and immunomodulation (Takkar et al., 2024) and fibromodulin (Fmod), a negative regulator of myostatin expression.

The functional enrichment analysis of upregulated genes in smoke exposed myotubes in relation to control (figure 5.10) revealed several significant terms with the highest in significance reported as “Reactive oxygen species biosynthetic process”. The functional enrichment analysis of downregulated genes in smoke exposed myotubes in relation to control (figure 5.12) revealed many interesting significant terms including “proteinaceous extracellular matrix”, “regulation of macrophage activation”, “extracellular structure organisation” and “regulation of cytokine secretion”.

5.9

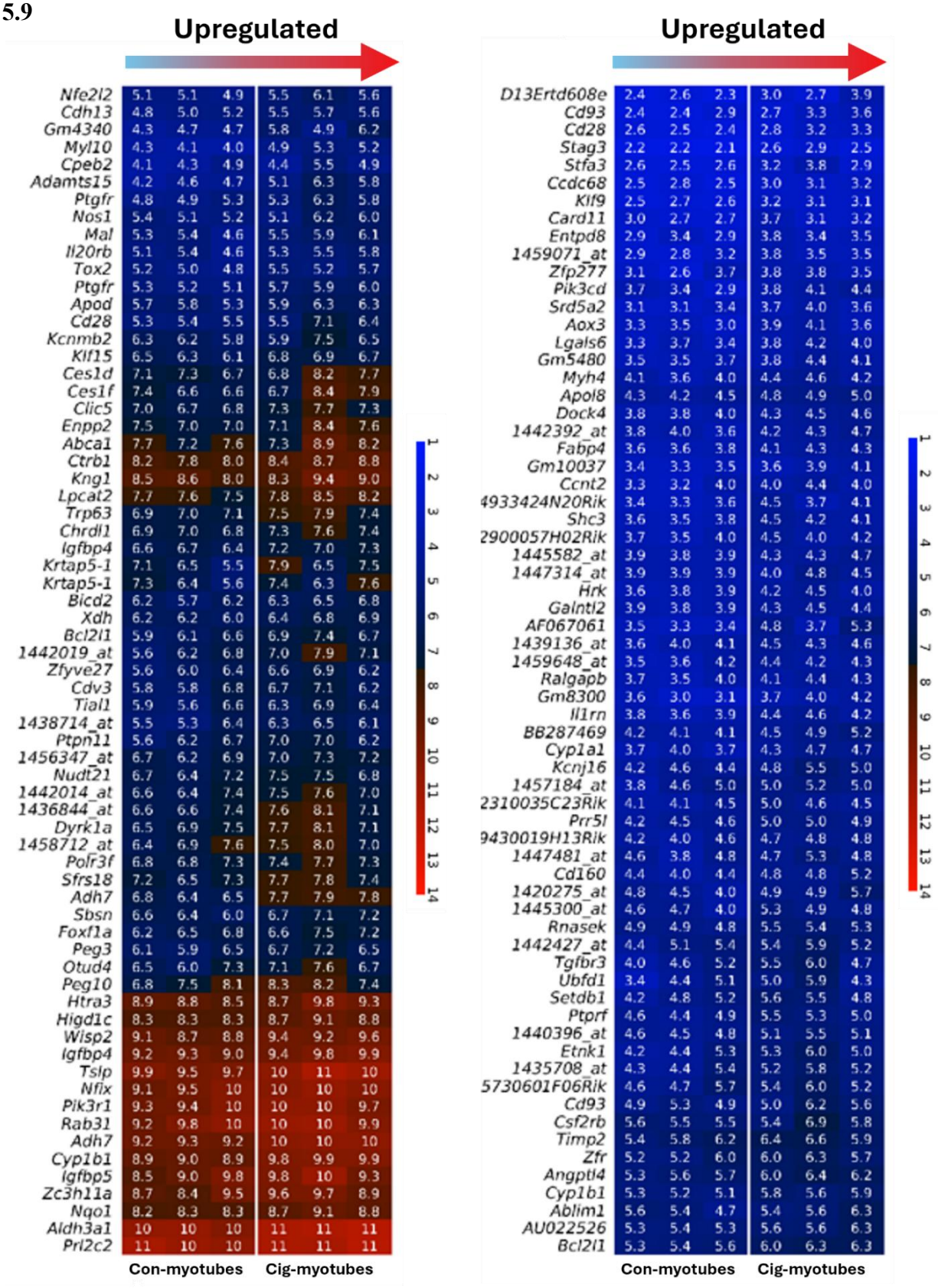

Figure 5.9. Heat map of up regulated genes in cigarette exposed myotubes in relation to control. Each column represents one sample. The colour bar on the side codifies gene expression in $\log_2$ scale, the higher the gene expression the more red the colour.

5.10

Figure 5.10. Bar plot of the significantly enriched terms of cigarette exposed myotubes up regulated in relation to control. Longer bars correspond to higher statistical significance of the enrichment (the p-values are given in parentheses)

5.11

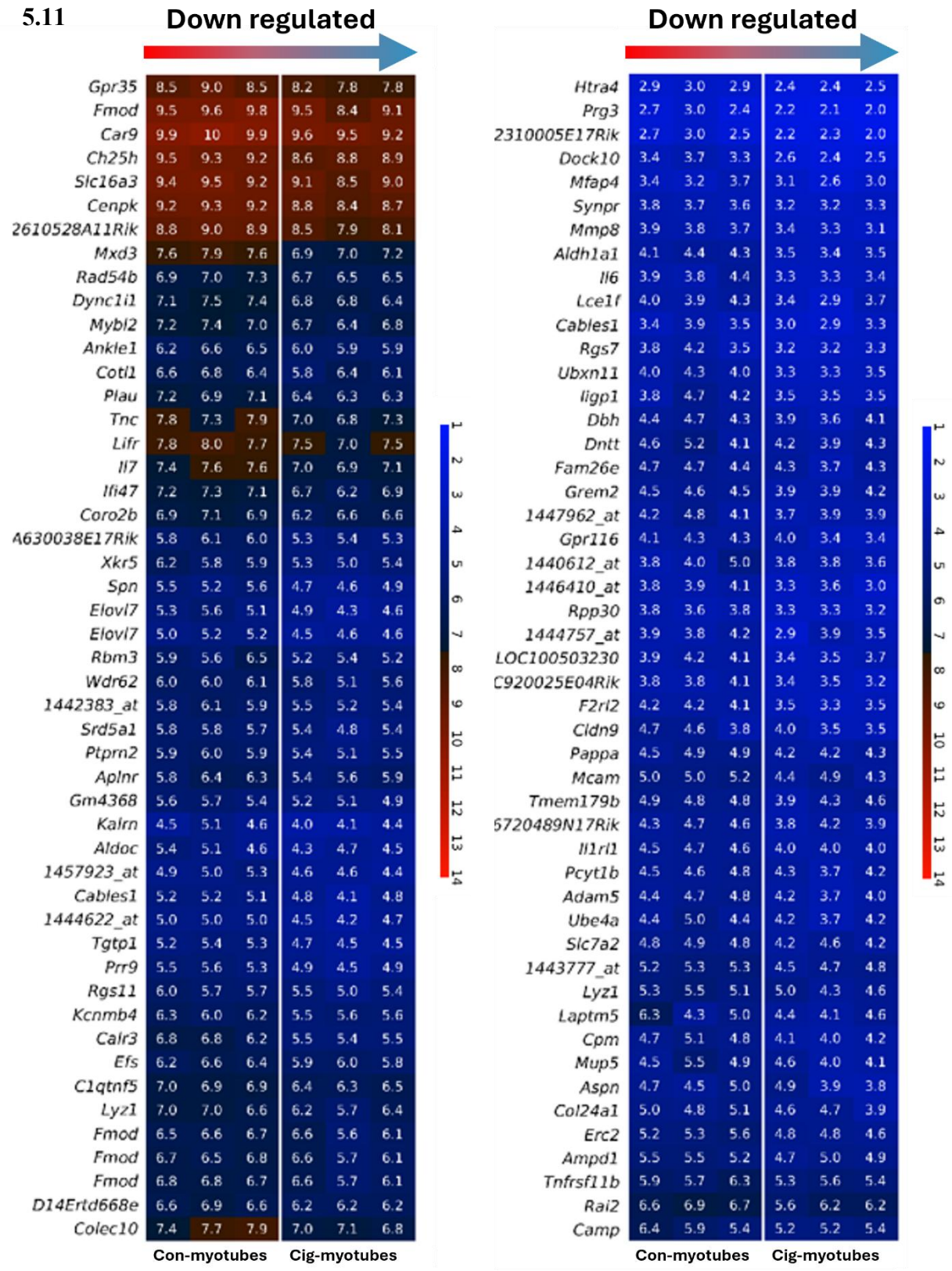

Figure 5.11. Heat map of down regulated genes in cigarette exposed myotubes in relation to control. Each column represents one sample. The colour bar on the side codifies gene expression in $\log_2$ scale, the higher the gene expression the more red the colour.

5.12

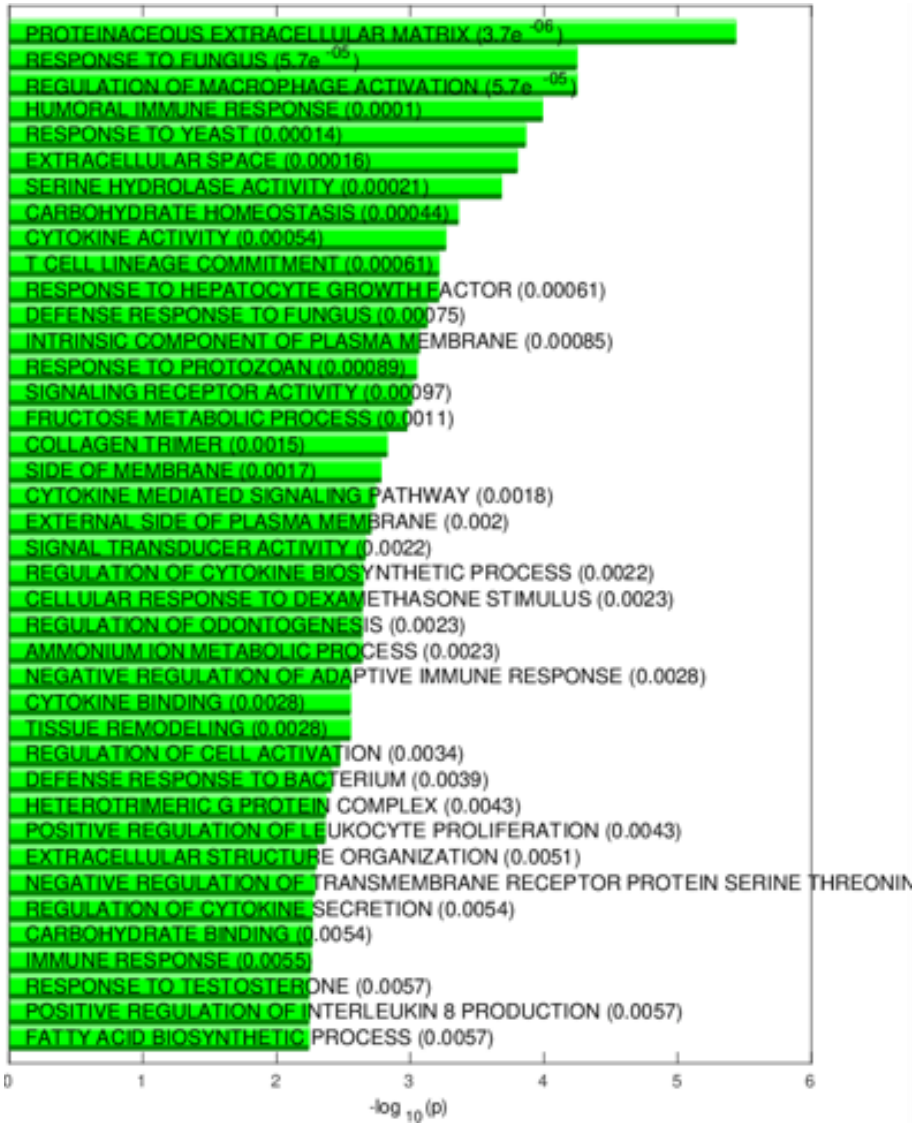

Figure 5.12. Bar plot of the significantly enriched terms of cigarette exposed myotubes down regulated in relation to control. Longer bars correspond to higher statistical significance of the enrichment (the p-values are given in parentheses).

5.2.2. C-mapping to identify compounds that may counteract the effects of cigarette smoke.

After identifying the differentially expressed genes, a connectivity mapping (CMAP) was generated by comparing the cigarette smoke specific differentially expressed genes (DEGs) to the Broad connectivity map database and the SPIED web portal to identify possible compounds that could potentially reverse or inhibit the effect of cigarette smoke. C-mapping is a database that identifies relationships among diseases, genetic perturbations and pharmacological compounds by comparing gene expression. This database holds hundreds of reference signatures collected from exposing human cell lines to a multitude of FDA approved chemical compounds. These signatures were used as a baseline against which our signatures were compared with. This comparison results in a positive or negative correlation which quantifies the degree of similarity or difference between our profiles and those of the database with the most significant being termed “hits”. The CMAP ‘hits’ were ranked according to their correlation with the cigarette smoke cohort DEGs. As previously performed with the microarray, we investigated the effects in both myoblasts and myotubes. Interrogating the microarray provided lists of compounds that potentially either escalated (highlighted in green) or receded (highlighted in red) the effects of CSM (figures 5.13 & 5.14). The compounds with the highest correlation to reduce the effects of CSM in the myoblast exposed cohort (figure 5.13) were asiaticoside, carisoprodol, harmine, hexesterol, fluoucinonide and others. Interestingly, we find etoposide which we had previously used to induce senescence in the list of compounds that escalate the effects of CSM in myoblasts.

5.13

Compound	Correlation	Significance
Kinetin	0.66	3.43 (22)
Bretylium tosilate	0.48	2.59 (27)
Etoposide	0.37	2.50 (45)
5253409	0.47	2.48 (27)
Trimethylcolchicinic acid	0.41	2.48 (36)
Terazosin	0.27	2.39 (76)
Bupivacaine	0.52	2.36 (20)
Thiamine	0.37	2.30 (39)
Fludrocortisone	0.22	2.28 (105)
Epitiostanol	0.43	2.28 (27)
Monobenzone	0.36	2.28 (39)
Pipemidic acid	0.35	2.26 (41)
Prednisone	0.35	2.21 (40)
Merbromin	0.24	2.17 (83)
Artemisinin	0.31	2.17 (50)
Gelsemine	0.51	2.17 (18)
(-)-isoprenaline	0.33	2.10 (41)
Primidone	0.41	2.08 (26)
Prestwick-981	0.37	2.04 (30)
Vorinostat	0.18	2.04 (130)
Acemetacin	0.31	2.03 (42)
Trimethoprim	0.31	2.02 (42)
Leflunomide	0.27	2.01 (57)
Galantamine	-0.30	2.03 (46)
Mefloquine	-0.27	2.03 (58)
Gramine	-0.39	2.03 (28)
Fluocinonide	-0.22	2.04 (87)
Miconazole	-0.32	2.04 (41)
Paroxetine	-0.42	2.04 (24)
Bergenin	-0.40	2.06 (27)
5155877	-0.31	2.10 (45)
Myosmine	-0.24	2.14 (80)
F0447-0125	-0.34	2.15 (39)
Androsterone	-0.45	2.19 (23)
Ramipril	-0.47	2.19 (21)
Conessine	-047	2.24 (22)
Hexestrol	-0.22	2.24 (101)
CP-645525-01	-0.28	2.31 (68)
Chicago Sky Blue 6B	-0.34	2.34 (48)
Estradiol	-0.35	2.42 (47)
Amylocaine	-0.46	2.43 (27)
Lysergol	-0.33	2.46 (55)
C-75	-0.39	2.58 (43)
Saquinavir	-0.46	2.92 (38)
BCB000038	-0.49	2.95 (33)
Mepyramine	-0.48	2.99 (35)
Harmine	-0.28	3.04 (114)
Carisoprodol	-0.54	3.06 (28)
Asiaticoside	-0.72	4.06 (23)

Figure 5.13. CMAP findings of cigarette smoke exposed myoblasts. Compounds that correlate (green) and anti-correlate (red) with the transcriptome of CSM exposed myoblasts.

The compounds with the highest correlation to reduce the effects of CSM in the myotubes exposed cohort (figure 5.14) were hexylcaine, clebopride, MK-886, diethylcarbamazine, 16-phenyltetranorprostaglandin_E2, diphemanil-metilsulfate, halofantrine, SR-95639A and xamoterol.

5.14

Compound	Correlation	Significance
Hydralazine	0.47	2.96 (36)
Tetramisole	0.53	2.91 (27)
L-methionine sulfoximine	0.52	2.88 (28)
Isoxsuprine	0.51	2.85 (29)
Terfenadine	0.33	2.63 (61)
Solanine	0.37	2.55 (45)
AG-013608	0.43	2.45 (32)
Fenoterol	0.30	2.44 (65)
Ioversol	0.44	2.43 (30)
Menadione	0.32	2.42 (56)
Cefazolin	0.44	2.41 (29)
Retrorsine	0.43	2.41 (31)
Sanguinarine	0.26	2.41 (82)
10-methoxyharmalan	0.37	2.38 (41)
Epiandrosterone	0.31	2.38 (57)
Desoxycortone	0.40	2.38 (34)
Parthenolide	0.27	2.34 (73)
Rottlerin	0.27	2.34 (75)
PNU-0251126	0.32	2.30 (50)
Mometasone	0.40	2.29 (32)
Fluphenazine	0.32	2.27 (49)
Sotalol	0.42	2.25 (29)
Hexylcaine	-0.48	2.01 (18)
Clebopride	-0.33	2.17 (43)
MK-886	-0.31	2.19 (50)
Diethylcarbamazine	-0.58	2.31 (15)
16-phenyltetranorprostaglandin E2	-0.46	2.32 (25)
Diphemanil metilsulfate	-0.43	2.49 (33)
Halofantrine	-0.39	2.50 (40)
SR-95639A	-0.40	2.53 (39)
Xamoterol	-0.43	2.77 (40)

Figure 5.14. CMAP findings of cigarette smoke exposed myotubes. Compounds that correlate (green) and anti-correlate (red) with the transcriptome of CSM exposed myotubes.

5.2.3. The effects of CSM exposure were not alleviated by asiaticoside and harmine in a viability setting.

The findings of the CMAP provided a comprehensive list of compounds that could be used to counteract the effects of CSM in-vitro. The list was dissected, and a few compounds were selected based on strength of correlation, availability, cost, solubility, lethality and previous use in literature. Based on these criteria we opted for asiaticoside and harmine from the myoblast exposed cohort. From the myotubes exposed cohort we selected xamoterol and halofantrine.

Harmine, is a naturally occurring organic compound mostly found in plants. Initially isolated in 1847 from the seed of *Peganum harmal*, has been found to have antimicrobial, antifungal, antioxidant and antitumorigenic properties (Patel et al., 2012). Recently harmine has been used to ameliorate some of the effects of spinal muscular atrophy in mice (Meijboom et al., 2021).

Asiaticoside is a triterpene compound isolated from *Centella asiatica,* an herbaceous plant that grows in the swampy areas of southeast asia. It has been reported to have several therapeutic properties as an anti-bacterial, anti-inflammatory and antioxidant (Bandopadhyay et al., 2023).

First the chemicals were solubilized, and a cytotoxicity assay was performed. Briefly, the cells were allowed to adhere overnight then incubated with the different concentrations Dimethyl-sulfoxide (DMSO), harmine and asiaticoside for 24 hours. This was then followed by adding the MTS reagent and incubating for a further 4 hours before measuring the absorbance at 490 nm. Since (DMSO) was used as a solvent, it was also used as the control in this experiment (figure 5.15 A). A concentration gradient was used starting from 1 to 50 µM. The DMSO (figure 5.15 B) had no effect on cell viability up to 50 µM where the absorbance was significantly high. Harmine (figure 5.15 C) presented with a significant decrease in absorbance at 50 µM and asiaticoside (figure 5.15 D) had no effect on absorbance in all concentrations.

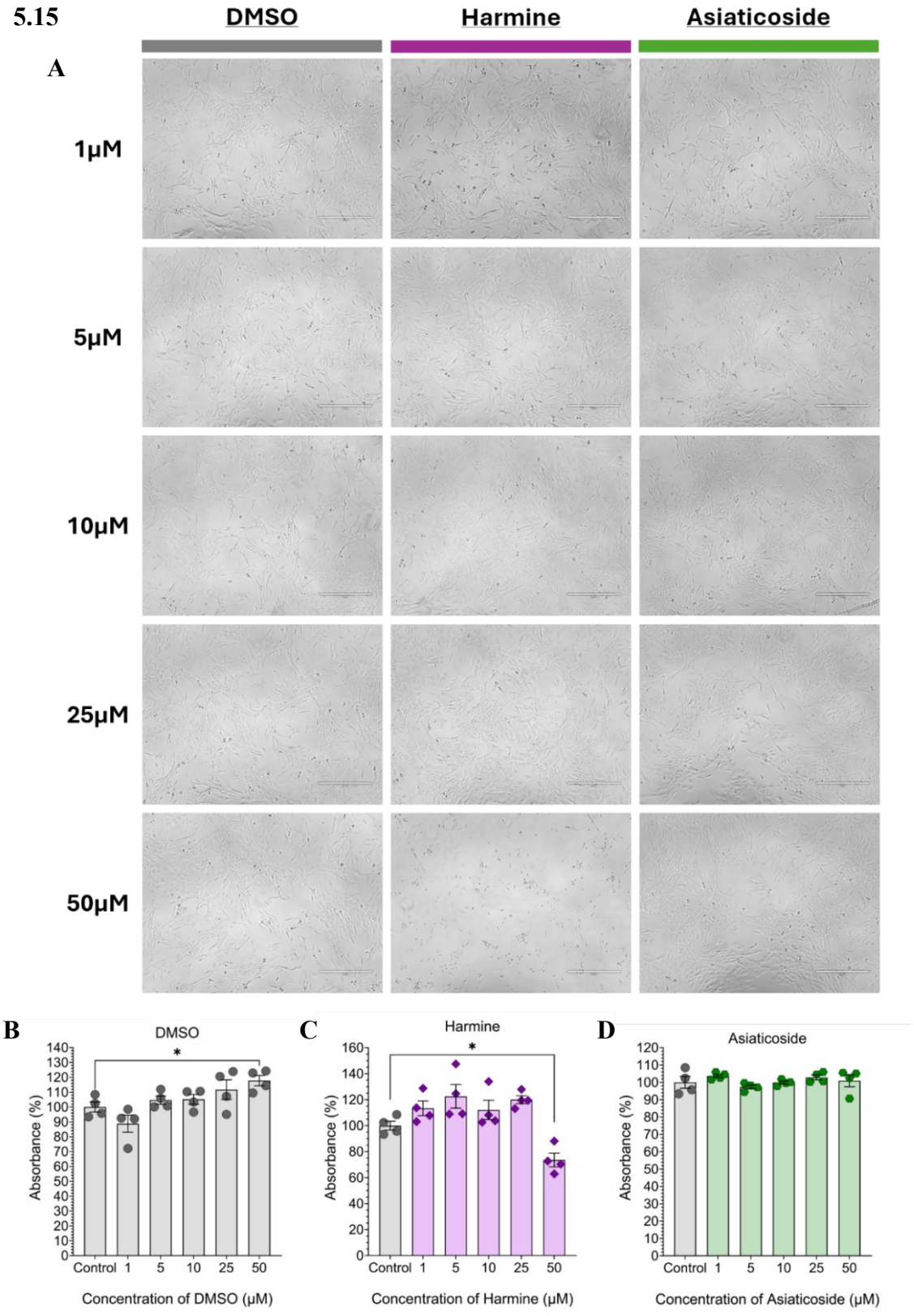

Figure 5.15. C_2C_{12} cytotoxicity assay incubated with harmine and asiaticoside. (A) representative images of C_2C_{12} myoblasts treated with a concentration gradient of DMSO, harmine or asiaticoside for 24 hours. (B, C, D) quantification of the cytotoxicity assay. Data presented as +/- SEM using one-way ANOVA with Dunnett's multiple comparison test. *$p<0.05$ (n=4). Scale bar is 400 µm.

Based on the findings of the cytotoxicity assay, going forward two concentrations of compound would be used to potentially counter the effects of cigarette smoke on myoblasts. Viability assays were performed using 5 and 25 μM concentrations of compound with the cells exposed to a concentration gradient of CSM (figure 5.16 & 5.17).

After 24 hours of incubation in CSM with 5 μM harmine (figure 5.16 B) there was no effect on the viability at the lower concentrations of CSM, however at the higher concentrations there was a significant decrease in viability that was not rescued by the 5 μM harmine. When 5 μM asiaticoside (figure 5.16 C) was incubated with CSM for 24 hours a significant drop in viability was seen between 0.01 CSM and 0.01 CSM + 5 μM asiaticoside. There was no effect in the 0.05 CSM and at 0.2 CSM there was no rescue. Interestingly though at 0.1 CSM with the addition of 5μM asiaticoside there was a significant increase in viability that suggests a rescue effect.

5.16

A

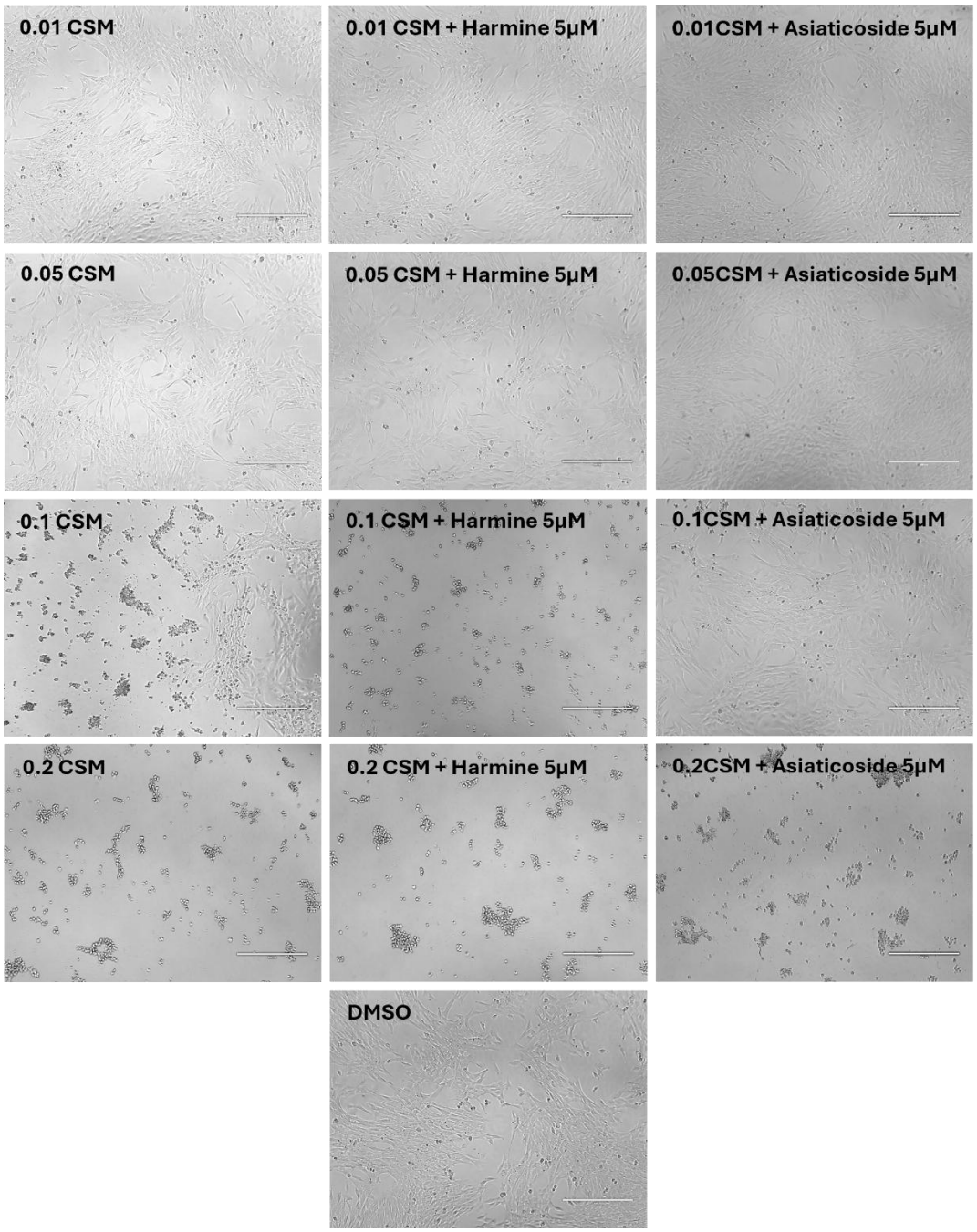
0.01 CSM
0.01 CSM + Harmine 5μM
0.01CSM + Asiaticoside 5μM
0.05 CSM
0.05 CSM + Harmine 5μM
0.05CSM + Asiaticoside 5μM
0.1 CSM
0.1 CSM + Harmine 5μM
0.1CSM + Asiaticoside 5μM
0.2 CSM
0.2 CSM + Harmine 5μM
0.2CSM + Asiaticoside 5μM
DMSO

B

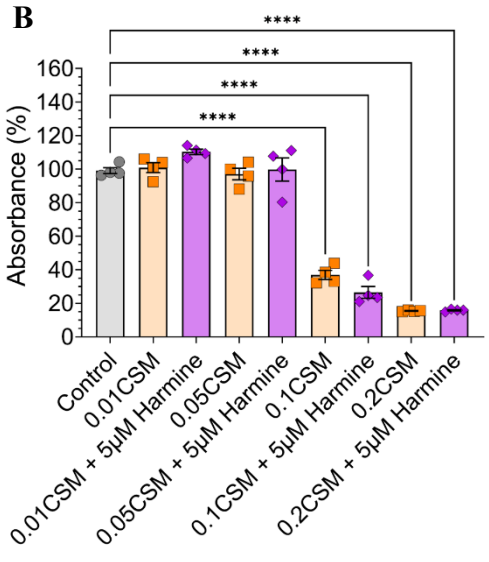
Absorbance (%)
0
20
40
60
80
100
120
140
160
****
****
****
****
Control
0.01CSM
0.01CSM + 5μM Harmine
0.05CSM
0.05CSM + 5μM Harmine
0.1CSM
0.1CSM + 5μM Harmine
0.2CSM
0.2CSM + 5μM Harmine

C

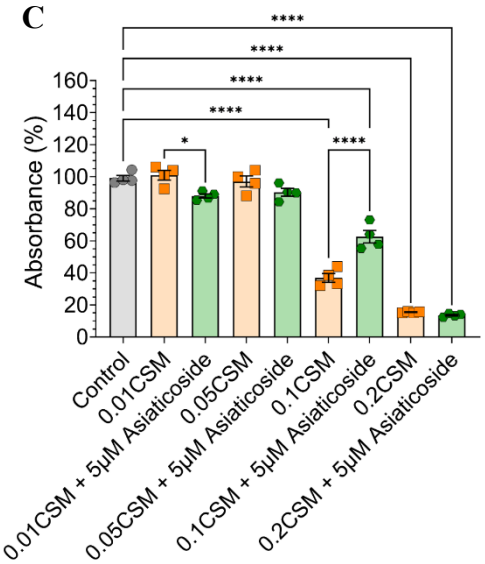
Absorbance (%)
0
20
40
60
80
100
120
140
160
****
****
****
*
****
Control
0.01CSM
0.01CSM + 5μM Asiaticoside
0.05CSM
0.05CSM + 5μM Asiaticoside
0.1CSM
0.1CSM + 5μM Asiaticoside
0.2CSM
0.2CSM + 5μM Asiaticoside

Figure 5.16. Effect of 5 µM harmine and asiaticoside on C_2C_{12} viability with CSM exposure. The myoblasts were incubated with different concentrations of CSM and 5 µM harmine or asiaticoside for 24 hours. Thereafter, the viability was assessed (using an MTS reagent). (A) representative images after 24 hours incubation. (B, C) quantification of the viability assay. Data presented as +/- SEM using one-way ANOVA with Tukey's multiple comparison test. *p<0.05, ****p<0.0001 (n=4). Scale bar is 400 µm.

Next, since the lower concentrations didn't provide convincing results, a viability assay was performed using higher concentrations of harmine and asiaticoside (figure 5.17). After 24 hours incubation in a concentration gradient of CSM with 25 μM harmine (figure 5.17 B) there was no increase in viability in any of the CSM exposed concentrations, in fact at 0.05 OD CSM the addition of 25 μM harmine further decreased viability. Similarly, and alarmingly the addition 25 μM asiaticoside to any concentration of CSM exacerbated the effect and a significant drop in viability was observed from the lowest concentration. These findings were clearly visible from the representative images seen in figure 5.17 A.

5.17

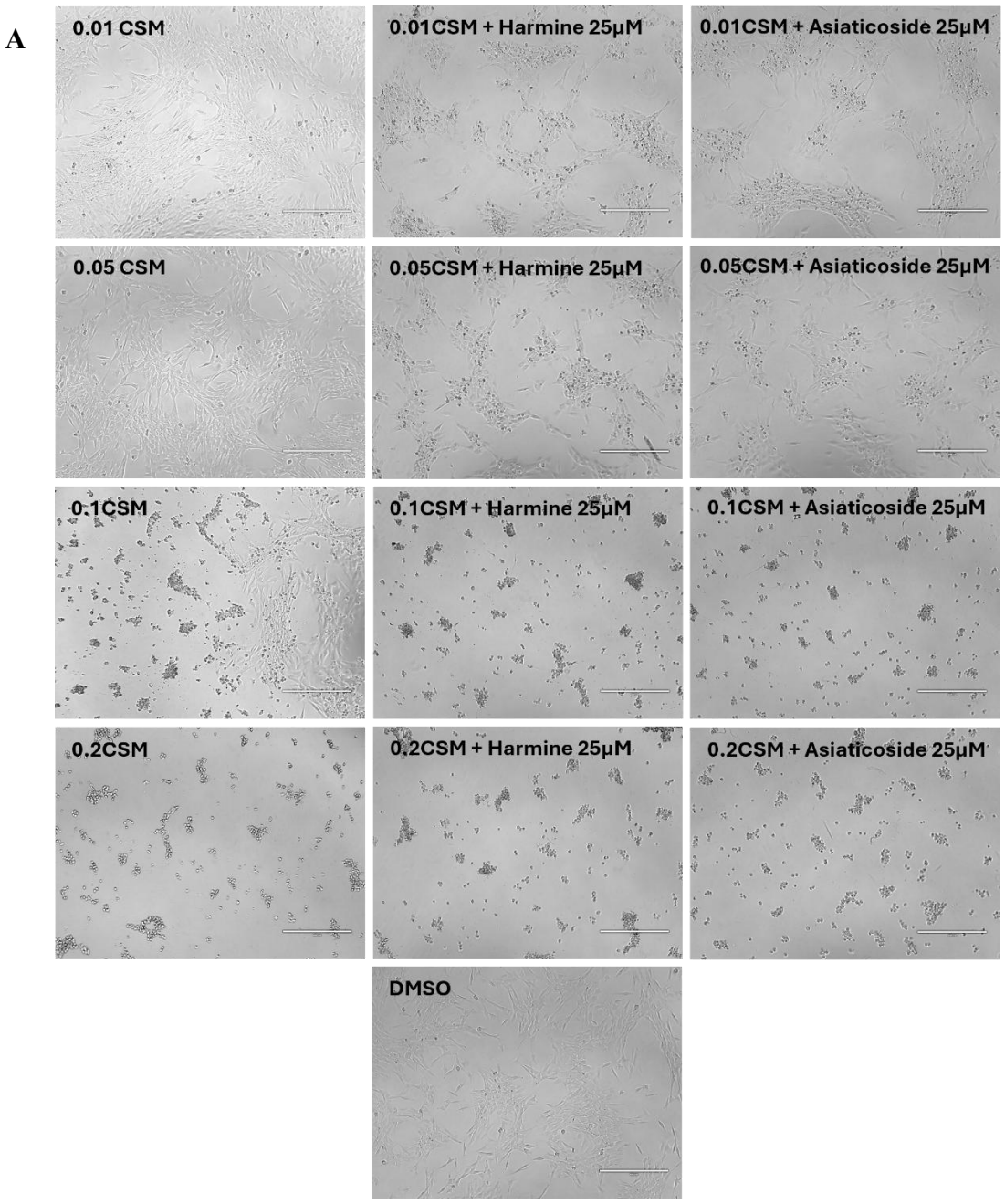
A
0.01 CSM
0.01CSM + Harmine 25µM
0.01CSM + Asiaticoside 25µM
0.05 CSM
0.05CSM + Harmine 25µM
0.05CSM + Asiaticoside 25µM
0.1CSM
0.1CSM + Harmine 25µM
0.1CSM + Asiaticoside 25µM
0.2CSM
0.2CSM + Harmine 25µM
0.2CSM + Asiaticoside 25µM
DMSO

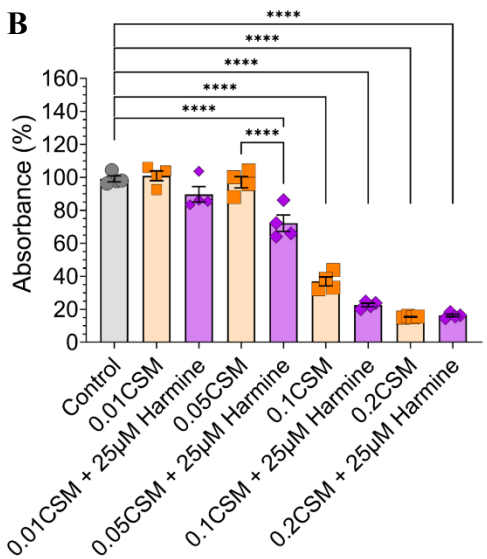
B
Absorbance (%)
Control
0.01CSM
0.01CSM + 25µM Harmine
0.05CSM
0.05CSM + 25µM Harmine
0.1CSM
0.1CSM + 25µM Harmine
0.2CSM
0.2CSM + 25µM Harmine

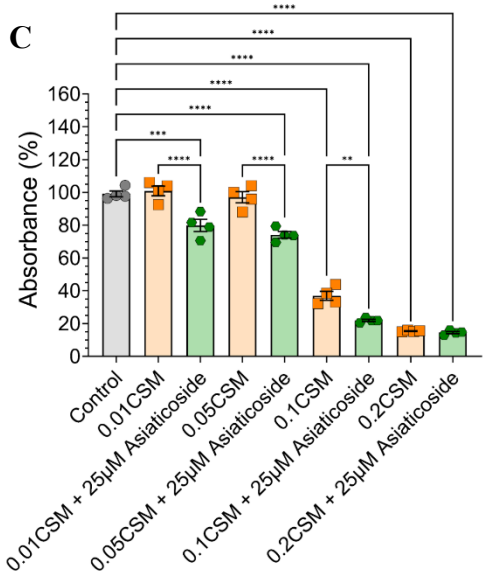
C
Absorbance (%)
Control
0.01CSM
0.01CSM + 25µM Asiaticoside
0.05CSM
0.05CSM + 25µM Asiaticoside
0.1CSM
0.1CSM + 25µM Asiaticoside
0.2CSM
0.2CSM + 25µM Asiaticoside

Figure 5.17. Effect of 25 µM harmine and asiaticoside on C_2C_{12} viability with CSM exposure. The myoblasts were incubated with different concentrations of CSM and 25 µM harmine or asiaticoside for 24 hours. Thereafter, the viability was assessed (using an MTS reagent). (A) representative images after 24 hours incubation. (B, C) quantification of the viability assay. Data presented as +/- SEM using one-way ANOVA with Tukey's multiple comparison test. **p<0.01, ***<p0.001, ****p<0.0001 (n=4). Scale bar is 400 µm.

5.3. Discussion

In this chapter we aimed to identify readily available compounds that could be used to reverse the effects of cigarette smoking. The microarray analysis was used as a stepping stone to identify the potential therapeutic compounds. Interestingly though, from the analysed data there were several differentially expressed genes. Notably Cyp1a1, Cyp1b1, Ahrr, Igfbp4, Actc1, Nov, Igf2, Fmod and Gm7325 (Mymx). The C-mapping data revealed several compounds with potential therapeutic outcomes, of which the two selected compounds, asiaticoside and harmine didn't rescue the myoblasts from CSM toxicity.

Cyp1a1 and Cyp1b1 are both members of the cytochrome P450 superfamily and involved in drug metabolism and synthesis of lipids, steroids and cholesterol. Mutations in these genes have been associated with an increased link to lung cancer (Androutsopoulos et al., 2009). Ahrr (Aryl hydrocarbon receptor repressor) is involved in the regulation of cell growth, differentiation and functions as a modulator for Cyp1a1 (Androutsopoulos et al., 2009). Insulin growth factors (IGFs) play a substantial role in growth, development and metabolism. IGFBP4 (Insulin like growth factor binding protein 4) is one of six high affinity binding proteins to IGFs. These proteins moderate the activity of IGFs and are capable of enhancing or inhibiting the IGF effects (Werner, 2023). Specifically, Igfbp4 has been found to inhibit the action of IGF1 in vitro (Mazerbourg et al., 2004) and over expression causes smooth muscle hypoplasia in transgenic mice (Wang et al., 1998). Gm7325 otherwise known as myomerger (myomixer) is muscle specific and essential to myoblast fusion. It has been shown that myocytes deficient in myomerger were able to differentiate but were fusion incompetent (Quinn et al., 2017). Our analysis showed down-expression of myomerger in myoblasts which could explain why the exposed cohort in vitro had a significantly lower fusion index. The microarray data is surprising, we expected from the results of previous chapters to find more differential expression in atrogenes involved in the ubiquitin-proteasome pathway (MuRF1, MAFbx, USP19). In fact, the only gene we could link to the

ubiquitin ligase family was Trim25 which was down expressed in myoblasts exposed to CSM. An interesting finding was the down regulation of fibromodulin (Fmod), a negative regulator of myostatin. This could be a potential explanation for the atrophy seen in the in vitro experiments (Lee et al., 2021) and could be investigated using Western blots. Much of the differential expression is found in genes responsible for metabolism. When comparing the heatmaps there weren't major changes in gene expression. It is possible that cigarette smoke exposure affects proteins rather than genes. The effect would be post translational and causes adducts altering the structure and function of the proteins. Several chemicals found in cigarette smoke such as acrolein, and formaldehyde had been previously shown to cause protein adducts (Kitaguchi et al., 2012; Metz et al., 2004; Spiess et al., 2011), therefore mass spectrometry could be used to identify any differentially expressed proteins. In fact, a recent study performed by Meijboom et al (Meijboom et al., 2021) attempting to identify muscle specific treatments for spinal muscular atrophy (SMA) combined transcriptomics with proteomics and connectivity mapping to identify potential targets of therapy. First, they identified compounds that reversed the disease signature of SMA in the transcriptome, then the proteome and overlapped them to come up with possible targets of therapy. Interestingly they single out harmine as a compound that upon testing in vivo improved several disease phenotypes that included lifespan and weight. However, when they investigated the effect in-vitro they found differential effects with low and high doses and specifically when testing on C_2C_{12} they found that harmine had inhibitory effects on proliferation and viability at higher doses. They contribute these findings to the fact that the CMAP resource is based on data from human cell lines which as we mention later on is a major limitation of our work as well.

The two compounds used, harmine and asiaticoside, are naturally occurring and derived from plants and widely used in traditional medicine. Our findings from the viability assay were unexpected, other than 0.1 OD CSM with 5μM asiaticoside there was no improvement

detected in all the other parameters. This could be the simple matter of the selected compounds weren't working or due to the concentrations selected, ideally the whole panel would be used but this wasn't feasible. Another explanation could be the setup of the experiment, we incubated the cells with both the CSM and therapeutic compounds, this may have led to interactions. Ideally variations where the cells were treated with the therapies prior to exposure or after, with fresh media would be performed. Ultimately this proves that C-mapping data isn't ironclad due to the data resource being from human cell lines but rather provides a platform for investigation of potential therapeutic targets.

5.4. Limitations and future work

Despite our findings in this chapter, there were limitations. The microarray and C-mapping were unfortunately only performed on the CSM exposed cohort. Consequently, the outcomes could not be compared to VM as they were in the previous chapters. Moreover, the experiments were only performed on the C_2C_{12} cell line and we only managed to analyse two of the compounds in a viability assay. Perhaps the biggest limitations are the use of C_2C_{12} only and microarrays alone, the use of proteomics would have given us a better understanding of the differential expression. The use of microarray is limited, since it measures gene expression by hybridising samples to a chip that contains thousands of known DNA sequences. This is useful but only provides a limited picture. RNA sequencing provides an objective and extensive view of the transcriptome and allows for the discovery of novel transcripts.

Future work to address the limitations faced in this chapter would include microarray analysis of the VM exposed C_2C_{12} with C-mapping. Further investigation of the compounds in a similar manner initially investigating cytotoxicity and viability. Should one prove to be beneficial then investigation would continue to include the potential effect on migration, differentiation, atrophy and proliferation. This will justify future work on mice. This would then be followed by translating this experiment to the AB1190 cell line as this would provide more insight and possibly different outcomes as it is more relative to the CMAP database, since AB1190 are of human origins. Finally, RNA sequencing would be performed on the samples collected from the mice exposed to CSM and VM in the in vivo experiments. The results, which would be more representative of smokers, would then be used in combination with the other transcriptomic and proteomic findings in a CMAP analysis in the hope of finding better therapeutic compounds.

5.5. Conclusion

We aimed to identify compounds that could revert the effect of cigarette smoke through identifying differentially expressed genes. We discovered that there weren't major changes in expression in-vitro, however they were substantial enough to illicit changes found previously. Harmine and asiaticoside didn't revert the effects of CSM but the C-map still provides a valuable resource of possible therapeutic targets.

Chapter 6: General Discussion

Smoking and now vaping are both popular amongst the population. Smoking outcomes have been studied for more than half a century with well documented findings. Vaping, however, is a more recent trend with much to be investigated. The principal aim of this study was to investigate the effect of both cigarette smoking and vaping on early muscle regeneration and to determine therapeutic agents that can be used to reverse said effects.

In this study, we investigated the effects of both CSM and VM in vitro on immortalized cells from mice and humans. We assessed viability, proliferation, migration, fusion, organellar and inflammatory response. We then moved into mouse models, and using the C57BL/6 mice we observed the outcomes on an organismal level. Our investigation monitored the rodents body weight, isolated muscle weights, fibre morphometrics, histopathological analysis, and inflammatory response. Finally, using gene expression analysis and the bio informatic tool, connectivity mapping, identified harmine and asiaticoside as possible therapeutics that could potentially reverse the effects of CSM.

First, we present a summary of the findings from this study on direct exposure of myoblasts (table 6.1).

	Viability	Senescence	Migration	Focal Adhesions	Fusion	Atrophy	Organelles	Inflammatory cytokines
CSM	Reduced in C_2C_{12}, AB1190, AB678 and AB1167.	Increased in AB1190. Increased in IMR-90.	Decreased in C_2C_{12}. Decreased in AB1190.	Area of FAs and SFs decreased in C_2C_{12}. Number and area of FAs increased in AB1190.	Decreased in C_2C_{12}. Decreased in AB1190.	Myofibre area decreased in C_2C_{12}. Myofibre area decreased in AB1190. sActRIIB rescues Atrophy in both.	Increase in area of nucleoli. Decrease in the number of nucleoli. Decrease in the number of nuclei. Decrease in area of nuclei. Increase in nuclear roundness. Decrease in cell area. Increased mitotracker area.	IL-8 elevated.
VM	No effect on C_2C_{12}. Increased in AB1190. Decreased in AB678. Decreased in AB1167.	No effect in AB1190. Increased in IMR-90.	No effect in C_2C_{12}. No effect in AB1190.	Number and area of FAs, area of SFs increased in C_2C_{12}. No effect in AB1190.	Decreased in C_2C_{12}. Decreased in AB1190.	No effect in C_2C_{12}. No effect in AB1190.	Increase in area of nucleoli. Decrease in the number of nuclei. Decrease in area of nuclei. Increase in nuclear roundness. Increased mitotracker intensity.	No Change

Table 6.1. A summary of the in-vitro results

There is a huge volume of data showing that smoking impacts muscle function and weight. In contrast, very little is known about the effects of vaping and its effect on this tissue. Numerous mouse models have been used where smoke inhalation brings about some of the detrimental effects seen in humans by the action of cigarettes. We wanted to establish in the first instance whether cigarette smoke or vaping had a direct effect on skeletal muscle. This is important as numerous studies have shown that the primary human tissue that is encountered by smoke are lung cells. Thereafter, the cells of the lung respond by producing various inflammatory cytokines. Therefore, in this scenario cigarette smoking needs to be considered to have two components one being the harmful chemicals that enter the circulation that originates from cigarettes and secondly molecules produced by human tissues particularly the lung as a reaction to cigarette smoke. By directly applying conditioned media containing either cigarette smoke extract or vaping extract we are in a position to dissect the direct role on skeletal muscle. Another important aspect addressed by our experiments was related to early stages of myogenesis. Most studies which are conducted on animals and those that concentrate on taking human skeletal muscle biopsies focus on mature myofibres. In our setup we aim to examine the outcome on early stages of muscle development. We focused on key properties of the myogenic programme that are not only important during the regeneration of this tissue but now having greater importance in maintaining adult muscle physiology. Here in the landscape of our understanding of muscle has changed considerably in that it was previously thought that the activity of satellite cells was only required during regeneration. Now we know that these cells are critical to replenish myonuclei that have been lost not through acute damage but simply by the wear and tear process that accompanies muscle contraction.

We used both human and mouse skeletal muscle cells as an experimental platform. Furthermore, we were in the position of using a number of different human lines. These revealed several important findings which we believe have major bearing on developing robust conclusions. Our studies using different cell lines found that there was very low level of agreement between the effect of cigarette smoke or vaping on a particular aspect of early muscle development. For example, cell viability was

reduced by cigarette smoke when applied to mouse cells whereas vape media failed to provoke any response. To further exemplify this point we found that all three human lines responded to cigarette smoke by decreasing viability. In contrast we found that one cell line increased viability when exposed to vape media. Of all the tests that we performed the most robust in terms of reproducibility across different cell lines and their origin were those related to senescence and fusion. Going forward we would advocate that the readouts assessing the function in terms of senescence and fusion are more conserved and more reliable as opposed to those investigating for example viability or migration or atrophy. The key question therefore to answer is why certain cells, even though they are all from humans respond whereas others don't. Presently we have no explanation for this other than to offer potential suggestions. Firstly, we need to take into account that the origin of the cells differs in that they are from various sites around the body which may impact their biology. We know from embryonic studies that the development of muscle occurs according to its location in that muscles of the body originate from cells of the myotome whereas those of the limb undergo a process of migration prior to activating their myogenic programme (Kablar et al., 1997; Ordahl & Douarin, 1992). Hence these differing experiences during development may have long lasting impact on the biology of these cells. More obvious could be factors such as age and sex of the donor from whom the muscle cells were obtained. Going forward these studies highlight that in order to generate robust data it is imperative that large number of cell lines are investigated to reach conclusions about effect of cigarette smoke and the efficacy of therapies when dealing at the population level.

One of the critical findings of our study was that the atrophy effect of cigarette smoke could be alleviated by a molecule that neutralised activin or myostatin signalling. We believe that these results are particularly informative because they offer a mechanistic explanation of muscle loss following smoking of cigarettes. As our experiments were performed solely on skeletal muscle cells these experiments would imply that cigarette smoke induced the expression of molecules that would work through the activin receptor which would induce atrophy. Furthermore, the addition of the soluble ligand trap neutralised this effect. Hence, we believe that this is the first proof that cigarette smoke

induces an autocrine effect resulting in muscle atrophy. We were unable to determine with certainty the nature of the ligand given that the expression of myostatin was not statistically elevated in our microarray expression data. Furthermore, it is possible that myostatin/activin levels could be increased by cigarette smoke without the need for transcription. It is possible that latent forms of either protein could become activated by cigarette smoke therefore bypassing the need for transcription. Future experiments could be designed to identify the molecule that is neutralised by the soluble ligand trap for example through the use of analyte specific ELISA assays.

	Animal weights	Muscle weights	Fiber area	IgG+ infiltration	eMYH area	Dystrophin	Fibrosis	Atrophy	Inflammatory cytokines
CSM	No effect	**Day 5:** Gastroc increased **Day 10:** No difference **Day 20**: No difference	No difference between damaged and undamaged.	**Day 5:** Same as control **Day 10:** Same as control **Day 20:** Same as control	**Day 5:** Same as control **Day 10:** Higher than control **Day 20:** Same as control	Incomplete perimeter	No change	No atrophy in contralateral fibres	**Dysregulated:** IL-5 ↓ significantly
VM	No effect	**Day 5:** R.TA increased **Day 10:** No difference **Day 20:** No difference	No difference between damaged and undamaged.	**Day 5:** Same as control **Day 10:** Same as control **Day 20:** Same as control	**Day 5:** Same as control **Day 10:** Higher than control **Day 20:** Same as control	Incomplete perimeter	No change	No atrophy in contralateral fibres	**Dysregulated:** GSF ↓ significantly IP-10 ↓ significantly LIX ↓ significantly

Table 6.2. A summary of the in-vivo results.

Moving on from the findings on muscle cells we aimed to assess the impact of cigarette smoke and vape media using the mouse as an experimental model with a particular emphasis on muscle regeneration. As previously stated, we saw that there were robust effects off cigarette smoke on senescence, fusion and migration when taken in the context of being conserved between cells of human and mouse origin. These processes are critical to the pathway that regulates muscle regeneration. However, we found that muscle regeneration took place quite well with the only notable exception being that it was slightly delayed compared to the untreated damaged muscle. Therefore, we need to offer explanations as to why cigarette smoke had a relatively minor role in regeneration. We propose a number of explanations. Firstly, we could contemplate that the dose that was applied put simply too low to bring about meaningful impact in our mouse experiments. We injected 100 microliters of a solution that had an optical density of 1.8 into mice weighing approximately 20 grammes. This equates to a dose that is approximately 10 times less than that used in our in vitro assays. We used the highest dose that we were permitted to do so under our home office licence guidelines. We could in future increase the dose not by using a higher volume but by making more concentrated condition media. One way to achieve this goal would be simply to draw the cigarette smoke from multiple cigarettes into a decreased volume of phosphate buffered saline.

We also noted that the procedure we used to mimic the effect of smoking, here by injection into the peritoneal cavity of smoke extract that had been collected in saline failed to bring about a decrease in body weight. Huge volumes of published data shows that cigarette smoke is very effective in reducing body weight in humans (Chao et al., 2019; Nemery et al., 1983; Williamson et al., 1991). A finding that has been repeated in studies involving smoke inhalation by rodents (Ajime et al., 2021; Stevens et al., 2024; Tan et al., 2025). Vaping has also been reported to decrease body mass in human population studies (Alqahtani et al., 2021)**.** Hence, we need to offer an explanation as to why our experiment failed to invoke loss in body mass. One possible explanation apart from that being centred around dosing is by understanding how we made our condition media. The process that we used collected only elements of cigarette smoke or vape smoke that dissolved in aqueous polar solution

(namely phosphate buffered saline). It is very likely that the highly organic molecules that are present in cigarette smoke were not captured in this solution. Hence it is highly likely that our cigarette smoke conditioned media only captures a fraction of harmful molecules. In future we could collect an organic fraction and then mix it with the one collected in an aqueous water-based media.

Our work also highlights how differing mechanisms induced by cigarette smoke/vape conditioned media that bring about body weight muscle loss. One potent means by which this occurs is simply through appetite control. This has been reported in humans and forms the basis of a slimming regime based on smoking and has been found in rodents (Ajime et al., 2021). A mechanistic explanation for this finding could be the fact that studies have shown that GDF 15 levels are elevated in the blood of smokers which acts on the brain to bring about appetite suppression (Klein et al., 2022; Wada et al., 2020). To our knowledge a similar assessment of measuring GDF15 levels in people using vaping has not been conducted and should be undertaken. However, our work suggests that at high enough doses, cigarette smoke works on muscle through the modulation of molecules in the activin/myostatin axis that control muscle mass. In order to assess the role of activin and myostatin during cigarette smoke induced muscle loss. We propose that it will be necessary to examine all molecules in this axis that work through the activin receptor. This could be done using ELISA assays that profile this entire axis. In order to do generate robust data it will be important to examine not only molecules that induce muscle atrophy (activin and myostatin) but also those that antagonise their action (Follistatin and FLT3) (Rodgers & Ward, 2022). Ideally this study should also examine the levels of GDF 15 hence determining the role of direct versus indirect regulation of body mass.

One aspect of our in vivo work that we didn't examine was the effect of cigarette smoke or vape conditioned media on senescence. The investigations we undertook using cell-based assays showed that both cigarette smoke and vape media induced senescence. Hence future work should be undertaken to histologically profile the appearance of β-Gal activity in muscle from mice that have been subjected to cigarette smoke or vape media. Our work nevertheless opens the possibility of a new pathological mechanism induced by cigarette smoke or vaping. Our results suggest that both of

these activities may affect muscle at the level of the myofibre (through atrophy) and in the satellite cell (through the induction of senescence). Hence it will be of interest to examine human muscle samples from people who have smoked or vaped and profile markers for senescence. There is already good evidence that cigarette smoke induces senescence in other cells particularly in the cells of lungs (Zheng et al., 2025). An indirect method would be to examine classical markers of SASP which causes the release of inflammatory cytokines and the decrease of anti-inflammatory molecules. Indeed, we saw a change in cytokine profile induced by both cigarette smoke and vaping. If there is evidence that either of these two activities bring about increase levels of senescence, then future health remedies based around decreasing the impact of senescent cells (senomorphics) or eliminating these aberrant cells (senolytics) should be considered. Indeed, a large number of such compounds being developed for clinical use and could be redirected towards pathology caused by cigarette smoke or vaping (Shi et al., 2024).

The Aim of this project was to ultimately identify treatments or skeletal muscle pathology induced by either cigarette smoke or vaping. To that end we used connectivity mapping to bring forward compounds that could be readily translated into a clinical setting. Connectivity mapping has been used over the past 10 years and identified a number of molecules that have been shown to address various aspects of muscle pathology. For example, the study of Dyle et al, discovered tomatidine which originates from tomatoes as an activator of mTOR signalling and had the ability to reduce skeletal muscle atrophy, promote growth of muscle fibres following a period of atrophy as well as to increase strength and exercise when used in animals (Dyle et al., 2014). Another compound that was discovered through connectivity mapping in the context of skeletal muscle was ursolic acid that promoted muscle growth in animals and stimulated hypertrophy. This molecule was thought to be potentially valuable in dealing with muscle loss in humans following fasting as well as spinal cord injury since it came up as a positive hit through connectivity mapping in samples from those suffering these two conditions (Kunkel et al., 2011). More recently the group of Bowerman have used the connectivity mapping approach to discover drugs to treat the muscle pathology for spinal muscular

atrophy (Hoolachan et al., 2024; Meijboom et al., 2021). In one of their studies, they found and showed that harmine, an alkaloid found in Syrian rue seeds, passionflower and lemon balm, was able to some degree reverse the impact of gene mutations that lead to muscle fibre atrophy.

Harmine was therefore an exciting prospect as it came up in our Connectivity mapping led investigations. However, we failed to detect any impact of this compound in any of the cell-based assays that we conducted. Hence it is important to explain this lack of effect. We believe that insights into lack of efficacy come from dissecting the experiences of other groups who have used this discovery platform. In particular the work of Meijboom (Meijboom et al., 2021) offers potential explanations. This group found that connectivity mapping when used with either gene expression lists or protein identifiers came up with different lead compounds. Furthermore, when they used differing setups that would all speak to the same output, that is muscle atrophy induced by changes to the *Smn* gene, again a different set of potential therapeutics came forward. Hence the connectivity map seems to be very sensitive to slight changes in the experimental setup, from which the input data as well as the type of input data is derived or used. This group came up to the conclusion that harmine was a strong lead through connectivity mapping when starting data from several experimental setups were used, and the same compound came through as and effective molecule. Furthermore, this group validated harmine by examining the expression of genes that it was predicted to regulate (Meijboom et al., 2021). Even after carrying out such robust preliminary investigations this compound was found to be efficacious only in certain spinal muscular atrophy models (Meijboom et al., 2021). Hence, we believe that in order to come up with robust leads using the connectivity mapping platform it will be essential to not only look at gene expression but also levels of proteins and to feed these into the discovery platform. The identification of compounds that come through using both approaches will add robustness to these experiments and go some ways towards mitigating against failure. Secondly, given our experiences with using different cell lines it would be judicious to examine gene expression in a number of these and only following leads which come out in a consistent, cell line independent

manner. Hence, we believe that until this is done, we should focus on molecules other than those identified in this study using our Connectivity Mapping data.

We suggest that from our data following the use of sActRIIB could be the basis of a treatment for cigarette smoke or vape induced muscle wasting. There is a huge body of data showing that muscle wasting can be readily prevented or slowed down by either neutralising the activity of activin or myostatin or through increasing the levels of molecules that neutralise their signalling capacity (Alqallaf et al., 2022; Lee et al., 2005; Zhou et al., 2010). Below is a list of molecules by no means extensive, that have progressed into clinical trials. We propose that these could be repurposed as a potential treatment for muscle wasting caused by either cigarette smoke or vaping.

Name	Developer	Indication	Phase	Safety	Outcomes
Apitegromab	Scholar Rock	Spinal muscular atrophy	Phase 3	No serious concerns	Improved motor function
Taldefgrobep Alfa	Biohaven	Spinal muscular atrophy	Phase 3	No serious concerns	Increase lean mass and bone strength with reduced fat
GYM329	Roche	Spinal muscular atrophy	Phase 2	NA	NA
Bimagrumab	Lilly	Obesity & diabetes	Phase 2	Diarrhoea and muscle spasms	Fat loss, lean mass gain and reduced HbA1c

Table 6.4. Drugs targeting the myostatin/activin pathway that are in clinical phase trial

Appendices

Appendix 1 – Immunohistochemistry antibodies

Primary antibodies

Antigen	Type	Immunoglobulin	Host species	Dilution	Supplier
MyHC A4.1025	Monoclonal	IgG	Mouse	1:100	DSHB
MyHC IIA A4.74	Monoclonal	IgG	Mouse	1:1	DSHB
MyHC IIB BF.F3	Monoclonal	IgM	Mouse	1:1	DSHB
MyHC III F1.652	Monoclonal	IgG	Goat	1:200	Santacruz biotechnology (sc-53091)
Laminin 1	Polyclonal	IgG	Rabbit	1:200	Sigma (L9393)
Dystrophin	Polyclonal	IgG	Rabbit	1:200	Santacruz biotechnology (sc-28535)
Fibrillarin	Polyclonal	IgG	Rabbit	1:100	Abcam (ab5821)
Paxillin	Monoclonal	IgG	Rabbit	1:200	Abcam (ab32084)

Secondary antibodies

Antibody	Immunoglobulin	Host species	Dilution	Supplier
Alexa-flour 488 anti-mouse	IgG	Goat	1:200	Invitrogen (A-11029)
Alexa-flour 488 anti-rabbit	IgG	Goat	1:200	Invitrogen (A-11008)
Alexa-flour 594 anti-mouse	IgM	Goat	1:200	Invitrogen (A-21044)
Alexa-flour 594 anti-mouse	IgG	Goat	1:200	Invitrogen (A-11005)
Alexa-flour 594 anti-rabbit	IgG	Goat	1:200	Invitrogen (A-11037)
Alexa flour 647 anti-rabbit	IgG	Goat	1:200	Invitrogen (A-21245)

Appendix 2 – Reagents, dyes and kits

Substance	Supplier
4% paraformaldehyde	Fisher scientific F/1501/PB08
Asiaticoside	Selleckchem.com (Cat#S3616)
Bouin	Abcam ab150681
B Galactosidase staining kit	Abcam ab102534
$CaCl_2$	Fisher Scientific 10161800
Collagenase	Sigma-Aldrich C0130
CellTrace Calcein Green	Invitrogen C34852
Chicken embryo extract	MP (2850145)
4' 6-diamidino-2-phenylindole, dihydrochloride (DAPI)	Fisher Scientific D1306
Dako fluorescence mounting medium	Dako north America Inc. S3023
DPX	Fisher scientific D/5319/05
Dulbecco's modified eagle medium (DMEM)	Gibco (11965118)
Eosin	Sigma-Aldrich 318906-500ML
Ethanol absolute	Sigma-Aldrich 32221-2.5L-M
Foetal bovine serum (FBS)	Gibco
Gentamycin	Gibco 15750-037
Glacial acetic acid	Fisher-scientific A38-500
Harmine	Selleckchem.com (Cat#S3868)
Haematoxylin (Harris)	Sigma-Aldrich HHS16
HCl	Fisher-scientific 7647-01-0
HEPES	Fisher-scientific BP410-500
Hoechst 33342	Merck
Horse serum (HS)	Gibco
KCN	Fisher-scientific 1059938
Methanol	Sigma-aldrich 34860
$MgCl_2$	Sigma-aldrich M2670-500
Mitotracker Orange	Invitrogen M7510
NaCl	Sigma-aldrich 71382
OCT	CellPath
PBS tablets	Oxoid BR0014G
Picrosirius red	Abcam ab150681
Penicllin-streptomycin	Gibco 15140-122
Rhodamine-conjugated Phalloidin	ThermoFisher scientific R415
Sodium azide	Fluka
Sodium succinate	Fisher-scientific 11418852
Sucrose	Fisher-scientific S/5860/53
TNF-alpha (Human) DuoSet ELISA kit	R&D Systems DY210
Triton X-100	Fisher-scientific T/3751/08
Xylene	Fisher-scientific 10588070

Appendix 3 – Solutions

Solution	Preperation
1x Phosphate buffered saline (PBS)	One PBS (oxoid) tablet was dissolved in distilled water (100 mL) and autoclaved.
4% Paraformaldehyde (PFA) in PBS	Paraformaldehyde powder (20 g) dissolved in 1x PBS (480 mL) at 65^{o} C, then the final volume was made up to 500 mL in 1x PBS.
Acidic alcohol	70% ethanol (200 mL) and HCl (200 µL).
Blocking wash buffer	Foetal bovine serum (FBS) (25 mL), sodium azide (200 mg) and Triton X-100 (250 µL) were dissolved in 1x PBS making a final volume of 500 mL.
DAPI	Add DAPI (7.5 µL) to Dako fluorescence mounting medium (15 mL).
Eosin 1%	70% ethanol (160 mL), Eosin Y and 5 wt% solution in water (40 mL) to make up a final volume of 200 mL of eosin 1%.
Permeabilisation buffer	Sucrose (20.54 g), HEPES (0.952 g), NaCl (0.584 g), $MgCl_2$ (0.260 g), Sodium azide (0.1 g), Triton X-100 (1 mL) and made up to a volume of 200 mL in distilled water then stored at 4^{o} C.
Acidified water	1L distilled water with 5ml Glacial acetic acid.
Collagenase solution	1 mL aliquot of 2 mg/mL type-1 collagenase solution for every two EDLs in DMEM.
Single fibre culture medium	10% (v/v) horse serum, 1% (v/v) penicillin-streptomycin), 0.5% (v/v) chick embryo extract and DMEM.
C_2C_{12} Growth medium	DMEM supplemented with 10% (v/v) FBS, 1% (v/v) penicillin-streptomycin.
Human cell lines Growth media	SMGM with supplement mix, 1% (v/v) gentamycin.
Differentiation media	DMEM supplemented with 5% (v/v) horse serum and 1% (v/v) penicillin-streptomycin.
Asiaticoside	Solubilised in DMSO to produce a stock solution of 1mM.
Harmine	Solubilised in DMSO to produce a stock solution of 1mM.

References

Abu-Hayyeh, S., Sian, M., Jones, K. G., Manuel, A., & Powell, J. T. (2001). Cadmium accumulation in aortas of smokers. *Arterioscler Thromb Vasc Biol*, *21*(5), 863-867. https://doi.org/10.1161/01.atv.21.5.863

Ajime, T. T., Serré, J., Wüst, R. C. I., Messa, G. A. M., Poffé, C., Swaminathan, A., Maes, K., Janssens, W., Troosters, T., Degens, H., & Gayan-Ramirez, G. (2021). Two Weeks of Smoking Cessation Reverse Cigarette Smoke-Induced Skeletal Muscle Atrophy and Mitochondrial Dysfunction in Mice. *Nicotine Tob Res*, *23*(1), 143-151. https://doi.org/10.1093/ntr/ntaa016

Alomari, M. A., & Al-Sheyab, N. A. (2016). Cigarette smoking lowers blood pressure in adolescents: the Irbid-TRY. *Inhal Toxicol*, *28*(3), 140-144. https://doi.org/10.3109/08958378.2016.1145769

Alonso, J. R., Cardellach, F., López, S., Casademont, J., & Miró, O. (2003). Carbon monoxide specifically inhibits cytochrome c oxidase of human mitochondrial respiratory chain. *Pharmacol Toxicol*, *93*(3), 142-146. https://doi.org/10.1034/j.1600-0773.2003.930306.x

Alqahtani, M. M., Alanazi, A. M. M., Almutairi, A. S., & Pavela, G. (2021). Electronic cigarette use is negatively associated with body mass index: An observational study of electronic medical records. *Obes Sci Pract*, *7*(2), 226-231. https://doi.org/10.1002/osp4.468

Alqallaf, A., Engelbeen, S., Palo, A., Cutrupi, F., Tanganyika-de Winter, C., Plomp, J., Vaiyapuri, S., Aartsma-Rus, A., Patel, K., & van Putten, M. (2022). The therapeutic potential of soluble activin type IIB receptor treatment in a limb girdle muscular dystrophy type 2D mouse model. *Neuromuscul Disord*, *32*(5), 419-435. https://doi.org/10.1016/j.nmd.2022.03.002

Amin, M. A., Matsunaga, S., Ma, N., Takata, H., Yokoyama, M., Uchiyama, S., & Fukui, K. (2007). Fibrillarin, a nucleolar protein, is required for normal nuclear morphology and cellular growth in HeLa cells. *Biochem Biophys Res Commun*, *360*(2), 320-326. https://doi.org/10.1016/j.bbrc.2007.06.092

Androutsopoulos, V. P., Tsatsakis, A. M., & Spandidos, D. A. (2009). Cytochrome P450 CYP1A1: wider roles in cancer progression and prevention. *BMC Cancer*, *9*, 187. https://doi.org/10.1186/1471-2407-9-187

Anerillas, C., Herman, A. B., Rossi, M., Munk, R., Lehrmann, E., Martindale, J. L., Cui, C.-Y., Abdelmohsen, K., De, S., & Gorospe, M. (2022). Early SRC activation skews cell fate from apoptosis to senescence. *Science Advances*, *8*(14), eabm0756. https://doi.org/doi:10.1126/sciadv.abm0756

Baba, T., Mimura, J., Gradin, K., Kuroiwa, A., Watanabe, T., Matsuda, Y., Inazawa, J., Sogawa, K., & Fujii-Kuriyama, Y. (2001). Structure and expression of the Ah receptor repressor gene. *J Biol Chem*, *276*(35), 33101-33110. https://doi.org/10.1074/jbc.M011497200

Bahmed, K., Lin, C. R., Simborio, H., Karim, L., Aksoy, M., Kelsen, S., Tomar, D., Madesh, M., Elrod, J., Messier, E., Mason, R., Unterwald, E. M., Eisenstein, T. K., Criner, G. J., & Kosmider, B. (2019). The role of DJ-1 in human primary alveolar type II cell injury induced by e-cigarette aerosol. *Am J Physiol Lung Cell Mol Physiol*, *317*(4), L475-L485. https://doi.org/10.1152/ajplung.00567.2018

Bandopadhyay, S., Mandal, S., Ghorai, M., Jha, N. K., Kumar, M., Radha, Ghosh, A., Prockow, J., Perez de la Lastra, J. M., & Dey, A. (2023). Therapeutic properties and pharmacological activities of asiaticoside and madecassoside: A review. *J Cell Mol Med*, *27*(5), 593-608. https://doi.org/10.1111/jcmm.17635

Barreiro, E., del Puerto-Nevado, L., Puig-Vilanova, E., Perez-Rial, S., Sanchez, F., Martinez-Galan, L., Rivera, S., Gea, J., Gonzalez-Mangado, N., & Peces-Barba, G. (2012). Cigarette smoke-induced oxidative stress in skeletal muscles of mice. *Respir Physiol Neurobiol*, *182*(1), 9-17. https://doi.org/10.1016/j.resp.2012.02.001

Barreiro, E., Peinado, V. I., Galdiz, J. B., Ferrer, E., Marin-Corral, J., Sanchez, F., Gea, J., Barbera, J. A., & Project, E. i. C. (2010). Cigarette smoke-induced oxidative stress: A role in chronic obstructive pulmonary disease skeletal muscle dysfunction. *Am J Respir Crit Care Med*, *182*(4), 477-488. https://doi.org/10.1164/rccm.200908-1220OC

Beauchamp, J. R., Heslop, L., Yu, D. S., Tajbakhsh, S., Kelly, R. G., Wernig, A., Buckingham, M. E., Partridge, T. A., & Zammit, P. S. (2000). Expression of CD34 and Myf5 defines the majority of quiescent adult skeletal muscle satellite cells. *J Cell Biol*, *151*(6), 1221-1234. https://doi.org/10.1083/jcb.151.6.1221

Beauval, N., Antherieu, S., Soyez, M., Gengler, N., Grova, N., Howsam, M., Hardy, E. M., Fischer, M., Appenzeller, B. M. R., Goossens, J. F., Allorge, D., Garçon, G., Lo-Guidice, J. M., & Garat, A. (2017). Chemical Evaluation of Electronic Cigarettes: Multicomponent Analysis of Liquid Refills and their Corresponding Aerosols. *J Anal Toxicol*, *41*(8), 670-678. https://doi.org/10.1093/jat/bkx054

Becher, B., Tugues, S., & Greter, M. (2016). GM-CSF: From Growth Factor to Central Mediator of Tissue Inflammation. *Immunity*, *45*(5), 963-973. https://doi.org/10.1016/j.immuni.2016.10.026

Benowitz, N. L. (2003). Cigarette smoking and cardiovascular disease: pathophysiology and implications for treatment. *Prog Cardiovasc Dis*, *46*(1), 91-111. https://doi.org/10.1016/s0033-0620(03)00087-2

Benowitz, N. L., & Jacob, P., 3rd. (1984). Daily intake of nicotine during cigarette smoking. *Clin Pharmacol Ther*, *35*(4), 499-504. https://doi.org/10.1038/clpt.1984.67

Bernhard, D., Csordas, A., Henderson, B., Rossmann, A., Kind, M., & Wick, G. (2005). Cigarette smoke metal-catalyzed protein oxidation leads to vascular endothelial cell contraction by depolymerization of microtubules. *Faseb j*, *19*(9), 1096-1107. https://doi.org/10.1096/fj.04-3192com

Betts, J. G. (2013). *Anatomy and Physiology*. OpenStax College, Rice University. https://books.google.com.kw/books?id=dvVgngEACAAJ

Bin Haidar, H., Almeida, J. R., Williams, J., Guo, B., Bigot, A., Senthilkumaran, S., Vaiyapuri, S., & Patel, K. (2024). Differential effects of the venoms of Russell's viper and Indian cobra on human myoblasts. *Sci Rep*, *14*(1), 3184. https://doi.org/10.1038/s41598-024-53366-9

Borgerding, M., & Klus, H. (2005). Analysis of complex mixtures--cigarette smoke. *Exp Toxicol Pathol*, *57 Suppl 1*, 43-73. https://doi.org/10.1016/j.etp.2005.05.010

Borghesan, M., Hoogaars, W. M. H., Varela-Eirin, M., Talma, N., & Demaria, M. (2020). A Senescence-Centric View of Aging: Implications for Longevity and Disease. *Trends Cell Biol*, *30*(10), 777-791. https://doi.org/10.1016/j.tcb.2020.07.002

Bottone, M. G., Santin, G., Aredia, F., Bernocchi, G., Pellicciari, C., & Scovassi, A. I. (2013). Morphological Features of Organelles during Apoptosis: An Overview. *Cells*, *2*(2), 294-305. https://doi.org/10.3390/cells2020294

Burke, A., & Fitzgerald, G. A. (2003). Oxidative stress and smoking-induced vascular injury. *Prog Cardiovasc Dis*, *46*(1), 79-90. https://doi.org/10.1016/s0033-0620(03)00076-8

Carnac, G., Ricaud, S., Vernus, B., & Bonnieu, A. (2006). Myostatin: biology and clinical relevance. *Mini Rev Med Chem*, *6*(7), 765-770. https://doi.org/10.2174/138955706777698642

Centers for Disease, C., Prevention, National Center for Chronic Disease, P., Health, P., Office on, S., & Health. (2010). Publications and Reports of the Surgeon General. In *How Tobacco Smoke Causes Disease: The Biology and Behavioral Basis for Smoking-Attributable Disease: A Report of the Surgeon General*. Centers for Disease Control and Prevention (US).

Chan, S. M. H., Cerni, C., Passey, S., Seow, H. J., Bernardo, I., van der Poel, C., Dobric, A., Brassington, K., Selemidis, S., Bozinovski, S., & Vlahos, R. (2020). Cigarette Smoking Exacerbates Skeletal Muscle Injury without Compromising Its Regenerative Capacity. *Am J Respir Cell Mol Biol*, *62*(2), 217-230. https://doi.org/10.1165/rcmb.2019-0106OC

Chao, A. M., Wadden, T. A., Ashare, R. L., Loughead, J., & Schmidt, H. D. (2019). Tobacco Smoking, Eating Behaviors, and Body Weight: A Review. *Curr Addict Rep*, *6*, 191-199. https://doi.org/10.1007/s40429-019-00253-3

Choi, S., Ferrari, G., & Tedesco, F. S. (2020). Cellular dynamics of myogenic cell migration: molecular mechanisms and implications for skeletal muscle cell therapies. *EMBO Mol Med*, *12*(12), e12357. https://doi.org/10.15252/emmm.202012357

Churg, A., Dai, J., Tai, H., Xie, C., & Wright, J. L. (2002). Tumor necrosis factor-alpha is central to acute cigarette smoke-induced inflammation and connective tissue breakdown. *Am J Respir Crit Care Med*, *166*(6), 849-854. https://doi.org/10.1164/rccm.200202-097OC

Cmarko, D., Smigova, J., Minichova, L., & Popov, A. (2008). Nucleolus: the ribosome factory. *Histol Histopathol*, *23*(10), 1291-1298. https://doi.org/10.14670/HH-23.1291

Coppe, J. P., Patil, C. K., Rodier, F., Sun, Y., Munoz, D. P., Goldstein, J., Nelson, P. S., Desprez, P. Y., & Campisi, J. (2008). Senescence-associated secretory phenotypes reveal cell-nonautonomous functions of oncogenic RAS and the p53 tumor suppressor. *PLoS Biol*, *6*(12), 2853-2868. https://doi.org/10.1371/journal.pbio.0060301

Correll, C. C., Bartek, J., & Dundr, M. (2019). The Nucleolus: A Multiphase Condensate Balancing Ribosome Synthesis and Translational Capacity in Health, Aging and Ribosomopathies. *Cells*, *8*(8). https://doi.org/10.3390/cells8080869

Davalos, A. R., Coppe, J. P., Campisi, J., & Desprez, P. Y. (2010). Senescent cells as a source of inflammatory factors for tumor progression. *Cancer Metastasis Rev*, *29*(2), 273-283. https://doi.org/10.1007/s10555-010-9220-9

Degens, H., Gayan-Ramirez, G., & van Hees, H. W. (2015). Smoking-induced skeletal muscle dysfunction: from evidence to mechanisms. *Am J Respir Crit Care Med*, *191*(6), 620-625. https://doi.org/10.1164/rccm.201410-1830PP

Derenzini, M., Montanaro, L., & Trere, D. (2009). What the nucleolus says to a tumour pathologist. *Histopathology*, *54*(6), 753-762. https://doi.org/10.1111/j.1365-2559.2008.03168.x

Di, L., Balesano, A., Jordan, S., & Shi, S. M. (2021). The Role of Alcohol Dehydrogenase in Drug Metabolism: Beyond Ethanol Oxidation. *AAPS J*, *23*(1), 20. https://doi.org/10.1208/s12248-020-00536-y

Dubois, M.-L., & Boisvert, F.-M. (2016). The Nucleolus: Structure and Function. In *The Functional Nucleus* (pp. 29-49). https://doi.org/10.1007/978-3-319-38882-3_2

Dyle, M. C., Ebert, S. M., Cook, D. P., Kunkel, S. D., Fox, D. K., Bongers, K. S., Bullard, S. A., Dierdorff, J. M., & Adams, C. M. (2014). Systems-based discovery of tomatidine as a natural small molecule inhibitor of skeletal muscle atrophy. *J Biol Chem*, *289*(21), 14913-14924. https://doi.org/10.1074/jbc.M114.556241

Eshraghian, E. A., & Al-Delaimy, W. K. (2021). A review of constituents identified in e-cigarette liquids and aerosols. *Tob Prev Cessat*, *7*, 10. https://doi.org/10.18332/tpc/131111

Famele, M., Palmisani, J., Ferranti, C., Abenavoli, C., Palleschi, L., Mancinelli, R., Fidente, R. M., de Gennaro, G., & Draisci, R. (2017). Liquid chromatography with tandem mass spectrometry method for the determination of nicotine and minor tobacco alkaloids in electronic cigarette refill liquids and second-hand generated aerosol. *J Sep Sci*, *40*(5), 1049-1056. https://doi.org/10.1002/jssc.201601076

Fan, L., Sweet, D. R., Prosdocimo, D. A., Vinayachandran, V., Chan, E. R., Zhang, R., Ilkayeva, O., Lu, Y., Keerthy, K. S., Booth, C. E., Newgard, C. B., & Jain, M. K. (2021). Muscle Kruppel-like factor 15 regulates lipid flux and systemic metabolic homeostasis. *J Clin Invest*, *131*(4). https://doi.org/10.1172/JCI139496

Farrell, K. R., Karey, E., Xu, S., Gibbon, G., Gordon, T., & Weitzman, M. (2021). E-Cigarette Use, Systemic Inflammation, and Depression. *Int J Environ Res Public Health*, *18*(19). https://doi.org/10.3390/ijerph181910402

Feng, H., Li, M., Altawil, A., Yin, Y., Zheng, R., & Kang, J. (2021). Cigarette smoke extracts induce apoptosis in Raw264.7 cells via endoplasmic reticulum stress and the intracellular Ca(2+)/P38/STAT1 pathway. *Toxicol In Vitro*, *77*, 105249. https://doi.org/10.1016/j.tiv.2021.105249

Foletta, V. C., White, L. J., Larsen, A. E., Leger, B., & Russell, A. P. (2011). The role and regulation of MAFbx/atrogin-1 and MuRF1 in skeletal muscle atrophy. *Pflugers Arch*, *461*(3), 325-335. https://doi.org/10.1007/s00424-010-0919-9

Forcina, L., Cosentino, M., & Musaro, A. (2020). Mechanisms Regulating Muscle Regeneration: Insights into the Interrelated and Time-Dependent Phases of Tissue Healing. *Cells*, *9*(5). https://doi.org/10.3390/cells9051297

Frank, D., Yusuf Rangrez, A., Friedrich, C., Dittmann, S., Stallmeyer, B., Yadav, P., Bernt, A., Schulze-Bahr, E., Borlepawar, A., Zimmermann, W. H., Peischard, S., Seebohm, G., Linke, W. A., Baba, H. A., Kruger, M., Unger, A., Usinger, P., Frey, N., & Schulze-Bahr, E. (2019). Cardiac alpha-Actin (ACTC1) Gene Mutation Causes Atrial-Septal Defects Associated With Late-Onset Dilated Cardiomyopathy. *Circ Genom Precis Med*, *12*(8), e002491. https://doi.org/10.1161/CIRCGEN.119.002491

Frontera, W. R., & Ochala, J. (2015). Skeletal muscle: a brief review of structure and function. *Calcif Tissue Int*, *96*(3), 183-195. https://doi.org/10.1007/s00223-014-9915-y

Gao, N., Liu, T., Wang, Y., Chen, M., Yu, L., Fu, C., & Xu, K. (2023). Assessing the association between smoking and hypertension: Smoking status, type of tobacco products, and interaction with alcohol consumption. *Front Cardiovasc Med*, *10*, 1027988. https://doi.org/10.3389/fcvm.2023.1027988

Gao, Q. Q., & McNally, E. M. (2015). The Dystrophin Complex: Structure, Function, and Implications for Therapy. *Compr Physiol*, *5*(3), 1223-1239. https://doi.org/10.1002/cphy.c140048

Gayraud-Morel, B., Chrétien, F., & Tajbakhsh, S. (2009). Skeletal muscle as a paradigm for regenerative biology and medicine. *Regen Med*, *4*(2), 293-319. https://doi.org/10.2217/17460751.4.2.293

Goniewicz, M. L., Knysak, J., Gawron, M., Kosmider, L., Sobczak, A., Kurek, J., Prokopowicz, A., Jablonska-Czapla, M., Rosik-Dulewska, C., Havel, C., Jacob, P., 3rd, & Benowitz, N. (2014). Levels of selected carcinogens and toxicants in vapour from electronic cigarettes. *Tob Control*, *23*(2), 133-139. https://doi.org/10.1136/tobaccocontrol-2012-050859

Gorgoulis, V., Adams, P. D., Alimonti, A., Bennett, D. C., Bischof, O., Bishop, C., Campisi, J., Collado, M., Evangelou, K., Ferbeyre, G., Gil, J., Hara, E.,

Krizhanovsky, V., Jurk, D., Maier, A. B., Narita, M., Niedernhofer, L., Passos, J. F., Robbins, P. D., . . . Demaria, M. (2019). Cellular Senescence: Defining a Path Forward. *Cell*, *179*(4), 813-827. https://doi.org/10.1016/j.cell.2019.10.005

Graziotti, G. H., Ríos, C. M., & Rivero, J.-L. L. (2001). Evidence for Three Fast Myosin Heavy Chain Isoforms in Type II Skeletal Muscle Fibers in the Adult Llama (Lama glama). *Journal of Histochemistry & Cytochemistry*, *49*(8), 1033-1044. https://doi.org/10.1177/002215540104900811

Grobet, L., Martin, L. J., Poncelet, D., Pirottin, D., Brouwers, B., Riquet, J., Schoeberlein, A., Dunner, S., Ménissier, F., Massabanda, J., Fries, R., Hanset, R., & Georges, M. (1997). A deletion in the bovine myostatin gene causes the double-muscled phenotype in cattle. *Nat Genet*, *17*(1), 71-74. https://doi.org/10.1038/ng0997-71

Guiraud, S., Edwards, B., Squire, S. E., Moir, L., Berg, A., Babbs, A., Ramadan, N., Wood, M. J., & Davies, K. E. (2019). Embryonic myosin is a regeneration marker to monitor utrophin-based therapies for DMD. *Hum Mol Genet*, *28*(2), 307-319. https://doi.org/10.1093/hmg/ddy353

Hagiwara, E., Takahashi, K. I., Okubo, T., Ohno, S., Ueda, A., Aoki, A., Odagiri, S., & Ishigatsubo, Y. (2001). Cigarette smoking depletes cells spontaneously secreting Th(1) cytokines in the human airway. *Cytokine*, *14*(2), 121-126. https://doi.org/10.1006/cyto.2001.0860

Hahad, O., Kuntic, M., Kuntic, I., Daiber, A., & Munzel, T. (2023). Tobacco smoking and vascular biology and function: evidence from human studies. *Pflugers Arch*, *475*(7), 797-805. https://doi.org/10.1007/s00424-023-02805-z

Han, S., Chen, H., Zhang, X., Liu, T., & Fu, Y. (2016). Levels of Selected Groups of Compounds in Refill Solutions for Electronic Cigarettes. *Nicotine Tob Res*, *18*(5), 708-714. https://doi.org/10.1093/ntr/ntv189

Hanahan, D., & Weinberg, R. A. (2011). Hallmarks of cancer: the next generation. *Cell*, *144*(5), 646-674. https://doi.org/10.1016/j.cell.2011.02.013

Hara, H., Araya, J., Ito, S., Kobayashi, K., Takasaka, N., Yoshii, Y., Wakui, H., Kojima, J., Shimizu, K., Numata, T., Kawaishi, M., Kamiya, N., Odaka, M., Morikawa, T., Kaneko, Y., Nakayama, K., & Kuwano, K. (2013). Mitochondrial fragmentation in cigarette smoke-induced bronchial epithelial cell senescence. *Am J Physiol Lung Cell Mol Physiol*, *305*(10), L737-746. https://doi.org/10.1152/ajplung.00146.2013

Heath, E., Tahri, D., Andermarcher, E., Schofield, P., Fleming, S., & Boulter, C. A. (2008). Abnormal skeletal and cardiac development, cardiomyopathy, muscle atrophy and cataracts in mice with a targeted disruption of the Nov (Ccn3) gene. *BMC Dev Biol*, *8*, 18. https://doi.org/10.1186/1471-213X-8-18

Heher, P., Ganassi, M., Weidinger, A., Engquist, E. N., Pruller, J., Nguyen, T. H., Tassin, A., Decleves, A. E., Mamchaoui, K., Banerji, C. R. S., Grillari, J., Kozlov, A. V., & Zammit, P. S. (2022). Interplay between mitochondrial reactive oxygen species, oxidative stress and hypoxic adaptation in facioscapulohumeral muscular dystrophy: Metabolic stress as potential therapeutic target. *Redox Biol*, *51*, 102251. https://doi.org/10.1016/j.redox.2022.102251

Hoffmann, D., & Hoffmann, I. (1997). The changing cigarette, 1950-1995. *J Toxicol Environ Health*, *50*(4), 307-364. https://doi.org/10.1080/009841097160393

Hoffmann, D., Hoffmann, I., & El-Bayoumy, K. (2001). The less harmful cigarette: a controversial issue. a tribute to Ernst L. Wynder. *Chem Res Toxicol*, *14*(7), 767-790. https://doi.org/10.1021/tx000260u

Hoffmann, R. F., Zarrintan, S., Brandenburg, S. M., Kol, A., de Bruin, H. G., Jafari, S., Dijk, F., Kalicharan, D., Kelders, M., Gosker, H. R., Ten Hacken, N. H., van der Want, J. J., van Oosterhout, A. J., & Heijink, I. H. (2013). Prolonged cigarette smoke exposure alters mitochondrial structure and function in airway epithelial cells. *Respir Res*, *14*(1), 97. https://doi.org/10.1186/1465-9921-14-97

Hoolachan, J. M., McCallion, E., Sutton, E. R., Cetin, O., Pacheco-Torres, P., Dimitriadi, M., Sari, S., Miller, G. J., Okoh, M., Walter, L. M., Claus, P., Wood, M. J. A., Tonge, D. P., & Bowerman, M. (2024). A transcriptomics-based drug repositioning approach to identify drugs with similar activities for the treatment of muscle pathologies in spinal muscular atrophy (SMA) models. *Hum Mol Genet*, *33*(5), 400-425. https://doi.org/10.1093/hmg/ddad192

Horinouchi, T., & Miwa, S. (2021). Comparison of cytotoxicity of cigarette smoke extract derived from heat-not-burn and combustion cigarettes in human vascular endothelial cells. *J Pharmacol Sci*, *147*(3), 223-233. https://doi.org/10.1016/j.jphs.2021.07.005

Horzum, U., Ozdil, B., & Pesen-Okvur, D. (2014). Step-by-step quantitative analysis of focal adhesions. *MethodsX*, *1*, 56-59. https://doi.org/10.1016/j.mex.2014.06.004

Hsieh, Y. T., & Chen, S. L. (2024). Visualization and Analysis of Neuromuscular Junctions Using Immunofluorescence. *Bio Protoc*, *14*(19), e5076. https://doi.org/10.21769/BioProtoc.5076

Hua, M., Alfi, M., & Talbot, P. (2013). Health-related effects reported by electronic cigarette users in online forums. *J Med Internet Res*, *15*(4), e59. https://doi.org/10.2196/jmir.2324

Jaccard, G., Djoko, D. T., Korneliou, A., Stabbert, R., Belushkin, M., & Esposito, M. (2019). Mainstream smoke constituents and in vitro toxicity comparative analysis of 3R4F and 1R6F reference cigarettes. *Toxicol Rep*, *6*, 222-231. https://doi.org/10.1016/j.toxrep.2019.02.009

Kablar, B., Krastel, K., Ying, C., Asakura, A., Tapscott, S. J., & Rudnicki, M. A. (1997). MyoD and Myf-5 differentially regulate the development of limb versus trunk skeletal muscle. *Development*, *124*(23), 4729-4738. https://doi.org/10.1242/dev.124.23.4729

Kamilari, E., Farsalinos, K., Poulas, K., Kontoyannis, C. G., & Orkoula, M. G. (2018). Detection and quantitative determination of heavy metals in electronic cigarette refill liquids using Total Reflection X-ray Fluorescence Spectrometry. *Food Chem Toxicol*, *116*(Pt B), 233-237. https://doi.org/10.1016/j.fct.2018.04.035

Kanithi, M., Junapudi, S., Shah, S. I., Matta Reddy, A., Ullah, G., & Chidipi, B. (2022). Alterations of Mitochondrial Network by Cigarette Smoking and E-Cigarette Vaping. *Cells*, *11*(10). https://doi.org/10.3390/cells11101688

Kanneganti, P., Harris, J. D., Brophy, R. H., Carey, J. L., Lattermann, C., & Flanigan, D. C. (2012). The effect of smoking on ligament and cartilage surgery in the knee: a systematic review. *Am J Sports Med*, *40*(12), 2872-2878. https://doi.org/10.1177/0363546512458223

Kasselimi, E., Pefani, D. E., Taraviras, S., & Lygerou, Z. (2022). Ribosomal DNA and the nucleolus at the heart of aging. *Trends Biochem Sci*, *47*(4), 328-341. https://doi.org/10.1016/j.tibs.2021.12.007

Kellers, F., Fernandez, A., Konukiewitz, B., Schindeldecker, M., Tagscherer, K. E., Heintz, A., Jesinghaus, M., Roth, W., & Foersch, S. (2022). Senescence-Associated Molecules and Tumor-Immune-Interactions as Prognostic Biomarkers in Colorectal Cancer. *Front Med (Lausanne)*, *9*, 865230. https://doi.org/10.3389/fmed.2022.865230

Kerr, J. F., Wyllie, A. H., & Currie, A. R. (1972). Apoptosis: a basic biological phenomenon with wide-ranging implications in tissue kinetics. *Br J Cancer*, *26*(4), 239-257. https://doi.org/10.1038/bjc.1972.33

Kim, D. H., & Wirtz, D. (2013). Focal adhesion size uniquely predicts cell migration. *Faseb j*, *27*(4), 1351-1361. https://doi.org/10.1096/fj.12-220160

Kitaguchi, Y., Taraseviciene-Stewart, L., Hanaoka, M., Natarajan, R., Kraskauskas, D., & Voelkel, N. F. (2012). Acrolein induces endoplasmic reticulum stress and causes

airspace enlargement. *PLoS One*, *7*(5), e38038. https://doi.org/10.1371/journal.pone.0038038
Klein, A. B., Kleinert, M., Richter, E. A., & Clemmensen, C. (2022). GDF15 in Appetite and Exercise: Essential Player or Coincidental Bystander? *Endocrinology*, *163*(1). https://doi.org/10.1210/endocr/bqab242
Koh, C. M., Gurel, B., Sutcliffe, S., Aryee, M. J., Schultz, D., Iwata, T., Uemura, M., Zeller, K. I., Anele, U., Zheng, Q., Hicks, J. L., Nelson, W. G., Dang, C. V., Yegnasubramanian, S., & De Marzo, A. M. (2011). Alterations in nucleolar structure and gene expression programs in prostatic neoplasia are driven by the MYC oncogene. *Am J Pathol*, *178*(4), 1824-1834. https://doi.org/10.1016/j.ajpath.2010.12.040
Kok, M. O., Hoekstra, T., & Twisk, J. W. (2012). The longitudinal relation between smoking and muscle strength in healthy adults. *Eur Addict Res*, *18*(2), 70-75. https://doi.org/10.1159/000333600
Kukurba, K. R., & Montgomery, S. B. (2015). RNA Sequencing and Analysis. *Cold Spring Harb Protoc*, *2015*(11), 951-969. https://doi.org/10.1101/pdb.top084970
Kumar, P. R., & Kumar, N. V. (1998). Effect of cigarette smoking on muscle strength of flexibility of athletes. *Indian J Exp Biol*, *36*(11), 1144-1146.
Kunkel, S. D., Suneja, M., Ebert, S. M., Bongers, K. S., Fox, D. K., Malmberg, S. E., Alipour, F., Shields, R. K., & Adams, C. M. (2011). mRNA expression signatures of human skeletal muscle atrophy identify a natural compound that increases muscle mass. *Cell Metab*, *13*(6), 627-638. https://doi.org/10.1016/j.cmet.2011.03.020
Kunzi, L., & Holt, G. E. (2019). Cigarette smoke activates the parthanatos pathway of cell death in human bronchial epithelial cells. *Cell Death Discov*, *5*, 127. https://doi.org/10.1038/s41420-019-0205-3
Lamb, J., Crawford, E. D., Peck, D., Modell, J. W., Blat, I. C., Wrobel, M. J., Lerner, J., Brunet, J. P., Subramanian, A., Ross, K. N., Reich, M., Hieronymus, H., Wei, G., Armstrong, S. A., Haggarty, S. J., Clemons, P. A., Wei, R., Carr, S. A., Lander, E. S., & Golub, T. R. (2006). The Connectivity Map: using gene-expression signatures to connect small molecules, genes, and disease. *Science*, *313*(5795), 1929-1935. https://doi.org/10.1126/science.1132939
Lange, S., Pinotsis, N., Agarkova, I., & Ehler, E. (2020). The M-band: The underestimated part of the sarcomere. *Biochim Biophys Acta Mol Cell Res*, *1867*(3), 118440. https://doi.org/10.1016/j.bbamcr.2019.02.003
Lee, E. J., Ahmad, S. S., Lim, J. H., Ahmad, K., Shaikh, S., Lee, Y. S., Park, S. J., Jin, J. O., Lee, Y. H., & Choi, I. (2021). Interaction of Fibromodulin and Myostatin to Regulate Skeletal Muscle Aging: An Opposite Regulation in Muscle Aging, Diabetes, and Intracellular Lipid Accumulation. *Cells*, *10*(8). https://doi.org/10.3390/cells10082083
Lee, J., Taneja, V., & Vassallo, R. (2012). Cigarette smoking and inflammation: cellular and molecular mechanisms. *J Dent Res*, *91*(2), 142-149. https://doi.org/10.1177/0022034511421200
Lee, J. S., Auyeung, T. W., Kwok, T., Lau, E. M., Leung, P. C., & Woo, J. (2007). Associated factors and health impact of sarcopenia in older chinese men and women: a cross-sectional study. *Gerontology*, *53*(6), 404-410. https://doi.org/10.1159/000107355
Lee, S. J., Lehar, A., Meir, J. U., Koch, C., Morgan, A., Warren, L. E., Rydzik, R., Youngstrom, D. W., Chandok, H., George, J., Gogain, J., Michaud, M., Stoklasek, T. A., Liu, Y., & Germain-Lee, E. L. (2020). Targeting myostatin/activin A protects against skeletal muscle and bone loss during spaceflight. *Proc Natl Acad Sci U S A*, *117*(38), 23942-23951. https://doi.org/10.1073/pnas.2014716117

Lee, S. J., Reed, L. A., Davies, M. V., Girgenrath, S., Goad, M. E., Tomkinson, K. N., Wright, J. F., Barker, C., Ehrmantraut, G., Holmstrom, J., Trowell, B., Gertz, B., Jiang, M. S., Sebald, S. M., Matzuk, M., Li, E., Liang, L. F., Quattlebaum, E., Stotish, R. L., & Wolfman, N. M. (2005). Regulation of muscle growth by multiple ligands signaling through activin type II receptors. *Proc Natl Acad Sci U S A*, *102*(50), 18117-18122. https://doi.org/10.1073/pnas.0505996102

Leone, A. (2011). Does Smoking Act as a Friend or Enemy of Blood Pressure? Let Release Pandora's Box. *Cardiol Res Pract*, *2011*, 264894. https://doi.org/10.4061/2011/264894

Li, Y., & Hecht, S. S. (2022). Carcinogenic components of tobacco and tobacco smoke: A 2022 update. *Food Chem Toxicol*, *165*, 113179. https://doi.org/10.1016/j.fct.2022.113179

Liu, C., Chu, D., Kalantar-Zadeh, K., George, J., Young, H. A., & Liu, G. (2021). Cytokines: From Clinical Significance to Quantification. *Adv Sci (Weinh)*, *8*(15), e2004433. https://doi.org/10.1002/advs.202004433

Liu, Q., Xu, W. G., Luo, Y., Han, F. F., Yao, X. H., Yang, T. Y., Zhang, Y., Pi, W. F., & Guo, X. J. (2011). Cigarette smoke-induced skeletal muscle atrophy is associated with up-regulation of USP-19 via p38 and ERK MAPKs. *J Cell Biochem*, *112*(9), 2307-2316. https://doi.org/10.1002/jcb.23151

Lluri, G., Langlois, G. D., McClellan, B., Soloway, P. D., & Jaworski, D. M. (2006). Tissue inhibitor of metalloproteinase-2 (TIMP-2) regulates neuromuscular junction development via a beta1 integrin-mediated mechanism. *J Neurobiol*, *66*(12), 1365-1377. https://doi.org/10.1002/neu.20315

Lugg, S. T., Scott, A., Parekh, D., Naidu, B., & Thickett, D. R. (2022). Cigarette smoke exposure and alveolar macrophages: mechanisms for lung disease. *Thorax*, *77*(1), 94-101. https://doi.org/10.1136/thoraxjnl-2020-216296

Luppi, F., Aarbiou, J., van Wetering, S., Rahman, I., de Boer, W. I., Rabe, K. F., & Hiemstra, P. S. (2005). Effects of cigarette smoke condensate on proliferation and wound closure of bronchial epithelial cells in vitro: role of glutathione. *Respir Res*, *6*(1), 140. https://doi.org/10.1186/1465-9921-6-140

Ma, T., Wang, X., Li, L., Sun, B., Zhu, Y., & Xia, T. (2021). Electronic cigarette aerosols induce oxidative stress-dependent cell death and NF-kappaB mediated acute lung inflammation in mice. *Arch Toxicol*, *95*(1), 195-205. https://doi.org/10.1007/s00204-020-02920-1

Mahdy, M. A. A. (2019). Skeletal muscle fibrosis: an overview. *Cell Tissue Res*, *375*(3), 575-588. https://doi.org/10.1007/s00441-018-2955-2

Mann, C. J., Perdiguero, E., Kharraz, Y., Aguilar, S., Pessina, P., Serrano, A. L., & Munoz-Canoves, P. (2011). Aberrant repair and fibrosis development in skeletal muscle. *Skelet Muscle*, *1*(1), 21. https://doi.org/10.1186/2044-5040-1-21

Maremanda, K. P., Sundar, I. K., & Rahman, I. (2021). Role of inner mitochondrial protein OPA1 in mitochondrial dysfunction by tobacco smoking and in the pathogenesis of COPD. *Redox Biol*, *45*, 102055. https://doi.org/10.1016/j.redox.2021.102055

Margham, J., McAdam, K., Forster, M., Liu, C., Wright, C., Mariner, D., & Proctor, C. (2016). Chemical Composition of Aerosol from an E-Cigarette: A Quantitative Comparison with Cigarette Smoke. *Chem Res Toxicol*, *29*(10), 1662-1678. https://doi.org/10.1021/acs.chemrestox.6b00188

Martinez, I. K. C., Sparks, N. R. L., Madrid, J. V., Talbot, P., & Zur Nieden, N. I. (2022). Exposure to Cigarette Smoke Impedes Human Osteoblast Differentiation Independently of Nicotine. *Nicotine Tob Res*, *24*(12), 1921-1926. https://doi.org/10.1093/ntr/ntac144

Masso-Silva, J. A., Byun, M. K., & Alexander, L. E. C. (2021). Acute and chronic effects of vaping electronic devices on lung physiology and inflammation. *Curr Opin Physiol*, *22*. https://doi.org/10.1016/j.cophys.2021.06.001

Mauro, A. (1961). Satellite cell of skeletal muscle fibers. *J Biophys Biochem Cytol*, *9*(2), 493-495. https://doi.org/10.1083/jcb.9.2.493

Mazerbourg, S., Callebaut, I., Zapf, J., Mohan, S., Overgaard, M., & Monget, P. (2004). Up date on IGFBP-4: regulation of IGFBP-4 levels and functions, in vitro and in vivo. *Growth Horm IGF Res*, *14*(2), 71-84. https://doi.org/10.1016/j.ghir.2003.10.002

McMahon, D., Anderson, P. A., Nassar, R., Bunting, J., Saba, Z., Oakeley, A. E., & Malouf, N. N. (1994). C2C12 cells: biophysical, biochemical, and immunocytochemical properties. *The American journal of physiology*, *266 6 Pt 1*, C1795-1802.

McNamara, J. W., & Sadayappan, S. (2018). Skeletal myosin binding protein-C: An increasingly important regulator of striated muscle physiology. *Archives of Biochemistry and Biophysics*, *660*, 121-128. https://doi.org/10.1016/j.abb.2018.10.007

McPherron, A. C., Lawler, A. M., & Lee, S. J. (1997). Regulation of skeletal muscle mass in mice by a new TGF-beta superfamily member. *Nature*, *387*(6628), 83-90. https://doi.org/10.1038/387083a0

Meijboom, K. E., Volpato, V., Monzon-Sandoval, J., Hoolachan, J. M., Hammond, S. M., Abendroth, F., de Jong, O. G., Hazell, G., Ahlskog, N., Wood, M. J., Webber, C., & Bowerman, M. (2021). Combining multiomics and drug perturbation profiles to identify muscle-specific treatments for spinal muscular atrophy. *JCI Insight*, *6*(13). https://doi.org/10.1172/jci.insight.149446

Melak, M., Plessner, M., & Grosse, R. (2017). Correction: Actin visualization at a glance. *J Cell Sci*, *130*(9), 1688. https://doi.org/10.1242/jcs.204487

Mescher, A. L. (2023). In *Junqueira's Basic Histology Text and Atlas, 16e*. McGraw Hill. accessartmed.mhmedical.com/content.aspx?aid=1203732657

Mescher, M., & Haarmann-Stemmann, T. (2018). Modulation of CYP1A1 metabolism: From adverse health effects to chemoprevention and therapeutic options. *Pharmacol Ther*, *187*, 71-87. https://doi.org/10.1016/j.pharmthera.2018.02.012

Metz, B., Kersten, G. F., Hoogerhout, P., Brugghe, H. F., Timmermans, H. A., de Jong, A., Meiring, H., ten Hove, J., Hennink, W. E., Crommelin, D. J., & Jiskoot, W. (2004). Identification of formaldehyde-induced modifications in proteins: reactions with model peptides. *J Biol Chem*, *279*(8), 6235-6243. https://doi.org/10.1074/jbc.M310752200

Millay, D. P. (2022). Regulation of the myoblast fusion reaction for muscle development, regeneration, and adaptations. *Exp Cell Res*, *415*(2), 113134. https://doi.org/10.1016/j.yexcr.2022.113134

Montecucco, A., Zanetta, F., & Biamonti, G. (2015). Molecular mechanisms of etoposide. *Excli j*, *14*, 95-108. https://doi.org/10.17179/excli2015-561

Montes de Oca, M., Loeb, E., Torres, S. H., De Sanctis, J., Hernández, N., & Tálamo, C. (2008). Peripheral muscle alterations in non-COPD smokers. *Chest*, *133*(1), 13-18. https://doi.org/10.1378/chest.07-1592

Morgan, J. E., Coulton, G. R., & Partridge, T. A. (1987). Muscle precursor cells invade and repopulate freeze-killed muscles. *J Muscle Res Cell Motil*, *8*(5), 386-396. https://doi.org/10.1007/bf01578428

Morgan, J. E., Prola, A., Mariot, V., Pini, V., Meng, J., Hourde, C., Dumonceaux, J., Conti, F., Relaix, F., Authier, F. J., Tiret, L., Muntoni, F., & Bencze, M. (2018). Necroptosis mediates myofibre death in dystrophin-deficient mice. *Nat Commun*, *9*(1), 3655. https://doi.org/10.1038/s41467-018-06057-9

Munzel, T., Hahad, O., Kuntic, M., Keaney, J. F., Deanfield, J. E., & Daiber, A. (2020). Effects of tobacco cigarettes, e-cigarettes, and waterpipe smoking on endothelial function and clinical outcomes. *Eur Heart J*, *41*(41), 4057-4070. https://doi.org/10.1093/eurheartj/ehaa460

Muqaddas, M., & Siddiqui, M. (2015). BIOCHEMICAL MECHANISMS OF ETOPOSIDE; UPSHOT OF CELL DEATH. *International Journal of Pharmaceutical Sciences And Research*, *6*, 4920. https://doi.org/10.13040/IJPSR.0975-8232.6(12).4920-39

Musarò, A. (2014). The Basis of Muscle Regeneration. *Advances in Biology*, *2014*, 1-16. https://doi.org/10.1155/2014/612471

Navani, N., Baldwin, D. R., Edwards, J. G., Evison, M., McDonald, F., Nicholson, A. G., Fenemore, J., Sage, E. K., & Popat, S. (2022). Lung Cancer in the United Kingdom. *J Thorac Oncol*, *17*(2), 186-193. https://doi.org/10.1016/j.jtho.2021.11.002

Nemery, B., Moavero, N. E., Brasseur, L., & Stănescu, D. C. (1983). Smoking, lung function, and body weight. *Br Med J (Clin Res Ed)*, *286*(6361), 249-251. https://doi.org/10.1136/bmj.286.6361.249

Ng, T. K., Huang, L., Cao, D., Yip, Y. W., Tsang, W. M., Yam, G. H., Pang, C. P., & Cheung, H. S. (2015). Cigarette smoking hinders human periodontal ligament-derived stem cell proliferation, migration and differentiation potentials. *Sci Rep*, *5*, 7828. https://doi.org/10.1038/srep07828

NHS. (2020). *Statistics on smoking, England 2020*. NHS. https://digital.nhs.uk/data-and-information/publications/statistical/statistics-on-smoking/statistics-on-smoking-england-2020#

NHS. (2025). *Lung cancer statistics*. Retrieved 22.05.2025 from https://www.cancerresearchuk.org/health-professional/cancer-statistics/statistics-by-cancer-type/lung-cancer

Nicholson, D. W., Ali, A., Thornberry, N. A., Vaillancourt, J. P., Ding, C. K., Gallant, M., Gareau, Y., Griffin, P. R., Labelle, M., Lazebnik, Y. A., & et al. (1995). Identification and inhibition of the ICE/CED-3 protease necessary for mammalian apoptosis. *Nature*, *376*(6535), 37-43. https://doi.org/10.1038/376037a0

Nogueira, L., Trisko, B. M., Lima-Rosa, F. L., Jackson, J., Lund-Palau, H., Yamaguchi, M., & Breen, E. C. (2018). Cigarette smoke directly impairs skeletal muscle function through capillary regression and altered myofibre calcium kinetics in mice. *J Physiol*, *596*(14), 2901-2916. https://doi.org/10.1113/JP275888

Nyunoya, T., Monick, M. M., Klingelhutz, A., Yarovinsky, T. O., Cagley, J. R., & Hunninghake, G. W. (2006). Cigarette smoke induces cellular senescence. *Am J Respir Cell Mol Biol*, *35*(6), 681-688. https://doi.org/10.1165/rcmb.2006-0169OC

Ordahl, C. P., & Douarin, N. M. L. (1992). Two myogenic lineages within the developing somite. *Development*, *114*(2), 339-353. https://doi.org/10.1242/dev.114.2.339

Orlander, J., Kiessling, K. H., & Larsson, L. (1979). Skeletal muscle metabolism, morphology and function in sedentary smokers and nonsmokers. *Acta Physiol Scand*, *107*(1), 39-46. https://doi.org/10.1111/j.1748-1716.1979.tb06440.x

Oxenhandler, R., Adelstein, E. H., & Hart, M. N. (1977). Immunopathology of skeletal muscle. The value of direct immunofluorescence in the diagnosis of connective tissue disease. *Hum Pathol*, *8*(3), 321-328. https://doi.org/10.1016/s0046-8177(77)80029-4

Patel, K., Gadewar, M., Tripathi, R., Prasad, S. K., & Patel, D. K. (2012). A review on medicinal importance, pharmacological activity and bioanalytical aspects of beta-carboline alkaloid "Harmine". *Asian Pac J Trop Biomed*, *2*(8), 660-664. https://doi.org/10.1016/S2221-1691(12)60116-6

Patel, R. A., Wilson, R. F., Patel, P. A., & Palmer, R. M. (2013). The effect of smoking on bone healing: A systematic review. *Bone Joint Res*, *2*(6), 102-111. https://doi.org/10.1302/2046-3758.26.2000142

Pepper, J. K., & Brewer, N. T. (2014). Electronic nicotine delivery system (electronic cigarette) awareness, use, reactions and beliefs: a systematic review. *Tob Control*, *23*(5), 375-384. https://doi.org/10.1136/tobaccocontrol-2013-051122

Petersen, A. M., Magkos, F., Atherton, P., Selby, A., Smith, K., Rennie, M. J., Pedersen, B. K., & Mittendorfer, B. (2007). Smoking impairs muscle protein synthesis and increases the expression of myostatin and MAFbx in muscle. *Am J Physiol Endocrinol Metab*, *293*(3), E843-848. https://doi.org/10.1152/ajpendo.00301.2007

Prokhorova, E. A., Zamaraev, A. V., Kopeina, G. S., Zhivotovsky, B., & Lavrik, I. N. (2015). Role of the nucleus in apoptosis: signaling and execution. *Cell Mol Life Sci*, *72*(23), 4593-4612. https://doi.org/10.1007/s00018-015-2031-y

Quinn, M. E., Goh, Q., Kurosaka, M., Gamage, D. G., Petrany, M. J., Prasad, V., & Millay, D. P. (2017). Myomerger induces fusion of non-fusogenic cells and is required for skeletal muscle development. *Nat Commun*, *8*, 15665. https://doi.org/10.1038/ncomms15665

Repine, J. E., Bast, A., & Lankhorst, I. (1997). Oxidative stress in chronic obstructive pulmonary disease. Oxidative Stress Study Group. *Am J Respir Crit Care Med*, *156*(2 Pt 1), 341-357. https://doi.org/10.1164/ajrccm.156.2.9611013

Rhee, M. Y., Na, S. H., Kim, Y. K., Lee, M. M., & Kim, H. Y. (2007). Acute effects of cigarette smoking on arterial stiffness and blood pressure in male smokers with hypertension. *Am J Hypertens*, *20*(6), 637-641. https://doi.org/10.1016/j.amjhyper.2006.12.017

Rodgers, B. D., & Ward, C. W. (2022). Myostatin/Activin Receptor Ligands in Muscle and the Development Status of Attenuating Drugs. *Endocr Rev*, *43*(2), 329-365. https://doi.org/10.1210/endrev/bnab030

Rossi, G., Bonfanti, C., Antonini, S., Bastoni, M., Monteverde, S., Innocenzi, A., Saclier, M., Taglietti, V., & Messina, G. (2017). Silencing Nfix rescues muscular dystrophy by delaying muscle regeneration. *Nat Commun*, *8*(1), 1055. https://doi.org/10.1038/s41467-017-01098-y

Saito, T., Miyatake, N., Sakano, N., Oda, K., Katayama, A., Nishii, K., & Numata, T. (2012). Relationship between cigarette smoking and muscle strength in Japanese men. *J Prev Med Public Health*, *45*(6), 381-386. https://doi.org/10.3961/jpmph.2012.45.6.381

Sass, F. A., Fuchs, M., Pumberger, M., Geissler, S., Duda, G. N., Perka, C., & Schmidt-Bleek, K. (2018). Immunology Guides Skeletal Muscle Regeneration. *Int J Mol Sci*, *19*(3). https://doi.org/10.3390/ijms19030835

Scharner, J., & Zammit, P. S. (2011). The muscle satellite cell at 50: the formative years. *Skeletal Muscle*, *1*(1), 28. https://doi.org/10.1186/2044-5040-1-28

Schiaffino, S., Rossi, A. C., Smerdu, V., Leinwand, L. A., & Reggiani, C. (2015). Developmental myosins: expression patterns and functional significance. *Skelet Muscle*, *5*, 22. https://doi.org/10.1186/s13395-015-0046-6

Schieweck, R., & Gotz, M. (2024). Pan-cellular organelles and suborganelles-from common functions to cellular diversity? *Genes Dev*, *38*(3-4), 98-114. https://doi.org/10.1101/gad.351337.123

Schuller, H. M., & Orloff, M. (1998). Tobacco-specific carcinogenic nitrosamines. Ligands for nicotinic acetylcholine receptors in human lung cancer cells. *Biochem Pharmacol*, *55*(9), 1377-1384. https://doi.org/10.1016/s0006-2952(97)00651-5

Schultz, E., Jaryszak, D. L., & Valliere, C. R. (1985). Response of satellite cells to focal skeletal muscle injury. *Muscle & Nerve*, *8*(3), 217-222. https://doi.org/https://doi.org/10.1002/mus.880080307

Scott, A., Lugg, S. T., Aldridge, K., Lewis, K. E., Bowden, A., Mahida, R. Y., Grudzinska, F. S., Dosanjh, D., Parekh, D., Foronjy, R., Sapey, E., Naidu, B., & Thickett, D. R. (2018). Pro-inflammatory effects of e-cigarette vapour condensate on human alveolar macrophages. *Thorax*, *73*(12), 1161-1169. https://doi.org/10.1136/thoraxjnl-2018-211663

Sharma, A., Lee, J., Fonseca, A. G., Moshensky, A., Kothari, T., Sayed, I. M., Ibeawuchi, S. R., Pranadinata, R. F., Ear, J., Sahoo, D., Crotty-Alexander, L. E., Ghosh, P., & Das, S. (2021). E-cigarettes compromise the gut barrier and trigger inflammation. *iScience*, *24*(2), 102035. https://doi.org/10.1016/j.isci.2021.102035

Sherwood, L. (2015). *Human Physiology: From Cells to Systems*. Cengage Learning. https://books.google.com.kw/books?id=_i5BBAAAQBAJ

Shi, Y., Zhang, Y., Zhang, Y., Yao, J., Guo, J., Xu, X., & Wang, L. (2024). Advances in Nanotherapy for Targeting Senescent Cells. *Int J Nanomedicine*, *19*, 8797-8813. https://doi.org/10.2147/IJN.S469110

Shinobu, N., Maeda, T., Aso, T., Ito, T., Kondo, T., Koike, K., & Hatakeyama, M. (1999). Physical interaction and functional antagonism between the RNA polymerase II elongation factor ELL and p53. *J Biol Chem*, *274*(24), 17003-17010. https://doi.org/10.1074/jbc.274.24.17003

Siegel, A. L., Atchison, K., Fisher, K. E., Davis, G. E., & Cornelison, D. D. W. (2009). 3D Timelapse Analysis of Muscle Satellite Cell Motility. *Stem Cells*, *27*(10), 2527-2538. https://doi.org/10.1002/stem.178

Singh, K. P., Miaskowski, C., Dhruva, A. A., Flowers, E., & Kober, K. M. (2018). Mechanisms and Measurement of Changes in Gene Expression. *Biol Res Nurs*, *20*(4), 369-382. https://doi.org/10.1177/1099800418772161

Sinicropi, D., Cronin, M., & Liu, M.-L. (2006). Gene Expression Profiling Utilizing Microarray Technology and RT-PCR. In *BioMEMS and Biomedical Nanotechnology* (pp. 23-46). https://doi.org/10.1007/978-0-387-25843-0_2

Sleiman, M., Logue, J. M., Montesinos, V. N., Russell, M. L., Litter, M. I., Gundel, L. A., & Destaillats, H. (2016). Emissions from Electronic Cigarettes: Key Parameters Affecting the Release of Harmful Chemicals. *Environ Sci Technol*, *50*(17), 9644-9651. https://doi.org/10.1021/acs.est.6b01741

Sloan, A., Hussain, I., Maqsood, M., Eremin, O., & El-Sheemy, M. (2010). The effects of smoking on fracture healing. *Surgeon*, *8*(2), 111-116. https://doi.org/10.1016/j.surge.2009.10.014

Smith, C. J., Perfetti, T. A., Garg, R., & Hansch, C. (2003). IARC carcinogens reported in cigarette mainstream smoke and their calculated log P values. *Food Chem Toxicol*, *41*(6), 807-817. https://doi.org/10.1016/s0278-6915(03)00021-8

Sopori, M. L., & Kozak, W. (1998). Immunomodulatory effects of cigarette smoke. *Journal of Neuroimmunology*, *83*(1), 148-156. https://doi.org/https://doi.org/10.1016/S0165-5728(97)00231-2

Spiess, P. C., Deng, B., Hondal, R. J., Matthews, D. E., & van der Vliet, A. (2011). Proteomic profiling of acrolein adducts in human lung epithelial cells. *J Proteomics*, *74*(11), 2380-2394. https://doi.org/10.1016/j.jprot.2011.05.039

Statistics, O. f. N. (2024). *Adult smoking habits in the UK: 2023*. Retrieved 23.02.2025 from https://www.ons.gov.uk/peoplepopulationandcommunity/healthandsocialcare/healthandlifeexpectancies/bulletins/adultsmokinghabitsingreatbritain/2023

Stevens, N. E., Loreti, M., Ramirez-Sanchez, I., Dos Reis, F. C. G., Sacco, A., Breen, E. C., & Nogueira, L. (2024). Cigarette smoke exposure impairs early-stage recovery from lengthening contraction-induced muscle injury in male mice. *Physiol Rep*, *12*(18), e70064. https://doi.org/10.14814/phy2.70064

Stupka, N., Kintakas, C., White, J. D., Fraser, F. W., Hanciu, M., Aramaki-Hattori, N., Martin, S., Coles, C., Collier, F., Ward, A. C., Apte, S. S., & McCulloch, D. R. (2013). Versican processing by a disintegrin-like and metalloproteinase domain with thrombospondin-1 repeats proteinases-5 and -15 facilitates myoblast fusion. *J Biol Chem*, *288*(3), 1907-1917. https://doi.org/10.1074/jbc.M112.429647

Suh, J., Kim, N. K., Lee, S. H., Eom, J. H., Lee, Y., Park, J. C., Woo, K. M., Baek, J. H., Kim, J. E., Ryoo, H. M., Lee, S. J., & Lee, Y. S. (2020). GDF11 promotes osteogenesis as opposed to MSTN, and follistatin, a MSTN/GDF11 inhibitor, increases muscle mass but weakens bone. *Proc Natl Acad Sci U S A*, *117*(9), 4910-4920. https://doi.org/10.1073/pnas.1916034117

Sundar, I. K., Maremanda, K. P., & Rahman, I. (2019). Mitochondrial dysfunction is associated with Miro1 reduction in lung epithelial cells by cigarette smoke. *Toxicol Lett*, *317*, 92-101. https://doi.org/10.1016/j.toxlet.2019.09.022

Szoka, P., Lachowicz, J., Cwiklińska, M., Lukaszewicz, A., Rybak, A., Baranowska, U., & Holownia, A. (2019). Cigarette Smoke-Induced Oxidative Stress and Autophagy in Human Alveolar Epithelial Cell Line (A549 Cells). *Adv Exp Med Biol*, *1176*, 63-69. https://doi.org/10.1007/5584_2019_373

Takkar, S., Sharma, G., Kaushal, J. B., Abdullah, K. M., Batra, S. K., & Siddiqui, J. A. (2024). From orphan to oncogene: The role of GPR35 in cancer and immune modulation. *Cytokine Growth Factor Rev*, *77*, 56-66. https://doi.org/10.1016/j.cytogfr.2024.03.004

Talhout, R., Schulz, T., Florek, E., van Benthem, J., Wester, P., & Opperhuizen, A. (2011). Hazardous compounds in tobacco smoke. *Int J Environ Res Public Health*, *8*(2), 613-628. https://doi.org/10.3390/ijerph8020613

Tan, Y., Ye, Y., Huang, C., Li, J., Huang, L., Wei, X., Liang, T., Qin, E., Xiong, G., & Bin, Y. (2025). Cigarette Smoking Induces Skeletal Muscle Atrophy in Mice by Activated Macrophage-Mediated Pyroptosis. *J Inflamm Res*, *18*, 2447-2464. https://doi.org/10.2147/JIR.S497631

Tarroni, P., Rubboli, F., Chini, B., Zwart, R., Oortgiesen, M., Sher, E., & Clementi, F. (1992). Neuronal-type nicotinic receptors in human neuroblastoma and small-cell lung carcinoma cell lines. *FEBS Lett*, *312*(1), 66-70. https://doi.org/10.1016/0014-5793(92)81411-e

Tattan-Birch, H., Jackson, S. E., Kock, L., Dockrell, M., & Brown, J. (2023). Rapid growth in disposable e-cigarette vaping among young adults in Great Britain from 2021 to 2022: a repeat cross-sectional survey. *Addiction*, *118*(2), 382-386. https://doi.org/10.1111/add.16044

Theron, A. J., Feldman, C., Richards, G. A., Tintinger, G. R., & Anderson, R. (2019). Electronic cigarettes: where to from here? *J Thorac Dis*, *11*(12), 5572-5585. https://doi.org/10.21037/jtd.2019.11.82

Tsurutani, J., Castillo, S. S., Brognard, J., Granville, C. A., Zhang, C., Gills, J. J., Sayyah, J., & Dennis, P. A. (2005). Tobacco components stimulate Akt-dependent proliferation and NFkappaB-dependent survival in lung cancer cells. *Carcinogenesis*, *26*(7), 1182-1195. https://doi.org/10.1093/carcin/bgi072

Turner, C. E. (2000). Paxillin and focal adhesion signalling. *Nature Cell Biology*, *2*(12), E231-E236. https://doi.org/10.1038/35046659

VanGuilder, H. D., Vrana, K. E., & Freeman, W. M. (2008). Twenty-five years of quantitative PCR for gene expression analysis. *Biotechniques*, *44*(5), 619-626. https://doi.org/10.2144/000112776

Vermes, I., Haanen, C., Steffens-Nakken, H., & Reutelingsperger, C. (1995). A novel assay for apoptosis. Flow cytometric detection of phosphatidylserine expression on early apoptotic cells using fluorescein labelled Annexin V. *J Immunol Methods*, *184*(1), 39-51. https://doi.org/10.1016/0022-1759(95)00072-i

Wada, H., Suzuki, M., Matsuda, M., Ajiro, Y., Shinozaki, T., Sakagami, S., Yonezawa, K., Shimizu, M., Funada, J., Takenaka, T., Morita, Y., Nakamura, T., Fujimoto, K., Matsubara, H., Kato, T., Unoki, T., Takagi, D., Wada, K., Wada, M., . . . Investigators, A. S. (2020). Impact of Smoking Status on Growth Differentiation Factor 15 and Mortality in Patients With Suspected or Known Coronary Artery Disease: The ANOX Study. *J Am Heart Assoc*, *9*(22), e018217. https://doi.org/10.1161/JAHA.120.018217

Wahl, E. A., Schenck, T. L., Machens, H. G., & Egana, J. T. (2016). Acute stimulation of mesenchymal stem cells with cigarette smoke extract affects their migration, differentiation, and paracrine potential. *Sci Rep*, *6*, 22957. https://doi.org/10.1038/srep22957

Wang, J., Niu, W., Witte, D. P., Chernausek, S. D., Nikiforov, Y. E., Clemens, T. L., Sharifi, B., Strauch, A. R., & Fagin, J. A. (1998). Overexpression of insulin-like growth factor-binding protein-4 (IGFBP-4) in smooth muscle cells of transgenic mice through a smooth muscle alpha-actin-IGFBP-4 fusion gene induces smooth muscle hypoplasia. *Endocrinology*, *139*(5), 2605-2614. https://doi.org/10.1210/endo.139.5.5986

Wang, J. B., Olgin, J. E., Nah, G., Vittinghoff, E., Cataldo, J. K., Pletcher, M. J., & Marcus, G. M. (2018). Cigarette and e-cigarette dual use and risk of cardiopulmonary symptoms in the Health eHeart Study. *PLoS One*, *13*(7), e0198681. https://doi.org/10.1371/journal.pone.0198681

Wang, L., Wang, Y., Chen, J., Yang, X. M., Jiang, X. T., Liu, P., & Li, M. (2021). Comparison of biological and transcriptomic effects of conventional cigarette and electronic cigarette smoke exposure at toxicological dose in BEAS-2B cells. *Ecotoxicol Environ Saf*, *222*, 112472. https://doi.org/10.1016/j.ecoenv.2021.112472

Wang, Q., Sundar, I. K., Li, D., Lucas, J. H., Muthumalage, T., McDonough, S. R., & Rahman, I. (2020). E-cigarette-induced pulmonary inflammation and dysregulated repair are mediated by nAChR alpha7 receptor: role of nAChR alpha7 in SARS-CoV-2 Covid-19 ACE2 receptor regulation. *Respir Res*, *21*(1), 154. https://doi.org/10.1186/s12931-020-01396-y

Wang, Y., Lu, J., & Liu, Y. (2022). Skeletal Muscle Regeneration in Cardiotoxin-Induced Muscle Injury Models. *Int J Mol Sci*, *23*(21). https://doi.org/10.3390/ijms232113380

Wang, Y. X., & Rudnicki, M. A. (2011). Satellite cells, the engines of muscle repair. *Nat Rev Mol Cell Biol*, *13*(2), 127-133. https://doi.org/10.1038/nrm3265

Watt, D. J., Morgan, J. E., Clifford, M. A., & Partridge, T. A. (1987). The movement of muscle precursor cells between adjacent regenerating muscles in the mouse. *Anat Embryol (Berl)*, *175*(4), 527-536. https://doi.org/10.1007/bf00309688

Werner, H. (2023). The IGF1 Signaling Pathway: From Basic Concepts to Therapeutic Opportunities. *Int J Mol Sci*, *24*(19). https://doi.org/10.3390/ijms241914882

WHO. (2020). *Summary results of the global youth tobacco survey in selected countries of the WHO european region*. WHO regional office for europe. WHO. (2020). "https://www.who.int/news-room/fact-sheets/detail/tobacco." Tobacco, 2021.

WHO. (2025). *Cancer*. Retrieved 22.05.2025 from https://www.who.int/news-room/fact-sheets/detail/cancer

Williamson, D. F., Madans, J., Anda, R. F., Kleinman, J. C., Giovino, G. A., & Byers, T. (1991). Smoking cessation and severity of weight gain in a national cohort. *N Engl J Med*, *324*(11), 739-745. https://doi.org/10.1056/nejm199103143241106

Wolfe, R. R. (2006). The underappreciated role of muscle in health and disease. *Am J Clin Nutr*, *84*(3), 475-482. https://doi.org/10.1093/ajcn/84.3.475

Wong, C. Y. J., Ong, H. X., & Traini, D. (2022). The application of in vitro cellular assays for analysis of electronic cigarettes impact on the airway. *Life Sci*, *298*, 120487. https://doi.org/10.1016/j.lfs.2022.120487

Wozniak, M. A., Modzelewska, K., Kwong, L., & Keely, P. J. (2004). Focal adhesion regulation of cell behavior. *Biochim Biophys Acta*, *1692*(2-3), 103-119. https://doi.org/10.1016/j.bbamcr.2004.04.007

Yin, H., Price, F., & Rudnicki, M. A. (2013). Satellite cells and the muscle stem cell niche. *Physiol Rev*, *93*(1), 23-67. https://doi.org/10.1152/physrev.00043.2011

Zheng, M., Yuan, G., Han, J., Li, J., Jiang, Y., Li, Z., & Yao, Y. (2025). FOXO1 contributes to cigarette smoke condensate-induced cellular senescence and fibrosis in lung fibroblasts through activating the TGF-beta1/Smad2/3 signaling pathway. *Immunol Res*, *73*(1), 94. https://doi.org/10.1007/s12026-025-09646-1

Zhou, X., Wang, J. L., Lu, J., Song, Y., Kwak, K. S., Jiao, Q., Rosenfeld, R., Chen, Q., Boone, T., Simonet, W. S., Lacey, D. L., Goldberg, A. L., & Han, H. Q. (2010). Reversal of cancer cachexia and muscle wasting by ActRIIB antagonism leads to prolonged survival. *Cell*, *142*(4), 531-543. https://doi.org/10.1016/j.cell.2010.07.011

Zong, H., Hu, Z., Li, W., Wang, M., Zhou, Q., Li, X., & Liu, H. (2024). Electronic cigarettes and cardiovascular disease: epidemiological and biological links. *Pflugers Arch*, *476*(6), 875-888. https://doi.org/10.1007/s00424-024-02925-0